AVOIDING & MITIGATING ALKALI-AGGREGATE REACTION (AAR) IN CONCRETE STRUCTURES

DIEGO JESUS DE SOUZA

Thesis submitted to the University of Ottawa
in partial Fulfillment of the requirements for the
DOCTOR OF PHILOSOPHY IN CIVIL ENGINEERING

Department of Civil Engineering
Faculty of Engineering
University of Ottawa

Abstract

Alkali-Aggregate Reaction (AAR) is one of the most harmful distress mechanisms affecting the serviceability and durability of concrete critical infrastructure worldwide. Over the past decades, several approaches and recommendations have been developed to assess the potential reactivity of aggregates in the laboratory and the efficiency of preventive measures (e.g., supplementary cementing materials – SCMs) to mitigate ASR in the field. Yet, recent findings suggest that the appropriate use of SCMs "only" delayed and does not entirely prevent ASR occurrence. Moreover, once ASR starts in the field, there is no "universal" solution that should be applied in various cases, and each situation should be evaluated as "unique". Nevertheless, artificially triggering healing agents have been studied in the late years, thus presenting an interesting "physical" solution to reduce the ingress of water and recover damaged concrete elements, which could present an interesting solution for durability-related distress due to ASR.

This Ph.D. project focuses on detailed laboratory investigations aiming first to understand the self-healing process of concrete (i.e., by the natural or engineered process). Then, its further influence on ASR-induced expansion and deterioration, either applied internally or externally to the concrete. To achieve this goal, concrete mixtures presenting a wide range of binder compositions, using distinct types of chemical admixtures (e.g., crystalline self-healing), and incorporating five different types/nature of highly reactive aggregates (i.e., coarse and fine) were combined to manufactured concrete specimens in the laboratory. Otherwise, in aging specimens, concrete samples were designed only with GU-cement as the binder material but incorporated two different types/nature of highly reactive aggregates. Then, the samples were exposed to ASR-induced development until they reached pre-determined expansion levels, in which a wide range of sealers and coating materials were applied on the surface of the affected specimens. Mechanical (i.e., stiffness damage test, modulus of elasticity, micro indentation, shear and compressive strengths) and microscopic (damage rating index and scanning electron microscopy) tests were performed on samples at different ages (up to two years of accelerated ASR development).

The results show that besides changing AAR-kinetics, the different binder compositions or the chemical admixtures could modify the distress mechanism due to AAR. The addition of crystalline

healing agents or their combination with SCMs in concrete not only delayed the development of inner damage but significantly lowered the compressive strength loss at equivalent expansion amplitudes than control specimens. Moreover, the combination of different binder materials modified the chemical and mechanical properties of the ASR-gel, changing its swelling properties and the further damage development in concrete. On the other hand, the wide range of surface treatments used were not able to alter ASR distress mechanism; yet, they changed ASR-kinetics. Moreover, their effectiveness to slower the reaction shows to be significantly influenced by the damage degree to which the surface treatment is applied. Finally, a comprehensive framework enabling the optimized selection of raw materials to prevent or mitigate ASR development is proposed.

Keywords: alkali-aggregate reaction, durability of concrete, supplementary cementitious materials, self-healing of concrete, surface treatment.

Acknowledgements

First of all, I would like to thank my wife, Daiana Joice Sehnem Gomes; without you, nothing would be possible. Every day, you give me the necessary strength to keep following my dreams and moving forward. You inspire me; you are the love of life; I am speechless about you. Honestly, thank you!

I would like to mention that during my bachelor's degree at the Federal University of Parana in Brazil, I have participated in numerous career services towards a scientific career, and I became passionate about it. The experiences during that time opened doors for me to initiate my Master's under the supervision of Prof. Dr. Marcelo Medeiros. He introduced me to Prof. Dr. Leandro Sanchez, who invited me to pursue a Ph.D. at the University of Ottawa.

I would like to warmly thank my friend and research supervisor, Prof. Dr. Leandro Sanchez, who was the one that gave me the opportunity to start a new journey in my life. I was convinced that I wanted to pursue a scientific career, and I always dreamed about developing a Ph.D. study in an international institution outside my home country (Brazil!). With the support of Prof. Dr. Leandro Sanchez, this dream became achievable. During my Ph.D. program, his guidance, advice, and even great opportunities were provided through exceptional teaching. Therefore, he became more than a Professor but a close friend I will always rely on and be in touch with for advice in my career. I am very grateful for everything he has done for me.

Also, I would like to dedicate this honour in my life to special members; for sure, without them, I would not be writing this acknowledgements section. My parents, Ovidio and Neusa, my brother Robson and my sister, Jucelma, always trusted me, celebrated every achievement I have made and encouraged me to welcome challenges and always move forward in my professional career. Furthermore, they have always given me all kinds of support I needed, even if it was necessary to sacrifice their plans, priorities and dreams. Therefore, I will always be grateful for all my family and special friends, responsible for making me stronger.

Also, my deepest thanks to all colleagues from the µStructure research group, friends whose every day motivated me. Moreover, helping me in laboratory activities assisted me with the collection of materials and data, supporting me in fabricating over 4000 concrete samples during my experimental campaign. Thanks to Hugo Deda, Gustavo Macioski, Agnes Bezerra, Mayra Grazia, Gabriella Puentes,

Andisheh and Rouzbeh. Particularly, I would like to express my sincere gratitude to Luan Antunes. I have no words to express how grateful I am to have all of you supporting me during the past years. I have learned a lot from all of you guys; thank you!

Finally, I would like to recognize two important members of uOttawa at the Faculty of Civil Engineering: the technical officers (TOs) of the Materials and Structures laboratory, Drs. Muslim Majeed, and Gamal Elnabelsya. They were essential during my experimental campaign, and I would like to thank them for all the support.

Table of Contents

List of Figures

List of Tables

Foreword

This Ph.D. thesis presents and analyses the results of a comprehensive investigation performed by the author in the laboratory. The main objective of this work is to perform an in-depth evaluation to understand the self-healing of the concrete (i.e., by the natural or engineered process) and its further influence on ASR-induced expansion and deterioration: 1) in new laboratory-made concrete specimens, and 2) in aging laboratory-made concrete specimens.

This Ph.D. thesis is divided into different sections, corresponding to five scientific papers covering specific but complementary research themes. In order to make the content of this paper-based Ph.D. thesis clear to readers, section 1 displays a brief synopsis introducing the global context and structure of this study. Section 2 presents a comprehensive literature review on AAR; hence, detailed background on techniques to avoid and mitigate ASR-induced development in new and aging concrete structures is presented. In the following section (Chapter 3), the problem statement is then established, and the summary of the current research gaps in the field is displayed. Next, the study's objectives are presented, followed by a summary of the proposed global experimental program (section 4). The scope and technical contents of the five scientific papers are then presented in section 5; from sections 6 to 10, all scientific papers are displayed in sequence.

Through this Ph.D. project, I first established, in collaboration with my director, since this project was performed as part of a contractual agreement with the Natural Science and Engineering Research Council of Canada (NSERC), as part of a Collaborative Research & Development between the University of Ottawa and Kryton International. Thus, I designed the experimental program, which was further optimized with the support and recommendations of my supervisor. Then, I personally performed and/or participated in all experimental works carried out in the laboratory. Likewise, I treated and analyzed all the data used, after which I wrote the first draft of each of the five scientific papers (sections 6 to 10). The manuscripts were all reviewed by my supervisor, who made suggestions to improve the manuscript. At the time of the final submission of the thesis, papers 1, 2, 3, and 4 have been submitted for publication in scientific journals. Paper 5 is expected to be submitted in 2022.

Finally, based on the results obtained in this study, the presentation of the conclusions and recommendations of the scientific papers are given in Section 11.

Chapter One: Introduction

1.1 Synopsis

Alkali-Aggregate Reaction (AAR) is one of the most harmful distress mechanisms affecting the serviceability and durability of concrete critical infrastructure worldwide [1]. The term alkali-aggregate reaction (AAR) describes chemical reactions between certain mineral phases from the aggregates and the alkali hydroxides from the concrete pore solution [1]. Overall, AAR can be divided into two main reaction types: Alkali-Silica Reaction (ASR) and Alkali-Carbonate Reaction (ACR); they differ in the type of mineral phases and mechanisms involved [2].

From the first ASR records by Stanton in 1940 and 1942 and the ACR by Swenson in 1957, many research and knowledge were developed to understand these deterioration mechanisms [3–9]. Several approaches and recommendations, including a comprehensive variety of laboratory test procedures, have been developed to assess the potential alkali-reactivity of concrete aggregates and the efficiency of preventive measures (i.e. control of the cement & concrete alkali content, use of supplementary cementing materials - SCMs, etc.) [1,10]. A number of engineers and researchers worldwide have been trying to develop mitigation & rehabilitation measures in the laboratory and in the field in order to avoid, cease or, at least, mitigate AAR-induced development. It has been shown that expansion & distress due to AAR could be avoided or reduced (chemically) by the appropriate use of supplementary cementing materials (SCMs). Many laboratory studies have confirmed this efficiency [11,12]. However, new studies are now finding that the deterioration is only delayed and not entirely prevented [13]. Moreover, it has been recently reported that some of the current standardized test methods used to determine the efficiency of SCMs in avoiding/mitigating AAR are not entirely reliable when compared to exposed field concrete structures.

The longer the concrete field exposure time, the lower the correlation with laboratory test methods. Otherwise, once AAR starts in the field, there is no “universal” solution that should be applied in various cases, and each situation should be evaluated as “unique”. Thus, various types of treatments, especially aiming to “physically” stop/reduce the ingress of moisture and/or to provide confinement of

the affected members. Multiple types of wrapping, coating and/or waterproofing materials have been used with more or less limited success. Although a number of contradictory data were also obtained [14,15], since the presence of cracks generally provides a point of entry for moisture and other aggressive agents, their effectiveness is reduced over time, which reflects the current lack of consensus in the area. Furthermore, it has been verified that some products (i.e. crystalline admixtures, bacteria-based products, etc.), either applied in the bulk paste or externally, can provide concrete with self-healing properties, which may present an interesting "physical" solution for durability-related distress in concrete, especially AAR [15–18]. Yet, very few data are available considering the competence of such products for mitigating/rehabilitating AAR-affected concrete, and some doubts remain regarding their ability to recover concrete integrity.

In this context, this study focuses on detailed laboratory investigations aiming first to understand the self-healing of the concrete (i.e., by the natural or engineered process). Then, its further influence on ASR-induced expansion and deterioration, either applied internally or externally to the concre.

1.2 Research Objectives

Researchers are constantly developing new materials and techniques to be applied in the concrete industry to lessen onerous human interventions in ageing concrete structures. Yet, these findings are in constant demand of evaluation and to verify their appraisal to maintain the concrete elements at "safe" working conditions and "free" from durability-related problems. Moreover, several techniques, supplementary cementing materials, chemical admixtures, and surface treatments have been used in the past, aiming to assess, prevent, and mitigate ASR development in the field. Although promising results have been obtained, there is a frequent need for improvement and optimization on materials without losing concrete performance. Thus, this PhD thesis is designed to meet the following objectives:

- Evaluate the combination of different types of supplementary cementing materials (SCMs) and crystalline admixtures to enhance the healing properties of concrete and prevent and/or mitigate (i.e., physically, chemically or both) concrete deterioration caused by ASR.

- Evaluate different surface treatments and techniques (i.e., water repellent, rigid coating based, lithium-based products, cementitious based systems with self-healing products, etc.) to stop, delay and/or mitigate ASR development in its initial, moderate, and advanced phases.

In order to do so, an extensive investigation program was developed and implemented in the laboratory, which involved the manufacturing and testing of a large number of concrete cylinders made from concrete mixtures with different raw materials, chemical admixtures, engineered triggering self-healing agents, coating and sealers. Finally, qualitative frameworks are proposed to optimize the selection of raw materials and/or surface treatment towards the prevention and/or mitigation of ASR in concrete.

This Ph.D. thesis presents and analyses the results of the investigation program mentioned above. It is divided into different sections, corresponding to five scientific papers covering specific but complementary research themes. In order to make the content of this paper-based this Ph.D. thesis clear to readers, section 1 displays a brief synopsis introducing the global context and structure of this study. On the other hand, section 2 displays a comprehensive literature review on AAR; furthermore, a detailed background on techniques to avoid and mitigate the development of alkali-aggregate reaction in new and ageing concrete structures. In following section (Chapter 3), a problem statement is then established and a summary of the current research gaps in the field is displayed. Next, the objectives of the study are presented, followed by a summary of the proposed global experimental program (section 4). Next, a summary of the scope and technical content of the five scientific papers is displayed (section 5). From section 6 to section 10 all scientific papers are presented. Finally, the presentation of the conclusions and recommendations of the scientific papers are given (Section 11).

1.3 References

[1] B. Fournier, M.-A. Bérubé, Alkali-aggregate reaction in concrete: a review of basic concepts and engineering implications, Can. J. Civ. Eng. 27 (2000) 167–191. doi:10.1139/cjce-27-2-167.

[2] M. Beyene, A. Snyder, R.J. Lee, M. Blaszkiewicz, Alkali Silica Reaction (ASR) as a root cause

of distress in a concrete made from Alkali Carbonate Reaction (ACR) potentially susceptible aggregates, Cem. Concr. Res. 51 (2013) 85–95. doi:10.1016/j.cemconres.2013.04.014.

[3] J.E. Gillott, C.A. Rogers, The behavior of silicocarbonatite aggregates from the Montreal area, Cem. Concr. Res. 33 (2003) 471–480. doi:10.1016/S0008-8846(02)00956-0.

[4] P. Štukovnik, T. Prinčič, R.S. Pejovnik, V. Bokan Bosiljkov, Alkali-carbonate reaction in concrete and its implications for a high rate of long-term compressive strength increase, Constr. Build. Mater. 50 (2014) 699–709. doi:10.1016/j.conbuildmat.2013.10.007.

[5] S. Diamond, Alkali silica reactions - Some paradoxes, Cem. Concr. Compos. 19 (1997) 391–401. doi:10.1016/s0958-9465(97)00004-8.

[6] L. Tong, M. Tang, Correlation between reaction and expansion of alkali-carbonate reaction, Cem. Concr. Res. 25 (1995) 470–476. doi:10.1016/0008-8846(95)00034-A.

[7] L.F.M. Sanchez, B. Fournier, M. Jolin, J. Bastien, Evaluation of the stiffness damage test (SDT) as a tool for assessing damage in concrete due to ASR: Test loading and output responses for concretes incorporating fine or coarse reactive aggregates, Cem. Concr. Res. 56 (2014) 213–229. doi:10.1016/j.cemconres.2013.11.003.

[8] L.F.M. Sanchez, B. Fournier, M. Jolin, M.A.B. Bedoya, J. Bastien, J. Duchesne, Use of Damage Rating Index to quantify alkali-silica reaction damage in concrete: Fine versus coarse aggregate, ACI Mater. J. 113 (2016) 395–407. doi:10.14359/51688983.

[9] L.F.M. Sanchez, B. Fournier, M. Jolin, D. Mitchell, J. Bastien, Overall assessment of Alkali-Aggregate Reaction (AAR) in concretes presenting different strengths and incorporating a wide range of reactive aggregate types and natures, Cem. Concr. Res. 93 (2017) 17–31. doi:10.1016/j.cemconres.2016.12.001.

[10] L. Sanchez, Contribution to the assessment of damage in aging concrete infrastructures affected by alkali-aggregate reaction, UNIVERSITE LAVAL, 2014.

[11] M.H. Shehata, M.D.A. Thomas, Use of ternary blends containing silica fume and fly ash to suppress expansion due to alkali-silica reaction in concrete, Cem. Concr. Res. 32 (2002) 341–

349. doi:10.1016/S0008-8846(01)00680-9.

[12] M. Thomas, The effect of supplementary cementing materials on alkali-silica reaction: A review, Cem. Concr. Res. 41 (2011) 1224–1231. doi:10.1016/j.cemconres.2010.11.003.

[13] B. Fournier, R. Chevrier, A. Bilodeau, P.P.C. Nkinamubanzi, N. Bouzoubaa, R. Chevrier, Comparative field and laboratory investigations on the use of supplementary cementing materials (SCMs) to control alkali-silica reaction (ASR) in concrete, in: 15th Int. Conf. Alkali-Aggregate React., Bernardes, H.M & Hasparyk, N.P., São Paulo, 2016.

[14] N. Bérubé, N. Smaoui, B. Fournier, B. Bissonnette, B. Durand, Evaluation of the expansion attained to date by concrete affected by alkali-silica reaction. Part III: Application to existing structures, Can. J. Civ. Eng. 32 (2005) 463.

[15] F. Rajabipour, E. Giannini, C. Dunant, J.H. Ideker, M.D.A. Thomas, Alkali-silica reaction: Current understanding of the reaction mechanisms and the knowledge gaps, Cem. Concr. Res. 76 (2015) 130–146. doi:10.1016/j.cemconres.2015.05.024.

[16] L.L. Kan, H.S. Shi, A.R. Sakulich, V.C. Li, Self-healing characterization of engineered cementitious composite materials, ACI Mater. J. 107 (2010) 617–624. doi:10.14359/51664049.

[17] P. Escoffres, C. Desmettre, J.P. Charron, Effect of a crystalline admixture on the self-healing capability of high-performance fiber reinforced concretes in service conditions, Constr. Build. Mater. 173 (2018) 763–774. doi:10.1016/j.conbuildmat.2018.04.003.

[18] P. Azarsa, R. Gupta, A. Biparva, Assessment of self-healing and durability parameters of concretes incorporating crystalline admixtures and Portland Limestone Cement, Cem. Concr. Compos. 99 (2019) 17–31. doi:10.1016/j.cemconcomp.2019.02.017.

2.1 Introduction

Alkali-aggregate reaction (AAR) is a chemical reaction that induces internal swelling and distress in affected concrete [1,2]. Moreover, it is a very complex anisotropic reaction, which is influenced by several parameters, such as temperature, alkali loading, type and nature/mineralogy of aggregates, presence of moisture, stress-state, etc. [3–6]. The first recorded cases of AAR are dated from the 1940s in California (USA); afterwards, many cases have been identified around the world. Nowadays, this deterioration mechanism is recognized as one of the most harmful processes affecting concrete structures' durability worldwide [1,5].

Overall, AAR can be divided into two main reaction types: Alkali-Silica Reaction (ASR) and Alkali-Carbonate Reaction (ACR). The most common, ASR, is conventionally defined as a chemical reaction between the alkali hydroxides (i.e., Na^+, K^+, OH^-) and metastable silica mineral forms present in both natural and synthetic aggregates [1,2,7]. The reaction generates a secondary product (the so-called *ASR-gel*) that induces expansive pressures within the reacting aggregate material(s) and the adjacent cement paste while moisture uptake [8]. Thus, causing microcracking, loss of material integrity (mechanical/durability), and, in some cases, functionality in the affected structure [9]. On the other hand, ACR is a much less common concrete distress whose mechanism is still mostly unknown. ACR is viewed by many as a reaction that occurs between alkali hydroxides and certain types of dolomitic limestones [2,3]. However, the threshold between ACR and ASR is not clear in many studies. It is generally agreed that ACR is accompanied by the process of dedolomitization and formation of calcite and brucite [10]. This reaction reduces the volume of solids by approximately 13% [10]; therefore, induced expansion is attributed to a parallel mechanism. Some authors [11,12] considered ACR a form of ASR, while others believe that ACR follows a completely different distress mechanism [2,3].

The most effective and easy way to prevent ASR is avoiding reactive aggregates; however, this is not always possible. Despite that, any preventive strategies/measures seeking to control at least one of the conditioning factors necessary for ASR occurrence are desirable.

2.2 Conditions for AAR development

AAR-induced expansion and damage in concrete members is quite heterogeneous and depends upon several parameters such as the exposed conditions, type and reactivity of the aggregates, the overall concrete mixture characteristics, temperature and humidity conditions, and mechanical confinement and restraints [2]. In other words, three conditions are simultaneously necessary for the development of AAR in a concrete [13,14]:

- Presence of reactive aggregates.
- High concentration of alkali hydroxides (*NaOH, KOH*) in the interstitial solution.
- High humidity conditions.

2.3 AAR-induced expansion and damage

AAR damage development is often directly correlated to the level of expansion triggered by the concrete under this physicochemical mechanism. Yet, important progress has been made in the last decades to better understand and explain the mechanical and microscopical distress development due to AAR in concrete. As widely studied by Sanchez et al. [15,16], at the beginning of the physicochemical reaction (i.e. low expansion levels up to 0.05%), it has been found that ASR-induced cracks are mainly generated within the aggregate particles. For moderate expansion levels (i.e., ± 0.12%), new cracks are still developed within the aggregate particles; yet, the pre-existing cracks keep growing in length and width, with some cracks reaching the cement paste. In higher expansion levels (i.e., ± 0.20%), most of the previously generated cracks may already be found in the cement paste. Furthermore, from this stage, it seems that due to the "minimum energy law," it is easier for ASR-induced expansion to keep increasing pre-existing cracks than generating new ones. Finally, for very high expansion levels (≥ 0.30%), the cracks previously formed throughout the whole physicochemical process connect to each other in the cement paste, which directly impacts the mechanical properties of the affected concrete, especially its compressive strength. Figure 2.1 illustrates the qualitative damage model described above [15,16].

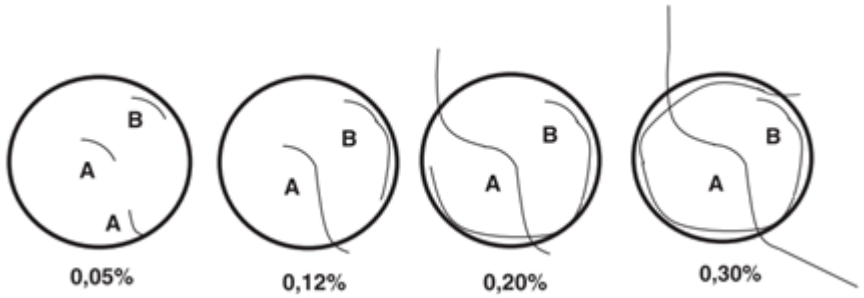

Figure 2.1: Qualitative damage model based on distinct levels of expansion [16] (*reproduced with permission of Elsevier*).

ACR-induced expansion and damage were different from ASR, at least in its microscopic damage features [9]. Furthermore, although there is no model proposed to explain ACR-crack pattern development (i.e. generation and propagation), it has been verified that very few cracks are found within the aggregate particles. In contrast, essential cracks are observed in the cement paste from the beginning of the physicochemical process. Moreover, minimal amounts of reaction products are observed, even at high expansion levels. Therefore, from an engineering and performance point of view, ACR should be considered a different mechanism than ASR, causing a distinct impact on the mechanical response of affected materials [8,9,17].

2.4 AAR influence on the mechanical properties of affected concrete structures

AAR damage development is usually directly related to the degree of induced expansion caused by this physicochemical mechanism [9]. Although conventional mechanical testing (i.e. compressive and tensile strengths, modulus of elasticity, etc.) are often used to evaluate the mechanical properties of AAR-affected concrete, a multi-level approach through the use of advanced microscopic and mechanical techniques was found to be extremely important to understand and explain AAR-induced damage development [9,16,18].

AAR *microscopic/macroscopic* distress degree and features depend upon the type and reactivity of the aggregates, the amount of alkalis, the temperature, relative humidity and confinement (i.e. reinforcement ratio, etc.) conditions of a given structure/structural member under analysis [9,18,19]. Literature data show that the stiffness (i.e. modulus of elasticity) and tensile strengths are the most

influenced mechanical properties of AAR-deteriorated concrete [9]. Furthermore, the compressive and shear strength seem to be less affected, although some contradictory results are found, especially in shear [17,20,21].

Concrete affected by AAR with expansion levels lower than 0.10% can generally still efficiently withstand service stresses; however, once the expansion becomes more significant, a complete structural evaluation should be performed [22–24]. It has been found that the compressive strength is a mechanical property that is not considerably influenced by AAR, at least in its early stages. Significant reductions in compressive strength are only observed for high and very high expansion levels (i.e. > 0.20%) as by [9,24,25], which disables its use for diagnostic purposes. Thus, compressive strength determinations on cores extracted from aging concrete infrastructure should be only used for determining the actual and residual strength of the material and not for assessing AAR damage degree and development.

Tensile strength is a mechanical property that is not directly used for designing reinforced concrete structures and is commonly adopted as being 10% of the material's compressive strength. However, past results demonstrate that the tensile strength is much more affected by internal swelling reaction mechanisms such as AAR than the compressive strength [9,25–27]. Moreover, it has been demonstrated that losses in tensile strength of AAR-affected concrete may vary up to 70%, even at low to moderate expansion developments [9]. However, very likely due to the test conditions (i.e. pure tension governed by fracture mechanics), overall tensile testing procedures seem not to be able to distinguish different damage scenarios beyond “moderate” damage degrees [9].

Shear strength in concrete is a property governed by tension and compression forces. Once cracked (and concrete will always present a certain amount of inner cracks, flaws, etc.), concrete may transfer shear forces across the cracks through two distinct mechanisms: a) dowel effect and; b) shear friction [28]. De Souza et al. [29] evaluated AAR-induced expansion and damage on the direct shear strength of affected concrete and found that the AAR significantly influences the direct shear strength of affected concrete as a function of its development. Moreover, the impact of the AAR on the shear strength was more significant for low (i.e., 0.05%) and moderate (i.e., 0.12%) expansions.

The overall stiffness of ordinary concrete is primarily governed by the mechanical properties of the aggregates, especially the coarse aggregate [30]. Therefore, this phenomenon is likely responsible for the significant decrease in AAR-affected concrete's modulus of elasticity (ME). Results demonstrate that ME losses can yield values up to 30% at low expansion amplitudes and up to 65% at higher levels. Moreover, although these values widely vary from different types of reactive aggregates, similar reduction trends were found in function of the expansion levels [9,18,19].

2.5 Tools and techniques for AAR assessment

2.5.1 Evaluation of aggregate reactivity

Among the various test procedures currently used to identify the potential reactivity of aggregates in concrete, one may mention the accelerated mortar bar test - AMBT (ASTM C1260/CSA A23.2-25A), the concrete prism test (ASTM C1293/ CSA A23.2-14A), petrographic analysis (ASTM C295/CSA A23.2-15A) and chemical test for detecting potential ACR reactivity (ASTM C586). Accelerated mortar bar test (i.e., CSA A23.2-25A, ASTM C1260) allows the assessment of ASR potential reactivity of coarse or fine aggregates within 16 days. After moulding and curing the mortar bars, the samples are soaked into a 1M NaOH solution at 80 ºC. Although this method can provide an interesting fast screening of ASR potential reactivity, it has been shown that false negatives and false positives can be found due to the severe conditions of exposure of mortars [31]. Moreover, there are criticisms regarding the use of SCMs as the exposure period in the test is too short to allow significant pozzolanic reactions [1,31–34].

Furthermore, to analyze other potential products for ASR mitigation, such as lithium, this method may present flaws compared to the behaviour of a concrete element in the field [31,35]. Moreover, the AMBT should not be used for rejecting aggregates; further testing using the Concrete Prism Test (CSA A23.2-14A or ASTM C 1293) is required for aggregates exceeding the proposed expansion limit. Yet, aggregates able to develop ACR may present false negatives using ASTM C1260/CSA A23.2-25A.

A relatively rapid indication of expansion reactivity for ACR can be performed according to ASTM C 586, which is an effective tool for tracking reactive carbonate and/or dolomitic aggregates. The studied rock samples (cylinders or prisms) are immersed in *1N NaOH* solution, and length changes are

measured at specified ages. Expansion equal to or greater than 0.10% at 28 days of exposure is indicative of high reactivity.

2.6 Techniques to evaluate damage in AAR affected concrete

2.6.1 Stiffness Damage Test (SDT)

The SDT was first developed by Walsh (1965) for assessing rock specimens [36], being afterwards somewhat modified and adapted for concrete by [37], [38] and [39]. Sanchez et al. [8,18,40] performed comprehensive research (i.e. using a wide variety of concrete strengths and reactive aggregate types) on the use of SDT for assessing damage in concrete affected by AAR and also by other internal swelling reactions (ISR). Details on the procedure developments and specific/practical considerations on its application as a diagnostic tool can be found in [8,18,40]. Briefly, after careful evaluation of the test outcomes, it was verified that the SDT needs to be performed at 40% of the material's compressive strength. Moreover, the method was found quite promising for appraising AAR (and ISR) damage in concrete, especially when indices are used as the test outcomes, namely *Stiffness Damage Index (SDI)* and *Plastic Deformation Index (PDI)*, which represent respectively the ratio of dissipated energy/plastic deformation to the total energy/deformation implemented over the five loading cycles in the system (Figure 2.2). Finally, following the works by Chrisp and co-workers [38], it was confirmed that the *Non-Linearity Index* (NLI; Sec 1/Sec 2 in the first cycle and the average Sec1/Sec2 value of the last four cycles – Figure 2.2) was also an interesting outcome to be considered, especially while studying inner cracks orientation.

a)

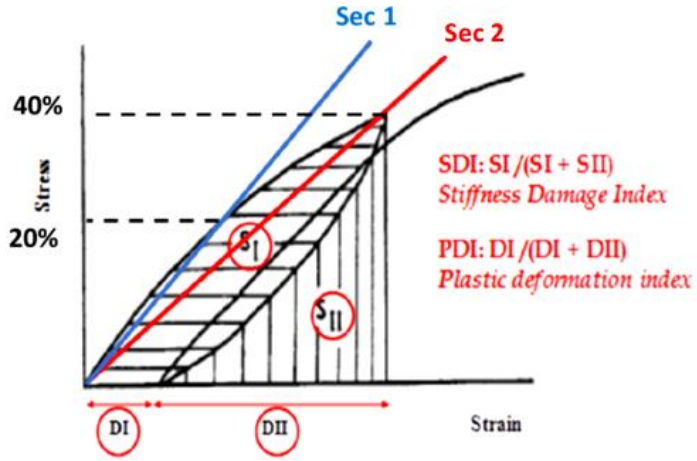

b)

Figure 2.2: a) Test setup for stiffness damage test; and b) Calculation of the stiffness damage index (SDI) and Plastic Deformation (PDI) [41] (*reproduced with permission of Elsevier*).

2.6.2 **Shear Strength**

Shear strength in concrete is a property governed by tension and compression forces. Once cracked (and concrete will always present a certain amount of inner cracks, flaws, etc.), concrete may transfer shear forces across the cracks through two distinct mechanisms: a) dowel effect and; b) shear friction [28]. A number of test methods have been developed over the years to evaluate the direct shear capacity and shear friction of reinforced and unreinforced concrete [42,43]. Barr & Hasso (1986) performed a comparative study on different setups to evaluate the direct shear of plain concrete. One of the most promising setups used was the modified cylinder specimen (i.e. double notched cylindrical specimen) [44].

De Souza et al. [29] evaluated AAR-induced expansion and damage on the direct shear strength of affected concrete and developed a simple yet reliable setup to assess AAR progress in the laboratory (Figure 2.3a). The authors found that the AAR significantly influences the direct shear strength of affected concrete's development. Moreover, the impact of the AAR on the shear strength was more significant for low (0.05%) and moderate (0.12%) expansions (Figure 2.3b). The proposed shear setup showed to be a fast and promising tool for detecting AAR-induced expansion and damage in the laboratory. Yet, only AAR-affected laboratory samples fabricated and monitored under accelerated and free expansion conditions were tested in this program [29].

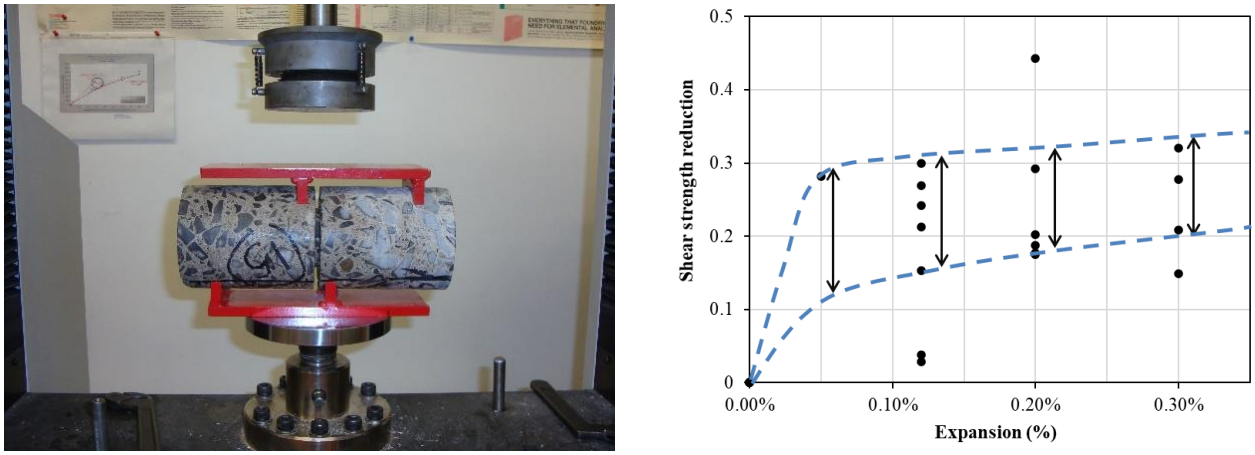

a) b)

Figure 2.3: a) Test setup for direct shear strength test [17]; and b) global shear strength loss of AAR affected concrete specimens [17] (*reproduced with permission of Elsevier*).

2.6.3 **Damage Rating Index (DRI)**

The DRI is a semi-quantitative microscopic procedure performed using a stereomicroscope (about 15-16x magnification) where the petrographic distress features associated with AAR (or ISR) are counted through a 1 cm^2 grid drawn on the surface of polished concrete sections [45]. The number of counts corresponding to each petrographic feature is then multiplied by a set of weighing factors whose purpose is to balance their relative importance towards the damage mechanism considered. The final DRI value is normalized to an area of 100 cm^2; overall, the higher the DRI number, the greater the deterioration of affected concrete [46–48]. Thus, the DRI is a complementary petrographic tool aiming to quantify the "damage degree" between different members from an affected structure or as a function of time within a specific concrete member.

A complete review of the DRI development and specific considerations on its application are given in Sanchez et al. [46–48]. The authors used the DRI to evaluate AAR distress with a wide range of reactive aggregates, different concrete strengths (25-45 MPa) and expansion levels (0.05% to 0.30%). It was found that the DRI is a powerful tool to detect AAR damage/progress in concrete whatever the aggregate type and concrete strength used, mainly when the aggregate particles are analyzed down to 1 mm. Moreover, [46–48] proposed the so-called "extended DRI version" in which the microscopic distress features could be presented in absolute values (counts) and relative (%), disregarding the

weighting factors, giving a more comprehensive assessment of the damaged concrete specimens. The damage features that could be found in the DRI assessment are presented in Figure 2.4a with their corresponding weighting factors; some of the damage features are observed in Figure 2.4b.

Petrographic features	Weighting factors
Closed cracks in aggregates (CCA)	0.25
Opened cracks in aggregates (OCA)	2
Opened crack with reaction product in aggregate (OCAG)	2
Coarse aggregate de-bonded (CAD)	3
Disaggregate/corroded aggregate particle (DAP)	2
Cracks in cement paste (CCP)	3
Cracks with reaction product in cement paste (CCPG)	3

a)

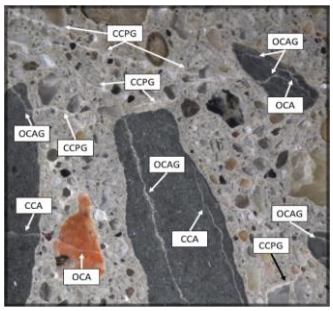

b)

Figure 2.4: Damage Rating Index: a) Current weighting factors as per [49] **and b) Micrograph illustrating a 1cm2 section where some of the petrographic features listed in A can be observed and identified.**

2.7 Preventive measures for AAR in concrete

The most common measures to minimize the risk of harmful expansion and cracking in new concrete structures due to alkali-aggregate reaction is CSA A23.2-14A or ASTM C 1293. These methods are believed to yield results close to the expected in the field [50]. Some variables are fixed for this test, such as the amount of cement per cubic meter (420 $\pm$ 10 kg/m^3), unit volume of coarse aggregate (0.70 $\pm$ 0.02), water/cement ratio (between 0.42 and 0.45) and alkali content of 1.25% by cement mass (equivalent to 5.25 kg/m^3 of concrete). The aggregates (or a combination of reactive aggregates and SCMs) are considered reactive if the expansion in 1 year of testing is equal to or greater than 0.04% (for exposure to a temperature of 38 + 2ºC and 100% RH). The main disadvantage of them is the period of testing, which is sometimes considered too long. Moreover, it has been suggested that in laboratory conditions, the expansions did not directly confirm the field performance [51]. Thomas et al. [51] demonstrated that greater levels of alkalis are required for the laboratory samples to produce expansion compared with field-exposed blocks. Thus, the suitability of present performance tests is questionable due to alkali-leaching problems [1].

Moreover, for designing concrete and structures that may be susceptible to AAR, CSA.A23.27A provides appropriate preventive measures concrete proportioning based on the degree of alkali-silica

reactivity of aggregates, the risk level associated with structure size and environment and the level of prevention related to service life requirements. The innovation of the CSA.A23.27A, unique in global scope, is that it presents a step-by-step decision-making procedure according to variables that can influence the development of AAR and that could be present in the application of the structure, making it easier to produce concrete that will present greater resistance to AAR.

2.8 Avoiding and Mitigating AAR in concrete structures

The most effective and easy way to prevent AAR is avoiding reactive aggregates; however, this is not always possible. Over the years, several approaches and recommendations, including a comprehensive variety of laboratory test procedures, have been developed around the world to assess the potential alkali-reactivity of concrete aggregates and the efficiency of preventive measures (i.e. control of the cement & concrete alkali content, use of SCMs, etc.) [2,8]. Therefore, the development of mitigation strategies (even palliative) to extend the service life of concrete structures needs to be investigated. Including the use of low alkali types of cement, supplementary cementitious materials, fillers, chemical admixtures such as lithium nitrate, sealants (silane/siloxane products), self-healing products, etc.

2.8.1 Minimizing alkalis through cement selection

The primary source of alkalis in concrete is Portland cement (PC); they are derived from the clay components present in the raw materials and coal used in the cement manufacturing process. Sodium and potassium portions are generally interconnected in the clicker main components C_2S, C_3S, C_3A and C_4AF [52]. Although, other constituents (e.g., supplementary cementing materials, aggregates, and admixtures) may also contribute to the total amount of alkalis.

Significant amounts of alkalis in the cement are favourable to maintain the pH of the concrete pore solution at higher levels (i.e., in between 12.6 and 13.1). Moreover, higher pH contributes to the chemical stability of the hydrated Portland cement products (i.e., *C-S-H*, AFm, etc.); besides, protecting reinforced concrete structures against corrosion [53–56]. On the other hand, high *pH* can contribute negatively to the development of AAR when combined with reactive aggregates and high R.H. [2,57,58].

In order to assess the total content of available alkalis present in cement or concrete, it has become a standard practice to express the alkali content in terms of "sodium oxide equivalent (expressed as $Na_2O_{eq.}$)" as per Equation 2.1.

$$Na_2O_{eq}(\%) = Na_2O + 0.658 \cdot K_2O$$

Equation 2.1

It is well known that AAR kinetics is generally accelerated by increasing the total alkali content (i.e. Na_2O_{eq}). Laboratory and field data show from several studies that Portland cement containing more than 0.6% of Na_2O_{eq} can trigger AAR to develop significant deterioration on concrete [1]. However, the threshold necessary to initiate and sustain deleterious AAR varies from one aggregate to another, according to their mineralogy (Figure 2.5) [2].

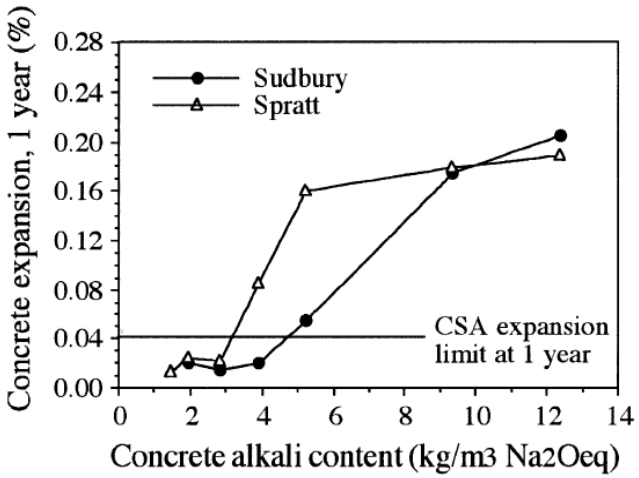

Figure 2.5: One-year CPT test as per ASTM C 1293 for concrete mixtures incorporating two reactive aggregates (Spratt limestone and Sudbury gravel) and different alkali contents [2] (*reproduced with permission of NRC Research Press*).

CSA A23.27A recommends limiting the alkali contribution from Portland cement based on the potential reactivity of the concrete mixture to develop AAR in the field. The standard presents those limits as Na_2O_{eq} kg/m³ of concrete, for example: < 3.0 kg/m³ for mild prevention; < 2.4 kg/m³ for moderate prevention; < 1.8 kg/m³ for strong prevention; and < 1.2 kg/m³ for very strong prevention.

Furthermore, concrete mixtures designed with similar Na_2O_{eq} content, but different *K/Na* ratios, can considerably change the AAR kinetics in accelerated laboratory tests [59]. Indicating that, in some cases, Na_2O_{eq} as the only parameter to assess the potential reactivity of concrete mixtures might be misleading in certain cases. It has been suggested that K and Na ions behave similarly in the ASR reaction, but the reaction rate is higher with K than with Na [60]. Moreover, it is possible to obtain misleading conclusions if two types of cement having equal sodium oxide equivalent. Still, extreme variations of Na_2O and K_2O levels are assumed to act similarly in a performance test [1].

On the other hand, the influence of the chemical composition of the cement in the AAR development is not just limited to the alkali content (Na^+ and K^+). Several studies [61–63] suggest that the CaO content is a crucial factor in AAR development. The swelling capacity of ASR-gel is related to the calcium ions present in the ASR-gel, which depends on the amount of Ca^{2+} available in the pore solution [64]. Microscopy and chemical analysis show that the reaction product within aggregates has crystalline properties with uniform composition, rich in Si ions [65]. However, when the damage caused by AAR development reaches the cement paste, the ASR-gel becomes richer in calcium with time. The reaction product takes up calcium from the cement paste and changes its structure from crystalline to amorphous, enhancing its swelling capacity and releasing alkalis to the concrete pore solution [65,66]. This alkali recycling during ASR reveals that the reaction may continue until all the reactive silica is transformed into ASR-gel.

Moreover, the amount of *portlandite* in concrete is controlled by the mineralogical composition of the clinker, which means that cement with a higher ratio of C_3S/C_2S will produce more $Ca(OH)_2$ [52]; therefore, cement with characteristics of high initial strength (high C_3S content) may favour degradation by AAR.

2.8.2 **Limiting moisture**

It is well known in the literature that relative humidity (R.H.) impacts significantly on AAR-kinetics and damage since high R.H. is one of the key requirements for AAR occurrence. It is generally agreed that the relative humidity should be greater than 80% to cause significant AAR development and damage in the concrete [2,19,67]. However, at a given alkali loading, the R.H. threshold is dependent on temperature and the reactive form of silica present within the aggregate [68]. Water plays two

critical roles in AAR reaction: first, as transport medium of the ions involved in AAR; and second, as a reactant (water is included in the amorphous gel formed). Figure 2.6 shows that higher external relative humidity accelerates ASR kinetics; moreover, indicating that R.H. above 95% is the worst-case scenario for AAR development. Furthermore, the results obtained at 96% humidity by [67] were slightly higher than those gathered at 100%, and the final expansion obtained on samples exposed to 96% R.H. is about 4.12 times higher when compared to 59% R.H.

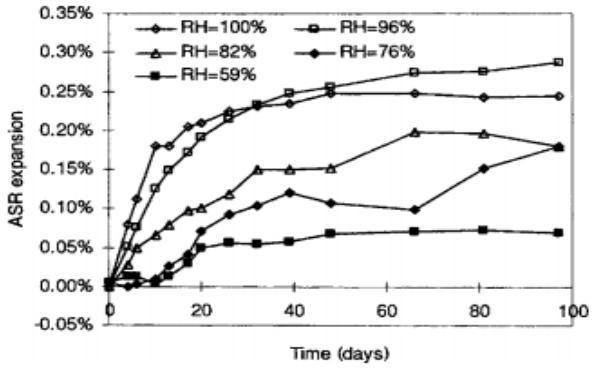

Figure 2.6: ASR swelling versus time for different constant external relative humidity [67] **(*reproduced with permission of ASCE*).**

Consequently, the porosity and permeability of the concrete have an essential role in the development of the AAR [70]. Higher porosity and permeability enable the easy transport of ions through the matrix. On the other hand, there will be more space to accommodate reaction products and delay the expansion and cracking initiation in the cement paste [71,72]. Yet, the use of finely ground materials, whether inert or reactive, will enhance the matrix microstructure, refining the porosity and permeability. In other words, besides the chemical effect of the SCMs [58,73,74], these materials can act simply as a physical barrier to water movement [75,76].

Hydrophobic impregnations and coatings have been used in various forms in the construction industry to help to prevent water and chloride ingress, and their benefits are well documented [77–82]. Breathable coating and sealants composed of siloxanes or silanes have shown promising results in reducing ASR-induced expansion [83,84]. Evidences from numerous studies demonstrate that the application of silanes significantly reduces water uptake [85,86], lowering ASR-induced expansion values by 40% [87] to 60% [88]. The removal of internal moisture prevents or slows the ASR-induced

expansion, and the water-repelling ability of silane prevents additional moisture from reaching the gel [89]. However, their performance is affected by surface imperfections, wetting and drying cycles, application technique and precision, surface preparation, application rates and local environmental conditions at the time of application [90]. In general, silane treatments are more effective if pre-wetting periods are lengthened [87]. Moreover, to effectively mitigate ASR-induced development, it has been demonstrated that extended pre-curing periods will permit the formation of solid oxygen bridging bonds between silane molecules and the substrate, which provides a surface with stable hydrophobic character [88].

2.8.3 **Influence of supplementary cementitious materials (SCMs) on AAR**

Preventive measures, including the use of supplementary cementing materials (SCMs) such as fly ash (FA) [74,91,92], granulated blast-furnace slag (GBFS) [93,94], silica fume (SF) [95,96] and metakaolin [92,97,98] have been widely studied to decrease the likelihood of ASR. SCMs can control ASR-induced development mainly by their capacity of reducing the alkalinity available in the system, thus limiting their availability to react with the aggregates [1,74,99]. Furthermore, it has been reported that the ability of SCMs to bind alkalis and hydroxyls ions seems to be strongly related to the CaO/SiO_2 ratio of the SCMs; i.e., the higher this ratio, the lower its binding capacity [99] (Figure 2.7).

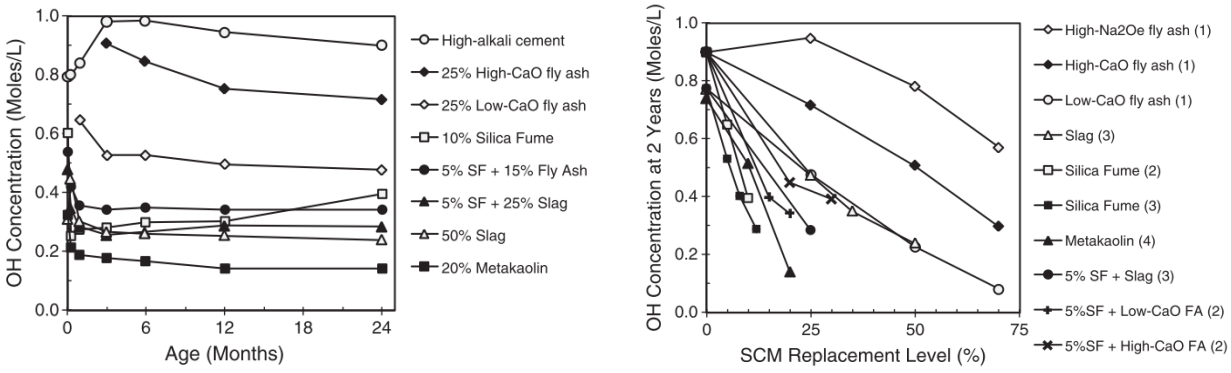

a) b)

Figure 2.7: Variation on the OH^- concentration in the pore solution: a) Evolution of the pore solution in pastes containing SCM [99]**; b) Effect of SCM type and replacement level on the pore solution hydroxyl ion concentration at two years** [99] **(*reproduced with permission of Elsevier*).**

Chemically, SCMs can dilute the alkalis available from the clinker and decrease the pH of the material by consuming $Ca(OH)_2$ from the pore solution [1,74,99]. Thus, the formation of "new" C-S-H due to SCMs reaction has a greater capacity to entrap alkalis and reduce even more the pH. Furthermore, these materials can change concrete microstructure, interfering with the pore size distribution and their interconnectivity among the binder paste. This effect reduces the mobility of ions and possibly slows the reaction rate [73,74,100]. Some authors suggested that alkali-silica reaction is very similar to pozzolanic reactions [60,99]. The main difference between them is the characteristics of the resulting products (i.e., C-S-H and ASR-gel, the latter with swelling properties). Moreover, the products formed through the pozzolanic reaction are homogenously distributed throughout the binder paste instead of accumulating around reactive aggregates [1]. Yet, the vast variety of SCMs (i.e., chemical composition, morphology, crystallinity, and reactivity) brings these materials to behave differently when exposed to AAR condition, moreover, their proportion in the concrete also varies completely from one type of SCM to other.

2.8.3.1 **Fly Ash (FA)**

Fly ashes are finely divided residue resulting from the combustion of powdered coal. FA consists mainly of SiO_2 and Al_2O_3; the amount of CaO is limited but highly variable depending on the origin of the fly ash [100]. Therefore, the effectiveness of concrete made of *fly ash (FA)* against ASR depends on the overall FA properties and calcium content (i.e., class F containing less than 15% of CaO, class CL for CaO content ranging from 15% to 20%, and class CH containing more than 20% of CaO) [101]. Besides both types of FA displayed some efficiency to prevent ASR development, FA class F has demonstrated better results [99], which is likely explained by the different CaO/SiO_2 ratios of FAs. In general, the lower the CaO/SiO_2 ratio of the FA, the higher its efficiency [14] to suppress ASR.

Class F fly ashes are generally efficient in controlling expansions related to ASR. Results demonstrate that after four years of exposure to the *NaOH* solution at 80ºC, concretes containing 40% fly ash had negligible expansion levels even with the formation of ASR gel [102]. This behaviour is attributed to the low viscosity of the reaction products due to the lower available calcium content [103]. On the other hand, Class CH fly ash may be challenging to suppress AAR development [99], yet, many contradictory data were obtained in the literature. After nine years of measurement (Figure 2.8),

replacing 40% of Portland cement by FA with CaO content up to 12% decreased the expansions to lower and "safe" levels (i.e., lower than 0.04%) [14]. Whereas, using 20% of FA, the average on expansion was 0.07%. However, FA containing a higher amount of CaO (i.e., 20.7%) for both 20% and 40% of replacement levels showed expansion higher than 0.12% (Moderate expansion due to ASR). Resulting in significant mechanical losses (i.e. 20-50% stiffness loss, compressive and tensile strengths up to 20% and 40-65%, respectively) [9].

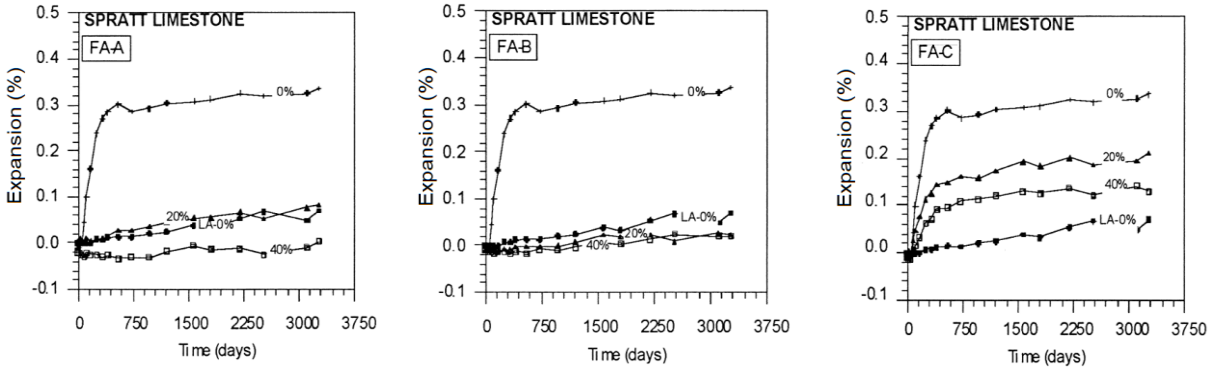

a) b) c)

Figure 2.8: Expansion of concrete prisms (CSA-A23.2-14A) made with Spratt Limestone reactive aggregate and various amounts of Fly Ash, cured at 100% RH and 38°C [14]: a) using FA with 1.87% of CaO; b) using FA with 12.00% of CaO; and, using FA with 20.70% of CaO (*reproduced with permission of Elsevier*).

2.8.3.2 **Silica Fume (SF)**

Silica fume consists nearly exclusively of SiO_2 (i.e. 85% to 99%) of very fine particle size and a relatively high pozzolanic activity. It is a by-product of the silicon and iron-silicon metal smelting process containing a high glassy-phase of silicon dioxide [105]. In general, the use of SF to mitigate ASR in concrete is recommended; yet its mechanism of mitigation is still not entirely understood [1,95]. Overall, SF particles rapidly bind alkalis (Figure 2.9), decreasing the alkalinity of the concrete pore solution [1,95]. However, at later ages, alkalis can eventually be released and re-increase alkali concentration [14,94]. In other words, SF can mitigate ASR at "safe" levels, yet longer periods of exposure can be challenging. Results have demonstrated that moderately and highly reactive aggregates combined with 7.5% to 12.5% of SF in concrete contributed to keeping expansion levels at safe levels

after ten years of exposure to ASR development. Conversely, concrete made of SF and highly reactive aggregates barely keep the expansion amplitudes under the above expansion level after 15 years of field exposure [14,106].

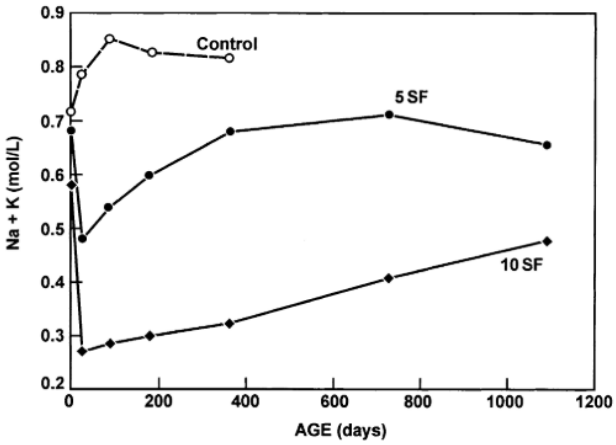

Figure 2.9: Effect of SF on the alkalinity of pore solution of pastes, represented by the sum of alkali cations in the pore solution [95] **(*reproduced with permission of Elsevier*).**

Finally, results demonstrated that the SiO_2 content of the SF plays a significant role in its effectiveness in preventing ASR occurrence [14]. By using two different types of SF (i.e., one with 94% and the other with 74% of SiO_2) at two different replacement levels (i.e., 5% and 10%) (Figure 2.10), [14] obtained that 5% of SF showed higher or similar expansion in comparison with only Portland cement as the binder material, for both types of SF. On the other hand, the authors presented that at 10% of replacement, SF significantly mitigates ASR after nine years of exposure. Moreover, the higher the SiO_2 content in the chemical composition of the SF, the higher the effectiveness of the concrete mixture to mitigate the reaction.

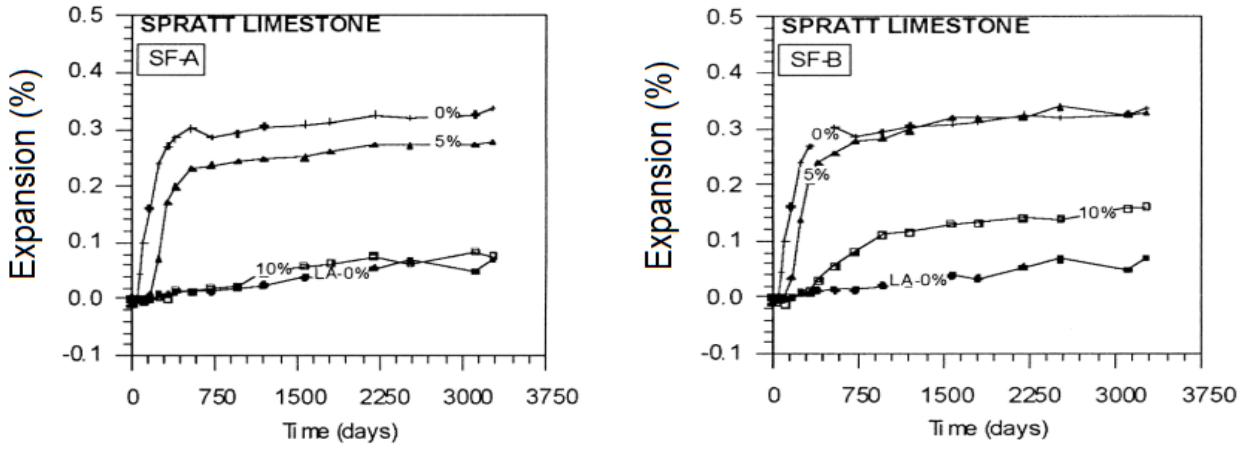

a) b)

Figure 2.10: Expansion of concrete prisms (CSA-A23.2-14A) made with two reactive aggregates and various amounts of two SF, cured at 100% RH and 38°C: a) Using SF with 94.17% of SiO_2; b) Using SF with 74.60% of SiO_2 (*reproduced with permission of Elsevier*).

2.8.3.3 **Metakaolin (MK)**

The use of highly reactive metakaolin (MK) as an SCMs has progressively increased in the construction industry during the last decades. MK is produced by calcinating kaolinite clay and is an aluminosilicate material rich in Al_2O_3 (i.e. 35% to 50% by mass). Different studies [97,107,108] have discussed the efficiency of the metakaolin (MK) to suppress ASR in concrete; yet, no threshold values have been defined. However, results suggest that mortar bars incorporating 10% MK by cement mass lessened ASR-induced expansion by about 70% [97,98], whereas 15% of PC replacement resulted in values up to 85% lower (Figure 2.11a, b and c) [107,109,110]. The mechanism of ASR mitigation by MK usage is commonly attributed to the increased aluminum content into the concrete pore solution, which is absorbed on reactive SiO_2 surfaces, slowing down its dissolution [97,107,108] to values close to zero [111]. Yet, decelerating the dissolution of reactive SiO_2 did not modify the chemical composition and morphology of the ASR-gel [97]. Furthermore, it is unlikely that the swelling potential of ASR products in cementitious materials incorporating MK is lessened [97].

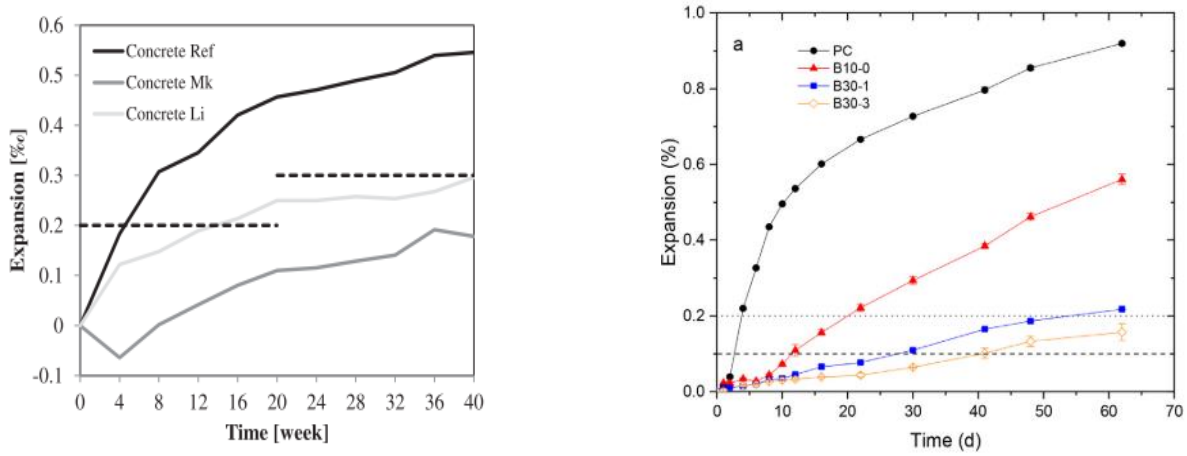

a) b)

Figure 2.11: a) Expansion of concrete Ref, Mk and Li versus time [97]**; b) ASR expansion of mortar bar specimens cement blends with substitution up to 30%** [98] **(*reproduced with permission of Elsevier*).**

2.8.3.4 Ground granulated blast-furnace slag

Compared to previously discussed SCMs, granulated blast-furnace slag (GBFS) contains significantly more CaO. GBFS is a by-product from the manufacturing of iron, is a finely ground glassy siliceous material formed when molten slag is rapidly cooled and then ground [105]. The chemical composition of GBFS is quite similar to Portland cement; yet, the extent of alkali release is much less than cement clinker. It has been discussed that GBFS as an SCM in concrete just delays the effect of ASR by temporarily modifying the gel composition [112]. At the same time, it does not significantly affect the amount and composition of the ASR-gel formed at early stages of ASR development [113]. In general, effective amounts of slag to suppress ASR development usually range from 25-50%, or more, depending on the reactivity of the aggregate and exposure conditions [114]; yet, no threshold values have been established to mitigate the ASR efficiently. Results demonstrated that replacing 50% (Figure 2.12) of PC with GBFS decreases the expansion rate to lower values than low-alkali PC concrete [14].

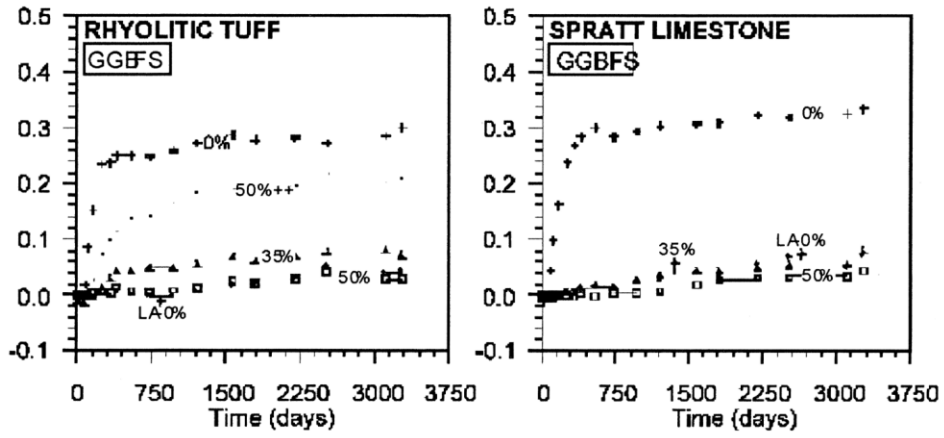

Figure 2.12: Expansion of concrete prisms (CSA-A23.2-14A) made with two reactive aggregates and various amounts of blast furnace slag, cured at 100% RH and 38°C (*reproduced with permission of Elsevier*) [14].

2.8.4 **Influence of lithium compounds on AAR development**

The use of chemical admixtures to reduce damage or delay AAR-induced development in concrete has been improving since the 1950s [115]. Although both the long-term efficiency and mechanisms of chemical admixtures in suppressing AAR have been considered for almost 50 years, the interest in their use recently increased either as admixtures for construction or as treatments of existing affected structures.

Among several products, lithium compounds show good response in modifying the reaction kinetics, as seen in recent research [97,116–119]. However, up till now, there is still a general lack of guidance and specifications for the proper use of chemical admixtures to control ASR-induced expansion due to the inconsistent outcomes and conclusions [120–122]. It has been suggested that metastable silica within the aggregate particles may react preferentially with Li ions, modifying the chemical structure of the ASR-product [120,121,123,124]. Later [125] and [63] assumed that Li ions are capable of reducing the solubility and the dissolution rate of silica. Finally, three lithium compositions have shown very promising results to mitigate ASR: lithium hydroxide, lithium carbonate and lithium nitrate. Lithium nitrate $(LiNO_3)$ was the lithium compound showing the best results in controlling ASR for the same

Li/(Na +K) ratio. Figure 2.13 shows the results obtained by [32] comparing ASR mitigation potential of admixtures by using different accelerated test methods.

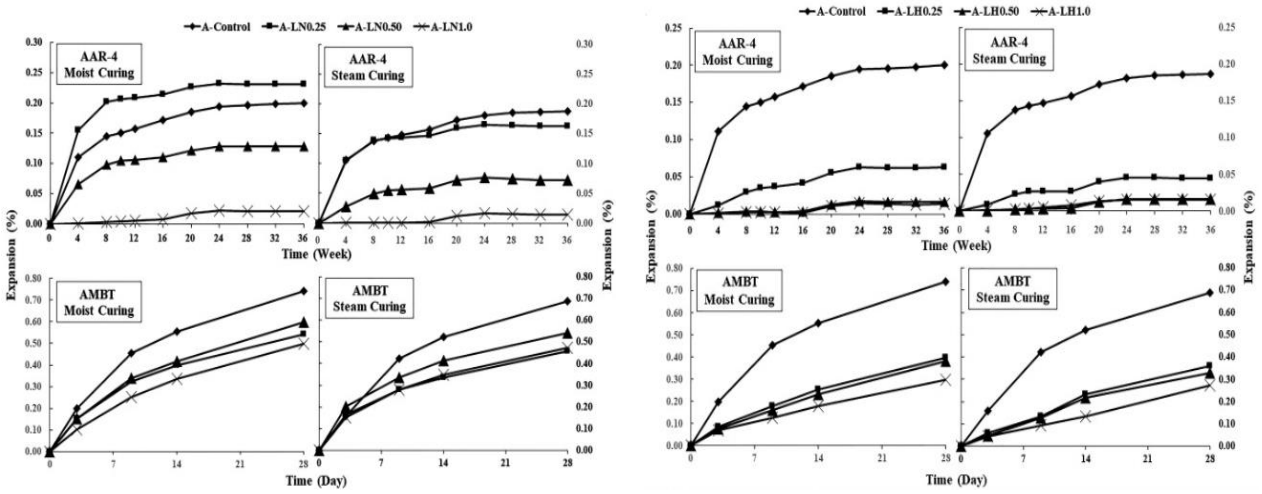

a) b)

Figure 2.13: a) Expansion curves of the Control and $LiNO_3$ containing mixtures; b) Expansion curves of the Control and LiOH containing mixtures (*reproduced with permission of Elsevier*).

Lithium nitrate stands out for good solubility and slightly modifies the pH of concrete pore solution [118,119]. Although the exact nature of the role of lithium ions in controlling ASR is still not clearly understood, several different mechanisms have been proposed. Figure 2.14 displays some of these proposed mechanisms, including: (1) formation of a physical barrier by insoluble silicon–lithium (Si–Li) reaction products [119,126,127], (2) formation of less expansive Si–Li reaction products, Li–Ca–Na–Si gel [119,127,128], and (3) increased chemical stability of reactive silica exposed to pore solution [118,119,129].

a) b)

Figure 2.14: a) Schematic diagram of a reaction system in the presence of lithium; b) SEM images of vycor glass disks immersed in alkaline solutions for 120d at 38 °C in 1N NaOH + 0.74N $LiNO_3$ + $Ca(OH)_2$, showing a matrix of ASR gel and Li–Si crystals [119] **(*reproduced with permission of Elsevier*).**

It was also reported that the mechanism of ASR mitigation using lithium could be likely explained by its ability to replace calcium in ASR gel rather than K^+ and Na^+ [118,127]. Lithium's efficiency in altering concrete swelling due to ASR depends significantly on the nature or reactivity of the aggregates used, lithium availability, and the amount of other alkalis. The minimum molar ratio between lithium and alkalis to efficiently suppress ASR generally varies between 0.67-1.20 for most of the lithium compounds studied and 0.72-0.93 for $LiNO_3$ [1,118,130].

In cases of structures that are already presenting ASR signs, Thomas *et al*. [131] recommend treatments that can be used to mitigate the reaction, such as:

- *Surface treatment*: application of the lithium solution directly on the surface of the affected concrete. The efficiency of the treatment depends on the level of deterioration of the concrete, the time when the solution is applied, and the methods used to apply the material (manual vs mechanical spraying). The solution of $LiNO_3$ is the most recommended because it presents better efficiency and a higher rate of penetration during the treatment; however, this solution must be associated with surfactants to guarantee a better percolation in the concrete [132,133];
- *Electrochemical impregnation*: a technique based on the electrochemical extraction of chloride, which involves the application of an electric field between the reinforcement and an external

electrode immersed in an electrolyte reservoir. Thus, a positive charge is applied inside the concrete in order to attract Li^+ ions to deeper regions of the member [131];

- *Vacuum impregnation*: negative pressure injection technique used to increase the penetration depth of lithium ions inside concrete affected by ASR.

Despite the research efforts and the number of publications concerning the use of lithium to mitigate ASR-induced development, contradictory results were found in the literature [116,119,124,127,130]. In general, the penetration depth of the lithium ions is limited to the first layers of the concrete, reaching depths of 5 mm to 50 mm, which significantly limits their effectiveness; thus, poor results can be found in the literature [134–137].

2.8.5 **Influence of the concrete surface treatment**

Various types of treatments, especially aiming to "physically" stop/reduce moisture ingress and/or to provide confinement of the affected members (e.g., silane/siloxane water repellents, coatings, prestress confinement, etc.) have been tested and have shown quite promising results. Hydrophobic impregnations have therefore been used in various forms in the construction industry to help to prevent water and chloride ingress, and their benefits are well documented [77–82]. Breathable sealants composed of siloxanes or silanes have shown promising results in reducing AAR-induced expansion [83,84]. Alkyl-Alkoxy-Silane is a water repellent agent, which prevents the penetration of water in the liquid state, acting indirectly in the mitigation of ASR by decreasing the internal moisture of the concrete [88,90,138].

Evidences from numerous studies demonstrate that the application of silanes significantly reduces water uptake [85,86]. However, their performance is affected by surface imperfections, wetting and drying cycles, application technique and precision, surface preparation, application rates and local environmental conditions at the time of application [90]. Silanes can penetrate into the surface layers of concrete, providing a layer that endures traffic wear for several years. The removal of internal moisture prevents or slows the ASR-induced expansion, and the water-repelling ability of silane prevents additional moisture from reaching the gel [89]. The mechanism of the silane's repellency is since

silanes react with alkalis in concrete and chemically bond water-repellent hydrocarbon molecules, thereby reducing the surface tension of concrete [87]. When the surface tension of the substrate is less than that of water, it will work as water-repellent [87,89].

Silane treatments are more effective if pre-wetting periods are lengthened. To effectively mitigate ASR-induced development, it is necessary to allow a minimum of 28 days of air curing. More extended pre-curing periods will permit the formation of strong oxygen bridging bonds between silane molecules and the substrate, which provides a surface with stable hydrophobic character [88]. However, many contradictory data were also obtained [13], reflecting the current lack of consensus in the area.

Overall, once ASR starts in the field, there is no efficient solution to mitigate the residual expansion and damage. However, it is somewhat clear that limiting moisture uptake demonstrates better results to modify the reaction kinetics. In addition, in the past decades, it has been verified that some crystalline waterproofing coating materials can provide concrete with interesting self-healing properties besides waterproofing, which may present a very interesting "physical" solution for durability-related distress in concrete [139–141].

2.9 **Improvement of the healing process of the concrete**

The costs related to human intervention in critical infrastructure have already become a significant field of interest [142,143]. Nevertheless, the implementation of continuous inspections and maintenance protocols is quite complex, especially in the case of large concrete structures, where considerable amounts of labour and funds are often required. To illustrate this situation, the U.S. Department of Transportation reports that a budget between $78 billion to $112 billion is estimated to address all structural and functional bridges' deficiencies in the United States [144]. Therefore, any preventive measures to preserve and improve the service life without onerous labour and capital requirements are highly desirable. In this regard, the development and use of cementing materials able to autogenously counteract the effects of cracking, the so-called self-healing (SH) products, became a topic of significant interest in civil engineering and concrete technology [145–148].

In the past decade, several studies have been conducted to understand the global self-healing of cement-based materials [149–151]. It is somewhat known that concrete can naturally/autogenously

self-heal cracks. However, although promising results can be observed when concrete is designed with high cement content, lower water to cement ratios and/or with supplementary cementing materials (SCMs) [152–154], autogenous healing has quite limited capacity on conventional concrete. Therefore, artificial/autonomous triggering healing agents, such as microencapsulated bacteria (MB) [155–158] or crystalline admixtures (CA) [146,159–162], have been introduced recently. Besides past studies have shown that MB and CA enhance the recovering of mechanical and durability properties of damaged concrete, the ACI committee [163] has reported that CAs are more reliable since these admixtures are hydrophilic by nature, increasing the density of the calcium silicate hydrate (CSH), and generating pore-blocking deposits resisting to water penetration. Nevertheless, both topics (i.e., naturally/autogenously and artificial/autonomous self-healing) are discussed as follows.

2.9.1 **Autogenous healing**

Autogenous crack healing in cementitious materials is a natural process, an intrinsic property of the material, and it has already been studied by many researchers [152,164–167]. The phenomenon takes place through four different main processes (Figure 2.15): a) formation of calcium carbonate ($CaCO_3$) in concrete; b) ongoing hydration of binder grains upon moisture uptake; c) swelling of cement paste; d) sedimentation of solid particles within cracks [160,168,169]. The first two are the most common autogenous healing processes; however, their efficiency significantly changes over time. At earlier ages of the concrete, continued hydration is the dominant mechanism due to the high content of unhydrated cement particles. Yet, calcium carbonate becomes the primary mechanism at later ages and more prolonged environmental exposure [169–172]. Moreover, besides being a natural process not easily controlled, autogenous healing properties can be enhanced. It has been demonstrated that pre-damaged concrete can recover, on average, 60% of its mechanical properties (i.e.., compressive strength, flexural strength and stiffness) [167,173–175]. In addition, significantly decrease concrete permeability and reduce chloride diffusivity [160,162,176] by lowering the water-to-binder (w/b) ratio and/or increasing the binder content. Yet, the later measure may raise the cost and carbon footprint of the concrete.

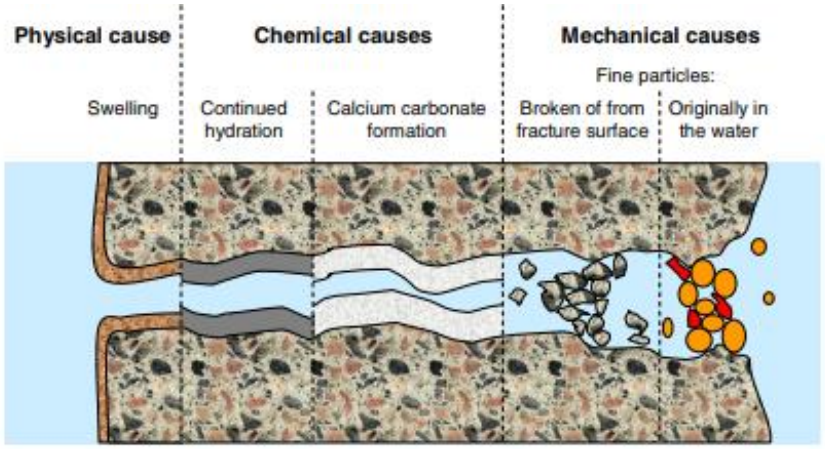

Figure 2.15: Different causes that can lead to autogenic self-healing [177]

Recently, to achieve greener concrete mixtures and further improve autogenous healing properties, several researchers [152–154,167] reported that the use of supplementary cementing materials (SCMs), partially replacing Portland cement (PC), is crucial. While the slower rate of hydration of blast furnace slag and fly ashes grains may slow early age processes of microstructure and strength developments, their capability to enhance self-healing is significantly higher than Portland cement [154]. Over time, tests on the healing capacity (1, 2, 7, 14 days, etc.) were performed in cementitious mortars incorporating different SCMs. Results show that SCMs can enhance the natural healing mechanism of cementitious materials as per Figure 2.16. Furthermore, it has been demonstrated that concrete made of a high volume of fly ash (i.e., 30% to 60% of PC's replacement) can recover 70% of the strength loss while reducing about 75% chloride diffusion after pre-cracking [152,178–181]. Moreover, combining two different techniques (e.g., selective dissolution and XRD-Rietveld analysis), Termkhajornkit et al. [180] calculated the total amount of C-S-H gel produced after 28 days of curing. The results demonstrate that replacing 50% of PC by fly ash class F had 560% more C-S-H between 28 days and 364 days; this, in turn, is an indication of later healing enhancement. Likewise, concrete made of blast furnace slag was found to heal 70% of cracks with widths until 200 µm and recover up to 80% of its compressive strength loss [154,182]. On the other hand, high volumes of SCMs may reduce the calcite precipitation process of healing [154,168,181] due to the lower amount of calcium carbonate formed in SCM-made concrete [154]. Overall, when the continued hydration is the main healing mechanism,

SCMs play an important role in the process; however, it is limited to self-seal cracks with width up to 250 µm, on average.

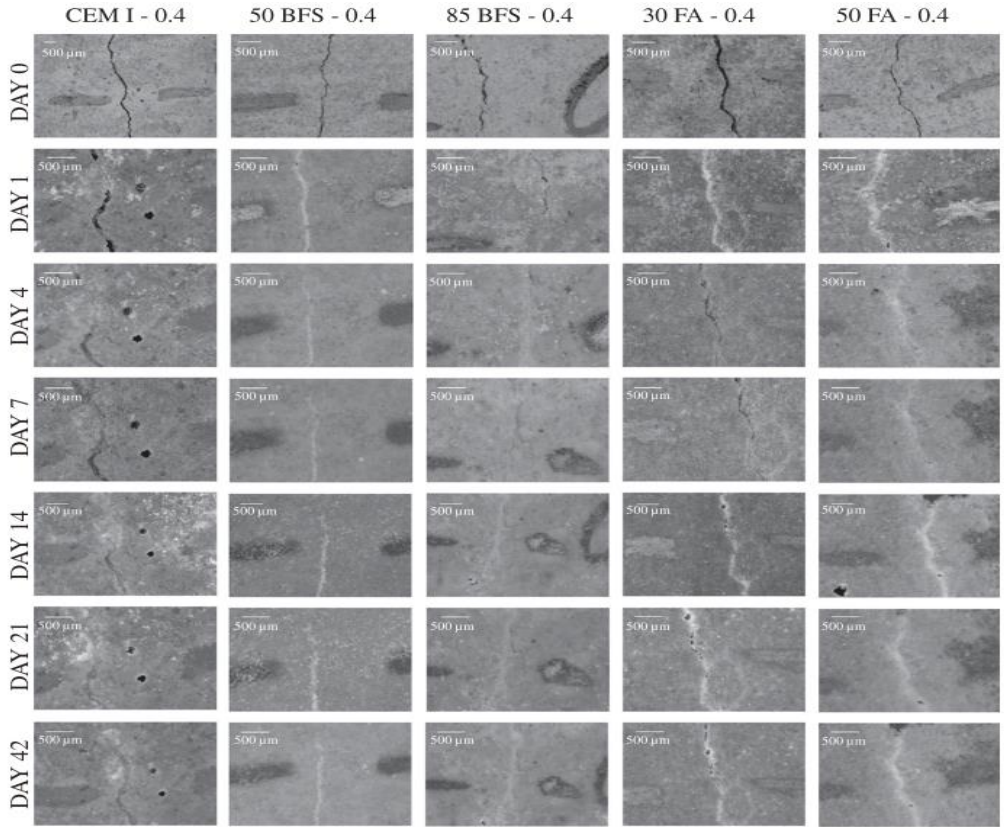

Figure 2.16: Evolution of the surface crack width over time due to autogenous crack healing: considering the use of blast furnace slag (BFS), fly ash (FA) and w/b of 0.40 [154] **(*reproduced with permission of Elsevier*).**

2.9.2 **Autonomous healing**

Autonomous healing is an engineered process designed to improve the healing properties of cementitious materials. Furthermore, autonomous/engineered healing can be further divided into "passive" and "active" modes. Activating the mechanism by human intervention is considered an "active mode" while without human intervention is defined as a "passive mode" [183]. Autonomous healing can be induced by two main groups of products: bacterial-based and crystalline admixtures, which are commonly added during concrete mixing [184].

2.9.2.1 **Bacterial-based healing (BBH)**

Bacterial-based healing involves the precipitation of $CaCO_3$ by direct bacterial activity [155,157] or by decomposition of urea by ureolytic bacteria [185,186]. *Bacillus Sphaericus* species (bio-agent for calcite precipitation) has been most commonly studied for concrete application due to its high tolerance to an alkaline environment [185,186]. Moreover, the bacterial activity is known by consuming oxygen; therefore, improving the durability of the reinforcement against corrosion.

Studies focusing on the use of BBH on concrete have progressively increased during the last decades: to increase lightweight concrete strength [187]; modify water mobility with hardened concrete and improve concrete strength and durability [188]; accelerate the setting time of concrete [156,189]; etc.

Bacillus Aerius bacteria combined with rice husk ash (RHA) concrete improved compressive strength in about 9% and 12% at 28 and 56 days. Moreover, the calcite precipitation by bacteria activity decreased water absorption and enhanced the microstructure, reducing the chloride ions penetration [188]. Different species of bacteria have also improved significantly concrete properties: *bacillus megaterium* were able to increase 24% of concrete compressive strength [190]; *sporoscarcina pasteurii* combined with fly ash or silica fume enhanced microstructure modifying chloride ions permeability [191]; *bacillus sphaericus* applied on concrete surface revealed promising results as an alternative for concrete surface treatment [192].

2.9.2.2 **Crystalline admixture for autonomous healing**

One of the smartest materials used for self-healing applications in concrete is the so-called crystalline admixtures (CA); these are permeability-reducing admixtures with a hydrophilic nature that easily react with water and can effectively serve also as self-healing engineered admixtures [163]. Moreover, the chemical reaction between CA, PC and water forms water-insoluble cracking deposits, increasing the density of calcium silicate hydrate (C-S-H), resulting in a more impermeable and resistant system against aggressive substances [145,146,153,159–162,183,193–195]. Furthermore, the reaction can also undergo a delayed activation whenever the material comes into contact with water and/or environmental moisture, enhancing the healing process at later ages [196].

However, the behaviour of these products is still partially unknown. Most of the studies in the literature focused on the variation of water and chloride permeability while using crystalline admixtures. Just a few authors have analyzed the effects on mechanical properties recovery, although most of them evaluated it through non-destructive techniques (NDTs). It has been suggested that in the presence of water, CA compounds may react with tricalcium silicate (C_3S), as seen in Equation 2.2, where a crystalline promoter, M_XR_X, reacts with C_3S and water to produce modified C-S-H and pore-blocking precipitates (i.e. M_XCaR_X –$(H_2O)x$) [197]. On the other hand, other authors [159] indicate that calcium hydroxide is the reactive component. Yet, the ability of CA to improve concrete properties may vary significantly with concrete mix-design, the chemical composition of the CA products, testing periods and methods of pre-inducing cracks on concrete for different studies (i.e., mechanical or durability-related) [161]. Furthermore, lower water-to-binder ratios and high cementitious material content seem to enhance the self-healing performance [152,154].

$$3CaO\text{-}SiO2+M_xR_x+H_2O\rightarrow Ca_xSi_xO_xR\text{-}(H_2O)_x+M_xCaR_x\text{-}(H_2O)_x$$

(C_3S+crystalline promoter+water→modified calcium silicate hydrate+pore blocking precipitate) **Equation 2.2**

Sisomphon and co-workers [159] demonstrated that by adding 1.5% and 4% (by PC mass) of CA in cement paste mixtures, cracks with widths ranging from 250 to 400 µm were closed entirely. Moreover, the healed paste specimens were demonstrated to be impermeable after 28 days of pre-induced cracking, and calcium carbonate was the major product found in the sealed cracks (Figure 2.17). Likewise, studies suggest that CA-concrete can achieve healing ratios of 0.98, for cracks up to 400 µm, after 42 days of curing [183]; complete sealing of cracks thinner than 300 µm [160]; 95% of strength regaining capacity [193]; and 50% lower water penetration, 30% lower chloride diffusivity and healing ratios close to 1.0 [169]. Moreover, it has been recently demonstrated that the combination of CA and SCMs (e.g., Blast Furnace Slag [182], fly ash [145,153,183,198] and silica fume [176]) could even reach higher values of self-healing ratios; yet overall, their efficiency lies between 90% to 105% depending on the exposure conditions [153]. It is worth mentioning that there is a relative agreement in the literature that cementitious materials soaked in water solutions tend to achieved higher self-healing ratios and faster healing rates, followed by wetting/drying cycles, water contact and air exposure conditions, respectively [147,152,153,160,169,176,183,196].

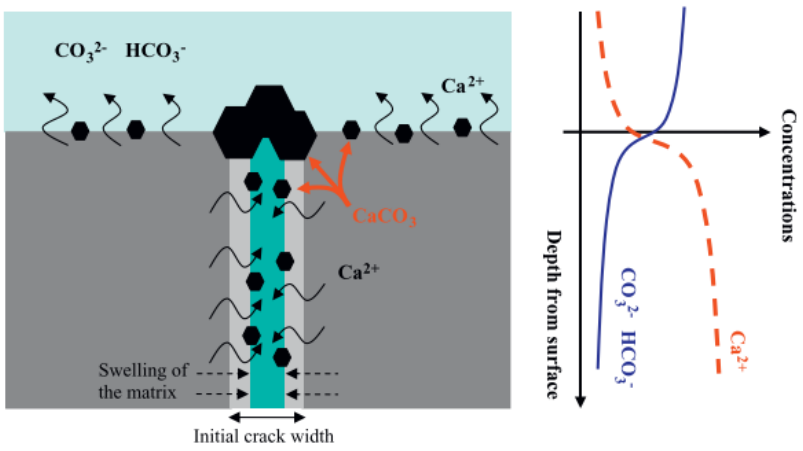

Figure 2.17: Schematic illustration of the precipitation of calcium carbonation [159] **(*reproduced with permission of Elsevier*).**

Besides, further investigation combining calcium sulfoaluminate-based admixture and CA showed optimum mechanical recovery at wet/dry conditions. On the other hand, air-cured samples contributed with no visible healing phenomenon and very low mechanical recovery [148]. Yet, results demonstrate that air exposure specimens placed in R.H. controlled rooms made of cement and CA (1% by cement weight) were highly effective in fully recovering concrete bending stiffness, load-bearing capacity, and visually closing cracks [196]. Moreover, in Roig-Flores et al. (2016), the average Healing Ratio reaches 0.99 and average Closing Ratio 0.98, for cracks up to 0.40 mm after 42 days of healing by samples soaked in water at 30 °C. Moreover, after pre-cracking concrete samples at 2 and 28 days, it was found that the mechanical properties were able to recover almost 100% [193]. Besides, the author indicates that CA can catalyze the healing capacity and was more systematic and reliable due to its hydrophilic nature.

Finally, several authors have studied the benefits of adding CAs in cement-based systems, either internally or externally, combined with cementitious coating material [147,160,169,176]. CA coatings' active ingredients can penetrate the cement paste and react with hydration products to form crystalline or gelatinous substances, which fill the capillary pores and micro-cracks [139]. It has been found that the healing products formed in the cracks display large calcium carbonate and ettringite contents, although C-S-H gel was also found [139,199]. Studies suggest that the penetration depths of CA from coatings can reach values between 33–80 mm, decreasing gas permeability values 11 times lower

[139], lessening in 70% the water absorption [200], enhanced the resistance to chloride penetration, and this improvement increases over-time in concrete [169]. Yet, these values seem to depend on the microstructure of the treated concrete, and the amount of coarse aggregates close to the surface [201,202].

2.10 References

[1] J. Lindgård, Ö. Andiç-Çakir, I. Fernandes, T.F. Rønning, M.D.A. Thomas, Alkali-silica reactions (ASR): Literature review on parameters influencing laboratory performance testing, Cem. Concr. Res. 42 (2012) 223–243. doi:10.1016/j.cemconres.2011.10.004.

[2] B. Fournier, M.-A. Bérubé, Alkali-aggregate reaction in concrete: a review of basic concepts and engineering implications, Can. J. Civ. Eng. 27 (2000) 167–191. doi:10.1139/cjce-27-2-167.

[3] M. Beyene, A. Snyder, R.J. Lee, M. Blaszkiewicz, Alkali Silica Reaction (ASR) as a root cause of distress in a concrete made from Alkali Carbonate Reaction (ACR) potentially susceptible aggregates, Cem. Concr. Res. 51 (2013) 85–95. doi:10.1016/j.cemconres.2013.04.014.

[4] B.P. Gautam, D.K. Panesar, S.A. Sheikh, F.J. Vecchio, Effect of coarse aggregate grading on the ASR expansion and damage of concrete, Cem. Concr. Res. 95 (2017) 75–83. doi:10.1016/j.cemconres.2017.02.022.

[5] F. Rajabipour, E. Giannini, C. Dunant, J.H. Ideker, M.D.A. Thomas, Alkali-silica reaction: Current understanding of the reaction mechanisms and the knowledge gaps, Cem. Concr. Res. 76 (2015) 130–146. doi:10.1016/j.cemconres.2015.05.024.

[6] C.M. Strack, E. Barnes, M.A. Ramsey, R.K. Williams, K.L. Klaus, R.D. Moser, Impact of aggregate mineralogy and exposure solution on alkali-silica reaction product composition and structure within accelerated test conditions, Constr. Build. Mater. 240 (2020) 117929. doi:10.1016/j.conbuildmat.2019.117929.

[7] M. Rashidi, M.C.L. Knapp, A. Hashemi, J.Y. Kim, K.M. Donnell, R. Zoughi, L.J. Jacobs, K.E. Kurtis, Detecting alkali-silica reaction: A multi-physics approach, Cem. Concr. Compos. 73 (2016) 123–135. doi:10.1016/j.cemconcomp.2016.07.001.

[8] L.F.M. Sanchez, Contribution to the assessment of damage in aging concrete infrastructures affected by alkali-aggregate reaction, 2014.

[9] L.F.M. Sanchez, B. Fournier, M. Jolin, D. Mitchell, J. Bastien, Overall assessment of Alkali-Aggregate Reaction (AAR) in concretes presenting different strengths and incorporating a wide range of reactive aggregate types and natures, Cem. Concr. Res. 93 (2017) 17–31. doi:10.1016/j.cemconres.2016.12.001.

[10] M.D.A. Thomas, K.J. Folliard, Concrete aggregates and the durability of concrete, in: Durab. Concr. Cem. Compos., 2007: pp. 247–281. doi:10.1533/9781845693398.247.

[11] T. Katayama, P.E. Grattan-Bellew, Petrography of the Kingston experimental sidewalk at age 22 years--ASR as the cause of deleteriously expansive, socalled alkali-carbonate reaction, in: Proc. 14th Int. Conf. Alkali-Aggregate React. Concr. Austin, Texas, USA, 2012: p. 10.

[12] T. Katayama, The so-called alkali-carbonate reaction (ACR) - Its mineralogical and geochemical details, with special reference to ASR, Cem. Concr. Res. 40 (2010) 643–675. doi:10.1016/j.cemconres.2009.09.020.

[13] N. Bérubé, N. Smaoui, B. Fournier, B. Bissonnette, B. Durand, Evaluation of the expansion attained to date by concrete affected by alkali-silica reaction. Part III: Application to existing structures, Can. J. Civ. Eng. 32 (2005) 463.

[14] J. Duchesne, M.A. Bérubé, Long-term effectiveness of supplementary cementing materials against alkali-silica reaction, Cem. Concr. Res. 31 (2001) 1057–1063. doi:10.1016/S0008-8846(01)00538-5.

[15] L.F.M. Sanchez, B. Fournier, M. Jolin, M.A.B. Bedoya, J. Bastien, J. Duchesne, Use of Damage Rating Index to quantify alkali-silica reaction damage in concrete: Fine versus coarse aggregate, ACI Mater. J. 113 (2016) 395–407. doi:10.14359/51688983.

[16] L.F.M. Sanchez, B. Fournier, M. Jolin, J. Duchesne, Reliable quantification of AAR damage through assessment of the Damage Rating Index (DRI), Cem. Concr. Res. 67 (2015) 74–92. doi:10.1016/j.cemconres.2014.08.002.

[17] D.J. De Souza, L.F.M. Sanchez, M.T. De Grazia, Evaluation of a direct shear test setup to quantify AAR-induced expansion and damage in concrete, Constr. Build. Mater. 229 (2019) 116806. doi:10.1016/j.conbuildmat.2019.116806.

[18] L.F.M. Sanchez, B. Fournier, M. Jolin, J. Bastien, Evaluation of the Stiffness Damage Test (SDT) as a tool for assessing damage in concrete due to alkali-silica reaction (ASR): Input parameters and variability of the test responses, Constr. Build. Mater. 77 (2015) 20–32. doi:10.1016/j.conbuildmat.2014.11.071.

[19] S. Poyet, A. Sellier, B. Capra, G. Foray, J.M. Torrenti, H. Cognon, E. Bourdarot, Chemical modelling of Alkali Silica reaction: Influence of the reactive aggregate size distribution, Mater. Struct. Constr. 40 (2007) 229–239. doi:10.1617/s11527-006-9139-3.

[20] V.E. Saouma, M.A. Hariri-Ardebili, Y. Le Pape, R. Balaji, Effect of alkali–silica reaction on the shear strength of reinforced concrete structural members. A numerical and statistical study, Nucl. Eng. Des. 310 (2016) 295–310. doi:10.1016/j.nucengdes.2016.10.012.

[21] J.W. Schmidt, S.G. Hansen, R.A. Barbosa, A. Henriksen, Novel shear capacity testing of ASR damaged full scale concrete bridge, Eng. Struct. 79 (2014) 365–374. doi:10.1016/j.engstruct.2014.08.027.

[22] R.S. Crouch, J.G.M. Wood, Damage evolution in AAR affected concretes, Eng. Fract. Mech. 35 (1990) 211–218. doi:10.1016/0013-7944(90)90199-Q.

[23] G.M. Wood, P. Norris, D. Leek, Physical behavior of AAR damaged concrete in structures and in test conditions, in: 8th Int. Conf. Alkali-Aggregate React. Concr., Kyoto (Japan), 1989.

[24] Y. Kubo, M. Nakata, Effect of reactive aggregate on mechanical properties of concrete affected by alkali-silica reaction, in: 14th Int. Conf. Alkali-Aggregate React. Concr., Austin (Texas), 2012: p. electronic.

[25] L.F.M. Sanchez, T. Drimalas, B. Fournier, D. Mitchell, J. Bastien, Comprehensive damage assessment in concrete affected by different internal swelling reaction (ISR) mechanisms, Cem. Concr. Res. 107 (2018) 284–303. doi:10.1016/j.cemconres.2018.02.017.

[26] A. Komar, J. Hartell, A.J. Boyd, Pressure tension test: reliability for assessing concrete deterioration., in: 7th Int. Conf. Concr. Under Sev. Cond. - Environ. Loading., Nanjing (China), 2013.

[27] G. Giaccio, R. Zerbino, J.M. Ponce, O.R. Batic, Mechanical behavior of concretes damaged by alkali-silica reaction, Cem. Concr. Res. 38 (2008) 993–1004. doi:10.1016/j.cemconres.2008.02.009.

[28] M. Haskett, D.J. Oehlers, M.S. Mohamed Ali, S.K. Sharma, Evaluating the shear-friction resistance across sliding planes in concrete, Eng. Struct. 33 (2011) 1357–1364. doi:10.1016/j.engstruct.2011.01.013.

[29] D.J. De Souza, L.F.M. Sanchez, M.T. De Grazia, Evaluation of a direct shear test setup to quantify AAR-induced expansion and damage in concrete, Constr. Build. Mater. 229 (2019) 116806. doi:10.1016/j.conbuildmat.2019.116806.

[30] P.K. Mehta, P.J.M. Monteiro, Concrete: Microstructure, Properties, and Materials, 3rd Edition, 2013. doi:10.1036/0071462899.

[31] C.S. Shon, S.L. Sarkar, Evaluation of modified ASTM C 1260 accelerated mortar bar test for alkali-silica reactivity, Cem. Concr. Res. 32 (2002) 1981–1987. doi:10.1016/S0008-8846(02)00903-1.

[32] H. Yazıcı, A. Beglarigale, K. Tosun Felekoğlu, S. Türkel, Comparing the alkali-silica reaction mitigation potential of admixtures by using different accelerated test methods, Constr. Build. Mater. 197 (2019) 597–614. doi:10.1016/j.conbuildmat.2018.11.227.

[33] N.P. Hasparyk, G. Gallo, T. Andrade, T.O. Santos, Potential of Metakaolin in Mitigating Expansions of Asr in Accelerated Tests, in: N.P. Bernardes, H.M. & Hasparyk (Ed.), 15th Int. Conf. Alkali-Aggregate React., São Paulo, 2016.

[34] R. Deschenes, M. Waidner, W.H. Hale, Mitigation of Alkali-Silica Reaction in Concrete Pavements By Silane Treatment, in: N.P. Bernardes, H.M. & Hasparyk (Ed.), 15th Int. Conf. Alkali-Aggregate React., São Paulo, 2016.

[35] X. Feng, B.J. Balcom, M.D.A. Thomas, T.W. Bremner, Na and Li ion diffusion in modified ASTM C 1260 test by Magnetic Resonance Imaging (MRI), Cem. Concr. Res. 38 (2008) 1409–1415. doi:10.1016/j.cemconres.2008.06.010.

[36] J.B. Walsh, The effect of cracks on the uniaxial elastic compression of rocks, J. Geophys. Res. 70 (1965) 399–411. doi:10.1029/JZ070i002p00399.

[37] R.S. Crouch, Specification for the determination of stiffness damage parameters from the low cyclic uniaxial compression of plain concrete cores. Revision A., 1987.

[38] T.M. Chrisp, P. Waldron, J.G.M. Wood, Development of a non-destructive test to quantify damage in deteriorated concrete, Mag. Concr. Res. 45 (1993) 247–256. doi:10.1680/macr.1993.45.165.247.

[39] N. Smaoui, M.-A. Bérubé, B. Fournier, B. Bissonnette, B. Durand, Evaluation of the expansion attained to date by concrete affected by alkali–silica reaction. Part I: Experimental study, Can. J. Civ. Eng. 31 (2004) 826–845. doi:10.1139/l04-051.

[40] L.F.M. Sanchez, B. Fournier, M. Jolin, J. Bastien, D. Mitchell, Practical use of the Stiffness Damage Test (SDT) for assessing damage in concrete infrastructure affected by alkali-silica reaction, Constr. Build. Mater. 125 (2016) 1178–1188. doi:10.1016/j.conbuildmat.2016.08.101.

[41] Y. Zhu, A. Zahedi, L.F.M. Sanchez, B. Fournier, S. Beauchemin, Overall assessment of alkali-silica reaction affected recycled concrete aggregate mixtures derived from construction and demolition waste, Cem. Concr. Res. 142 (2021) 106350. doi:10.1016/j.cemconres.2020.106350.

[42] D.F. Adams, D.E. Walrath, Current status of the Iosipescu shear test method, J. Compos. Mater. 21 (1987) 494–507. doi:10.1177/002199838702100601.

[43] L. Banks-Sills, M. Arcan, An edge-cracked Mode II fracture specimen., Exp. Mech. 23 (1983) 257–261.

[44] B. Barr, E.B.D. Hasso, Development of a compact cylindrical shear test specimen, J. Mater. Sci. Lett. 5 (1986) 1305–1308. doi:10.1007/BF01729401.

[45] V. Villeneuve, B. Fournier, Determination of the damage in concrete affected by ASR–the

damage rating index (DRI), in: 14th Int. Conf. Alkali-Aggregate React. Concr., Austin (Texas), 2012: p. electronic.

[46] L.F.M. Sanchez, B. Fournier, M. Jolin, M.A.B. Bedoya, J. Bastien, J. Duchesne, Use of Damage Rating Index to quantify alkali-silica reaction damage in concrete: Fine versus coarse aggregate, ACI Mater. J. 113 (2016) 395–407. doi:10.14359/51688983.

[47] L.F.M. Sanchez, Contribution to the assessment of damage in aging concrete infrastructures affected by alkali-aggregate reaction, (2014) 341.

[48] L.F.M. Sanchez, B. Fournier, M. Jolin, J. Duchesne, Reliable quantification of AAR damage through assessment of the Damage Rating Index (DRI), Cem. Concr. Res. 67 (2015) 74–92. doi:10.1016/j.cemconres.2014.08.002.

[49] V. Villeneuve, B. Fournier, Determination of the damage in concrete affected by ASR–the damage rating index (DRI), in: 14th Int. Conf. Alkali-Aggregate React. Concr., Austin (Texas), 2012: p. electronic.

[50] G. Gudmundsson, H. Olafsson, Alkali-silica reactions and silica fume: 20 years of experience in Iceland, Cem. Concr. Res. 29 (1999) 1289–1297. doi:10.1016/S0008-8846(98)00239-7.

[51] M. Thomas, A. Dunster, P. Nixon, B. Blackwell, Effect of fly ash on the expansion of concrete due to alkali-silica reaction - Exposure site studies, Cem. Concr. Compos. 33 (2011) 359–367. doi:10.1016/j.cemconcomp.2010.11.006.

[52] H.F.W. Taylor, Cement Chemistry, Harcourt Brace Jovanovich, London, 1990.

[53] M.H. Samarakoon, P.G. Ranjith, T.D. Rathnaweera, M.S.A. Perera, Recent advances in alkaline cement binders: A review, J. Clean. Prod. 227 (2019) 70–87. doi:10.1016/j.jclepro.2019.04.103.

[54] J. Stark, Recent advances in the field of cement hydration and microstructure analysis, Cem. Concr. Res. 41 (2011) 666–678. doi:10.1016/j.cemconres.2011.03.028.

[55] A. James, E. Bazarchi, A.A. Chiniforush, P. Panjebashi Aghdam, M.R. Hosseini, A. Akbarnezhad, I. Martek, F. Ghodoosi, Rebar corrosion detection, protection, and rehabilitation of reinforced concrete structures in coastal environments: A review, Constr. Build. Mater. 224

(2019) 1026–1039. doi:10.1016/j.conbuildmat.2019.07.250.

[56] C.G. Berrocal, K. Lundgren, I. Löfgren, Corrosion of steel bars embedded in fibre reinforced concrete under chloride attack: State of the art, Cem. Concr. Res. 80 (2016) 69–85. doi:10.1016/j.cemconres.2015.10.006.

[57] Z. Shi, A. Leemann, D. Rentsch, B. Lothenbach, Synthesis of alkali-silica reaction product structurally identical to that formed in field concrete, Mater. Des. 190 (2020) 108562. doi:10.1016/j.matdes.2020.108562.

[58] H.T. Le, H.M. Ludwig, Alkali silica reactivity of rice husk ash in cement paste, Constr. Build. Mater. 243 (2020) 118145. doi:10.1016/j.conbuildmat.2020.118145.

[59] A. Leemann, B. Lothenbach, The influence of potassium-sodium ratio in cement on concrete expansion due to alkali-aggregate reaction, Cem. Concr. Res. 38 (2008) 1162–1168. doi:10.1016/j.cemconres.2008.05.004.

[60] X. Hou, L.J. Struble, R.J. Kirkpatrick, Formation of ASR gel and the roles of C-S-H and portlandite, Cem. Concr. Res. 34 (2004) 1683–1696. doi:10.1016/j.cemconres.2004.03.026.

[61] S. Chatterji, Chemistry of alkali-silica reaction and testing of aggregates, Cem. Concr. Compos. 27 (2005) 788–795. doi:10.1016/j.cemconcomp.2005.03.005.

[62] H. Maraghechi, F. Rajabipour, C.G. Pantano, W.D. Burgos, Effect of calcium on dissolution and precipitation reactions of amorphous silica at high alkalinity, Cem. Concr. Res. 87 (2016) 1–13. doi:10.1016/j.cemconres.2016.05.004.

[63] A. Leemann, G. Le Saout, F. Winnefeld, D. Rentsch, B. Lothenbach, Alkali-Silica reaction: The Influence of calcium on silica dissolution and the formation of reaction products, J. Am. Ceram. Soc. 94 (2011) 1243–1249. doi:10.1111/j.1551-2916.2010.04202.x.

[64] A. Gholizadeh Vayghan, F. Rajabipour, J.L. Rosenberger, Composition-rheology relationships in alkali-silica reaction gels and the impact on the Gel's deleterious behavior, Cem. Concr. Res. 83 (2016) 45–56. doi:10.1016/j.cemconres.2016.01.011.

[65] A. Leemann, P. Lura, E-modulus of the alkali-silica-reaction product determined by micro-

indentation, Constr. Build. Mater. 44 (2013) 221–227. doi:10.1016/j.conbuildmat.2013.03.018.

[66] T.C. Powers, H.H. Steinour, An Interpretation of Some Published Researches on the Alkali-Aggregate Reaction Part 1-The Chemical Reactions and Mechanism of Expansion, ACI J. Proc. 51 (1955). doi:10.14359/11691.

[67] S. Poyet, A. Sellier, B. Capra, G. Thè-venin-Foray, J.M. Torrenti, H. Tournier-Cognon, E. Bourdarot, Influence of water on alkali-silica reaction: Experimental study and numerical simulations, J. Mater. Civ. Eng. 18 (2006) 588–596. doi:10.1061/(ASCE)0899-1561(2006)18:4(588).

[68] R.A. Deschenes, E.R. Giannini, T. Drimalas, B. Fournier, W.M. Hale, Effects of moisture, temperature, and freezing and thawing on Alkali-Silica reaction, ACI Mater. J. 115 (2018) 575–584. doi:10.14359/5170219.

[69] R.N. Swamy, The Alkali-Silica Reaction in Concrete, 1st ed., Blackie, London, 1992.

[70] D.W. Hobbs, Alkali–silica reaction in concrete, Thomas-Telford, London, 1988.

[71] S. Kamali, B. Gérard, M. Moranville, Modelling the leaching kinetics of cement-based materials - Influence of materials and environment, Cem. Concr. Compos. 25 (2003) 451–458. doi:10.1016/S0958-9465(02)00085-9.

[72] S. Kamali, M. Moranville, S. Leclercq, Material and environmental parameter effects on the leaching of cement pastes: Experiments and modelling, Cem. Concr. Res. 38 (2008) 575–585. doi:10.1016/j.cemconres.2007.10.009.

[73] P. Lawrence, M. Cyr, E. Ringot, Mineral admixtures in mortars, Cem. Concr. Res. 33 (2003) 1939–1947. doi:10.1016/S0008-8846(03)00183-2.

[74] A.K. Saha, M.N.N. Khan, P.K. Sarker, F.A. Shaikh, A. Pramanik, The ASR mechanism of reactive aggregates in concrete and its mitigation by fly ash: A critical review, Constr. Build. Mater. 171 (2018) 743–758. doi:10.1016/j.conbuildmat.2018.03.183.

[75] E.T. Bueno, J.M. Paris, K.A. Clavier, C. Spreadbury, C.C. Ferraro, T.G. Townsend, A review of ground waste glass as a supplementary cementitious material: A focus on alkali-silica reaction, J.

Clean. Prod. 257 (2020) 120180. doi:10.1016/j.jclepro.2020.120180.

[76] J.J. Chen, A.K.H. Kwan, Y. Jiang, Adding limestone fines as cement paste replacement to reduce water permeability and sorptivity of concrete, Constr. Build. Mater. 56 (2014) 87–93. doi:10.1016/j.conbuildmat.2014.01.066.

[77] T. Bader, R. Lackner, Acrylic surface treatment applied to architectural High-Performance Concrete (HPC): Identification of potential pitfalls on the way to long-lasting protection, Constr. Build. Mater. 237 (2020) 117415. doi:10.1016/j.conbuildmat.2019.117415.

[78] S. Weisheit, S.H. Unterberger, T. Bader, R. Lackner, Assessment of test methods for characterizing the hydrophobic nature of surface-treated High Performance Concrete, Constr. Build. Mater. 110 (2016) 145–153. doi:10.1016/j.conbuildmat.2016.02.010.

[79] P.A.M. Basheer, L. Basheer, D.J. Cleland, A.E. Long, Surface treatments for concrete: Assessment methods and reported performance, Constr. Build. Mater. 11 (1997) 413–429. doi:10.1016/S0950-0618(97)00019-6.

[80] Z. Liu, W. Hansen, Effect of hydrophobic surface treatment on freeze-thaw durability of concrete, Cem. Concr. Compos. 69 (2016) 49–60. doi:10.1016/j.cemconcomp.2016.03.001.

[81] S.R.C. Madduru, K.S. Shaik, R. Velivela, V.K. Karri, Hydrophilic and hydrophobic chemicals as self curing agents in self compacting concrete, J. Build. Eng. 28 (2020) 101008. doi:10.1016/j.jobe.2019.101008.

[82] A.A. Almusallam, F.M. Khan, S.U. Dulaijan, O.S.B. Al-Amoudi, Effectiveness of surface coatings in improving concrete durability, Cem. Concr. Compos. 25 (2003) 473–481. doi:10.1016/S0958-9465(02)00087-2.

[83] M.. Berube, B. Fournier, Influence of Wetting-Drying and Freezing-Thawing Cycles, and Effectiveness of Sealers on ASR, in: Ahmad Sheyan (Ed.), 10th Int. Conf. Alkali-Aggregate React. Concr., Melbourne, 1996: pp. 1056–1063.

[84] D. Stark, The moisture condition of field concrete exhibiting alkali-silica reactivity, in: 2nd Int. Conf. Durab. Concr., ACI Publication SP, 1991: pp. 973–987.

[85] M.H.F. Medeiros, P. Helene, Surface treatment of reinforced concrete in marine environment: Influence on chloride diffusion coefficient and capillary water absorption, Constr. Build. Mater. 23 (2009) 1476–1484. doi:10.1016/j.conbuildmat.2008.06.013.

[86] R.S.C. Woo, H. Zhu, M.M.K. Chow, C.K.Y. Leung, J.K. Kim, Barrier performance of silane-clay nanocomposite coatings on concrete structure, Compos. Sci. Technol. 68 (2008) 2828–2836. doi:10.1016/j.compscitech.2007.10.028.

[87] R.D. Lute, K.J. Folliard, T. Drimalas, C.K. Rust, Coatings and sealers for mitigation of alkali-silica reaction and/or delayed ettringite formation, in: H.M. Bernardes, N.P. Hasparyk (Eds.), 15th Int. Conf. Alkali-Aggregate React., São Paulo, 2016.

[88] K. Tosun, B. Felekoglu, B. Baradan, Effectiveness of alkyl alkoxy silane treatment in mitigating alkali-silica reaction, ACI Mater. J. 105 (2008) 20–27. doi:10.14359/19203.

[89] C.D. Murray, R.A. Deschenes, W.M. Hale, Durability of silane sealer in highly alkaline environment, ACI Mater. J. 113 (2016) 387–393. doi:10.14359/51688982.

[90] C. Christodoulou, C.I. Goodier, S.A. Austin, J. Webb, G.K. Glass, Long-term performance of surface impregnation of reinforced concrete structures with silane, Constr. Build. Mater. 48 (2013) 708–716. doi:10.1016/j.conbuildmat.2013.07.038.

[91] Y. Kawabata, K. Yamada, The mechanism of limited inhibition by fly ash on expansion due to alkali–silica reaction at the pessimum proportion, Cem. Concr. Res. 92 (2017) 1–15. doi:10.1016/j.cemconres.2016.11.002.

[92] Z. Shi, C. Shi, J. Zhang, S. Wan, Z. Zhang, Z. Ou, Alkali-silica reaction in waterglass-activated slag mortars incorporating fly ash and metakaolin, Cem. Concr. Res. 108 (2018) 10–19. doi:10.1016/j.cemconres.2018.03.002.

[93] D. Hester, C. McNally, M. Richardson, A study of the influence of slag alkali level on the alkali-silica reactivity of slag concrete, Constr. Build. Mater. 19 (2005) 661–665. doi:10.1016/j.conbuildmat.2005.02.016.

[94] M.C.G. Juenger, R. Siddique, Recent advances in understanding the role of supplementary

cementitious materials in concrete, Cem. Concr. Res. (2015). doi:10.1016/j.cemconres.2015.03.018.

[95] M.H. Shehata, M.D.A. Thomas, Use of ternary blends containing silica fume and fly ash to suppress expansion due to alkali-silica reaction in concrete, Cem. Concr. Res. 32 (2002) 341–349. doi:10.1016/S0008-8846(01)00680-9.

[96] T. Nochaiya, W. Wongkeo, A. Chaipanich, Utilization of fly ash with silica fume and properties of Portland cement-fly ash-silica fume concrete, Fuel. 89 (2010) 768–774. doi:10.1016/j.fuel.2009.10.003.

[97] A. Leemann, L. Bernard, S. Alahrache, F. Winnefeld, ASR prevention - Effect of aluminum and lithium ions on the reaction products, Cem. Concr. Res. 76 (2015) 192–201. doi:10.1016/j.cemconres.2015.06.002.

[98] J. Wei, B. Gencturk, A. Jain, M. Hanifehzadeh, Mitigating alkali-silica reaction induced concrete degradation through cement substitution by metakaolin and bentonite, Appl. Clay Sci. 182 (2019) 105257. doi:10.1016/j.clay.2019.105257.

[99] M. Thomas, The effect of supplementary cementing materials on alkali-silica reaction: A review, Cem. Concr. Res. 41 (2011) 1224–1231. doi:10.1016/j.cemconres.2010.11.003.

[100] B. Lothenbach, K. Scrivener, R.D. Hooton, Supplementary cementitious materials, Cem. Concr. Res. 41 (2011) 1244–1256. doi:10.1016/j.cemconres.2010.12.001.

[101] CSA A23.1-14, Concrete materials and methods of concrete construction, Can. Stand. Assoc. (2019).

[102] R.F. Bleszynski, The performance and durability of concrete with ternary blends of silica fume and blast-furnace slag, 2002.

[103] M.H. Shehata, M.D.A. Thomas, R.F. Bleszynski, The effects of fly ash composition on the chemistry of pore solution in hydrated cement pastes, Cem. Concr. Res. 29 (1999) 1915–1920. doi:10.1016/S0008-8846(99)00190-8.

[104] J. Duchesne, M.A. Bérubé, Long-term effectiveness of supplementary cementing materials

against alkali-silica reaction, Cem. Concr. Res. 31 (2001) 1057–1063. doi:10.1016/S0008-8846(01)00538-5.

[105] S.W. Forster, R.L. Boone, M.S. Hammer, J.F. Lamond, D.S. Lane, R.E. Miller, S.E. Parker, A. Pergalsky, J.S. Pierce, M.Q. Robert, J.W. Schmitt, R.E. Tobin, State-of-the-Art Report on Alkali-Aggregate Reactivity Reported by ACI Committee 221, 98 (1998) 1–31.

[106] B. Fournier, R. Chevrier, A. Bilodeau, P.C. Nkinamubanzi, N. Bouzoubaa, Comparative field and laboratory investigations on the use of supplementary cementing materials (SCMs) to control alkali-silica reaction (ASR) in concrete, in: 15th Int. Conf. Alkali-Aggregate React., Bernardes, H.M & Hasparyk, N.P., São Paulo, 2016.

[107] T. Chappex, K.L. Scrivener, The influence of aluminium on the dissolution of amorphous silica and its relation to alkali silica reaction, Cem. Concr. Res. 42 (2012) 1645–1649. doi:10.1016/j.cemconres.2012.09.009.

[108] T. Chappex, K. Scrivener, Alkali fixation of C-S-H in blended cement pastes and its relation to alkali silica reaction, Cem. Concr. Res. 42 (2012) 1049–1054. doi:10.1016/j.cemconres.2012.03.010.

[109] A. Mirdamadi, H. Layssi, M.H. Eftekhar, M. Shekarchi, Comparative Study of Metakaolin and Silica Fume To Prevent Alkali-Silica Reaction in Concrete, in: N.P. Bernardes, H. M. & Hasparyk (Ed.), 13th Int. Conf. Alkali-Aggregate React. Concr., 2008.

[110] F.A.. Munhoz, Y. Kihara, M.A. Cincotto, Effect of Mineral Admixtures on To the Mitigation of Alkali-Silica Reaction in Concrete, in: 13th Int. Conf. Alkali-Aggregate React. Concr., Trondheim, Norway, 2008.

[111] K.-J. Huenger, M. Kositz, M. Huenger, J. Krey, M. Muehlstaedt, Surface Coating of Siliceous Parts of Aggregate Grains By Alumina Containing Scm`S in Alkaline Solutions, in: N.P. Bernardes, H. M. & Hasparyk (Ed.), 15th Int. Conf. Alkali-Aggregate React., São Paulo, 2016.

[112] Q. Zhao, J. Stark, E. Freyburg, M. Zhou, The Mechanism of Gbfs Preventing AAR: a Discussion, in: 13th Int. Conf. Alkali-Aggregate React. Concr., Trondheim, Norway, 2008.

[113] N. Arano, M. Kawamura, Comparative consideration on the mechanism of ASR suppression due to different mineral admixtures., in: B.D. M.A. Bérubé, B. Fournier (Ed.), 11th Int. Conf. Alkali–Aggregate React. Concr. (ICAAR)., Quebéc, 2000: pp. 553–562.

[114] V.M. Malhotra, B. Fournier, Overview of Research on Alkali-Aggregate Reactions., in: Int. Work. Alkali-Aggregate React. Concr., Nova Scotia, 1995: pp. 1–45.

[115] B.W.J. Mccoyt, A.G. Caldwelu, New Approach to Inhibiting Alkali-Aggregate Expansion, ACI J. Proc. 47 (1951) 693–706. doi:10.14359/12030.

[116] J. Zapała-Sławeta, Z. Owsiak, The role of lithium compounds in mitigating alkali-gravel aggregate reaction, Constr. Build. Mater. 115 (2016) 299–303. doi:10.1016/j.conbuildmat.2016.04.058.

[117] T. Kim, J. Olek, The effects of lithium ions on chemical sequence of alkali-silica reaction, Cem. Concr. Res. 79 (2016) 159–168. doi:10.1016/j.cemconres.2015.09.013.

[118] C. Tremblay, M.A. Bérubé, B. Fournier, M.D. Thomas, K.J. Folliard, Experimental investigation of the mechanisms by which LiNO3 is effective against ASR, Cem. Concr. Res. 40 (2010) 583–597. doi:10.1016/j.cemconres.2009.09.022.

[119] X. Feng, M.D.A. Thomas, T.W. Bremner, K.J. Folliard, B. Fournier, New observations on the mechanism of lithium nitrate against alkali silica reaction (ASR), Cem. Concr. Res. 40 (2010) 94–101. doi:10.1016/j.cemconres.2009.07.017.

[120] X. Mo, Y. Zhang, J. Yao, G. Li, Y. Feng, Influence of various parameters on Li2CO3 against alkali-silica reaction, Constr. Build. Mater. 22 (2008) 1668–1674. doi:10.1016/j.conbuildmat.2007.06.005.

[121] X. Mo, Laboratory study of LiOH in inhibiting alkali-silica reaction at 20 °c: A contribution, Cem. Concr. Res. 35 (2005) 499–504. doi:10.1016/j.cemconres.2004.06.003.

[122] X. Mo, T. Jin, G. Li, K. Wang, Z. Xu, M. Tang, Alkali-aggregate reaction suppressed by chemical admixture at 80 °c, Constr. Build. Mater. 19 (2005) 473–479. doi:10.1016/j.conbuildmat.2004.07.012.

[123] M. Kawamura, H. Fuwa, Effects of lithium salts on ASR gel composition and expansion of mortars, Cem. Concr. Res. 33 (2003) 913–919. doi:10.1016/S0008-8846(02)01092-X.

[124] X. Mo, B. Fournier, Investigation of structural properties associated with alkali-silica reaction by means of macro- and micro-structural analysis, Mater. Charact. 58 (2007) 179–189. doi:10.1016/j.matchar.2006.04.018.

[125] D. Bulteel, E. Garcia-Diaz, P. Dégrugilliers, Influence of lithium hydroxide on alkali-silica reaction, Cem. Concr. Res. 40 (2010) 526–530. doi:10.1016/j.cemconres.2009.08.019.

[126] L.D. Mitchell, J.J. Beaudoin, P. Grattan-Bellew, The effects of lithium hydroxide solution on alkali silica reaction gels created with opal, Cem. Concr. Res. 34 (2004) 641–649. doi:10.1016/j.cemconres.2003.10.011.

[127] A. Leemann, L. Lörtscher, L. Bernard, G. Le Saout, B. Lothenbach, R.M. Espinosa-Marzal, Mitigation of ASR by the use of LiNO3 - Characterization of the reaction products, Cem. Concr. Res. 59 (2014) 73–86. doi:10.1016/j.cemconres.2014.02.003.

[128] M. Prezzi, P.J.M. Monteiro, G. Sposito, Alkali-silica reaction - Part 2: The effect of chemical admixtures, ACI Mater. J. 95 (1998) 3–10. doi:10.14359/346.

[129] C.L. Collins, J.H. Ideker, G.S. Willis, K.E. Kurtis, Examination of the effects of LiOH, LiCl, and LiNO3 on alkali-silica reaction, Cem. Concr. Res. 34 (2004) 1403–1415. doi:10.1016/j.cemconres.2004.01.011.

[130] R.B. Figueira, R. Sousa, L. Coelho, M. Azenha, J.M. de Almeida, P.A.S. Jorge, C.J.R. Silva, Alkali-silica reaction in concrete: Mechanisms, mitigation and test methods, Constr. Build. Mater. 222 (2019) 903–931. doi:10.1016/j.conbuildmat.2019.07.230.

[131] M.D.A. Thomas, B. Fournier, K.J. Folliard, J.H. Ideker, Y. Resendez, The Use of Lithium To Prevent or Mitigate Alkali-Silica Reaction in Concrete Pavements and Structures., Washington, DC, 2007.

[132] D.P. Johnston, R. Surdahl, D.P. Stokes, A Case Study of a Lithium-Based Treatment of an ASR-Affected Pavement., in: B.D. M.A. Berube, B. Fournier (Ed.), 11th Int. Conf. Alkali- Aggreg.

React., Quebéc, 2000: pp. 1149–1158.

[133] K.J. Folliard, R. Barborak, T. Drimalas, L. Du, S. Garber, J. Ideker, T. Ley, S. Williams, M. Juenger, B. Fournier, M.D.A. Thomas, Preventing ASR/DEF in new concrete:final report., Austin (Texas), 2006.

[134] M. Kawamura, T. Kodera, Effects of externally supplied lithium on the suppression of ASR expansion in mortars, Cem. Concr. Res. 35 (2005) 494–498. doi:10.1016/j.cemconres.2004.04.032.

[135] S. Ekolu, G. Rakgosi, D. Hooton, Long-term mitigating effect of lithium nitrate on delayed ettringite formation and ASR in concrete – Microscopic analysis, Mater. Charact. 133 (2017) 165–175. doi:10.1016/j.matchar.2017.09.025.

[136] K. Kobayashi, Y. Takagi, Penetration of pressure-injected lithium nitrite in concrete and ASR mitigating effect, Cem. Concr. Compos. 114 (2020) 103709. doi:10.1016/j.cemconcomp.2020.103709.

[137] L.M.S. Souza, R.B. Polder, O. Çopuroğlu, Lithium migration in a two-chamber set-up as treatment against expansion due to alkali–silica reaction, Constr. Build. Mater. 134 (2017) 324–335. doi:10.1016/j.conbuildmat.2016.12.052.

[138] L. Shen, H. Jiang, T. Wang, K. Chen, H. Zhang, Performance of silane -based surface treatments for protecting degraded historic concrete, Prog. Org. Coatings. 129 (2019) 209–216. doi:10.1016/j.porgcoat.2019.01.016.

[139] Y. Zhang, L. Zuo, J. Yang, X. Cai, Y. Zhao, X. Zeng, Effect of cementitious capillary crystalline waterproofing coating on the gas permeability of mortar, Struct. Concr. 20 (2019) 1763–1770. doi:10.1002/suco.201900016.

[140] Y. Zhang, X. Du, Y. Li, F. Yang, Z. Li, Research on cementitious capillary crystalline waterproofing coating for underground concrete works, Adv. Mater. Res. 450–451 (2012) 286–290. doi:10.4028/www.scientific.net/AMR.450-451.286.

[141] G. Lu, W. Zhao, D. Dai, Study on Preparation of cementitious capillary crystalline

waterproofing coating, Proc. 3rd Int. Conf. Mechatronics, Robot. Autom. 15 (2015) 79–84. doi:10.2991/icmra-15.2015.16.

[142] E. Watanabe, Bridge Maintenance, Safety, Management and Cost, 2014. doi:10.1201/9781482290127.

[143] Y. Yoon, M. Hastak, Annual rehabilitation costs estimation for a bridge network, KSCE J. Civ. Eng. 21 (2017) 27–36. doi:10.1007/s12205-016-1175-0.

[144] H. Tabatabai, A. Ghorbanpoor, M.D. Pritzl, Evaluation of Select Methods of Corrosion Prevention, Corrosion Control, and Repair in Reinforced Concrete Bridges, Wisconsin Highw. Res. Progr. (2009) 1–343.

[145] T. Chandra Sekhara Reddy, A. Ravitheja, Macro mechanical properties of self healing concrete with crystalline admixture under different environments, Ain Shams Eng. J. 10 (2019) 23–32. doi:10.1016/j.asej.2018.01.005.

[146] M. Roig-Flores, S. Moscato, P. Serna, L. Ferrara, Self-healing capability of concrete with crystalline admixtures in different environments, Constr. Build. Mater. 86 (2015) 1–11. doi:10.1016/j.conbuildmat.2015.03.091.

[147] S. Guzlena, G. Sakale, Self-healing concrete with crystalline admixture - A review, IOP Conf. Ser. Mater. Sci. Eng. 660 (2019). doi:10.1088/1757-899X/660/1/012057.

[148] K. Sisomphon, O. Copuroglu, E.A.B. Koenders, Effect of exposure conditions on self healing behavior of strain hardening cementitious composites incorporating various cementitious materials, Constr. Build. Mater. 42 (2013) 217–224. doi:10.1016/j.conbuildmat.2013.01.012.

[149] A.E.M. Abd-Elmoaty, Self-healing of polymer modified concrete, Alexandria Eng. J. 50 (2011) 171–178. doi:10.1016/j.aej.2011.03.002.

[150] D.G. Bekas, K. Tsirka, D. Baltzis, A.S. Paipetis, Self-healing materials: A review of advances in materials, evaluation, characterization and monitoring techniques, Compos. Part B Eng. 87 (2016) 92–119. doi:10.1016/j.compositesb.2015.09.057.

[151] M. Getnet Meharie, Factors Affecting the Self-Healing Efficiency of Cracked Concrete

Structures, Am. J. Appl. Sci. Res. 3 (2017) 80. doi:10.11648/j.ajasr.20170306.12.

[152] M. Şahmaran, S.B. Keskin, G. Ozerkan, I.O. Yaman, Self-healing of mechanically-loaded self consolidating concretes with high volumes of fly ash, Cem. Concr. Compos. 30 (2008) 872–879. doi:10.1016/j.cemconcomp.2008.07.001.

[153] T.C.S.R. Reddy, A.R. Theja, C. Sashidhar, Self-Healing Ability of High-Strength Fibre-Reinforced Concrete with Fly Ash and Crystalline Admixture, Civ. Eng. J. 4 (2018) 971. doi:10.28991/cej-0309149.

[154] K. Van Tittelboom, E. Gruyaert, H. Rahier, N. De Belie, Influence of mix composition on the extent of autogenous crack healing by continued hydration or calcium carbonate formation, Constr. Build. Mater. 37 (2012) 349–359. doi:10.1016/j.conbuildmat.2012.07.026.

[155] H. Kalhori, R. Bagherpour, Application of carbonate precipitating bacteria for improving properties and repairing cracks of shotcrete, Constr. Build. Mater. 148 (2017) 249–260. doi:10.1016/j.conbuildmat.2017.05.074.

[156] M. Luo, C. Qian, Influences of bacteria-based self-healing agents on cementitious materials hydration kinetics and compressive strength, Constr. Build. Mater. 121 (2016) 659–663. doi:10.1016/j.conbuildmat.2016.06.075.

[157] K. Vijay, M. Murmu, S. V. Deo, Bacteria based self healing concrete – A review, Constr. Build. Mater. 152 (2017) 1008–1014. doi:10.1016/j.conbuildmat.2017.07.040.

[158] L. Jiang, G. Jia, C. Jiang, Z. Li, Sugar-coated expanded perlite as a bacterial carrier for crack-healing concrete applications, Constr. Build. Mater. 232 (2020) 117222. doi:10.1016/j.conbuildmat.2019.117222.

[159] K. Sisomphon, O. Copuroglu, E.A.B. Koenders, Self-healing of surface cracks in mortars with expansive additive and crystalline additive, Cem. Concr. Compos. 34 (2012) 566–574. doi:10.1016/j.cemconcomp.2012.01.005.

[160] E. Cuenca, A. Tejedor, L. Ferrara, A methodology to assess crack-sealing effectiveness of crystalline admixtures under repeated cracking-healing cycles, Constr. Build. Mater. 179 (2018)

619–632. doi:10.1016/j.conbuildmat.2018.05.261.

[161] P. Escoffres, C. Desmettre, J.P. Charron, Effect of a crystalline admixture on the self-healing capability of high-performance fiber reinforced concretes in service conditions, Constr. Build. Mater. 173 (2018) 763–774. doi:10.1016/j.conbuildmat.2018.04.003.

[162] M. Nasim, U.K. Dewangan, S. V. Deo, Autonomous healing in concrete by crystalline admixture: A review, Mater. Today Proc. 32 (2020) 638–644. doi:10.1016/j.matpr.2020.03.116.

[163] ACI 212.3R, ACI 212 . 3R-10 Report on Chemical Admixtures for Concrete, American Concrete Institute, 2015.

[164] S. Granger, A. Loukili, G. Pijaudier-Cabot, G. Chanvillard, Experimental characterization of the self-healing of cracks in an ultra high performance cementitious material: Mechanical tests and acoustic emission analysis, Cem. Concr. Res. 37 (2007) 519–527. doi:10.1016/j.cemconres.2006.12.005.

[165] S. Jacobsen, J. Maschand, L. Boisvert, Effect of cracking and healing on chloride transport in OPC concrete, Cem. Concr. Res. 26 (1996) 869–881.

[166] W. Zamorowski, The phenomenon of self-regeneration of concrete., Int. J. Cem. Compos. Light. Concr. 7 (1985) 199–201. doi:10.1139/b87-051.

[167] K. Van Tittelboom, N. De Belie, Self-healing in cementitious materials-a review, 2013. doi:10.3390/ma6062182.

[168] W. Zhang, Q. Zheng, A. Ashour, B. Han, Self-healing cement concrete composites for resilient infrastructures: A review, Compos. Part B Eng. 189 (2020) 107892. doi:10.1016/j.compositesb.2020.107892.

[169] P. Azarsa, R. Gupta, A. Biparva, Assessment of self-healing and durability parameters of concretes incorporating crystalline admixtures and Portland Limestone Cement, Cem. Concr. Compos. 99 (2019) 17–31. doi:10.1016/j.cemconcomp.2019.02.017.

[170] M. Wu, B. Johannesson, M. Geiker, A review: Self-healing in cementitious materials and engineered cementitious composite as a self-healing material, Constr. Build. Mater. 28 (2012)

571–583. doi:10.1016/j.conbuildmat.2011.08.086.

[171] G. Yildirim, Ö.K. Keskin, S.B.I. Keskin, M. Şahmaran, M. Lachemi, A review of intrinsic self-healing capability of engineered cementitious composites: Recovery of transport and mechanical properties, Constr. Build. Mater. 101 (2015) 10–21. doi:10.1016/j.conbuildmat.2015.10.018.

[172] W. Tang, O. Kardani, H. Cui, Robust evaluation of self-healing efficiency in cementitious materials - A review, Constr. Build. Mater. 81 (2015) 233–247. doi:10.1016/j.conbuildmat.2015.02.054.

[173] K. van Breugel, Is there a market for self-healing cement-based materials?, 1St Int. Conf. Self-Healing Mater. (2007) 1–9.

[174] W. Ramm, M. Biscoping, Autogenous healing and reinforcement corrosion of water-penetrated separation cracks in reinforced concrete, Nucl. Eng. Des. 179 (1998) 191–200. doi:10.1016/S0029-5493(97)00266-5.

[175] H.W. Reinhardt, M. Jooss, Permeability and self-healing of cracked concrete as a function of temperature and crack width, Cem. Concr. Res. 33 (2003) 981–985. doi:10.1016/S0008-8846(02)01099-2.

[176] T.C.S. Reddy, A. Ravitheja, C. Sashidhar, Micromechanical Properties of Self-Healing Concrete with Crystalline Admixture and Silica Fume, ACI Mater. J. 117 (2020) 63–74. doi:10.14359/51722395.

[177] M. Rooij, K. Van Tittelboom, N. De Belie, E. Schlangen, Recovery against Environmental Action, in: RILEM (Ed.), Self-Healing Phenom. Cem. Mater., Springer, 2013: pp. 65–117. doi:10.1007/978-94-007-6624-2.

[178] E.H. Yang, Y. Yang, V.C. Li, Use of high volumes of fly ash to improve ECC mechanical properties and material greenness, ACI Mater. J. 104 (2007) 620–628. doi:10.14359/18966.

[179] S. Wang, V.C. Li, Engineered cementitious composites with high-volume fly ash, ACI Mater. J. 104 (2007) 233–241. doi:10.14359/18668.

[180] P. Termkhajornkit, T. Nawa, Y. Yamashiro, T. Saito, Self-healing ability of fly ash-cement

systems, Cem. Concr. Compos. 31 (2009) 195–203. doi:10.1016/j.cemconcomp.2008.12.009.

[181] Z. Zhang, S. Qian, H. Ma, Investigating mechanical properties and self-healing behavior of micro-cracked ECC with different volume of fly ash, Constr. Build. Mater. 52 (2014) 17–23. doi:10.1016/j.conbuildmat.2013.11.001.

[182] G. Li, S. Liu, M. Niu, Q. Liu, X. Yang, M. Deng, Effect of granulated blast furnace slag on the self-healing capability of mortar incorporating crystalline admixture, Constr. Build. Mater. 239 (2020) 117818. doi:10.1016/j.conbuildmat.2019.117818.

[183] M. Roig-Flores, F. Pirritano, P. Serna, L. Ferrara, Effect of crystalline admixtures on the self-healing capability of early-age concrete studied by means of permeability and crack closing tests, Constr. Build. Mater. 114 (2016) 447–457. doi:10.1016/j.conbuildmat.2016.03.196.

[184] H. Huang, G. Ye, C. Qian, E. Schlangen, Self-healing in cementitious materials: Materials, methods and service conditions, Mater. Des. 92 (2016) 499–511. doi:10.1016/j.matdes.2015.12.091.

[185] J.Y. Wang, H. Soens, W. Verstraete, N. De Belie, Self-healing concrete by use of microencapsulated bacterial spores, Cem. Concr. Res. 56 (2014) 139–152. doi:10.1016/j.cemconres.2013.11.009.

[186] J. Wang, K. Van Tittelboom, N. De Belie, W. Verstraete, Use of silica gel or polyurethane immobilized bacteria for self-healing concrete, Constr. Build. Mater. 26 (2012) 532–540. doi:10.1016/j.conbuildmat.2011.06.054.

[187] W. Khaliq, M.B. Ehsan, Crack healing in concrete using various bio influenced self-healing techniques, Constr. Build. Mater. 102 (2016) 349–357. doi:10.1016/j.conbuildmat.2015.11.006.

[188] R. Siddique, K. Singh, P. Kunal, M. Singh, V. Corinaldesi, A. Rajor, Properties of bacterial rice husk ash concrete, Constr. Build. Mater. 121 (2016) 112–119. doi:10.1016/j.conbuildmat.2016.05.146.

[189] Y. Zhang, H.X. Guo, X.H. Cheng, Role of calcium sources in the strength and microstructure of microbial mortar, Constr. Build. Mater. 77 (2015) 160–167.

doi:10.1016/j.conbuildmat.2014.12.040.

[190] R. Andalib, M.Z. Abd Majid, M.W. Hussin, M. Ponraj, A. Keyvanfar, J. Mirza, H.S. Lee, Optimum concentration of Bacillus megaterium for strengthening structural concrete, Constr. Build. Mater. 118 (2016) 180–193. doi:10.1016/j.conbuildmat.2016.04.142.

[191] N. Chahal, R. Siddique, A. Rajor, Influence of bacteria on the compressive strength, water absorption and rapid chloride permeability of concrete incorporating silica fume, Constr. Build. Mater. 37 (2012) 645–651. doi:10.1016/j.conbuildmat.2012.07.029.

[192] W. De Muynck, K. Cox, N. De Belie, W. Verstraete, Bacterial carbonate precipitation as an alternative surface treatment for concrete, Constr. Build. Mater. 22 (2008) 875–885. doi:10.1016/j.conbuildmat.2006.12.011.

[193] T.C.S. Reddy, A. Ravitheja, Macro mechanical properties of self healing concrete with crystalline admixture under different environments, Ain Shams Eng. J. 10 (2019) 23–32. doi:10.1016/j.asej.2018.01.005.

[194] C. Zhang, L. Sorelli, B. Fournier, J. Duchesne, J. Bastien, Z. Chen, Stress-relaxation of crystalline alkali-silica reaction products: Characterization by micro- and nanoindentation and simplified modeling, Constr. Build. Mater. 148 (2017) 455–464. doi:10.1016/j.conbuildmat.2017.05.069.

[195] A. Ravitheja, T.C.S. Reddy, C. Sashidhar, Self-healing concrete with crystalline admixture - A review, J. Wuhan Univ. Technol. - Mater. SCi. Ed. 34 (2019) 1143–1154. doi:10.1088/1757-899X/660/1/012057.

[196] L. Ferrara, V. Krelani, M. Carsana, A “fracture testing” based approach to assess crack healing of concrete with and without crystalline admixtures, Constr. Build. Mater. 68 (2014) 535–551. doi:10.1016/j.conbuildmat.2014.07.008.

[197] A.C. 212, Report on Chemical Admixtures for concrete, American Concrete Institute, 2010.

[198] B. Park, Y.C. Choi, Self-healing capability of cementitious materials with crystalline admixtures and super absorbent polymers (SAPs), Constr. Build. Mater. 189 (2018) 1054–1066.

doi:10.1016/j.conbuildmat.2018.09.061.

[199] G. Li, X. Huang, J. Lin, X. Jiang, X. Zhang, Activated chemicals of cementitious capillary crystalline waterproofing materials and their self-healing behaviour, Constr. Build. Mater. 200 (2019) 36–45. doi:10.1016/j.conbuildmat.2018.12.093.

[200] M.J. Al-Kheetan, M.M. Rahman, D.A. Chamberlain, Moisture evaluation of concrete pavement treated with hydrophobic surface impregnants, Int. J. Pavement Eng. 21 (2020) 1746–1754. doi:10.1080/10298436.2019.1567917.

[201] R. Al-Rashed, M. Jabari, Dual-crystallization waterproofing technology for topical treatment of concrete, Case Stud. Constr. Mater. 13 (2020) e00408. doi:10.1016/j.cscm.2020.e00408.

[202] R. Al-Rashed, M. Al-Jabari, Concrete protection by combined hygroscopic and hydrophilic crystallization waterproofing applied to fresh concrete, Case Stud. Constr. Mater. 15 (2021) e00635. doi:10.1016/j.cscm.2021.e00635.

Chapter Three: Problem statement, current gaps, and objectives of the study.

Alkali-aggregate reaction (AAR) is one of the main processes affecting the durability of concrete infrastructure in Canada and worldwide. Over the years, several approaches and recommendations, including a comprehensive variety of laboratory test procedures, have been developed around the world to assess the potential alkali-reactivity of concrete aggregates and the effectiveness of preventive measures (i.e. control of the cement & concrete alkali content, use of supplementary cementing materials, etc.) before their use in the field.

A number of engineers and researchers worldwide have been trying to develop mitigation & rehabilitation measures in the laboratory and in the field in order to avoid, cease or, at least, mitigate AAR-induced development. It has been shown that expansion & distress due to AAR could be avoided or reduced (chemically) by the appropriate use of supplementary cementing materials (SCMs). Many laboratory studies have confirmed this efficiency. However, new studies are now finding that the deterioration is only delayed and not entirely prevented. Moreover, it has been recently reported that some of the current standardized test methods used to determine the efficiency of SCMs in avoiding/mitigating AAR are not entirely reliable when compared to exposed field concrete structures.

The longer the concrete field exposure time, the lower the correlation with laboratory test methods. Otherwise, once AAR starts in the field, there is no “universal” solution that should be applied in various cases, and each situation should be evaluated as “unique”. Thus, various types of treatments, especially aiming to “physically” stop/reduce the ingress of moisture and/or to provide confinement of the affected members. Multiple types of wrapping, coating and/or waterproofing materials have been used with more or less limited success. Although a number of contradictory data were also obtained, since the presence of cracks generally provides a point of entry for moisture and other aggressive agents, their effectiveness is reduced over time, which reflects the current lack of consensus in the area.

Furthermore, it has been verified that some products (i.e., using different types of bacteria or crystalline admixtures) are able to provide concrete with self-healing properties, which may present a very interesting “physical” solution for durability-related distress in concrete, especially AAR. Yet, no data are available considering the effectiveness of such products for mitigating/rehabilitating AAR-affected concrete, and some doubts remain regarding their ability to recover concrete integrity. Furthermore, the

use of self-healing products with the presence of SCMs forming a binary chemical-physical treatment is absent in available literature, leaving room for major developments in this area.

Based on the gaps in the current available literature, this PhD thesis is designed to meet the following objectives:

- Understanding of the efficiency of natural and engineered triggering self-healing agents in ordinary concrete mixtures through the use of multi-level techniques (i.e., mechanical and microscopical procedures).
- Understanding the influence of natural healing processes in concrete affected by ASR
- Evaluate the combination of different types of supplementary cementing materials (SCMs) and crystalline admixtures to enhance the healing properties of concrete and prevent and/or mitigate (i.e. physically, chemically or both) concrete deterioration caused by AAR;
- Evaluate different surface treatments and techniques (i.e. water repellent, rigid coating based, lithium-based products, cementitious based systems with self-healing products, etc.) to stop, delay and/or mitigate AAR development in its initial, moderate and advanced phases.
- Propose a framework for the optimized selection of raw materials and surface treatments to avoid and/or mitigate ASR-induced development in concrete.

Chapter Four: Research Program.

The comprehensive experimental program developed in this research is divided in two main parts: 1) testing performed on new laboratory-made concrete specimens (Figure 4.1), and 2) testing conducted on aging laboratory-made concrete specimens (Figure 4.2).

4.1 Experimental procedures, part 1: new laboratory-made concrete specimens

In the first part of the Ph.D. project, a conventional Portland cement, four different types of supplementary cementing materials, four commercially available hydrophilic permeability reducer admixtures (i.e., crystalline admixtures – CA), four chemically modified versions of CA, lithium nitrate, nano-silica, and five different reactive aggregate types/natures (i.e., coarse and fine reactive aggregates) were selected for this study to manufacture distinct concrete mixtures. The coarse aggregates ranged from 5 to 20 mm in size. Non-reactive fine and coarse aggregates were combined with the reactive aggregate materials for concrete manufacturing.

Concrete cylinders with100 by 200 mm in size, were investigated in this study. Considering the huge amount of different concrete mixtures, they are only presented in the scientific papers. Yet, they were mix-proportioned as per ASTM C1293 to present the same water to binder ratio (w/b of 0.45) and amount of binder materials (420 ± 10 kg/m^3). However, adjustments were made in the volume of non-reactive aggregates to maintain the volume of reactive aggregate constant in all mixtures, since the replacement of PC with the SCMs modified the total volume of binder paste. The amounts of $LiNO_3$, NS, and crystalline admixtures were fixed as per the manufacturers' recommendation and according to what is used in field applications. The amounts of SCMs selected in this study were quite variable and relied upon each type of SCMs used; yet, in general a minimum of two different percentages of each type of SCMs were selected. All characteristics of the aggregates and concrete mixtures used in this PhD are presented in the six scientific papers of the thesis. The specimens were then divided into two streams of evaluation: i.e, evaluation of the self-healing without reactive aggregate and evaluation of the self-healing containing reactive aggregates.

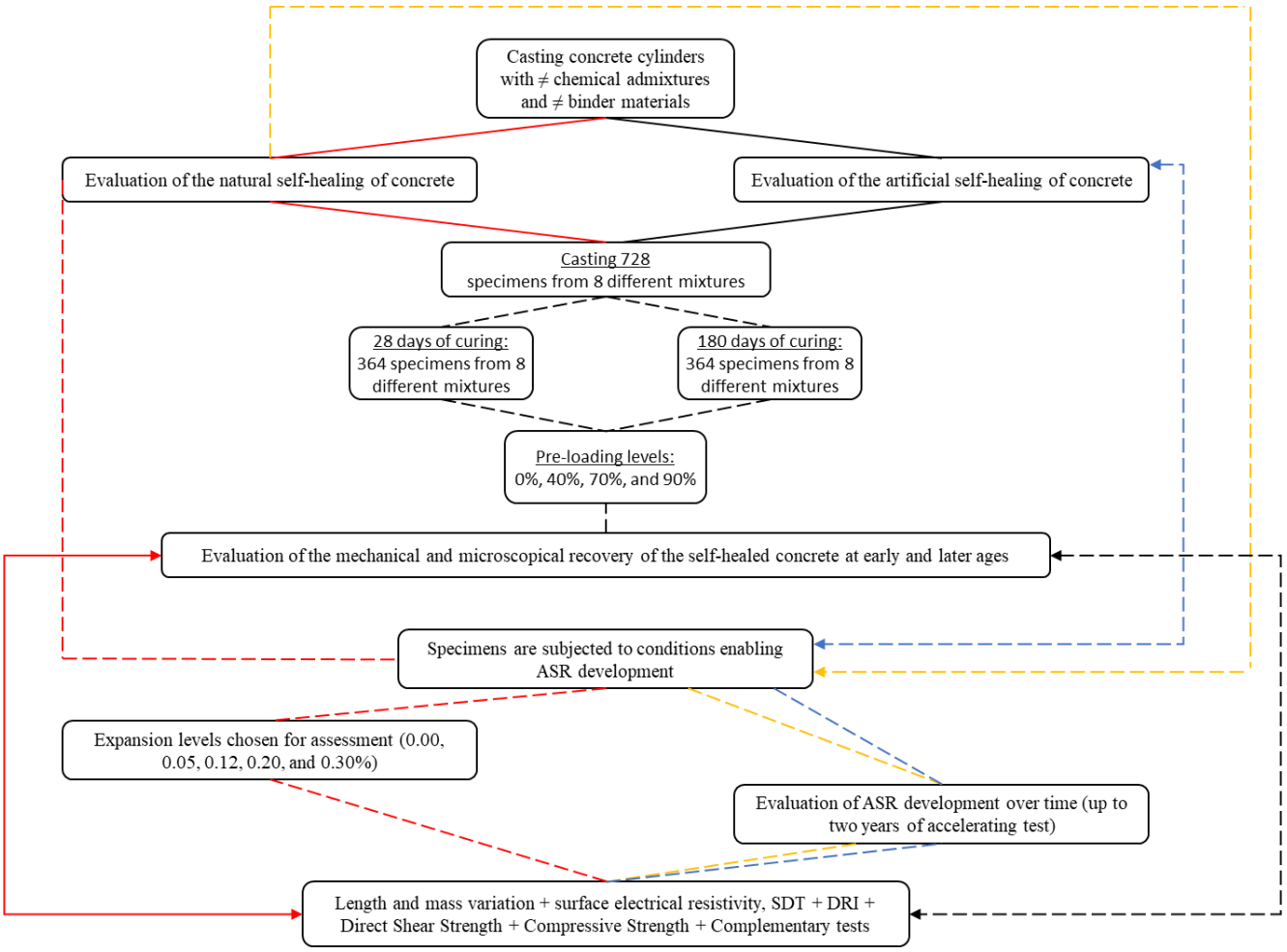

Figure 4.1: Structure of the part one of the Ph.D. project: new laboratory-made concrete specimens

4.1.1 Evaluation of the self-healing without reactive aggregate

Twenty-four hours after casting, the samples were demoulded, separated into two initial curing groups, and placed in a moist curing room at 20°C and 100% RH, where they were left curing for two different periods (i.e., 28 days and 180 days). The goal of splitting the total amount of specimens into two groups was to evaluate the self-healing ability of the concrete mixtures at early and later ages. Therefore, after the first initial curing periods (i.e., 28 days and 180 days), the compressive strength of each concrete mixture was determined. Next, the specimens were divided into four groups of pre-loading levels per mixture (i.e., 0%, 40%, 70% and 90% of their corresponding compressive strength). It is worth mentioning that the loading rate for the pre-loaded samples was the same as used for the compressive strength test (i.e., 0.25 $\pm$ 0.05 MPa/s).

Furthermore, after reaching the pre-determined load, the latter was kept constant for three minutes for better damage development in the samples, then released at the same rate of 0.25 ± 0.05 MPa/s. Afterwards, the specimens were placed back in the moist curing room at 20℃ and 100% RH until 3 (to partially recover the pre-load deformations), 30 and 90 days of the second curing period (self-healing time). Moreover, the specimens were placed in sealed bucked to minimize further carbonation of the samples, even within the controlled chamber. Hereafter, to identify the different initial curing periods and second curing periods in the text, the specimens will be named as, for instance, 28+3, 28+30, 28+90, 180+3, 180+30 and 180+90 days, which 28 and 180 days are the initial curing and 3, 30, and 90 are the periods of second curing after pre-loading.

4.1.2 **Evaluation of the self-healing containing reactive aggregate**

Twenty-four hours after casting, the samples were demoulded and stored in a moist curing room for another 24 h. Then, small holes (5 mm in diameter by 15 mm deep) were drilled at the two flat ends of the samples, in which steel gauge studs were glued in place with a fast-setting cement slurry for longitudinal expansion measurements. Afterwards, the samples were taken for the zero reading, being finally placed in sealed plastic buckets lined with a damp cloth and stored at 38 °C and 100% RH. The AAR-affected cylinders were monitored for length changes over time for a total period of two years. As per ASTM C1293, the buckets were cooled to 23 °C for 16 ± 4 h before the periodic measurements. Finally, to perform each test selected, the samples were prepared according to the test procedure explained in the following section.

4.1.3 **Testing methods**

4.1.3.1 **Non-destructive tests methods (NDTs)**

Two different non-destructive test methods, ultrasonic pulse velocity (UPV) and bulk electrical resistivity (BER) were selected for this study to assess the inner “quality” of the sound and damaged concrete. Both NDTs’ measurements were performed on six 100 by 200 mm cylinders per group of mixtures at the ages of 1, 3, 7, 14, 28, 90 and 180 days; then, in three samples for each of the period evaluated, 28+3, 28+30, 28+90, 180+3, 180+30 and 180+90 days and each pre-load level (i.e., 0%, 40%, 70% and 90%). All cylinders were removed one by one from the moist curing room and tested at the saturated surface dry condition at 20 ± 3 °C.

A commercially available two-probe BER meter was employed in this study, and the test was performed following the ASTM C1876. An alternating current was applied at a fixed frequency of 1 kHz through the concrete specimen. It is worth mentioning that to ensure a proper electrical connection between the two circular stainless-steel plates electrodes and the concrete samples, two moist sponges were added at the interface concrete-electrodes. The UPV was obtained using direct transmission according to ASTM C597, and the equipment used was the portable ultrasonic non-destructive digital indicating tester (PUNDIT). A viscoelastic gel was applied between both transducers and the specimen to achieve a good connection; a frequency of 54 kHz was fixed.

4.1.3.2 **Porosity**

The porosity of the concrete samples was evaluated according to the Archimedes immersion method at each of the six periods (i.e., 28+3, 28+30, 28+90, 180+3, 180+30, and 180+90 days). First, the concrete cylinders selected for the porosity test were cut in half longitudinally using a diamond-bladed masonry saw. One-half of the specimens were then separated for the DRI test. The remaining half of the samples were next cut back (perpendicularly to the first cut) into three similar slices (i.e., about 40 mm high). Afterwards, the sliced samples were dried at 60℃ for ten days and weighed to obtain their dry mass (M_D). Next, the samples were fully immersed in water under the constant pressure of 28-30Hg for twenty-four hours and then wiped to remove their surface moisture and weighted in a high precision scale to record their wet mass (M_{SSD}).

4.1.3.3 **Stiffness Damage Test (SDT)**

Concrete specimens were subjected to five cycles of loading/unloading at a controlled loading rate of 0.10 MPa/s. The SDT procedure was performed using a loading level corresponding to 40% of the non-damaged 28-day compressive strength. The results presented in this work (i.e., stiffness damage index and modulus of elasticity) average three concrete specimens from the same mix at a given age.

4.1.3.4 **Compressive Strength (CS)**

Compressive strength was measured through two different approaches with different and specific goals. First, to characterize all mixtures at 28, 56, 90, and 180 days, the samples were wrapped and placed at 12 °C, since some of the specimens contained highly reactive aggregates and ASTM C39 method could not be followed as they could develop some AAR. Cylinders of all mixtures were maintained at 12 °C

for 47-, 93-, 150- and 300-days periods (maturity equivalent to 28, 56, 90 and 180 days, respectively), according to the maturity concept as by ASTM C 1074. Moreover, it is worth noting that no strength gain was observed after 300 days under the above storage conditions. Thus, the compressive strength of sound concrete after 360 and 720 days were considered as the values measured at 180 days. Likewise, to determine the SDT loading level, the 40% of CS used were the values obtained at each specific age of the concrete (i.e., 90 and 180, while for 360 and 720, it was considered the CS found at 180 days). Second, the compressive strength measurements were carried out on two specimens from each concrete mixture after being subjected to SDT to verify the compressive strength loss of the material as ASR develops. This procedure was adopted and considered valid as largely non-destructive character of the SDT.

4.1.3.5 **Damage Rate Index (DRI)**

The DRI was conducted on one specimen from each concrete mixture at the 6 time periods (28+3, 28+30, 28+90, 180+3, 180+30 and 180+90 days). The remaining half of the samples from the porosity test were polished with grits of 30, 60, 140, 280(80–100 µm), 600 (20–40 µm), 1200 (10–20 µm) and 3000 (4–8µm) and 1cm^2 grids were drawn on the surface of the polished sections. Then a stereomicroscope (16× magnification) was used to perform the test. The DRI final number presented hereafter is the normalized 100 cm^2 value.

4.2 **Experimental procedures, part 2: aging laboratory-made concrete specimens**

In the second part of the Ph.D., a conventional Portland cement and two different reactive aggregate types/natures (i.e., coarse and fine reactive aggregates) were selected for this study to manufacture distinct concrete mixtures. The coarse aggregates ranged from 5 to 20 mm in size. Non-reactive fine and coarse aggregates were combined with the reactive aggregate materials for concrete manufacturing.

A total of one thousand, three hundred and twenty concrete specimens (sixty samples per each of the twenty-two groups of surface treatment), 100 by 200 mm in size, were investigated in this study. The two concrete mixtures were mix-proportioned as per ASTM C1293 to present the same water to binder ratio (w/b of 0.45) and amount of binder materials (420 kg/m^3).

Twenty-four hours after casting, the samples were demoulded, and small holes (5 mm in diameter by 15 mm deep) were drilled at the two flat ends of the samples, in which steel gauge studs were glued in

place with a fast-setting cement slurry for longitudinal expansion measurements. Afterwards, the specimens were left to harden at 20 °C and 100% RH over 24 hours (totalizing 2 days after casting) before the zero reading was taken. Next, one hundred and thirty-two specimens per mixture were randomly selected and separated for surface treatment and application of coating materials, as described in the following section. The remaining samples were finally placed in sealed plastic buckets lined with a damp cloth and stored at 38 °C and 100% RH. The specimens were monitored for length variations until they reached different expansion levels (i.e., 0.05%, 0.12%, 0.20% and 0.30%). As per ASTM C1293, the buckets were cooled down to 23 °C for 16 ± 4 h before the periodic measurements. Then, when the cylinders reached the specified expansion levels, they were taken for surface treatment and further application of coating materials.

4.2.1 **Surface treatment and coating materials**

It is worth noting that the application of coated materials requires a surface treatment of concrete for better adherence and achieve better performance. The overall surface treatment used in this study can be divided into three main steps: a) surface preparation, b) drying the specimens, c) coating application. The first two were implemented on all specimens, even for control specimens in which the coating materials were applied. The third was determined accordingly with the specification of each material used. After achieving the pre-determined expansion levels, i.e., 0.00%, 0.05%, 0.12%, 0.20% and 0.30%, twelve specimens per group of coating materials and for each concrete mixture were taken and fully wrapped with sponges saturated with a low acid solution (98% of distilled water and 2% of acetic acid) for 24 hours at 12 ^{o}C. It is important to mention that to avoid further evaporation and changes in acid concentration, the covered specimens were also wrapped in plastic film and placed in sealed buckets. Next, the specimens were unwrapped, and the surface was gently scrubbed with a wire bristle brush to increase rugosity and enhance the adherence of the coating materials, then cleaned with a nylon brush and water. Afterwards, the samples were placed at 12 ^{o}C, and 60% RH yet kept unwrapped out of the sealed buckets for 120 hours.

The coating mixtures were then applied following each specification of the commercially available materials and following what is used in field applications. Just before applying the coating materials, clear water was gently spayed at the surface of the concrete specimens to improve adherence. Finally, the specimens were placed back in sealed buckets and left for 14 days at 12 ^{o}C and 60% RH for hardening purposes and to provide a surface with stable hydrophobic character. Afterwards, the

specimens were stored at 38 °C and 100% RH. As per ASTM C1293, the buckets were cooled down to 23 °C for 16 ± 4 h prior to the periodic length measurements (i.e., 45, 90, 180, 360, and 720 days). Moreover, mechanical and microscopical tests were performed at 360 and 720 days as per section 4.1.3.

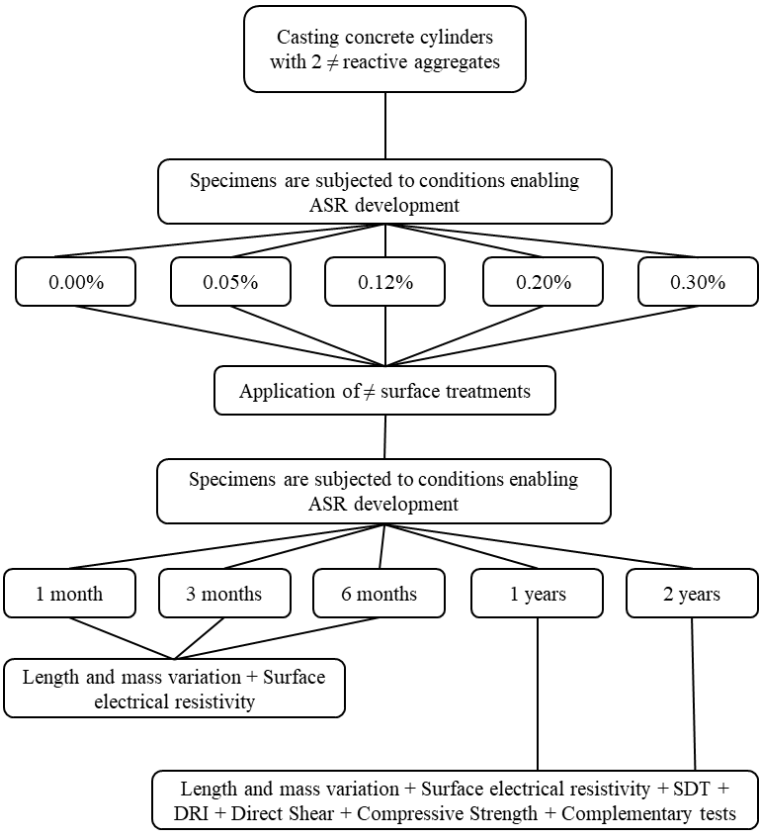

Figure 4.2: Structure of the part two of the Ph.D. project: aging laboratory-made concrete specimens

5.1 Introduction

In order to report and evaluate the results obtained as part of the experimental program implemented in this Ph.D. project, five scientific papers were strategically prepared. They cover all the major themes of the research, thus enabling them to meet the distinct objectives of the Ph.D. project. Figure 5.1 illustrates the links between the papers.

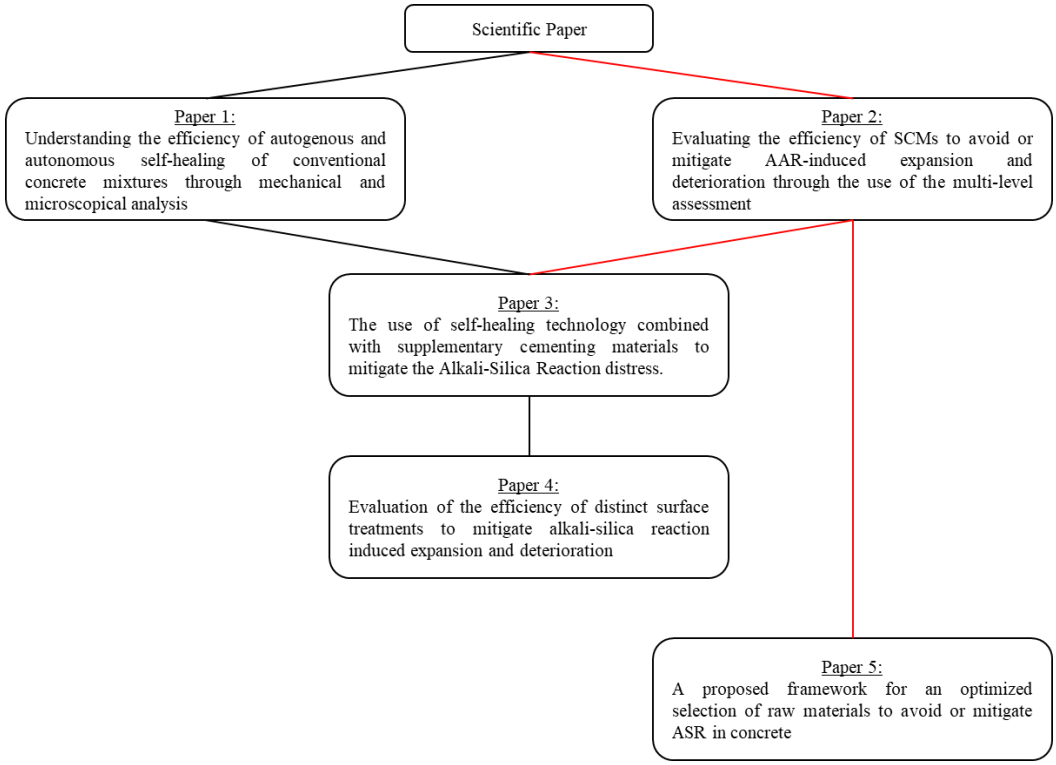

Figure 5.1: Core of the Ph.D. Thesis – links between the scientific papers.

Paper 1 is focuses on understanding the efficiency of autogenous and autonomous self-healing of conventional concrete mixtures through mechanical and microscopical analysis. To achieve this goal, a commercially available crystalline admixture, different types of supplementary cementing materials, and chemically modified versions of CA were combined with Portland cement to proportioned distinct concrete mixtures. With the intriguing results obtained in paper 1 regarding the efficiency of SCMs to enhance the natural self-healing of the concrete, paper 2 displays the results of a multi-level assessment

conducted to appraise AAR damage evolution in SCMs-made concrete specimens as a function of induced expansion (i.e., 0.00%, 0.05%, 0.12%, 0.20% and 0.30%).

The promising data gathered in papers 1 and 2 motivated the extensive analysis on the use of self-healing technology combined with SCMs to mitigate ASR-induced deterioration in new concrete (paper 3). Furthermore, paper 4 appraises the ability of waterproofing self-healing coating mixtures to mitigate concrete deterioration caused by ASR in its initial, moderate and advanced phases. Therefore, qualitative charts were proposed to provide engineers with better "decision making" through a more convenient selection of coating and sealers and the most appropriate "timing" to apply them in ASR-affected concrete.

Paper 5 proposes a framework for optimizing binder materials towards the prevention and/or mitigation of ASR in concrete. This new "approach" is based on selecting the blended binder materials as per their combined chemical compositions using the ternary main oxides plot.

Chapter Six: Understanding the efficiency of autogenous and autonomous self-healing of conventional concrete mixtures through mechanical and microscopical analysis

Diego J. De Souza[1], Leandro F. M. Sanchez[1]

[1]Department of Civil Engineering, University of Ottawa, Ottawa, Canada.

Abstract

Concrete is one of the most used construction materials worldwide, yet it is constantly vulnerable to cracking formation, keeping the need for maintenance, repair, and rehabilitation considerably high. In this regard, cementing materials that can autogenously counter the effects of cracking by self-healing became a topic of significant interest in civil engineering. Thus, this research aims to understand the efficiency of autogenous and autonomous self-healing in concrete specimens through mechanical and microscopical analysis. To achieve this goal, a commercially available crystalline admixture (CA), different types of supplementary cementing materials, and chemically modified versions of CA were combined with Portland cement to proportioned distinct concrete mixtures. In which were pre-loaded and damaged at 28 and 180, the specimens were then evaluated over 90 days of curing through non-destructive (i.e., bulk electrical resistivity and ultrasonic pulse velocity), porosity, microscopic (i.e., Damage Rating Index and Scanning Electron Microscopy), mechanical (i.e., Stiffness Damage Test, modulus of elasticity, compressive strength), and micro-indentation analyses. The results indicate that SCMs significantly enhanced the natural healing of concrete. Yet, mixtures to which CA was added demonstrated the highest healing ratios, indicating promising recovery of the mechanical properties.

Keywords: Crystalline Admixtures, Self-Healing, Supplementary Cementing Materials

6.1 Introduction

Concrete is the most common construction material used in critical infrastructure worldwide. The lifespan of reinforced concrete structures varies according to the structure type and purpose, yet 50 to 70 years are often targeted according to distinct standards [1]. When properly fabricated, placed and cured, concrete can be durable under most natural and industrial environments. However, while predictable and partially avoidable, cracks will inevitably exist in concrete [2–4]. Furthermore, in more critical and advanced phases, they can work as easy paths for the ingress of harmful substances, potentially affecting the durability of reinforced concrete, decreasing its mechanical properties and service life [5–8]. This scenario indicates the need to rehabilitate aging concrete infrastructure displaying visible deterioration signs (i.e., crack networks).

The costs related to human intervention in critical infrastructure have already become a significant field of interest [9,10]. Nevertheless, the implementation of continuous inspections and maintenance protocols is quite complex, especially in the case of large concrete structures, where considerable amounts of labour and funds are often required. To illustrate this situation, the U.S. Department of Transportation reports that a budget between $78 billion to $112 billion is estimated to address all structural and functional bridges' deficiencies in the United States [11]. Therefore, preventive measures to preserve and improve the service life without onerous labour and capital requirements are highly desirable. In this regard, the development and use of cementing materials to autogenously counteract the effects of cracking, the so-called self-healing (SH) products, became a topic of significant interest in civil engineering and concrete technology [12–15].

Several studies have been conducted to understand the global self-healing of cement-based materials [16–18] in the past decade. It is somewhat known that concrete can naturally/autogenously self-heal cracks. However, although promising results can be observed when concrete is designed with high cement content, lower water to cement ratios and/or with supplementary cementing materials (SCMs) [19–21], autogenous healing has quite limited capacity on conventional concrete. Therefore, artificial/autonomous triggering healing agents, such as microencapsulated bacteria (MB) [22–25] or crystalline admixtures (CA) [13,26–29], have been introduced recently. Besides past studies have shown that MB and CA enhance the recovering of mechanical and durability properties of damaged concrete, the ACI committee [30] has reported that CAs are more reliable since these admixtures are

hydrophilic by nature, increasing the density of the calcium silicate hydrate (CSH), and generating pore-blocking deposits resisting to water penetration.

It has been demonstrated that CA-concrete can significantly decrease the water penetration depth [31], enhance the resistance to chloride penetration [27,29,32] and almost fully recover mechanical properties [20,33,34]. Furthermore, when exposed to high humid conditions or soaked in water-based solutions [13,34,35]; moreover, combining CA with SCMs can reach even more beneficial results [20,32,36]. Yet, most past studies have focused on using high binder contents (≈ 500 kg/m3 or higher), low water to binder ratios (≈ 0.20 – 0.35), fibre-reinforced concrete, or focused on evaluating Portland cement mortars or paste. Hence, to the best knowledge of the authors, there is currently a lack of literature attesting the efficiency of conventional concrete combined with a) commercial CAs, b) chemically modified CA's, and c) commercial CA's combined with distinct SCMs, to recover the material's microstructure quality and engineering properties, which makes room for further developments in this area.

6.2 Background

6.2.1 Self-Healing approach in concrete

6.2.1.1 Autogenous healing

Autogenous crack healing in cementitious materials is a natural process that has already been studied [19,37–40]. The phenomenon takes place through four different main processes: a) formation of calcium carbonate ($CaCO_3$) in concrete; b) continuous hydration of binder grains upon moisture uptake; c) swelling of cement paste; d) sedimentation of solid particles within cracks [27,31,41]. The first two are the most common autogenous healing processes; however, their efficiency significantly changes over time. At earlier ages of the concrete, continued hydration is the dominant mechanism due to the high content of unhydrated cement particles. Yet, calcium carbonate becomes the primary mechanism at later ages and more prolonged environmental exposure [31,42–44]. Moreover, besides being a natural process not easily controlled, autogenous healing properties can be enhanced. It has been demonstrated that pre-damaged concrete can recover, on average, 60% of its mechanical properties (i.e.., compressive strength, flexural strength and stiffness) [40,45–47]. Likewise, significantly decrease concrete permeability and reduce chloride diffusivity [27,29,32], only by

lowering the water-to-binder (w/b) ratio and/or increasing the binder content. Yet, the later measure may raise the cost and carbon footprint of the concrete.

Recently, to achieve greener concrete mixtures and further improve autogenous healing properties, several researchers [19–21,40] reported that the use of supplementary cementing materials (SCMs), partially replacing Portland cement (PC), is crucial. While the slower rate of hydration of blast furnace slag and fly ashes grains may slow early age processes of microstructure and strength developments, their capability to enhance self-healing is significantly higher than Portland cement [21]. It has been demonstrated that concrete made of a high volume of fly ash (i.e., 30% to 60% of PC's replacement) can recover 70% of the strength loss while reducing about 75% chloride diffusion after pre-cracking [19,48–51]. Moreover, combining two different techniques (e.g., selective dissolution and XRD-Rietveld analysis), Termkhajornkit et al. [50] calculated the total amount of C-S-H gel produced after 28 days of curing. The results show that replacing 50% of PC by fly ash class F had 560% more C-S-H between 28 days and 364 days; this indicates later healing enhancement. Likewise, concrete made of blast furnace slag was found to heal 70% of cracks with widths until 200 µm and recover up to 80% of its compressive strength loss [21,36]. On the other hand, high volumes of SCMs may reduce the calcite precipitation process of healing [21,41,51] due to the lower calcium carbonate formed in SCM-made concrete [21]. Overall, when the continued hydration is the primary healing mechanism, SCMs play an important role in the process; however, it is limited to self-seal cracks with width up to 250 µm, on average.

6.2.1.2 **Autonomous healing by using crystalline admixtures (CA)**

Autonomous or engineered healing can be further divided into "passive" or "active" modes. Activating the healing process by human intervention is considered an "active" mode, while the process without such an intervention is defined as "passive" [35]. One of the smartest materials used for self-healing applications in concrete is the so-called crystalline admixtures (CA); these are permeability-reducing admixtures with a hydrophilic nature that easily react with water and can effectively serve as well self-healing engineered admixtures [30]. Moreover, the chemical reaction between CA, PC and water forms water-insoluble cracking deposits, increasing the density of calcium silicate hydrate (C-S-H), resulting in a more impermeable and resistant system against aggressive substances [12,13,20,26–29,34,35,52,53]. Furthermore, the reaction can also undergo a delayed activation whenever the material

comes into contact with water and/or environmental moisture, which enhances the healing process at later ages [33].

In early 2010's, one of the pioneering research on the use of CA, Sisomphon and co-workers [26] demonstrated that adding 1.5% and 4% (by PC mass) of CA in cement paste mixtures, cracks with widths ranging from 250 to 400 μm were closed entirely. Moreover, the healed paste specimens were demonstrated to be impermeable after 28 days of pre-induced cracking, and calcium carbonate was the primary product found in the sealed cracks. Likewise, studies suggest that CA-concrete can achieve healing ratios of 0.98, for cracks up to 400 μm, after 42 days of curing [35]; complete sealing of cracks thinner than 300 μm [27]; 95% of strength regaining capacity [34]; and 50% lower water penetration, 30% lower chloride diffusivity and healing ratios close to 1.0 [31]. Moreover, it has been recently demonstrated that the combination of CA and SCMs (e.g., Blast Furnace Slag [36], fly ash [12,20,35,54] and silica fume [32]) could even reach higher values of self-healing ratios. Yet, overall, their efficiency lies between 90% to 105% depending on the exposure conditions [20]. It is worth mentioning that there is a relative agreement in the literature that cementitious materials soaked in water solutions tend to achieved higher self-healing ratios and faster healing rates, followed by wetting/drying cycles, water contact and air exposure conditions, respectively [14,19,20,27,31–33,35].

Different technics and methodologies have been proposed to better understand the autonomous healing and mechanical recovery, such as, water permeability test [13,28,35,54], gas permeability [55], Flexural strength recovery [15,28,33], splitting tensile strength [12], compressive strength [12,33], ultrasonic pulse velocity [16,17,19,33], electrical resistivity [17,31,32] and rapid chloride diffusivity [19,31,51]. Among them, permeability tests, electrical resistivity, and rapid chloride diffusivity as durability parameters revealed the most promising results. However, the load and damage recovery (calculated from flexural stiffness values) indicate suitable trends to evaluate self-healing efficiency [33]. Finally, it can be addressed that measuring the self-healing efficiency of concrete is not standardized. There are still some lacks in the literature, such as adequate procedures to measure the rate of self-healing, influence on the length of the crack, reports attesting the dynamic of crack healing versus concrete age, and quantitative data of the mechanical properties of the deposited material within the crack. Moreover, enriching the importance of using different tools and techniques to understand the mechanical response of self-healed conventional concrete mixtures.

6.2.2 **Tools for damage assessment**

6.2.2.1 **Stiffness Damage Test (SDT)**

The SDT was first developed by Walsh (1965) for assessing rock specimens [56], who detected an interesting correlation between the inner crack density and the cycles of loading/unloading (stress/strain relationship) of rock specimens. Afterwards, the method was modified and adapted to quantify the distress degree of concrete affected by alkali-silica reaction (ASR). It initially consisted of applying five compression cycles (loading/unloading) using a fixed stress level of 5,5MPa [57,58]. Later, Smaoui et al. [59] increased the fixed stress level to 10MPa to improve the diagnostic character of the procedure. Finally, Sanchez et al. [60–62] continued the works from [59] and performed comprehensive research (i.e., using a wide variety of concrete strengths and reactive aggregate types) on the use of SDT for assessing damage in concrete affected by ASR and also by other internal swelling reactions (ISR). Details on the procedure developments and specific/practical considerations on its application as a diagnostic tool can be found in [60–62]. Briefly, after careful evaluation of the test outcomes, it has been verified that the SDT needs to be performed at 40% of the material's compressive strength. Moreover, the method was found quite promising for appraising AAR (and ISR) damage in concrete, especially when indices are used as the test outcomes, namely *Stiffness Damage Index (SDI)* and *Plastic Deformation Index (PDI)*, which represent respectively the ratio of dissipated energy/plastic deformation to the total energy/deformation implemented over the five loading cycles in the system (Figure 2.2). Finally, following the works by Chrisp and co-workers [57], it was confirmed that the *Non-Linearity Index* (NLI; Sec 1/Sec 2 in the first cycle and the average Sec1/Sec2 value of the last four cycles – Figure 2.2) was also an interesting outcome to be considered, especially while studying inner cracks orientation.

a)

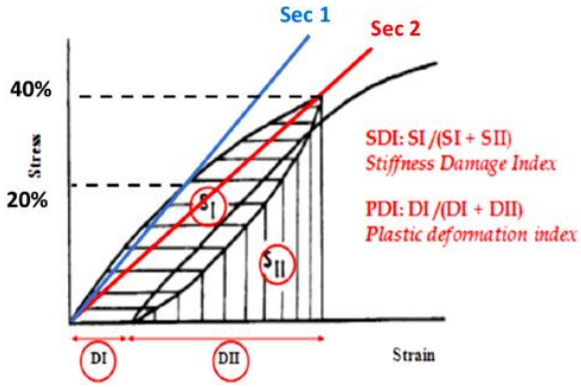

b)

Figure 6.1: a) Test setup for stiffness damage test; and b) Calculation of the stiffness damage index (SDI) and Plastic Deformation (PDI) [63].

6.2.2.2 Damage Rating Index (DRI)

The DRI is a petrographic analysis performed with the use of a stereomicroscope (15–16× magnification) where damage features generally associated with ASR or ISR are counted through a 1 cm^2 grid (i.e., 10 × 10 mm units) drawn on the surface of polished concrete sections [64]. The number of counts corresponding to each type of petrographic feature is then multiplied by weighting factors, whose purpose is to balance their relative importance towards the mechanism of distress under consideration, for instance, ASR [64]. The factors used in the method were selected logically but relatively arbitrarily; they were recently modified to reduce the variability between the petrographers performing the test [65]. Ideally, a surface of at least 200 cm^2 should be used for DRI analysis, and it may be more significant in the case of mass concrete incorporating larger aggregate particles. However, the final DRI value is normalized to a 100 cm^2 area [66]. The goal of DRI is to appraise the damage degree or extent of affected concrete, complementing conventional petrographic analysis whose main purpose is to detect the cause of the deterioration. Furthermore, presenting a direct correlation with expansion level, a damage scale to distinguish low, moderate, and high damage levels caused by ASR were proposed by Sanchez et al. [60,64]. Yet, similar results were presented by [67,68] with concreted cores extracted from ASR-affected structures.

6.3 Scope of the work

As previously stated, there is currently a need for a thorough, quantitative, and systematic study on the impact of autogenous and autonomous healing processes on conventional concrete. This work presents the results of a multi-level evaluation comparing mechanical and microscopical properties recovery of early (28 days) and later (180 days) deterioration in conventional concrete. Portland cement Type 1 in combination with a commercially available crystalline admixture (CA), different types of supplementary cementing materials (i.e., fly ash and silica fume), and chemically modified versions of CA (as described in section 4) were used to fabricate concrete specimens. The specimens were stored in a moist-curing chamber (i.e., 20℃ and 100% RH) for 28 and 180 days. The 28 and 180-days compressive strengths were gathered and assumed as the average ultimate capacity of the different concrete mixtures. Then, all the remaining samples were pre-loaded until 90% of their ultimate compressive strength capacity and stored back in 20℃ and 100% RH for 90 days. At selected periods (i.e., 0, 30, and 90 days), non-destructive (i.e., bulk electrical resistivity and ultrasonic pulse velocity), microscopic (i.e., Damage Rating Index), mechanical (i.e., Stiffness Damage Test, modulus of elasticity, compressive strength), micro-indentation, and porosity analyses were conducted on the specimens to evaluate the evolution of deterioration caused by the pre-loading process over time and thus to appraise the self-healing capacity of the distinct mixtures.

6.4 Experimental program

6.4.1 Materials and mix proportioning

A conventional Portland cement (GU type, equivalent to ASTM C150 Type I [69]) and two distinct supplementary cementing materials (i.e. SCMs; fly ash class F - FA and silica fume - SF) were combined with either a commercially available hydrophilic permeability reducer admixture (or Crystalline Admixture – CA) or two chemically modified versions of the CA with the use of metakaolin (MK) and magnesium sulphate (MS). The chemical and physical properties of the selected binder materials are provided in Table 6.1. The particle size distribution (PSD) of the PC, SCMs and CA were obtained through laser diffraction spectroscopy (Figure 6.2). CA displays a coarser PSD (D50 of 56 mm) around 3.7 times rougher than PC (D50 of 15 mm). Moreover, silica fume revealed the lowest D50 among all fine materials (i.e., D50 of 7 mm), while metakaolin presented a similar PSD to

PC, yet slightly lower (i.e., D50 of 14 mm). Otherwise, fly ash particles were, on average, twice coarser than PC (D50 of 31 mm).

Table 6.1: Chemical properties of the Binder materials.

	PC	FA	SF	MK	MS
SiO_2 (%)	20.10	56.31	92.86	52.48	0.12
Al_2O_3 (%)	5.03	23.27	0.05	44.35	0.19
CaO (%)	61.93	10.29	0.62	0.12	1.92
Fe_2O_3 (%)	3.80	3.57	0.12	0.61	0.09
SO_3 (%)	3.38	0.19	0.07	0.04	64.46
MgO (%)	2.42	1.07	0.19	0.08	32.51
Na_2O_{eq} (%)	0.91	3.17	0.52	0.38	0.21
C_3S (%)	43.24	-	-	-	-
C_2S (%)	25.02	-	-	-	-
C_3A (%)	6.90	-	-	-	-
C_4AF (%)	11.56	-	-	-	-
Specific Gravity	3.12	2.01	2.20	2.29	2.61
Lost on Ignition (%)	2.91	0.98	5.05	0.69	1.02

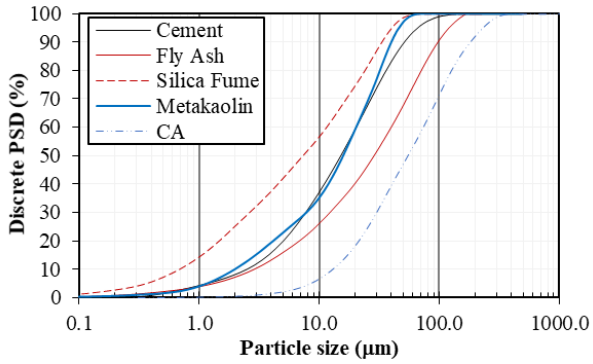

Figure 6.2: Particle size distribution (PSD) of the GU Portland cement, silica fume, fly ash class F, metakaolin and crystalline admixture.

6.4.2 Mixture proportions, curing, sample preparation and exposure conditions

A total of seven hundred and sixty-eight concrete cylinders (ninety-six samples per each of the eight mixtures), 100 by 200 mm in size, were investigated in this study. Table 6.2 summarizes the concrete mix designs employed in this work. It may be noticed that the volume of binder materials, fine and coarse aggregates were kept constants for all mixtures; likewise, the water-to-binder ratio (w/b) of all mixtures was fixed at 0.45, and the CA and its modified versions were added to the mixes. The amount of CA (and its modified versions, i.e., CA2- CA + MK and CA3 - CA + coarse MK + MS) was selected as per the manufacturer's recommendation, following the conventional amounts typically used in field applications. A coarse limestone aggregate ranging from 5 to 20 mm in size, the specific gravity of 2.79

and fine natural aggregate with fineness modulus and specific gravity of 2.79 and 2.67, respectively, were selected for this research.

Table 6.2: Concrete mix proportions.

Mixture	w/b = 0.45		Aggregates (kg/m^3)		Admixtures[a] (kg/m3)			SCMs (kg/m^3)	
	Water (kg/m^3)	Cement (kg/m^3)	Fine	Coarse	CA1	MK	MS	FA	SF
Control	189	420	788	1010	-	-	-	-	-
FA	177	275	788	1010	-	-	-	118	-
SF	186	372	788	1010	-	-	-	-	41
CA1	189	420	788	1010	8	-	-	-	-
CA-FA	177	275	788	1010	8	-	-	118	-
CA-SF	186	372	788	1010	8	-	-	-	41
CA2	189	420	788	1010	6.4	1.6	-	-	-
CA3	189	420	788	1010	6.4	0.8b)	0.8	-	-

[a] MK and MS were considered as part of the chemical admixture once they were used to chemically modify the CA.
[b] For CA3, the metakaolin was sieved and only the fraction above 40 µm was used.

Twenty-four hours after casting, the samples were demoulded, separated into two initial curing groups, and placed in a moist curing room at 20°C and 100% RH, where they were left curing for two different periods (i.e., 28 days and 180 days), as illustrated in Figure 6.3. The goal of splitting the total amount of specimens into two groups was to evaluate the self-healing ability of the concrete mixtures at early and later ages. Therefore, after the first initial curing periods (i.e., 28 days and 180 days), the compressive strength of each concrete mixture was determined. Next, the specimens were divided into four groups of pre-loading levels per mixture (i.e., 0%, 40%, 70% and 90% of their corresponding compressive strength). It is worth mentioning that the loading rate for the pre-loaded samples was the same as used for the compressive strength test (i.e., 0.25 $\pm$ 0.05 MPa/s) [70].

Furthermore, after reaching the pre-determined load, the latter was kept constant for three minutes for better damage development in the samples, then released at the same rate of 0.25 $\pm$ 0.05 MPa/s. Afterwards, the specimens were placed back in the moist curing room at 20°C and 100% RH until 3 (to partially recover the pre-load deformations), 30 and 90 days of the second curing period (self-healing time). Moreover, the specimens were placed in sealed bucked to minimize further carbonation of the samples, even within the controlled chamber. Hereafter, to identify the different initial curing periods and second curing periods in the text, the specimens will be named as, for instance, 28+3, 28+30, 28+90, 180+3, 180+30 and 180+90 days, which 28 and 180 days are the initial curing and 3, 30, and 90

are the periods of second curing after pre-loading. Finally, to perform each test selected, the samples were prepared according to the test procedure explained in the following section.

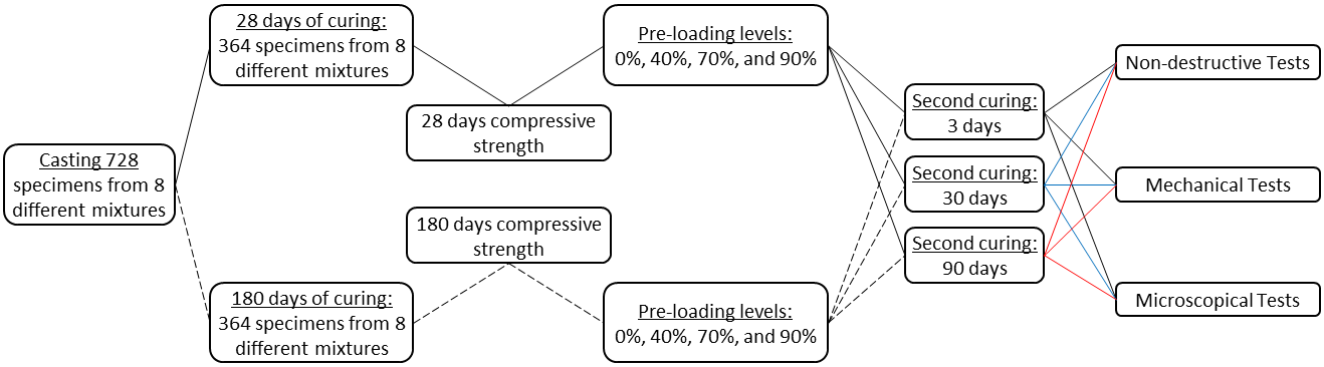

Figure 6.3: Illustration of the overall experimental program developed to multi-level assess the self-healed specimens' physical and mechanical properties recovery.

6.4.3 **Testing methods**

6.4.3.1 **Non-destructive tests methods (NDTs)**

Two different non-destructive test methods, ultrasonic pulse velocity (UPV) and bulk electrical resistivity (BER) were selected for this study to assess the inner "quality" of the sound and damaged concrete. Both NDTs' measurements were performed on six 100 by 200 mm cylinders per group of mixtures at the ages of 1, 3, 7, 14, 28, 90 and 180 days; then, in three samples for each of the period evaluated, 28+3, 28+30, 28+90, 180+3, 180+30 and 180+90 days and each pre-load level (i.e., 0%, 40%, 70% and 90%). All cylinders were removed one by one from the moist curing room and tested at the saturated surface dry condition at 20 ± 3 °C.

A commercially available two-probe BER meter was employed in this study, and the test was performed following the ASTM C1876 [71]. An alternating current was applied at a fixed frequency of 1 kHz through the concrete specimen. It is worth mentioning that to ensure a proper electrical connection between the two circular stainless-steel plates electrodes and the concrete samples, two moist sponges were added at the interface concrete-electrodes. The UPV was obtained using direct transmission according to ASTM C597 [72], and the equipment used was the portable ultrasonic non-destructive digital indicating tester (PUNDIT). A viscoelastic gel was applied between both transducers and the specimen to achieve a good connection; a frequency of 54 kHz was fixed.

6.4.3.2 **Porosity**

The porosity of the concrete samples was evaluated according to the Archimedes immersion method at each of the six periods (i.e., 28+3, 28+30, 28+90, 180+3, 180+30, and 180+90 days). First, the concrete cylinders selected for the porosity test were cut in half longitudinally using a diamond-bladed masonry saw. One-half of the specimens were then separated for the DRI test as per the description presented in 4.1.3.5. The remaining half of the samples were next cut back (perpendicularly to the first cut) into three similar slices (i.e., about 40 mm high). Afterwards, the sliced samples were dried at 60°C for ten days and weighed to obtain their dry mass (M_D). Next, the samples were fully immersed in water under the constant pressure of 28-30Hg for twenty-four hours and then wiped to remove their surface moisture and weighted in a high precision scale to record their wet mass (M_{SSD}). Finally, on a hydrostatic scale, the submerged mass (Ms) was recorded. Thus, the apparent porosity can be calculated through the following Equation 6.1.

$$\boldsymbol{AP} = \frac{M(ssd) - M(d)}{M(ssd) - M(s)} \qquad \textbf{Equation 6.1}$$

6.4.3.3 **Stiffness Damage Test (SDT)**

Concrete specimens were subjected to five cycles of loading/unloading at a controlled loading rate of 0.10 MPa/s. The SDT procedure was performed as per Sanchez et al. [61,62,73], i.e., using a loading level corresponding to 40% of the non-damaged 28-day compressive strength. The results presented in this work (i.e., stiffness damage index and modulus of elasticity) average three concrete specimens from the same mix at a given age.

6.4.3.4 **Compressive Strength (CS)**

At 28 and 180 days after casting, three specimens from each mixture were selected, and the compressive strength was conducted according to ASTM C39 [70] with two different and specific goals. First, to obtain the ultimate capacity of the mixtures designed and to determine the maximum load per pre-load level selected (0%, 40%, 70% and 90%). Second, the compressive strength measurements were performed on three cylinders used for stiffness damage testing after 3, 30 and 90 days from the pre-load application, intending to verify the compressive strength loss/recovery of the

material as a function of the pre-load damage and self-healing activity. The procedure of testing CS after SDT was adopted and considered valid after Sanchez et al. [60,74] confirmed the non-destructive character of the SDT.

6.4.3.5 **Damage Rate Index (DRI)**

The DRI was conducted as per [60,74] on one specimen from each concrete mixture at the 6 time periods (28+3, 28+30, 28+90, 180+3, 180+30 and 180+90 days). The remaining half of the samples from the porosity test were polished with grits of 30, 60, 140, 280(80–100 µm), 600 (20–40 µm), 1200 (10–20 µm) and 3000 (4–8µm) and 1cm^2 grids were drawn on the surface of the polished sections. Then a stereomicroscope (16× magnification) was used to perform the test. The DRI final number presented hereafter is the normalized 100 cm^2 value.

6.5 **Results**

6.5.1 **Non-Destructive tests**

In this section, the results of bulk electrical resistivity (BER) and ultrasonic pulse velocity (UPV) developments over-time are presented for all mixtures manufactured in the laboratory with different binder compositions (i.e., PC, FA, and SF) and using different crystalline admixtures (i.e., CA and the modified versions CA2 and CA3). Figure 6.4 displays the results of BER obtained over 180 days of curing without any pre-load (Figure 6.4a), while Figure 6.4b), c) and d) illustrate the BER variation of the different mixtures over 90 days of healing after pre-load levels of 40%, 70% and 90%, respectively.

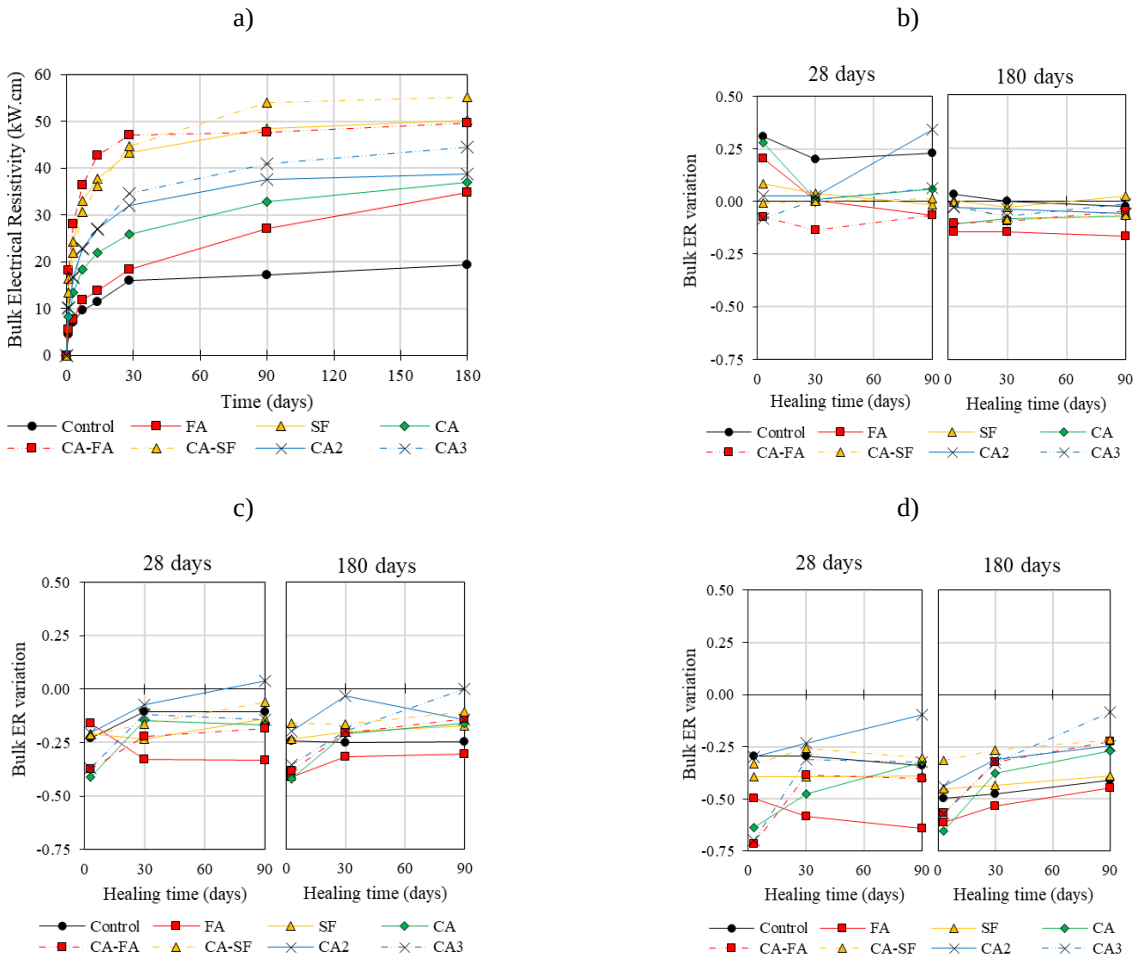

Figure 6.4: Bulk Electrical Resistivity: a) BER of the specimens over 180 days without any pre-load applied; BER evolution of specimen pre-loaded at 28 and 180 days with b) 40% of the total load; c) 70% of the total load; d) 90% of the total load.

Evaluating the data, one observes that replacing the PC with any SCMs or adding the CAs decreases the conductivity of the specimens, increasing the ER (Figure 6.4a). Moreover, samples made of silica fume with (CA-SF) or without CA (SF) and CA-FA showed the highest values (i.e., 55, 50 and 49 kΩ·cm at 180 days of curing, respectively). Among all groups of samples, FA demonstrated the higher BER enhancement between 28 and 180 days of curing, from 18.2 to 34.8 kΩ·cm (improvement of 90.7%), followed by CA and CA3. Thus, increasing the BER by 43.4% and 28.7% between 28 and 180 days of curing.

Overall, the higher the pre-load (PL) level, the higher the BER loss, either at 28 or 180 days of curing. Yet, pre-loading the specimens at 40% of their corresponding CS (Figure 6.4b) did not significantly change the BER. Moreover, the BER variations along the 90 days of healing time (HT) were relatively

"stable" for most mixtures. On the other hand, both pre-load levels of 70% and 90% have averagely decreased BER; besides, the period from 3 to 90 days displays a significant recovery on BER (Figure 6.4c and d) either for PL at 28 or 180 days. The latter is directly affected by the different binder compositions used. Globally, FA mixtures enhanced early and later BER recovery, while concrete made of SF yielded lower recovery than the control mixture. Likewise, the addition of CA, either the commercial formula or modified versions, significantly enhanced BER recovery over the 90 days of healing time, either after pre-loading the specimen at 28 days or 180 days. Finally, the behaviour of the different mixes tested through UPV was quite similar to those measured by BER (Figure 6.5a, b, c and d).

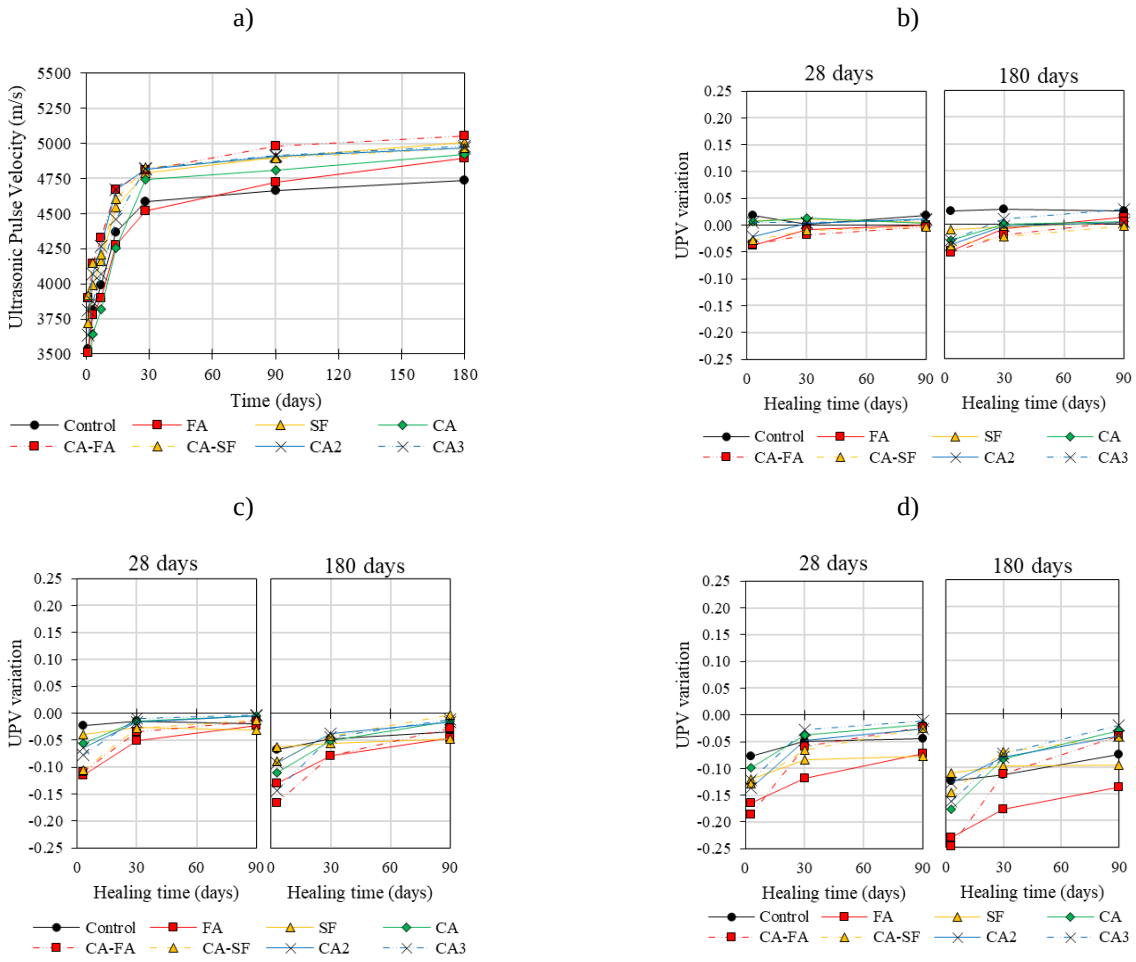

Figure 6.5: Ultrasonic Pulse Velocity: a) UPV of the specimens over 180 days without any pre-load applied; UPV evolution of specimen pre-loaded at 28 and 180 days with b) 40% of the total load; c) 70% of the total load; and d) 90% of the total load.

6.5.2 **Porosity**

Figure 6.6 provides the porosity results measured over 28, 28+30, 28+90, 180, 180+30 and 180+90 days of curing without any pre-load (Figure 6.6a), while Figure 6.6b), c) and d) presents the BER variation of the different mixtures over 90 days of self-healing time after pre-load levels of 40%, 70% and 90%, respectively. Overall, all specimens with no induced damage (Figure 6.6a) displayed a close range of porosity (between 5.1% and 7.3%) over the 180+90 days of curing; moreover, the values of each mixture slightly changed over time. The only exception was the FA mixture, which shows a porosity of 7.3% at 28 days, and a decrease to an average of 5.7% at the end of the evaluated period. The highest average porosity values measured were 6.9% and 6.7%, respectively, for the control and SF mixtures. On the other hand, the combination of crystalline admixtures and SCMs showed the lowest porosity average values (i.e., 5.5% and 5.8% for CA-FA and CA-SF, respectively). It is worth mentioning that applying a pre-load of 40% at 28 and 180 days did not change the trends observed for PL of 0%; yet, the range of variation for the porosity results was between 5.3% and 7.0% (Figure 6.6b), slightly lower than PL of 0% (Figure 6.6a).

Increasing the pre-load level changed the porosity; the higher the PL, the higher the average porosity. In general, PL of 70% increased 28.1% and 36% at 28+3 and 180+3 days, while PL of 90% reached 53.1% and 61.5% higher average values than PL of 0%. Despite that, the self-healing period of 90 days significantly changes the porosity of the concrete specimens at early and later ages. Overall, FA mixtures displayed the highest porosity enhancement over the curing period, while SF, the lowest. However, combining SF with CA significantly improved the healing behaviour (i.e., 42% and 233% for PL of 70% and 90% at 28 days; 450% and 94% for PL of 70% and 90% at 180 days). The combination of CA and FA also presented similar trends. The modified versions of the crystalline admixture (i.e., CA2 and CA3) improved in about 26% the self-healing when compared with CA, the only exception was seen for PL of 90% applied at 180 days, in which CA displays the highest recovery of porosity (i.e., 12.1% to 8.0%).

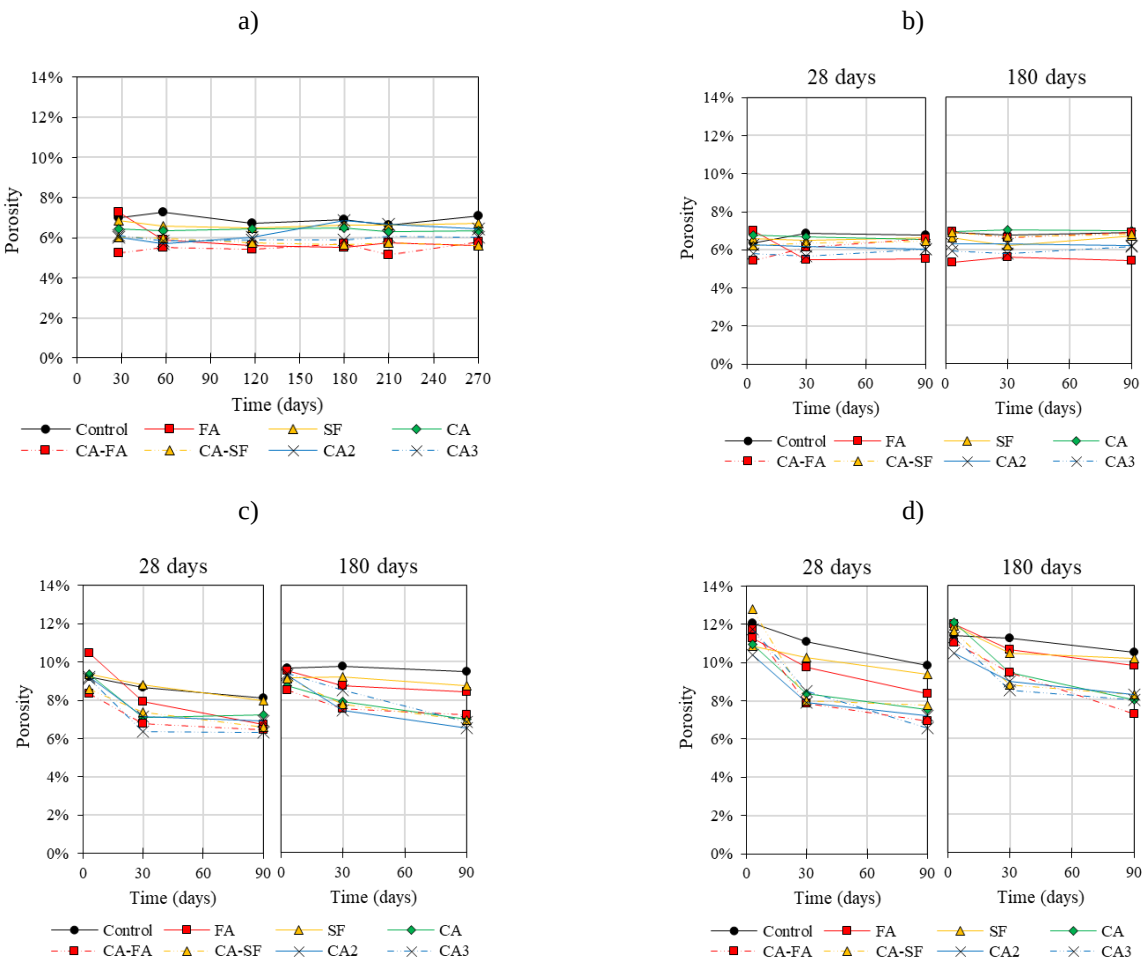

Figure 6.6: Porosity evolution of specimen pre-loaded at 28 and 180 days with a) 0% of the total load; b) 40% of the total load; c) 70% of the total load; and d) 90% of the total load.

6.5.3 **Mechanical Properties**

6.5.3.1 **Stiffness Damage Index (SDI)**

Figure 6.7 displays the results of SDI obtained without any pre-load (Figure 6.7a), while Figure 6.7b), c) and d) presents the SDI of the different mixtures over 90 days of healing after pre-load levels of 40%, 70% and 90%, respectively. Overall, the SDI values gathered for sound concrete were somewhat similar among the different concrete mixtures, ranging from 0.07 (CA3 at 180+90) to 0.12 (CA, CA-FA, CA3 at 28+30). Moreover, applying 40% of the total strength (Figure 6.7b) did not significantly change SDI values in both 28 and 180 days of initial curing. Besides, the trend observed during the 90 days of HT was quite horizontally linear on average with just a few exceptions (i.e., CA at 28+3 and control at 28+3 and 180+3). Otherwise, both pre-load levels of 70% and 90% have averagely increased

energy dissipation during the tests, increasing SDI (Figure 6.7c and d). After 90 days of HT, the samples containing CA dropped SDI values in 0.04, on average, whereas control, FA, and SF, presented a drop of 0.01 in SDI values; furthermore, similar trends were also displayed by the specimens pre-loaded at 90% of the total strength. Finally, modifying the chemical composition of the CA did not significantly impact on the SDI results.

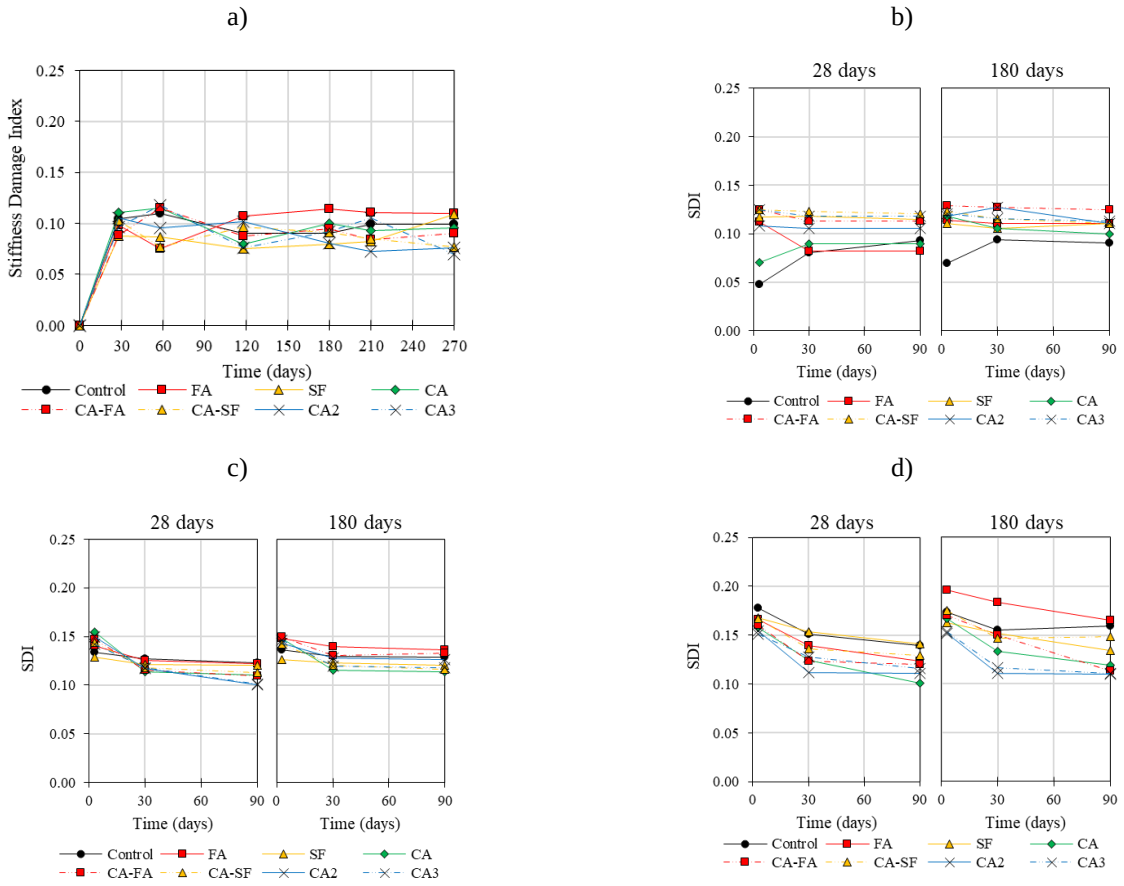

Figure 6.7: Stiffness damage index (SDI) of the pre-loaded samples at 28 and 180 days with a) 0% of the total load; b) 40% of the total load; c) 70% of the total load; and d) 90% of the total load.

6.5.3.2 Modulus of Elasticity (ME)

The modulus of elasticity (ME) of the mixtures can be seen in Figure 6.8a, while the average variation ratios are displayed in Figure 6.8b, c, and d) for pre-load levels of 40%, 70% and 90% of the total strength of the concrete mixtures, respectively. The eight different concrete mixtures displayed close ME over the curing period with PL of 0% (Figure 6.8a). The average ME ranged from 28.5 GPa to 32.4 GPa. Moreover, pre-loading the specimens with 40% of the total strength slightly decreased the

average ratio of ME in -0.01 and -0.02 when applied at 28 and 180 days, respectively (Figure 6.8b). Yet, there is no significant variation of ME considering the healing time after applying PL of 40%. On the other hand, increasing the pre-load level, the ME significantly changed just after pre-loading and over the self-healing period.

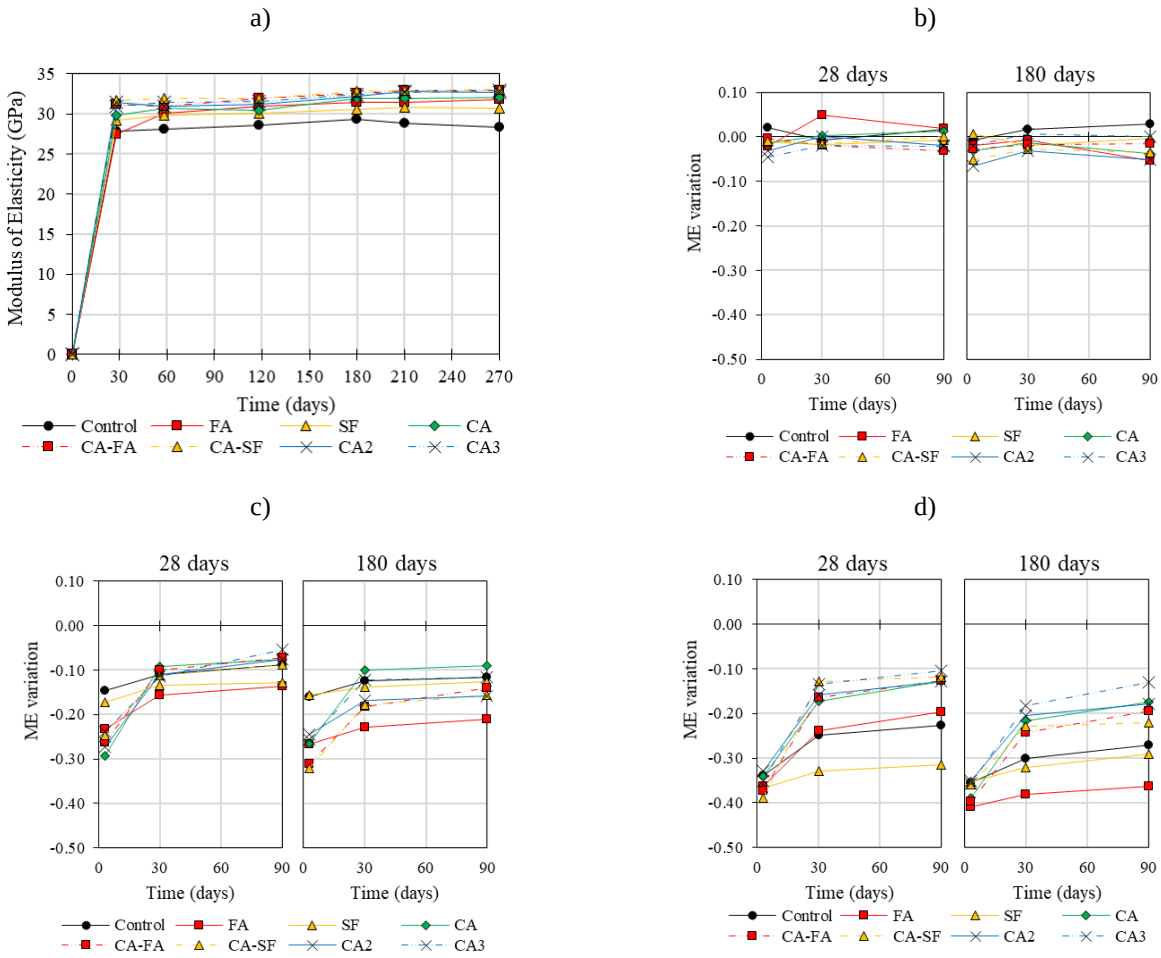

Figure 6.8: Modulus of Elasticity of the pre-loaded samples at 28 and 180 days with a) 0% of the total load; b) 40% of the total load; c) 70% of the total load; and d) 90% of the total load.

In general, the average drop measured in ME for PL of 70% was -0.23 at 28+3 days and -0.25 at 180+3 days (Figure 6.8c). Although the mixtures containing CA displayed the higher losses, they showed the most expressive recovery ratios (i.e., CA reached 0.22, variation from -0.29 to -0.08) and followed by CA2 (0.20), CA-FA (0.19), CA3 (0.18), CA-SF (0.16), FA (0.10), control (0.06) and SF (0.04). However, damaging the concrete specimens at higher age significantly impacted on the ME recovery results. The mixture CA specimens sustained a higher recovery ratio, yet 23% lower than the values obtained for early damage (i.e., variation ratio of 0.17, variation from -0.26 to -0.09), the same ratio

was also displayed by CA-FA, and followed by CA-SF (0.16), CA3 (0.14), CA2 (0.09), FA (0.06), control (0.04) and SF (0.03). Similar trends with higher losses can also be seen for PL of 90 (Figure 6.8d).

6.5.3.3 **Compressive Strength (CS)**

Figure 6.9a displays the compressive strength results over the evaluated period without any pre-load and the variation of the different mixtures over 90 days of self-healing after pre-load levels of 40%, 70% and 90% (Figure 6.9b, c, and d, respectively). The highest average CS obtained over the evaluated curing period were 55.8 MPa for CA-FA mixtures and 51.7 MPa for CA3 (Figure 6.9a). The Control specimens presented the lowest average (41.5 MPa), followed by SF (47.5 MPa), CA2 (47.7 MPa), CA (48.6 MPa), FA (50.8 MPa) and CA-SF (51.6 MPa). FA specimens displayed the highest variation between 28 days (34.9 MPa) and the last measurement at 180+90 (56.1 MPa), whereas CA-SF had the lowest. The application of a PL level of 40% (Figure 6.9b), in general, did not change the average CS. Yet, it is important to notice that the control specimens presented a slight increase in CS after applying the pre-load in both 28 and 180 days (average of 4.1% and 5.5%, respectively). On the other hand, CA-FA displays a higher decrease in CS just after the application of PL.

Increasing the pre-load levels to 70% and 90% significantly decreased CS averages; in addition, the periods from 3 to 90 days indicate significant recovery of CS (Figure 6.9c and d) whether for PL at 28 or 180 days. Moreover, the recovery of CS is highlighted using SCMs and, especially, by adding crystalline admixtures (i.e., CA1, CA2 and CA3). The most expressive regaining CS measure over the 90 days of HT was for CA-FA, which moved the average ratio loss from -0.17 to +0.02 (difference of 0.19), representing a gain of 17.6 MPa. Yet, the combination of the crystalline admixture and silica fume also display an expressive recovery. Finally, it is worth mentioning that the lowest ratio of recovery measured after 90 days of HT was for SF specimens (i.e., 0.02 average ratio), followed by Control (0.05), FA (0.08), CA (0.09), CA2 (0.11) and CA3 (0.13). Similar trends were also seen for pre-load applied at 180 days of curing.

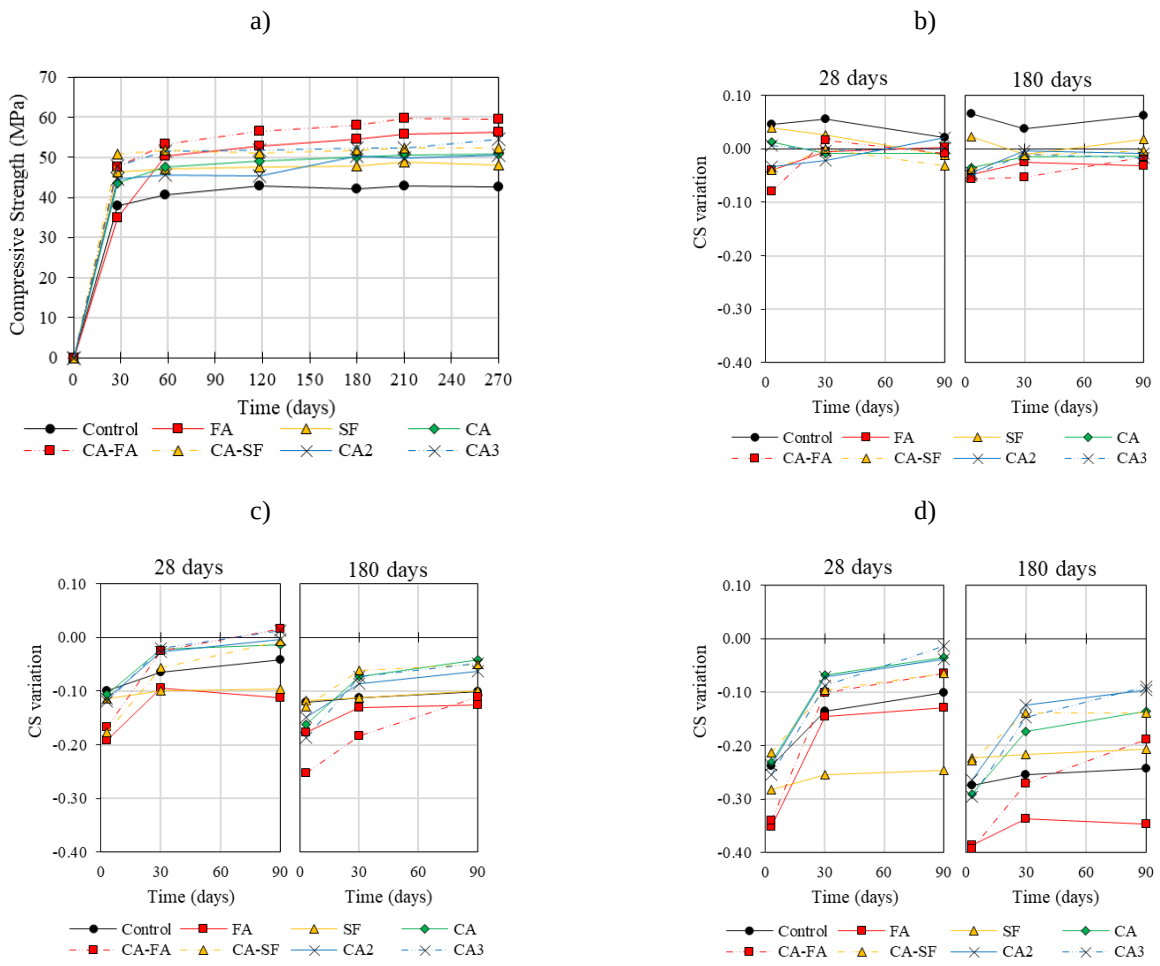

Figure 6.9: Compressive strength of the pre-loaded samples at 28 and 180 days with a) 0% of the total load; b) 40% of the total load; c) 70% of the total load; and d) 90% of the total load.

6.5.4 **Microscopic Evaluation**

6.5.4.1 **Damage Rating Index (DRI)**

Figure 6.10 provides the DRI numbers obtained from the specimens without any pre-load (Figure 6.10a). In contrast, Figure 6.10b), c) and d) presents the SDI of the different mixtures over 90 days of healing after the pre-load levels of 40%, 70% and 90%, respectively. Although a constantly higher DRI number was observed for mixtures incorporating silica fume (i.e., an average of 148), the DRI number of the different mixtures were relatively constant along the curing period for samples without pre-loading (Figure 6.10a) within the variation range of 10% of the method [60,74]. Moreover, most of the cracks were found in the crushed coarse aggregate, even for "undamaged" concrete specimens. Samples displayed similar results with a PL of 40% (Figure 6.10b).

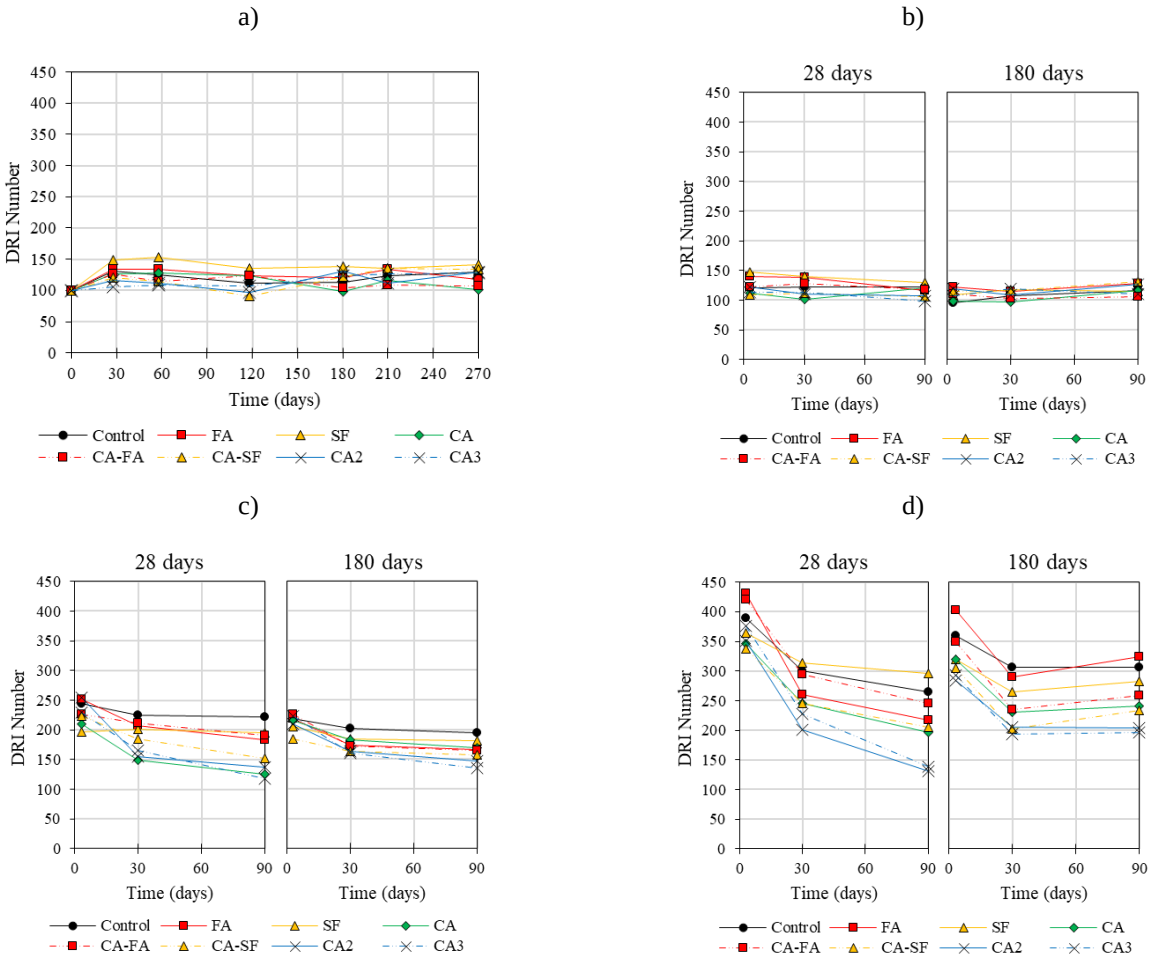

Figure 6.10: Damage Rating Index (DRI) number of the pre-loaded samples at 28 and 180 days with a) 0% of the total load; b) 40% of the total load; c) 70% of the total load; and d) 90% of the total load.

Increasing the PL to 70% (Figure 6.10c), on the other hand, significantly changed the DRI average numbers; pre-loading the specimens at 28 days resulted in total DRI numbers of 254, 252, 244, 230, 226, 223, 210 and 196 for CA2, FA, control, FA, CA3, CA-FA, CA-SF, CA and SF, respectively. However, it is worth noting that over the self-healing period, all mixtures had the DRI number considerably decreased, yielding values of 221 (control), 183 (FA), 196 (SF), 125 (CA), 191 (CA-FA), 152 (CA-SF), 137 (CA2) and 118 (CA3). Furthermore, similar behaviour can also be seen for samples pre-loaded after 180 days of curing. For PL of 90% (Figure 6.10d), the specimens presented 50% more cracks than PL of 70%, on average; however, the recovery ranges were more expressive for PL of 90%. At 28 days, control, FA, SF, CA, CA-FA, CA-SF, CA2 and CA3 presented DRI of 389, 430, 365, 347,

421, 337, 350 and 376, which, after 90 days of HT curing, they decreased in 32%, 49%, 22%, 43%, 42%, 38%, 62% and 63%, respectively. On the other hand, damaging the samples at 180 days, the recovery rate of the mixtures was significantly affected, especially for FA mixtures. For PL of 90% at 180 days, control, FA, SF, CA, CA-FA, CA-SF, CA2 and CA3 presented recovery ranges of 15%, 18%, 12%, 25%, 27%, 22%, 29% and 34%.

6.6 Discussion

6.6.1 Distress development in the pre-loaded specimens

First, to evaluate the self-healing capacity, either natural or artificial, of the different concrete mixtures, it is imperative to understand the distress generation caused by the different pre-load levels on each one of them. Based on the results previously presented, it is clear that the higher the pre-load level (PL), the higher the "damage" in the concrete. One verifies that Sanchez et al. [75] defined the term "damage" as the harmful consequences of various types of deterioration mechanisms (i.e., loadings, creep, durability-related, etc.) on the mechanical properties, physical integrity and durability of concrete. It is worth noting that all concrete mixtures already presented a few measurable damage before the application of PL, mostly closed cracks within the aggregates, which could be generated over crushing/weathering processes, and very limited microcracking randomly spread through the cement paste. Likewise, pre-loading the concrete samples up to 40% of the compressive strength capacity seems not significantly to change the pattern displayed for PL of 0%; overall, physical, mechanical, and microscopic results obtained for PL of 0% and PL of 40% are pretty similar.

Nevertheless, a very few cracks might be formed under PL of 40% due to differential stresses concentration at pre-existent microcracks, irregular air-entrapped pores, and the interfacial transition zone between the cement paste and aggregates. Furthermore, pre-existent opened cracks could be closed, and others may have their widths slightly widened after PL of 40%, depending on the position and angle of the cracks. This behaviour can be seen in Figure 6.11a and b, where the total DRI numbers are quite similar for PL of 0% and PL of 40% for all mixtures, yet the DRI features slightly changed between these two PLs.

a)

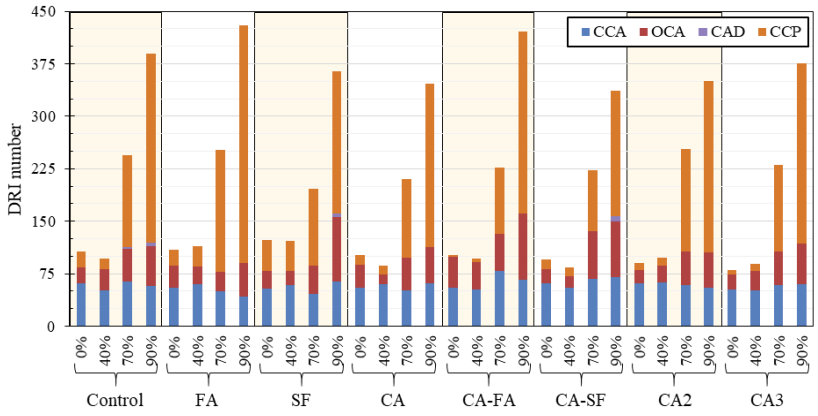

b)

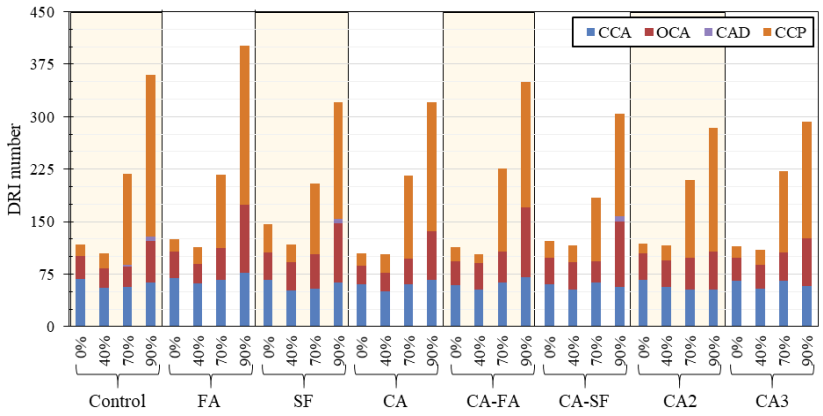

Figure 6.11: Damage features and total DRI number of the pre-loaded concrete specimens: a) at 28+3 days of initial curing and b) at 180+3 days of initial curing.

Figure 6.11 also provides the microscopic damage features and DRI numbers obtained 3 days after applying the determined pre-loads (i.e., 0%, 40%, 70% and 90%) in the concrete specimens at 28 and 180 days of initial curing. One may notice that the rise of the total DRI numbers is mainly related to the increase in cracks in the cement paste (CCP) as a function of the pre-loading level. Yet, for PL of 90%, a significant number of open cracks in aggregates (OCA) are verified for SF, CA-FA, and CA-SF mixtures at 28-3 days and FA, SF and CA-FA mixtures at 180-3 days. Overall, for PL of 70% the average of CCP were 123 (6.8 times higher than CCP for PL of 0%) at 28+3 and 112 at 180+3 (5.1 times higher than CCP for PL of 0% in the same age), while for PL of 90% the averages were equal to 249 and 184 (13.8 and 8.4 times higher than PL of 0% at the same ages, 28+3 and 180+3, respectively).

Based on the analysis of the DRI numbers illustrated in Figure 6.11 and their qualitative description, the following damage model (Figure 6.12) of the overall distress development against the pre-loading level was applied. It is worth mentioning that the PL levels in the presented model are only indicative values. Moreover, the descriptions are based on a "macroscale" evaluation made under a stereomicroscope at a magnification of 15-16x.

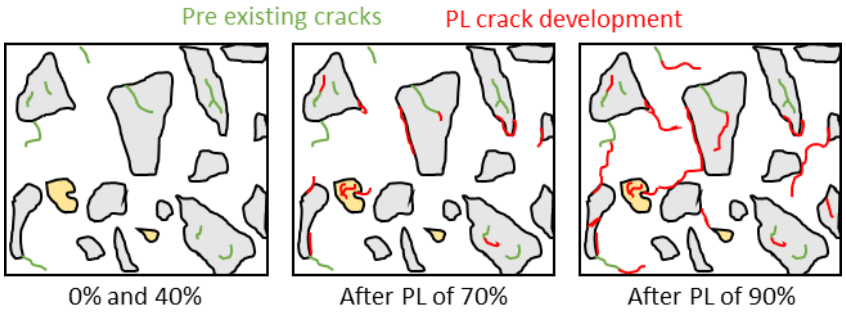

Figure 6.12: Qualitative damage development vs. pre-load level.

As previously mentioned, at pre-load levels of 0% and 40%, a few measurable deteriorations were found in all different concrete mixtures specimens even without any induced damage (i.e., PL of 0%). Globally, the cracks are primarily within the aggregate particles and consist of sharp closed cracks resulting from aggregate processing or weathering. Figure 6.13a and b highlight two examples of pre-existent cracks (indicated by the red arrows) within the crushed limestone coarse aggregate. Moreover, a few cracks can also be found in the cement paste; they are very thin, and although randomly spread in the specimen, they are often linked with the ITZ. This type of crack could result from different mechanisms, such as autogenous or drying shrinkage, plastic deformation, bleeding, settlement, etc. Furthermore, they would facilitate further cracks development or work as an easy path for cracks' propagation and network under higher pre-load levels (i.e., PL of 70% and 90%). Likewise, increasing the stress level in the specimens to 70% of the total strength, the pre-existing cracks start to become unstable and keep growing. Moreover, weaker regions such as irregular air-entrapped pores, ITZ (Figure 6.13c) and areas with higher stress concentration begin to develop cracks. At PL of 90%, the cracks keep growing, mainly through the cement paste, linking to each other and connecting different ITZs forming an important crack network (Figure 6.13d.

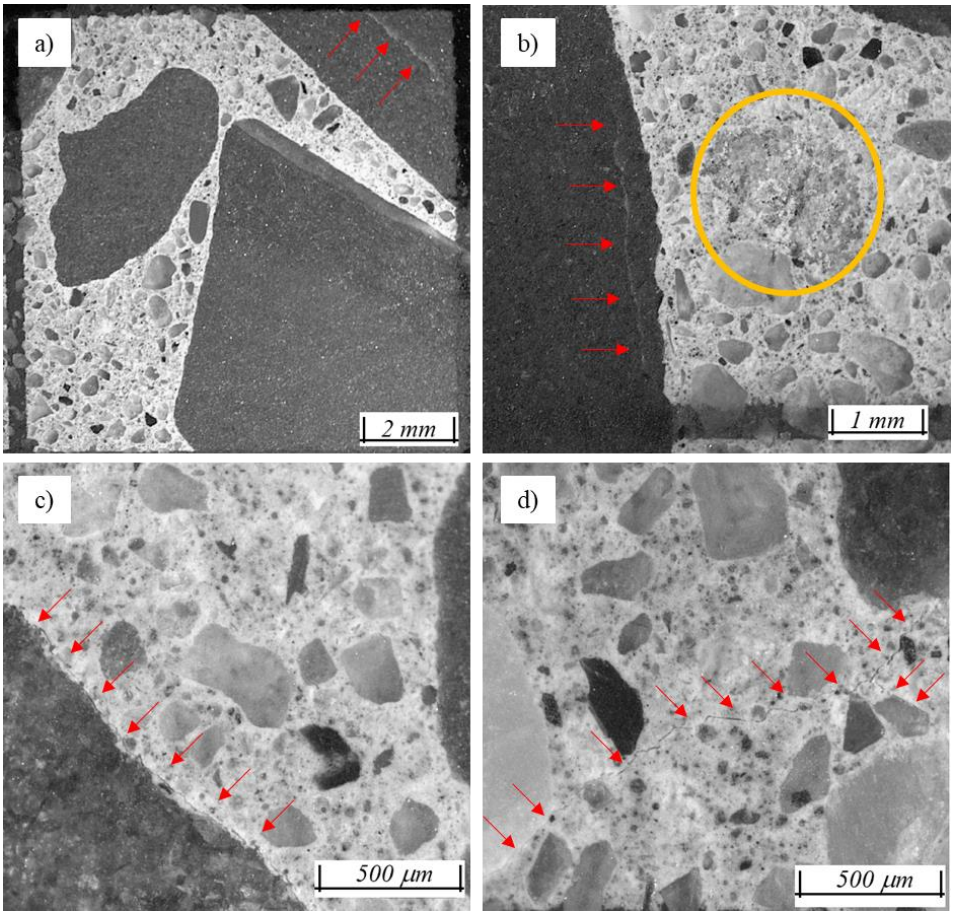

Figure 6.13: Cracking features found in the concrete mixtures

One may notice that the binder composition of the different mixtures influences the damage developed in the specimens, especially for samples pre-loaded at 90%, likely because the mixtures displayed different compressive strengths (Figure 6.9a) even for the same w/b. For instance, at 28 days, the FA and control revealed the lowest CS values (35 MPa and 38 MPa, respectively) and CA-SF the highest (50.9 MPa). Likewise, at 180 days, the control mixture presented the lowest CS value (42.1 MPa), whereas CA-FA and FA yielded the highest (58.1 MPa and 54.6 MPa, respectively). Thus, globally, the highest the corresponding compressive strength of the concrete mixtures, the highest the amount of cracks formed within the aggregate particles after PL of 90%.

Finally, the DRI features analysis revealed that concrete specimens with higher compressive strength exhibited more cracks within the coarse aggregates after PL of 90%. This interesting trend is displayed in Figure 6.14 and is instead explained by the mechanical properties of the crushed limestone coarse aggregate used in this study. In other words, the highest the corresponding compressive strength of the concrete mixtures, the highest the number of cracks formed within the aggregate particles after PL of

90%. Moreover, increasing the number of cracks within the aggregate, the higher the losses in ME. Likewise, the self-healing ability of each mixture is also affected by the type of agents (i.e., natural or artificial); hence cracks within the aggregate particles cannot be properly healed.

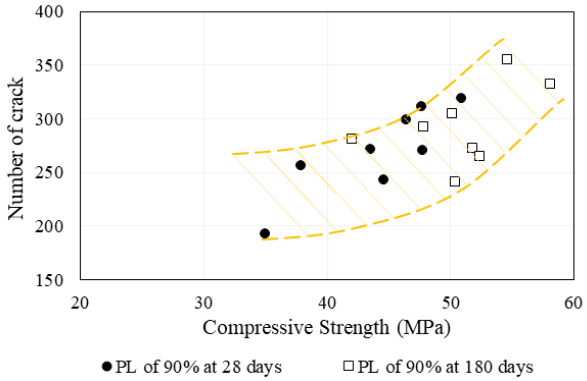

Figure 6.14: Correlation between the number of cracks in aggregates (CCA + OCA) without weighting factors found in PL of 90% specimens vs. the compressive strength.

6.6.2 Effect of natural healing on physical and mechanical properties recovery of concrete specimens

Generally, the mixtures without CA displayed relatively satisfactory self-healing properties; the latter is directly affected by the different binder compositions used. It is important to notice that the w/b, the volume of paste, and fine and coarse aggregates were kept constant for all mixtures to compare similar systems. Moreover, the specimens were kept inside buckets with hermetic lids at 20 ^{o}C and 100% of R.H., which minimized the natural carbonation of the superficial layers of the concrete samples. However, the two main natural healing mechanisms accounted for in this study are the continued hydration and the formation of calcium carbonate.

The replacement of PC either by fly ash or silica fume influenced the rate of development of the physical and mechanical properties of the concrete specimens. Through the non-destructive tests, it has been found that SF mixtures developed greater values of ER and UPV and compressive strength at 28 days (i.e., 22% higher than control specimens). This behaviour suggests faster hydration kinetics of the SF mixtures. Moreover, this could indicate that fewer unhydrated PC's particles will be available for autogenous healing after damaging the concrete specimens, which seems to be the case for SF concrete specimens. To "quantify" the healing performance, the average ratio of recovery (RR) was calculated as per Equation 6.2. The RR of SF concrete mixtures was 36% lower than control mixtures for samples

pre-loaded at 28 days as displayed in Figure 6.15; likewise, 8% lower for PL applied at 180 days. Moreover, the slight difference between RR at 28+90 days and 180+90 days presented by SF mixtures (0.03) indicates that the silica fume particles significantly affected the early self-healing. Furthermore, the DRI features observed for SF concrete specimens show a higher amount of CCA and OCA (Figure 6.11), either for 28 or 180 days, which somewhat decreased the mechanical properties recovery rate once cracks in aggregates cannot be easily healed.

$$Ratio\ of\ Recovery\ (RR) = \frac{Property\ Variation_{initial} - Property\ Variation_{90\ days\ of\ SH}}{Property\ Variation_{initial}} \qquad \textbf{Equation 6.2}$$

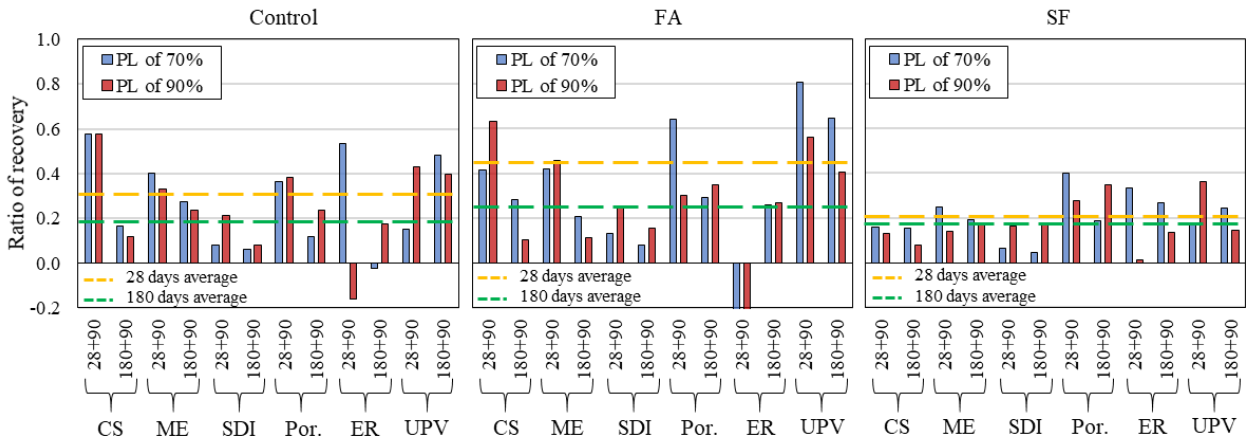

Figure 6.15: Ratio of recovery of control, FA, and SF mixtures for compressive strength (CS), modulus of elasticity (ME), stiffness damage index (SDI), apparent porosity (Por.), bulk electrical resistivity (ER) and ultrasonic pulse velocity (UPV) after 90 days of Self-Healing.

Another good indicator of the lower ability of self-healing of the SF concrete mixture is the evaluation of the counts of cracks in the cement paste over the 90 days of the healing period. As a "parallel" evaluation, the samples prepared and evaluated through DRI analysis at 28+3 and 180+3 (just after the application of PL of 90%) were further re-stored at 20 °C and 100% of R.H. for 90 days. The goal of this analysis was to evaluate and count the number of cracks healed over time. It is worth mentioning that the remaining DRI specimens had their polished surface protected with a plastic sheet before re-storing in the moist curing room. The results of these observations are displayed in Figure 6.16 and Figure 6.17, which illustrate the cracks observed in the cement paste for each cm^2 and without weighting factors. At 28+3 days, the SF specimen presented a total number of CCP of 116, the lowest amongst the control and FA mixtures; furthermore, the cracks were more spread in the polished surface

of the specimen. After 30 days of self-healing activity, 14.7% of the cracks were sealed, while after 90 days, the number found was 23.3% lower than the initial. At 180+3 days, similar behaviour was observed for the SF mixture.

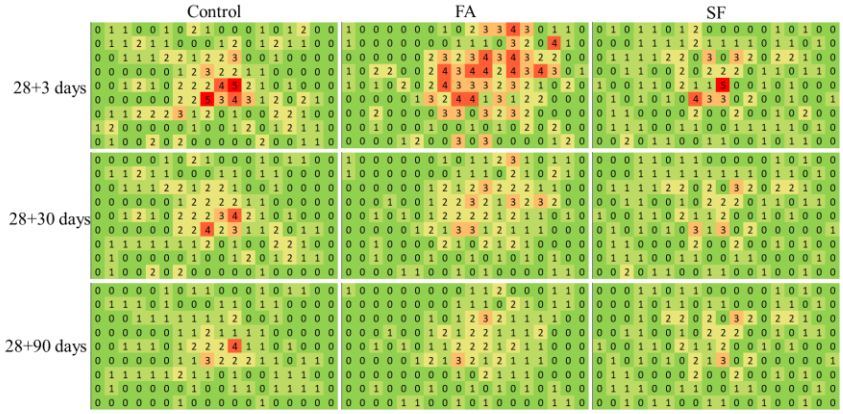

Figure 6.16: Total number of cracks found in the cement paste through DRI analysis for control, FA, and SF specimens after applying 90% of the total strength applied at 28 days and cured for 30 and 90 days for healing evaluation.

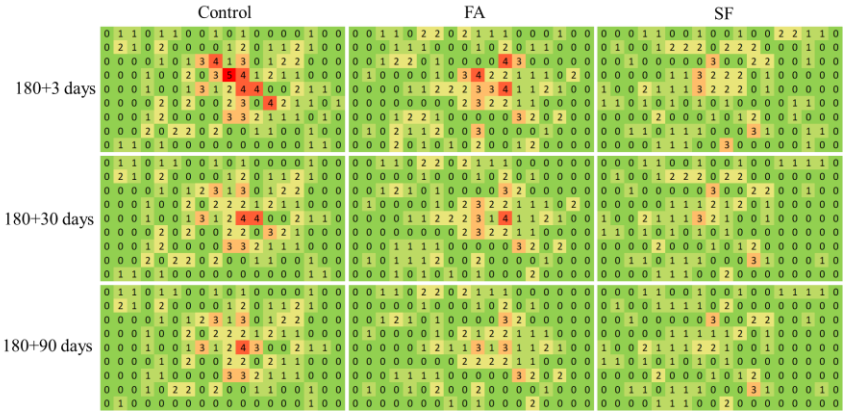

Figure 6.17: Total number of cracks found in the cement paste through DRI analysis for control, FA, and SF specimens after applying 90% of the total strength applied at 180 days and cured for 30 and 90 days for healing evaluation.

The specimen made of fly ash displayed the best results of physical and mechanical properties recovery of the mixtures without any crystalline admixtures added. Once again, as in SF mixtures, the chemical and physical properties of the SCMs play an essential role in the self-healing ability of the specimens. Unlike what has been observed for the silica fume, FA presented coarser particles than PC as observed in its particle size distribution in Figure 6.2. Moreover, the evaluation of ER and UPV made at 1, 3, 7 and 14 days for FA mixtures showed similar results to the control mixture; likewise, the CS was 8%

lower than control at 28 days, yet 30% higher at 180 days. The later gain of strength seen for FA mixtures likely explains the significantly higher recovery ratio displayed by the FA mixture in Figure 6.15 (i.e., 43% and 36% higher than control at 28+90 and 180+90 days). Evaluating the DRI features, it was clear that at 28 days, FA specimens developed more cracks through the cement paste (Figure 6.16); moreover, it was found that FA concrete specimens were able to seal 52.6% after 90 of healing, for cracks formed at 28 days and 28.3% at 180+90 (Figure 6.17). However, it verifies that an important number of cracks within aggregates were noticed in the FA specimens pre-loaded at 180 days (Figure 6.11), which may have somewhat helped decrease the later age mechanical properties recovery of the mixture.

Finally, the control specimens displayed results in between those found for FA and SF mixtures, either RR (i.e., 0.32 at 28+90 days and 0.19 at 180+90 days) or amount of self-healed cracks (i.e., 38.3% for PL applied at 28 days and 17.0% for PL applied at 180 days). Moreover, it is worth mentioning that the second DRI analysis revealed that a few cracks were only partially healed, which decreased the overall self-healing performance of the control samples. Figure 6.18 displays two pictures taken before and after 90 days of healing and shows the evolution of the self-healing in the specimen. It is clear that the healing products filled the crack in the ITZ, yet in the yellow dashed area, it can be seen that the crack is still slightly opened.

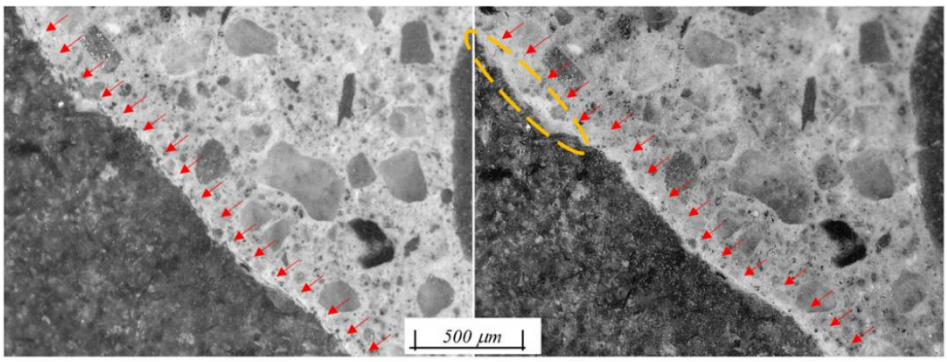

Figure 6.18: Self-healing evolution of a crack in the ITZ found in the control specimen: in the left a picture taken just after pre-loading the sample and in the right, the same sample after 90 days of curing.

6.6.3 Effect of artificial healing on physical and mechanical properties recovery of concrete specimens

6.6.3.1 Efficiency of the crystalline admixture combined with supplementary cementing materials.

The addition of CA in concrete significantly impacted the SH ability displayed by the concrete specimens. Only adding 1.91% of CA in binder mass resulted in faster development and better microstructure quality, as indicated by the ER and UPV results. Moreover, at 28 days, the compressive strength of the CA mixture was 15% higher than the control and at 180 days, 19% higher; furthermore, CA specimens displayed significantly higher recovery of physical and mechanical properties after being damaged. The RR for CA mixtures (Figure 6.19) were found as 0.67 and 0.61 for PL of 70% and 90% at 28 and 180 days (average values). One may notice that CA specimens pre-loaded either at 70% or 90% at 28 days were able to recover 0.85 and 0.86 of CS after 90 days of curing; at 180 days, these numbers are smaller (0.74 and 0.53 for PL of 70% and PL of 90%, respectively).

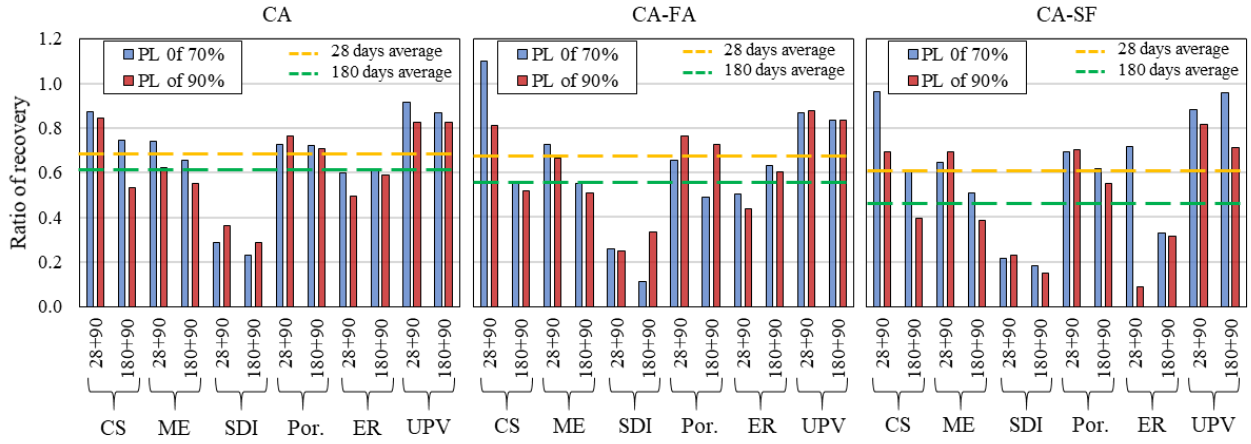

Figure 6.19: Ratio of recovery of CA, CA-FA, and CA-SF mixtures for compressive strength (CS), modulus of elasticity (ME), stiffness damage index (SDI), apparent porosity (Por.), bulk electrical resistivity (ER) and ultrasonic pulse velocity (UPV) after 90 days of Self-Healing.

The differences obtained for PLs at 28 and 180 days could be explained by the fact that after applying PL of 90%, the number of cracks within the aggregate particles increased (Figure 6.11). Yet, this also may indicate that the CA mixture had its potential to self-heal decrease. Through the analysis of the number of cracks healed over time (Figure 6.20 and Figure 6.21), the CA mixture fully healed 82.1% of cracks in the cement paste after 90 days of self-healing curing. However, at 180 days, those numbers were 25% lower, which indicates that the overall self-healing ability has decreased, at least for the same curing period (i.e., 90 days). In general, there was a trend of cracks' development over the diagonals and a higher concentration of cracks surrounding the center of the polished concrete sections.

However, over the 90 days of curing at 100% R.H., the CA mixtures seem to have their self-healing ability enhanced in layers close to the external faces of the specimens, which were directly exposed to higher environment humidity (100%).

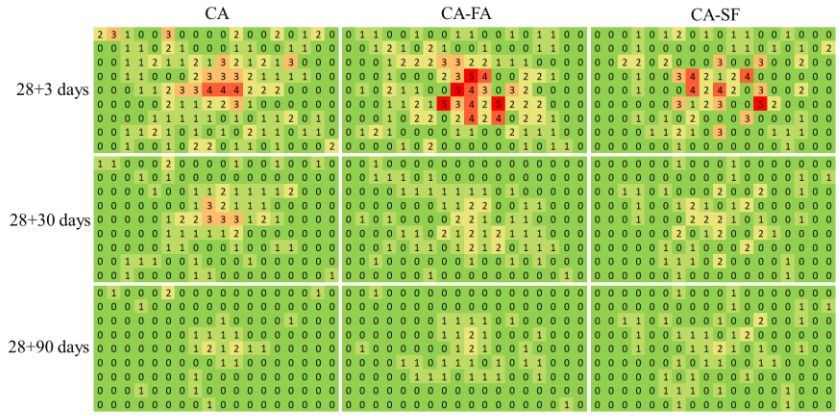

Figure 6.20: Total number of cracks found in the cement paste through DRI analysis for CA, CA-FA, and CA-SF specimens after applying 90% of the total strength applied at 28 days and cured for 30 and 90 days for healing evaluation.

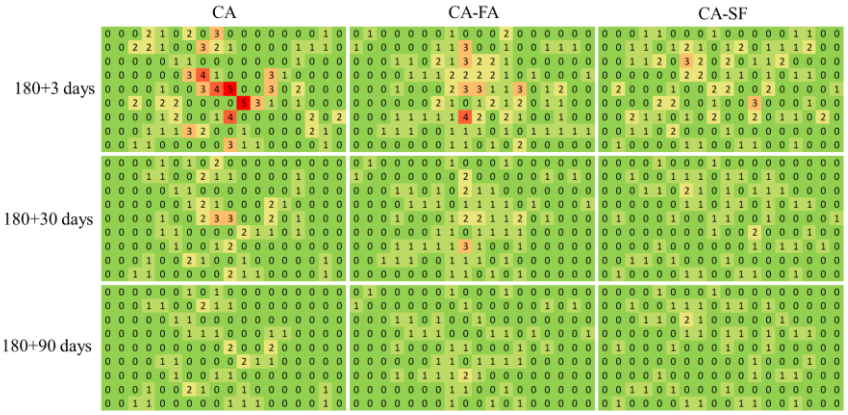

Figure 6.21: Total number of cracks found in the cement paste through DRI analysis for CA, CA-FA, and CA-SF specimens after applying 90% of the total strength applied at 180 days and cured for 30 and 90 days for healing evaluation.

Combining CA and FA (CA-FA) also resulted in substantial improvement of the self-healing properties. The results of ER, UPV and CS at 28 days indicate that CA accelerates the hydration rate of the mixture; comparing CA-FA with FA data, ER, UPV and CS were 158%, 6% and 36% higher for CA-FA. Furthermore, the latter displayed recovery ratios 43% and 112% higher than the FA mixture for pre-damaging at 28 and 180 days, respectively. One of the most impressive results obtained with CA-FA mixture was the recovery ratio of the compressive strength after PL of 70% (i.e., 1.10),

indicating that even after being damaged, the CS after 90 days of curing was even higher than the one obtained for PL of 0%. On the other hand, the CS recovery for PL of 90% specimens did not reach similar values (i.e., RR of 0.81); yet, higher than control mixtures.

Additionally, the variation from 1.10 to 0.81 may be a consequence of the notable amount of cracks found within the aggregates (Figure 6.13). Evaluating the total amount of cracks healed in the cement paste (Figure 6.20 and Figure 6.21), CA-FA displayed a considerable concentration of cracks surrounding the center of the polished surface of the sample at 28+3, whereas a more spread pattern at 180+3. Furthermore, after 30 and 90 days of curing, CA-FA could heal 59.1% and 77.2% of the CCP at 28+30 and 28+90 days and 38.6% and 58.4% at 180+30 180+90 days. The overall coarser particle size distribution and slower pozzolanic kinetics of the fly ash extended the hydration period of the concrete, contributing to further self-healing as long as unhydrated fly ash and $Ca(OH)_2$ keeps forming later C-S-H. Moreover, besides the delayed activation of CA particles under contact with water and environmental moisture, the catalyst properties of crystalline material improved fly ash hydration over the global hydration of the CA-FA mixture and after delayed activation, once the concrete specimen was damaged. Thus, increasing the strength at 28 days and improved the self-healing ability of CA-FA once compared with FA and CA mixtures.

CA-SF displayed the lowest recovery ratios among the mixtures containing the commercially available CA, yet higher than all values obtained for mixtures without CA. Besides, analyzing the efficiency to heal cracks through the DRI analysis, in Figure 6.20 and Figure 6.21 can be seen that CA-SF were able to heal 58.4% of the cracks after 90 days of HT curing for PL at 28 days (2.51 times higher than SF) and 51.2% at 180+90 (2.02 times higher than SF). In other words, the lower volume of silica fume, lower particle size distribution and well-known faster pozzolanic kinetics than fly ash enhanced the early strength gain of the concrete. However, withholding the self-healing ability of both the SF and the CA-SF mixtures. These results highlight that either natural healing or the crystalline admixtures responses towards self-healing are pretty susceptible to the presence of unhydrated PC's and SCMs particles.

6.6.3.2 **Efficiency of the chemically modified crystalline admixture.**

The modified versions of the crystalline admixture, either CA2 or CA3, significantly changed the overall self-healing behaviour of the mixtures. In general, both CA2 and CA3 mixtures reached similar mechanical properties (i.e., CS, ME, and SDI), close cracks in the cement paste and comparable crack

patterns after being damaged. However, the addition of reactive SiO_2 and Al_2O_3 rich metakaolin particles in the crystalline admixture to produce the so-called mix CA2, were able to make concrete mixture able to increase the recovery ratios of specimens damaged at 28 days by 9% than the values obtained for CA concrete (Figure 6.22). Besides the mass of MK combined with CA only represents 0.38% of the PC weight, the higher RR value could have been due to the contribution of the reactive SiO_2 and Al_2O_3 from MK. Conversely, the latter self-healing ability measured for specimens damaged at 180 days decreased compared to CA (i.e., RR of CA2 was 17% lower than CA). In this case, the MK grains may have fully reacted as a pozzolanic material; moreover, there is a decrease of 20% of the CA particles content, the ability of CA2 mixtures to recover physical and mechanical properties was affected.

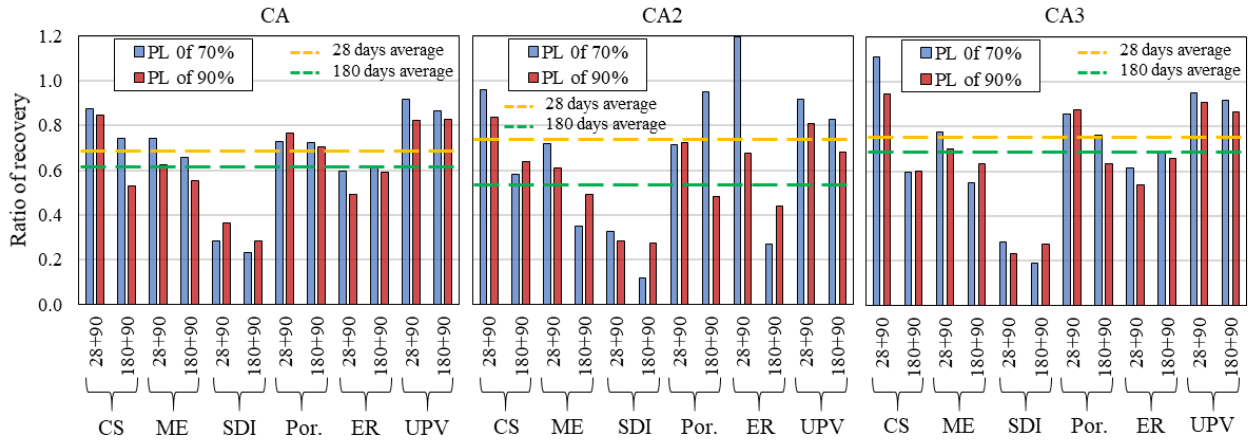

Figure 6.22: Ratio of recovery of CA, CA2 and CA3 mixtures for compressive strength (CS), modulus of elasticity (ME), stiffness damage index (SDI), apparent porosity (Por.), bulk electrical resistivity (ER) and ultrasonic pulse velocity (UPV) after 90 days of Self-Healing.

On the other hand, besides the mentioned changes in the recovery ratio achieved by CA2 mixtures, the ability to heal crack in the cement paste observed through the DRI analysis shows very similar behaviour to the CA mixture. For PL of 90% at 28 days, CA2 specimens developed a total of 140 cracks, the same number as found for CA mixture; moreover, after 90 days of curing, CA2 mixture was able to heal 83.6% of the cracks, while CA, 82.1%. For later age, this trend continued; CA2 specimens had 67.3% of the cracks in the cement paste self-healed, CA mixtures self-healed 61.5% (Figure 6.23). This behaviour may indicate that the modifications on CA enhanced the overall healing ability of the concrete. Yet, the mechanical properties of the healing products might have been negatively affected towards the improvement of CA with MK.

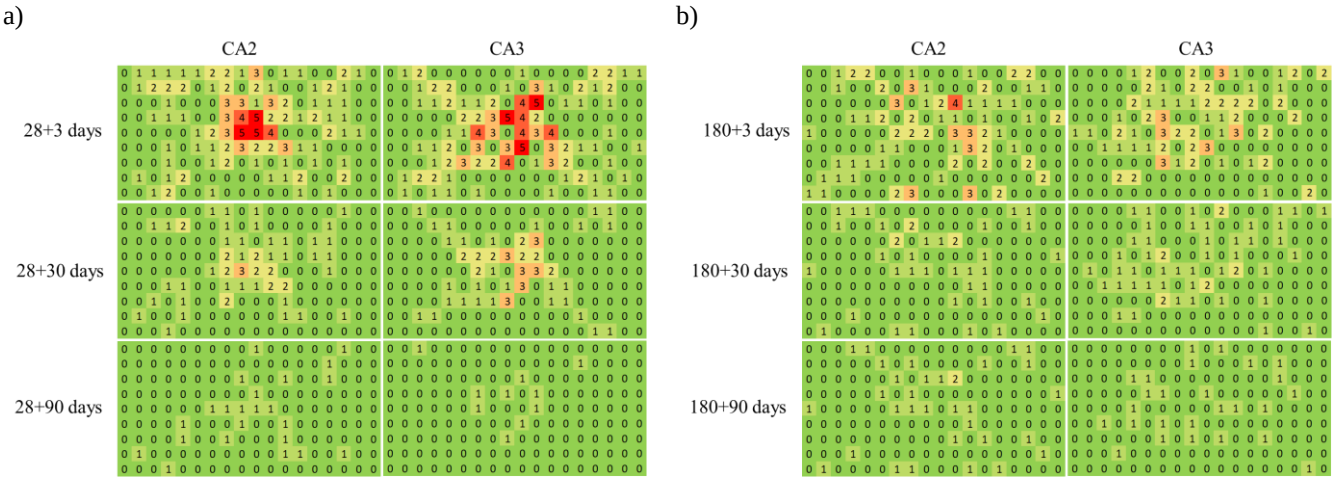

Figure 6.23: Total number of cracks found in the cement paste through DRI analysis for CA2 and CA3 specimens after applying 90% of the total strength applied at a) 28 days and b) 180 days and cured for 30 and 90 days for healing evaluation.

Focusing on the improvement of the overall self-healing capability of the mixtures, especially at later ages, for CA3, the MK was sieved in a 40 μm mesh, and the retained material was then combined with magnesium sulphate (MS) and mixed with CA (80% of CA, 10% of coarse MK and 10% of MS). The general physical and mechanical properties of the sound CA3 concrete were quite similar to CA and CA2. However, the CA3 mixture performed the highest recovery ratios for both early and later ages, among all other mixtures. For pre-loads applied at 28 days, the recovery ratio was 132% higher than control specimens, whereas 12% and 3% greater values than CA and CA2, respectively. Moreover, it is worth mentioning that the compressive strength recovery 90 days after pre-loading CA3 at 28 days with 70% of its ultimate strength achieved values higher than the "undamaged" samples, such as what was found for CA-FA. For PL of 90%, the CS recovery ratio reached 0.95, the highest value obtained. Likewise, for PLs applied at 180 days, the CS recovery ratios were also maintained at high levels, for PL of 70%, the obtained ratio was equal to 0.74, the same value as CA; yet, for PL of 90%, the results of recovery for CA3 were 31% higher than CA.

Evaluating the DRI features, the total number of CCP found was slightly higher than CA and CA2; however, at 28+90, CA3 mixture was able to self-healed 93.2% of the cracks (Figure 6.23); while at 180+90 days, this number was found as 73.2%, the highest among all concrete mixtures. Figure 6.24 shows an example this impressive self-healing efficiency of the CA3 mixture. Figure 6.24a, on the left, one sees a crack developed/propagated through the ITZ of the coarse aggregate and cement paste linking different ITZs from several fine aggregate particles and, b) on the right, the crack is thoroughly

sealed at 15-16x magnification after 90 days of curing. The coarser particles of MK provided by the modified CA3 are SiO_2 and Al_2O_3 rich. Yet, conversely than CA2, they had slower reactivity, decelerating the release of SiO_2 and Al_2O_3 to combined with $Ca(OH)_2$ and further forming C-S-H, precipitating in pores and cracks and improving the self-healing. Moreover, another hypothesis is that the magnesium sulphate may increase the formation of gypsum, ettringite and brucite inside the crack.

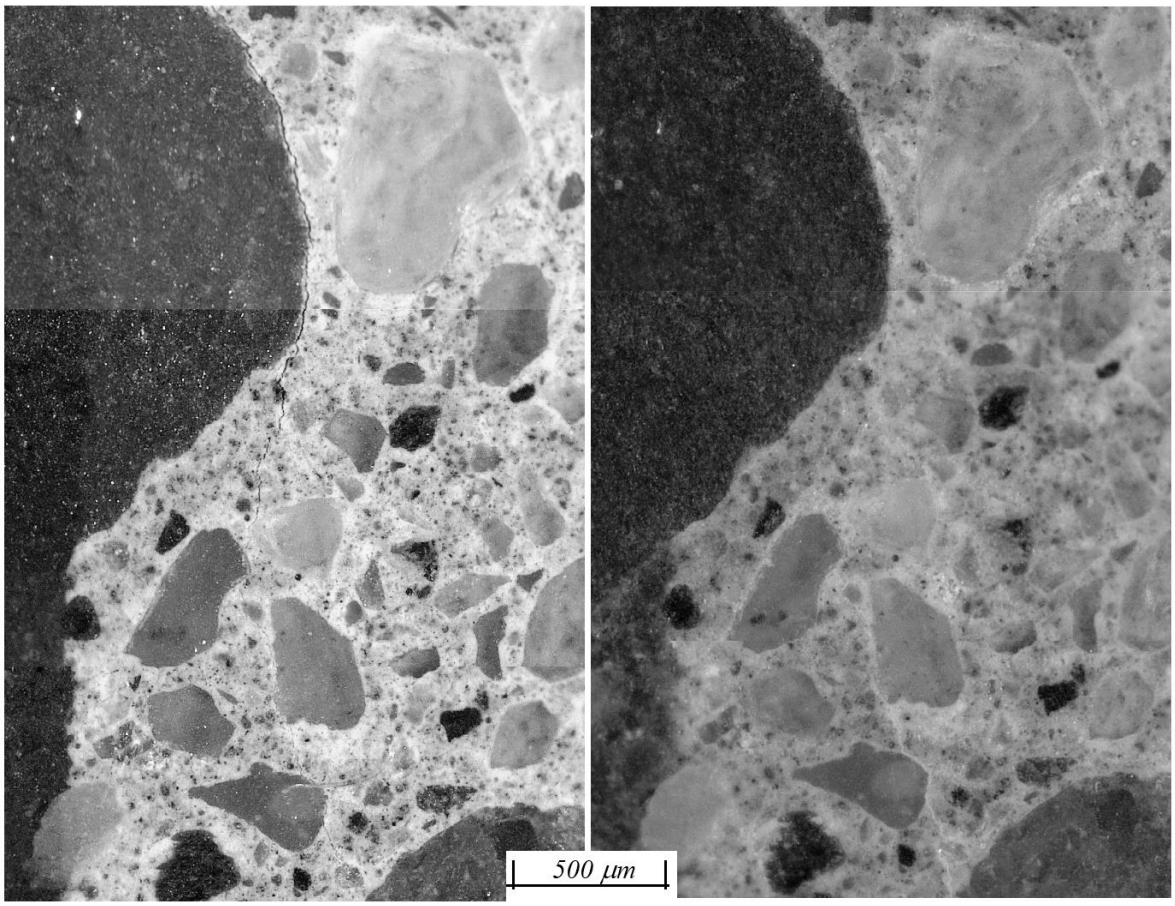

Figure 6.24: Self-healing evolution of a crack spread through different ITZs, and cement paste found in the CA3 specimen: in the left a picture taken just after pre-loading the sample and in the right, the same sample after 90 days of curing.

6.6.4 **Chemo-mechanical properties of the healing products**

The previously displayed results and discussions revealed promising findings; it was clear that the self-healing ability of the concrete mixtures can be improved naturally (i.e., by using SCMs) and artificially (i.e., the addition of crystalline admixtures). However, the different concrete mixtures achieved distinct self-healing efficiencies and affecting differently each mechanical, physical or microscopical property of the concrete. In other words, besides the apparent volume of cracks healed, the different products

precipitated in the opened cracks might impact on the overall data gathered. In that regard, a further qualitative chemical (i.e., scanning electron microscopy/energy-dispersive X-ray spectroscopy, SEM/EDS) and quantitative mechanical (i.e., micro indentation) were performed in the healing products found in the concrete specimens. The SEM and EDS were performed in an EVO MA-10, Carl Zeiss AG equipment in the high-vacuum mode, set at 15 kV, using secondary electron imaging and EDS. Backscattered electron images were taken at different magnifications (i.e., x200, x300, x500, x1000 and x2000), yet the main focus of the analysis was to identify the chemical composition of the products found in cracks. Figure 6.25 shows the SEM images of one partially healed crack (Figure 6.25a) and the self-healing products precipitated within the crack (Figure 6.25b). Globally, quite fibrous materials were observed covering the surface of the products in the cracks; such interesting results have been documented previously in [33,76]. Moreover, the main products identified were calcium carbonate, followed by $Ca(OH)_2$, C-S-H, and ettringite nails. Therefore, comparing the different concrete mixtures, no expressive differences were found with EDS analysis. The exception was the mixtures containing SCMs, either fly ash or silica fume, which had precipitated less amount of calcium carbonate in the cracks. Thus, the main product found in FA, SF, CA-FA, and CA-SF mixtures was C-S-H gel.

a) b)

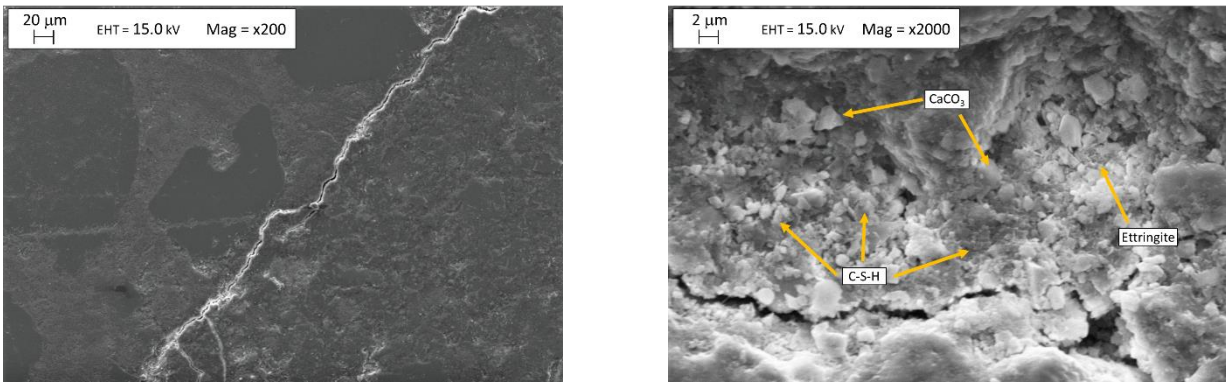

Figure 6.25: Illustration of SEM-image of the studied self-healed concrete after 90 days of curing: a) taken at a magnitude of x200 and b) magnitude of x2000.

The mechanical analysis of the self-healing products was evaluated through the micro-indentation test. In this regard, the remaining specimens selected for DRI analysis at 28+3 and 180+3 were, as aforementioned, carefully inspected to assess and quantify the total amount of healed cracks over time through the stereomicroscope to localize cracks and to follow their healing process. Following this

evaluation, cracks with average widths of 100 µm and 200 µm, self-healed after 90 days of curing, were identified to perform the standard Vickers hardness tests (micro-indentation). It was used a diamond indenter and 0.4903 N (490.3 mN) load for Vickers indentations (Struers Duramin Machine), a dwell time of 10 s was fixed and a total of 5 points per region were measured to cover statistics and to obtain the Vickers micro-hardness (HV) averages as per [77–79]. Figure 6.26 displays the results obtained for micro-indentation hardness tested at 28+3, 28+90, 180+3 and 180+90 days of curing. Its worth noting that the results of cement paste as indicated were conducted in sound specimens.

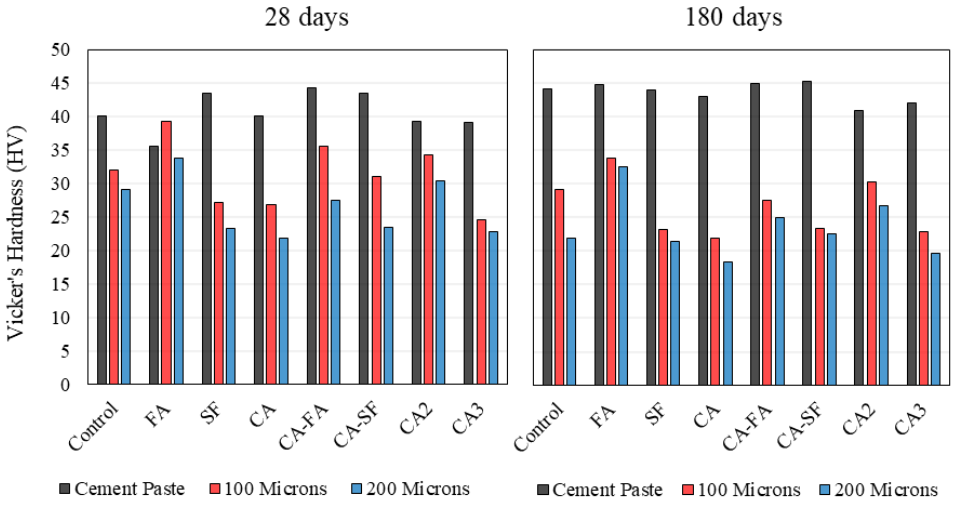

Figure 6.26: Micro-indentation hardness (HV) results obtained for specimens pre-loaded at 28 and 180 days and after 90 days of healing.

The results indicate that the overall HV of the binder matrix, either at 28 or 180 days, was averagely higher than the HV of the products formed in the cracks. The only exception for HV values was FA specimens which showed similarly and higher HV in the healing products formed in cracks with a width of 100 µm and 200 µm. This behaviour indicates that a denser material filled the cracks of FA mixtures with mechanical properties similar to the binder matrix, which is likely explained by the highest strength gain that the FA mixture achieved between 28 days and 28+90 days. In other words, the continued hydration of the fly ash grains after damaging at 28 days played a significant role in the crack healing. For induced cracks formed at 180 days, on the other hand, the properties of the healing products for FA specimens were significantly lower than the paste matrix, which reinforces the later statement.

In general, the products formed from natural healing processes provided higher HV than the artificial ones. Moreover, both mixtures CA and CA3 displayed the lowest average values of HV while, on the other hand, provided the highest ratio of recovery and percentage of healed cracks. It suggests that the "volume" of cracks healed plays a major role in the final physical and mechanical properties recovery. At the same time, the inner "quality" of the healing products seems to be less critical. It is worth highlighting that different from CA, CA2, and CA3 mixtures, the incorporation of SCMs proportioned concrete specimens with the highest compressive strength results. Consequently, the pre-loading resulted in an expressively higher amount of cracks formed within the aggregate particles, as revealed in the DRI analysis. Moreover, it was clear that cracks in aggregates could not be healed, which directly impacted the overall performance and efficiency of the concrete mixtures to recover the mechanical properties.

6.7 **Conclusions**

The main objective of the current comprehensive experimental campaign was performed to better understand the influence of autogenous and autonomous healing to recover the physical and mechanical properties of damaged concrete specimens at an early and later age (i.e., 28 and 180 days). Therefore, after pre-loading, the samples using four different load levels (0%, 40%, 70% and 90% of the total strength) at 28 and 180 days, the self-healing ability of the concrete cylinders were then evaluated over 90 days of curing, and the main conclusions of the above investigations are presented hereafter:

- The higher the pre-loading (PL) level in the concrete specimens, the higher the damage. However, PL of 40% of the ultimate compressive strength did not change the concrete samples' physical or mechanical properties. Yet, higher PL levels (70% and 90%) were able to generate internal cracking measured by microscopic analysis and increased the total porosity of the specimens. Thus, decreasing their compressive strength, modulus of elasticity, bulk electrical resistivity, ultrasonic pulse velocity and increasing stiffness damage index.

- Both autonomous or autogenous healing processes partially recovered the physical and mechanical properties of the concrete specimens after 90 days of curing. Moreover, both approaches could self-heal only cracks formed in the cement paste; pre-existent and PL generated cracks within the aggregates were not even partially healed.

- The autonomous healing property was significantly improved by replacing 30% of Portland cement (PC) with fly ash class F (FA); however, this property was negatively affected by the replacement of 10% of PC by silica fume (SF). Generally, control specimens could recover 32% of their physical and mechanical properties (on average) when damaged at 28 days and 19% at 180 days. On the other hand, FA concrete specimens achieved 46% and 26% at 28 and 180 days, while SF samples values were 21% and 18% at the same ages, respectively. Moreover, the control, FA, and SF mixtures could self-heal about 38%, 52% and 23% of their cracks in the cement paste for PL applied at 28 days, whereas they reached 17%, 26% and 25% of cracks healed at 180 days.

- Concrete specimens treated with the commercially available crystalline admixture (CA), CA, CA-FA, CA-SF mixtures were able to achieve an average recovery of 67%, 66% and 61% of their physical and mechanical properties, respectively. Moreover, early age damage CA, CA-FA, and CA-SF samples self-healed 82%, 77% and 58% of cracks formed in the paste matrix. For specimens damaged at 180 days, the recovery ratio obtained was 61%, 55% and 48%, whereas the number of self-healed cracks was 61%, 58% and 50% for CA, CA-FA and CA-SF, respectively.

- The chemically modified version of the CA (CA2 and CA3) reached even higher average values: the specimens of both mixtures were able to recover 73% of their physical and mechanical properties and self-seal 84% (CA2) and 93% (CA3) of the cracks in the paste matrix when damaged at 28 days. For specimens damaged at 180 days, the results showed that 51% and 69% of mechanical properties recovery and 67% and 74% of the cracks were self-healed for CA2 and CA3, respectively.

- Finally, the chemo-mechanical evaluation of the products formed within the cracks showed a higher C-S-H formation was found in healed cracks of SCMs-made concrete specimens. On the other hand, in concrete mixtures without SCMs, the main products found filling the cracks were calcium carbonate first, followed by portlandite, C-S-H, and ettringite. Moreover, the Vickers' Hardness (HV) analysis suggests that the HV of autonomous healed samples was higher, while the specimens made of CA and CA3 displayed the lowest HV values. This behaviour suggests that the "volume" of cracks healed plays a major role in the final physical and mechanical

properties recovery of the concrete. At the same time, the inner "quality" of the healing products seems to be less important.

6.8 Acknowledgment

The authors would like to thank Dr. Gamal Elnabelsya and Dr. Muslim Majeed, technical officers of the Materials and Structures Laboratory in the Department of Civil Engineering at the University of Ottawa. Likewise, the authors would like to express their sincere gratitude and appreciation to Kryton International, Mr. Alireza Biparva, Mary Grace Rosalin, Dr. Pejman Azarsa. As well as De Souza benefits from the University of Ottawa Excellence Scholarship, Collaborative Research & Development by NSERC (Natural Science and Engineering Research Council of Canada), and the prestigious Vanier CGS scholarship, also financed by the NSERC.

6.9 References

[1] Canadian Standard Association, CSA A23.3-14 Design of concrete structures, (2014) 297.

[2] M. An, H. Huang, Y. Wang, G. Zhao, Effect of thermal cycling on the properties of high-performance concrete: Microstructure and mechanism, Constr. Build. Mater. 243 (2020) 118310. doi:10.1016/j.conbuildmat.2020.118310.

[3] M. Malik, S.K. Bhattacharyya, S. V. Barai, Thermal and mechanical properties of concrete and its constituents at elevated temperatures: A review, Constr. Build. Mater. 270 (2021) 121398. doi:10.1016/j.conbuildmat.2020.121398.

[4] L. Wu, N. Farzadnia, C. Shi, Z. Zhang, H. Wang, Autogenous shrinkage of high performance concrete: A review, Constr. Build. Mater. 149 (2017) 62–75. doi:10.1016/j.conbuildmat.2017.05.064.

[5] D.J. De Souza, M.H.F. Medeiros, J. Hoppe, L.F.M. Sanchez, The uses of finely ground materials to mitigate the external sulphate attack (ESA) on cementitious materials, 2020. doi:10.1007/978-3-030-20331-3_11.

[6] D.J. Souza, L.Y. Yamashita, F. Dranka, M.H.F. Medeiros, R.A. Medeiros-Junior, Repair Mortars Incorporating Multiwalled Carbon Nanotubes: Shrinkage and Sodium Sulfate Attack, J. Mater. Civ. Eng. 29 (2017) 1–12. doi:10.1061/(ASCE)MT.1943-5533.0002105.

[7] X. Huang, S. Hu, F. Wang, L. Yang, M. Rao, Y. Mu, C. Wang, The effect of supplementary

cementitious materials on the permeability of chloride in steam cured high-ferrite Portland cement concrete, Constr. Build. Mater. 197 (2019) 99–106. doi:10.1016/j.conbuildmat.2018.11.107.

[8] Y. Wang, Z. Shui, Y. Huang, T. Sun, P. Duan, Properties of coral waste-based mortar incorporating metakaolin: Part II. Chloride migration and binding behaviors, Constr. Build. Mater. 174 (2018) 433–442. doi:10.1016/j.conbuildmat.2018.04.076.

[9] E. Watanabe, Bridge Maintenance, Safety, Management and Cost, 2014. doi:10.1201/9781482290127.

[10] Y. Yoon, M. Hastak, Annual rehabilitation costs estimation for a bridge network, KSCE J. Civ. Eng. 21 (2017) 27–36. doi:10.1007/s12205-016-1175-0.

[11] H. Tabatabai, A. Ghorbanpoor, M.D. Pritzl, Evaluation of Select Methods of Corrosion Prevention, Corrosion Control, and Repair in Reinforced Concrete Bridges, Wisconsin Highw. Res. Progr. (2009) 1–343.

[12] T. Chandra Sekhara Reddy, A. Ravitheja, Macro mechanical properties of self healing concrete with crystalline admixture under different environments, Ain Shams Eng. J. 10 (2019) 23–32. doi:10.1016/j.asej.2018.01.005.

[13] M. Roig-Flores, S. Moscato, P. Serna, L. Ferrara, Self-healing capability of concrete with crystalline admixtures in different environments, Constr. Build. Mater. 86 (2015) 1–11. doi:10.1016/j.conbuildmat.2015.03.091.

[14] S. Guzlena, G. Sakale, Self-healing concrete with crystalline admixture - A review, IOP Conf. Ser. Mater. Sci. Eng. 660 (2019). doi:10.1088/1757-899X/660/1/012057.

[15] K. Sisomphon, O. Copuroglu, E.A.B. Koenders, Effect of exposure conditions on self healing behavior of strain hardening cementitious composites incorporating various cementitious materials, Constr. Build. Mater. 42 (2013) 217–224. doi:10.1016/j.conbuildmat.2013.01.012.

[16] A.E.M. Abd-Elmoaty, Self-healing of polymer modified concrete, Alexandria Eng. J. 50 (2011) 171–178. doi:10.1016/j.aej.2011.03.002.

[17] D.G. Bekas, K. Tsirka, D. Baltzis, A.S. Paipetis, Self-healing materials: A review of advances in materials, evaluation, characterization and monitoring techniques, Compos. Part B Eng. 87 (2016) 92–119. doi:10.1016/j.compositesb.2015.09.057.

[18] M. Getnet Meharie, Factors Affecting the Self-Healing Efficiency of Cracked Concrete Structures, Am. J. Appl. Sci. Res. 3 (2017) 80. doi:10.11648/j.ajasr.20170306.12.

[19] M. Şahmaran, S.B. Keskin, G. Ozerkan, I.O. Yaman, Self-healing of mechanically-loaded self

consolidating concretes with high volumes of fly ash, Cem. Concr. Compos. 30 (2008) 872–879. doi:10.1016/j.cemconcomp.2008.07.001.

[20] T.C.S.R. Reddy, A.R. Theja, C. Sashidhar, Self-Healing Ability of High-Strength Fibre-Reinforced Concrete with Fly Ash and Crystalline Admixture, Civ. Eng. J. 4 (2018) 971. doi:10.28991/cej-0309149.

[21] K. Van Tittelboom, E. Gruyaert, H. Rahier, N. De Belie, Influence of mix composition on the extent of autogenous crack healing by continued hydration or calcium carbonate formation, Constr. Build. Mater. 37 (2012) 349–359. doi:10.1016/j.conbuildmat.2012.07.026.

[22] H. Kalhori, R. Bagherpour, Application of carbonate precipitating bacteria for improving properties and repairing cracks of shotcrete, Constr. Build. Mater. 148 (2017) 249–260. doi:10.1016/j.conbuildmat.2017.05.074.

[23] M. Luo, C. Qian, Influences of bacteria-based self-healing agents on cementitious materials hydration kinetics and compressive strength, Constr. Build. Mater. 121 (2016) 659–663. doi:10.1016/j.conbuildmat.2016.06.075.

[24] K. Vijay, M. Murmu, S. V. Deo, Bacteria based self healing concrete – A review, Constr. Build. Mater. 152 (2017) 1008–1014. doi:10.1016/j.conbuildmat.2017.07.040.

[25] L. Jiang, G. Jia, C. Jiang, Z. Li, Sugar-coated expanded perlite as a bacterial carrier for crack-healing concrete applications, Constr. Build. Mater. 232 (2020) 117222. doi:10.1016/j.conbuildmat.2019.117222.

[26] K. Sisomphon, O. Copuroglu, E.A.B. Koenders, Self-healing of surface cracks in mortars with expansive additive and crystalline additive, Cem. Concr. Compos. 34 (2012) 566–574. doi:10.1016/j.cemconcomp.2012.01.005.

[27] E. Cuenca, A. Tejedor, L. Ferrara, A methodology to assess crack-sealing effectiveness of crystalline admixtures under repeated cracking-healing cycles, Constr. Build. Mater. 179 (2018) 619–632. doi:10.1016/j.conbuildmat.2018.05.261.

[28] P. Escoffres, C. Desmettre, J.P. Charron, Effect of a crystalline admixture on the self-healing capability of high-performance fiber reinforced concretes in service conditions, Constr. Build. Mater. 173 (2018) 763–774. doi:10.1016/j.conbuildmat.2018.04.003.

[29] M. Nasim, U.K. Dewangan, S. V. Deo, Autonomous healing in concrete by crystalline admixture: A review, Mater. Today Proc. 32 (2020) 638–644. doi:10.1016/j.matpr.2020.03.116.

[30] ACI 212.3R, ACI 212 . 3R-10 Report on Chemical Admixtures for Concrete, American Concrete Institute, 2015.

[31] P. Azarsa, R. Gupta, A. Biparva, Assessment of self-healing and durability parameters of concretes incorporating crystalline admixtures and Portland Limestone Cement, Cem. Concr. Compos. 99 (2019) 17–31. doi:10.1016/j.cemconcomp.2019.02.017.

[32] T.C.S. Reddy, A. Ravitheja, C. Sashidhar, Micromechanical Properties of Self-Healing Concrete with Crystalline Admixture and Silica Fume, ACI Mater. J. 117 (2020) 63–74. doi:10.14359/51722395.

[33] L. Ferrara, V. Krelani, M. Carsana, A "fracture testing" based approach to assess crack healing of concrete with and without crystalline admixtures, Constr. Build. Mater. 68 (2014) 535–551. doi:10.1016/j.conbuildmat.2014.07.008.

[34] T.C.S. Reddy, A. Ravitheja, Macro mechanical properties of self healing concrete with crystalline admixture under different environments, Ain Shams Eng. J. 10 (2019) 23–32. doi:10.1016/j.asej.2018.01.005.

[35] M. Roig-Flores, F. Pirritano, P. Serna, L. Ferrara, Effect of crystalline admixtures on the self-healing capability of early-age concrete studied by means of permeability and crack closing tests, Constr. Build. Mater. 114 (2016) 447–457. doi:10.1016/j.conbuildmat.2016.03.196.

[36] G. Li, S. Liu, M. Niu, Q. Liu, X. Yang, M. Deng, Effect of granulated blast furnace slag on the self-healing capability of mortar incorporating crystalline admixture, Constr. Build. Mater. 239 (2020) 117818. doi:10.1016/j.conbuildmat.2019.117818.

[37] S. Granger, A. Loukili, G. Pijaudier-Cabot, G. Chanvillard, Experimental characterization of the self-healing of cracks in an ultra high performance cementitious material: Mechanical tests and acoustic emission analysis, Cem. Concr. Res. 37 (2007) 519–527. doi:10.1016/j.cemconres.2006.12.005.

[38] S. Jacobsen, J. Maschand, L. Boisvert, Effect of cracking and healing on chloride transport in OPC concrete, Cem. Concr. Res. 26 (1996) 869–881.

[39] W. Zamorowski, The phenomenon of self-regeneration of concrete., Int. J. Cem. Compos. Light. Concr. 7 (1985) 199–201. doi:10.1139/b87-051.

[40] K. Van Tittelboom, N. De Belie, Self-healing in cementitious materials-a review, 2013. doi:10.3390/ma6062182.

[41] W. Zhang, Q. Zheng, A. Ashour, B. Han, Self-healing cement concrete composites for resilient infrastructures: A review, Compos. Part B Eng. 189 (2020) 107892. doi:10.1016/j.compositesb.2020.107892.

[42] M. Wu, B. Johannesson, M. Geiker, A review: Self-healing in cementitious materials and

engineered cementitious composite as a self-healing material, Constr. Build. Mater. 28 (2012) 571–583. doi:10.1016/j.conbuildmat.2011.08.086.

[43] G. Yildirim, Ö.K. Keskin, S.B.I. Keskin, M. Şahmaran, M. Lachemi, A review of intrinsic self-healing capability of engineered cementitious composites: Recovery of transport and mechanical properties, Constr. Build. Mater. 101 (2015) 10–21. doi:10.1016/j.conbuildmat.2015.10.018.

[44] W. Tang, O. Kardani, H. Cui, Robust evaluation of self-healing efficiency in cementitious materials - A review, Constr. Build. Mater. 81 (2015) 233–247. doi:10.1016/j.conbuildmat.2015.02.054.

[45] K. van Breugel, Is there a market for self-healing cement-based materials?, 1St Int. Conf. Self-Healing Mater. (2007) 1–9.

[46] W. Ramm, M. Biscoping, Autogenous healing and reinforcement corrosion of water-penetrated separation cracks in reinforced concrete, Nucl. Eng. Des. 179 (1998) 191–200. doi:10.1016/S0029-5493(97)00266-5.

[47] H.W. Reinhardt, M. Jooss, Permeability and self-healing of cracked concrete as a function of temperature and crack width, Cem. Concr. Res. 33 (2003) 981–985. doi:10.1016/S0008-8846(02)01099-2.

[48] E.H. Yang, Y. Yang, V.C. Li, Use of high volumes of fly ash to improve ECC mechanical properties and material greenness, ACI Mater. J. 104 (2007) 620–628. doi:10.14359/18966.

[49] S. Wang, V.C. Li, Engineered cementitious composites with high-volume fly ash, ACI Mater. J. 104 (2007) 233–241. doi:10.14359/18668.

[50] P. Termkhajornkit, T. Nawa, Y. Yamashiro, T. Saito, Self-healing ability of fly ash-cement systems, Cem. Concr. Compos. 31 (2009) 195–203. doi:10.1016/j.cemconcomp.2008.12.009.

[51] Z. Zhang, S. Qian, H. Ma, Investigating mechanical properties and self-healing behavior of micro-cracked ECC with different volume of fly ash, Constr. Build. Mater. 52 (2014) 17–23. doi:10.1016/j.conbuildmat.2013.11.001.

[52] A. Ravitheja, T.C.S. Reddy, C. Sashidhar, Self-healing concrete with crystalline admixture - A review, J. Wuhan Univ. Technol. - Mater. SCi. Ed. 34 (2019) 1143–1154. doi:10.1088/1757-899X/660/1/012057.

[53] C. Zhang, L. Sorelli, B. Fournier, J. Duchesne, J. Bastien, Z. Chen, Stress-relaxation of crystalline alkali-silica reaction products: Characterization by micro- and nanoindentation and simplified modeling, Constr. Build. Mater. 148 (2017) 455–464. doi:10.1016/j.conbuildmat.2017.05.069.

[54] B. Park, Y.C. Choi, Self-healing capability of cementitious materials with crystalline admixtures and super absorbent polymers (SAPs), Constr. Build. Mater. 189 (2018) 1054–1066. doi:10.1016/j.conbuildmat.2018.09.061.

[55] X. Wang, C. Fang, D. Li, N. Han, F. Xing, A self-healing cementitious composite with mineral admixtures and built-in carbonate, Cem. Concr. Compos. 92 (2018) 216–229. doi:10.1016/j.cemconcomp.2018.05.013.

[56] J.B. Walsh, The effect of cracks on the uniaxial elastic compression of rocks, J. Geophys. Res. 70 (1965) 399–411. doi:10.1029/JZ070i002p00399.

[57] T.M. Chrisp, P. Waldron, J.G.M. Wood, Development of a non-destructive test to quantify damage in deteriorated concrete, Mag. Concr. Res. 45 (1993) 247–256. doi:10.1680/macr.1993.45.165.247.

[58] R.S. Crouch, J.G.M. Wood, Damage evolution in AAR affected concretes, Eng. Fract. Mech. 35 (1990) 211–218. doi:10.1016/0013-7944(90)90199-Q.

[59] N. Smaoui, M.A. Bérubé, B. Fournier, B. Bissonnette, B. Durand, Evaluation of the expansion attained to date by concrete affected by alkali-silica reaction. Part I: Experimental study, Can. J. Civ. Eng. (2004). doi:10.1139/L04-051.

[60] L.F.M. Sanchez, B. Fournier, M. Jolin, M.A.B. Bedoya, J. Bastien, J. Duchesne, Use of Damage Rating Index to quantify alkali-silica reaction damage in concrete: Fine versus coarse aggregate, ACI Mater. J. 113 (2016) 395–407. doi:10.14359/51688983.

[61] L.F.M. Sanchez, B. Fournier, M. Jolin, J. Bastien, Evaluation of the stiffness damage test (SDT) as a tool for assessing damage in concrete due to ASR: Test loading and output responses for concretes incorporating fine or coarse reactive aggregates, Cem. Concr. Res. 56 (2014) 213–229. doi:10.1016/j.cemconres.2013.11.003.

[62] L.F.M. Sanchez, B. Fournier, M. Jolin, D. Mitchell, J. Bastien, Overall assessment of Alkali-Aggregate Reaction (AAR) in concretes presenting different strengths and incorporating a wide range of reactive aggregate types and natures, Cem. Concr. Res. 93 (2017) 17–31. doi:10.1016/j.cemconres.2016.12.001.

[63] Y. Zhu, A. Zahedi, L.F.M. Sanchez, B. Fournier, S. Beauchemin, Overall assessment of alkali-silica reaction affected recycled concrete aggregate mixtures derived from construction and demolition waste, Cem. Concr. Res. 142 (2021) 106350. doi:10.1016/j.cemconres.2020.106350.

[64] L.F.M. Sanchez, B. Fournier, M. Jolin, J. Duchesne, Reliable quantification of AAR damage through assessment of the Damage Rating Index (DRI), Cem. Concr. Res. 67 (2015) 74–92.

doi:10.1016/j.cemconres.2014.08.002.

[65] V. Villeneuve, B. Fournier, J. Duchesne, Determination of the damage in concrete affected by ASR- the damage rating index (DRI), in: Proc. 14th Int. Conf. Alkali-Aggregate React. Concr., 2012.

[66] P.E. Grattan-Bellew, L.D. Mitchell, Quantitative Petrographic Analysis of Concrete – The Damage Rating Index (DRI) Method , A Review, in: 8th CANMET/ACI Int. Conf. Recent Adv. Concr. Technol., 2006.

[67] M.D.A. Thomas, K.J. Folliard, B. Fournier, P. Rivard, T. Drimalas, S.I. Garber, Methods for Evaluating and Treating ASR-Affected Structures: Results of Field Application and Demonstration Projects. Volume II: Details of Field Applications and Analysis Final Report, Fed. Highw. Adm. FHWA-HIF-1 (2013) 338.

[68] F. Shrimer, Use of the damage rating index as input for service life prediction in Alkali-Silica reaction affected concrete, in: ASTM Spec. Tech. Publ., 2018. doi:10.1520/STP161320W0246.

[69] ASTM C150, Standard Specification for Portland Cement, 2018.

[70] ASTM C39, Standard Test Method for Compressive Strength of Cylindrical Concrete Specimens, 2018. doi:10.1520/C0039.

[71] ASTM C1876, Standard Test Method for Bulk Electrical Resistivity or Bulk Conductivity of Concrete, 2019.

[72] ASTM C597, Standard Test Method for Pulse Velocity Through Concrete, 2016.

[73] L.F.M. Sanchez, T. Drimalas, B. Fournier, D. Mitchell, J. Bastien, Comprehensive damage assessment in concrete affected by different internal swelling reaction (ISR) mechanisms, Cem. Concr. Res. 107 (2018) 284–303. doi:10.1016/j.cemconres.2018.02.017.

[74] L.F.M. Sanchez, Contribution to the assessment of damage in aging concrete infrastructures affected by alkali-aggregate reaction, (2014) 341.

[75] L.F.M. Sanchez, B. Fournier, M. Jolin, D. Mitchell, J. Bastien, Overall assessment of Alkali-Aggregate Reaction (AAR) in concretes presenting different strengths and incorporating a wide range of reactive aggregate types and natures, Cem. Concr. Res. 93 (2017) 17–31. doi:10.1016/j.cemconres.2016.12.001.

[76] R. Gagné, M. Argouges, A study of the natural self-healing of mortars using air-flow measurements, Mater. Struct. Constr. 45 (2012) 1625–1638. doi:10.1617/s11527-012-9861-y.

[77] H. Liu, X. Ren, J. Li, Indentation tests based multi-scale random media modeling of concrete, Constr. Build. Mater. 168 (2018) 209–220. doi:10.1016/j.conbuildmat.2018.02.050.

[78] W. Zhu, P.J.M. Bartos, Application of depth-sensing microindentation testing to study of interfacial transition zone in reinforced concrete, Cem. Concr. Res. 30 (2000) 1299–1304. doi:10.1016/S0008-8846(00)00322-7.

[79] P. Lura, P. Trtik, B. Münch, Validity of recent approaches for statistical nanoindentation of cement pastes, Cem. Concr. Compos. 33 (2011) 457–465. doi:10.1016/j.cemconcomp.2011.01.006.

Chapter Seven: Evaluating the efficiency of SCMs to avoid or mitigate AAR-induced expansion and deterioration through the use of the multi-level assessment

Diego J. De Souza[1], Leandro F. M. Sanchez[1]

[1]Department of Civil Engineering, University of Ottawa, Ottawa, Canada.

Abstract

Alkali-Silica Reaction (AAR) is one of the most harmful distress mechanisms affecting the durability and serviceability of concrete infrastructure worldwide. It has been found that AAR-induced expansion and distress may be prevented by the appropriate use of supplementary cementing materials (SCMs). Yet, recent studies find that the deterioration is "only" delayed and does not entirely prevent AAR occurrence. In this context, besides the impact of the SCMs on AAR-kinetics, it is imperative to establish a correlation between the *microscopic/macroscopic* distress degree and features of SCMs-made concrete. Moreover, very little research has been conducted on understanding the elastic properties of ASR-gel and the influence of the use of SCMs on it. This research presents the results of a multi-level assessment of AAR-induced damage development incorporating a wide range of reactive aggregate and SCMs at selected "unrestrained or free" expansion levels (i.e., 0.00%, 0.05%, 0.12%, 0.20% and 0.30%). Moreover, it focuses on the distress generated at distinct locations of affected concrete: aggregate particles, ITZ and cement paste. The latter is expected to aid in understanding the material's deterioration as a function of AAR development.

Keywords: Alkali-silica reaction, the durability of concrete, micro-indentation, overall assessment of the damage

7.1 Introduction

Alkali-Aggregate reaction (AAR) is one of the most harmful distress mechanisms affecting the durability and serviceability of concrete infrastructure worldwide. AAR can be divided into two main reaction types: Alkali-Silica Reaction (ASR), the most common by far, and Alkali-Carbonate Reaction (ACR). Both reaction types generate secondary products that induce swelling pressures within the reacting aggregate material(s) and the adjacent cement paste upon moisture uptake [1–4]. AAR-induced deterioration leads to microcracking, loss of material's integrity and functionality of the affected structure [1–4], significantly impacting on the stiffness, tensile and shear strength of affected concrete, whereas the losses in compressive strength are observed as less significant [5–8].

Over the past decades, several approaches and recommendations, including a variety of accelerated laboratory test procedures, have been developed to assess the potential reactivity of aggregates in the laboratory as well as the efficiency of preventive measures (i.e., supplementary cementing materials such as fly ash, silica fume, blast furnace slag, metakaolin, etc.) to mitigate ASR in the field [4,9–17]. Overall, SCMs can enhance concrete microstructure, impacting ions' mobility and possibly slowing the reaction rate [18–20]. Likewise, these materials can dilute the alkalis available from the clinker and change the properties of the ASR reaction products by consuming $Ca(OH)_2$ from the concrete pore solution [2,9,20]. However, it has been reported that SCMs do not suppress the expansion generated by ACR [21]. Conversely, studies suggest that ASR-induced expansion and distress may be prevented by the appropriate use of SCMs [2,9,17]; yet, recent studies are now finding that the deterioration is "only" delayed and does not entirely prevent ASR occurrence [22]. Furthermore, besides the ASR-induced distress development is well described by Sanchez et al. [23,24], there are no established correlations between the expansion development, and *microscopic/macroscopic* distress of AAR affected SCMs-made concrete.

In that regard, a global understanding of the chemo-mechanical properties of the AAR reaction products (e.g., ASR-gel) and the impact of SCMs on it is imperative to predict and prevent damage in concrete structures and structural components. Furthermore, it is anticipated that ASR-gel features may influence the damage generation and propagation in concrete, especially in field structures/structural components presenting a wide range of exposure conditions and confinement effects. However, there is currently limited information in the literature in this regard. This work presents the results of a multi-

level assessment of AAR-induced damage development addressing the distress generated at distinct locations of affected SCMs-made concrete: aggregate particles, ITZ and binder paste. The latter is expected to aid in the understanding of the material's deterioration as a function of AAR development

7.2 **Background**

AAR damage development is often directly correlated to the level of expansion triggered by the concrete under this physicochemical mechanism. Yet, in the last decades, important progress has been made to better understand and explain the mechanical and microscopical distress development due to AAR in concrete. As widely studied by Sanchez et al. [23,24], cracks are formed within the aggregate particles at the beginning of the physicochemical reaction (i.e., expansion level of about 0.05%). As the ASR-induced damage raises, new cracks are still developed within the aggregate particles; yet the pre-existing cracks keep increasing in length and width, reaching the cement paste. At higher levels of expansion (i.e., expansion of 0.30%), the cracks keep propagating through the aggregate particles and cement paste and due to the "minimum energy law", they start connecting, forming a high crack networking and compromising the mechanical properties of the affected concrete [23,24]. As ASR-induced cracking development begins within the aggregate and propagates to the cement paste, ASR-gel diffuses through the cracks and voids of the different phases of concrete microstructure.

On the other hand, ACR is a much less common concrete distress whose mechanism is still mostly unknown. ACR is viewed by many as a reaction that occurs between the alkali hydroxides of concrete pore solution and certain types of dolomitic limestones [4,25]. It is generally agreed that ACR is accompanied by the process of dedolomitization and formation of calcite and brucite [26]. Although different studies [1,27–29] considered ACR as a form of ASR, the microscopic damage features of the ACR-induced expansion and damage were quite different from ASR [5]. Moreover, currently, there is no model which qualitatively explains ACR-cracking pattern development. Yet, it was found that very few cracks may be found within the aggregate, differently from ASR-affected concrete, at the beginning of the ACR deterioration. In contrast, important cracks are observed in the cement paste. Furthermore, a limited amount of reaction products are observed through the progress of ACR development [5,10].

7.2.1 **Techniques for assessing AAR damage in concrete**

AAR development is frequently associated with its degree of induced expansion [5]; however, it is known that induced expansion leads to critical damage in the affected concrete. Sanchez et al. [5] defined the term "damage" as the harmful consequences of various types of deterioration mechanisms (i.e., loadings, creep, ASR, freezing and thawing, etc.) on the mechanical properties, physical integrity and durability of concrete. Thus, these authors proposed the use of a multi-level assessment protocol composed of microscopic and mechanical test procedures to appraise the damage extent of ASR-affected concrete successfully. Among the multi-level test methods proposed, the Damage Rating Index (DRI) and the Stiffness Damage Test (SDT) are the most promising.

7.2.1.1 **Damage Rating Index (DRI)**

The Damage Rating Index (DRI) is a semi-quantitative microscopic analysis performed using a stereomicroscope (about 15-16 x magnification) where the petrographic damage features associated with AAR are counted through a grid of 1 cm^2 (i.e., 10 × 10 mm units) drawn on the surface of a polished concrete section [23,30]. The number of counts corresponding to each petrographic characteristic is then multiplied by a set of weighting factors, whose purpose is to balance their relative importance towards the distress mechanism. The final DRI value is normalized to an area of 100 cm^2; overall, the higher the DRI number, the more significant the deterioration of affected concrete [3,23,24]. Thus, the DRI is instead a complementary petrographic tool aiming at quantifying the "damage degree" between different members from an affected structure or as a function of time within a specific concrete member.

A complete review of the DRI development and specific considerations on its application are given in Sanchez et al. [3,23,24]. The authors used the DRI to evaluate AAR distress with a wide range of reactive aggregates, different concrete strengths (25-45 MPa) and expansion levels (0.05% to 0.30%). It was found that the DRI is a powerful tool to detect AAR damage/progress in concrete whatever the aggregate type and concrete strength used, mainly when the aggregate particles are analyzed down to 1 mm. Moreover, [3,23,24] proposed the so-called "extended DRI version" in which the microscopic distress features could be presented in absolute values (counts) and relative (%), disregarding the weighting factors, giving a more comprehensive assessment of the damaged concrete specimens.

7.2.1.2 Stiffness Damage Test (SDT)

The Stiffness Damage Test (SDT) was first developed by Walsh (1965) for evaluating the quality of rocks specimens [31], being afterwards adapted for assessing concrete by Crouch [32]. The test procedure is based on a cyclic loading (in compression) of concrete specimens and can quantify the degree of damage or physical integrity of distressed concrete. Both researchers selected the use of fixed loads of either 5.5 or 10 MPa, respectively, at a loading rate of 0.10 MPa. The outcomes of the SDT are the modulus of elasticity, the hysteresis area or the dissipated energy (hysteresis area), the plastic deformation and the non-linearity index (NLI) [3,33].

Details on the test procedure and specific considerations on its application as a diagnostic tool for assessing ASR-affected concrete can be found in Sanchez et al. [3,34]. The method was found very promising for assessing AAR damage and progress in concrete and the authors indicated that 40% of the concrete design strength provided the best correlation between SDT output parameters (Stiffness Damage Index – SDI, Plastic Deformation Index - PDI and Non-Linearity Index - NLI) and the expansion of the ASR-affected concrete. However, since in most practical cases, the 28-day strength of aging concrete structures is unknown, Sanchez [3] suggested that the most suitable approach would be to first determine the compressive strength on cores extracted from locations that are not/less damaged in the structural member under investigation and then use 40% of this value for stiffness damage testing.

7.2.1.3 Compressive strength technique (CS)

Compressive strength is commonly used for structural concrete design. Yet, several past studies also aimed to use it to quantify AAR damage and development with more or less success. In AAR-affected concrete, the compressive strength is a mechanical property that is the least affected by the chemical reaction due to AAR microscopic features (i.e., mainly cracks within the aggregate particles). Significant reductions in compressive strength are only observed for high and very high expansion levels (i.e. >0.20%) as by [5,35], which disables its use for diagnostic purposes.

7.2.1.4 Direct Shear test (DS)

Shear strength in concrete is a property governed by tension and compression forces. Once cracked (and concrete will always present a certain amount of inner cracks, flaws, etc.), concrete may transfer

shear forces across the cracks through two distinct mechanisms: a) dowel effect and; b) shear friction [36]. Several test methods have been developed over the years to evaluate the direct shear capacity and shear friction of reinforced and unreinforced concrete [37–39].

De Souza et al. [10] evaluated AAR-induced expansion and damage on the direct shear strength of affected concrete and developed a simple yet reliable setup to assess AAR progress in the laboratory. The authors found that the AAR significantly influences the direct shear strength of affected concrete's development. Moreover, the impact of the AAR on the shear strength was more significant for low (0.05%) and moderate (0.12%) expansions. Thus, the proposed shear setup showed to be a fast and promising tool for detecting AAR-induced expansion and damage in the laboratory. Yet, only AAR-affected laboratory samples fabricated and monitored under accelerated and free expansion conditions were tested in this program [10].

7.2.2 **Assessment of the mechanical properties of ASR-gel through micro-indentation technique**

Indentation hardness testing has been used to evaluate the mechanical properties of materials [40–44]. More recently, the advent of nano- and micro-scale science, engineering and technology, coupled with substantial progress in instrumentation, has resulted in depth-sensing indentation [45]. A typical measurement via an indenter can record load and displacements from the surface of a material. Amongst these properties, the elastic modulus, E, and hardness, H, are timely obtainable without complicated testing apparatus [45]. The micro-hardness is an important index reflecting the mechanical properties of the material. The principle of the indentation, or Vickers hardness tester, is pressing the diamond corner-cone indenter with a particular shape into the surface of the tested piece under a specific test force [40,41,43]. The test force is maintained for a present time and then removed. The two diagonal lengths of the indentation are measured, and the hardness can be obtained from these lengths.

Indentation has been used in concrete samples in recent years; in general, to assess the mechanical properties of the ITZ and distinct phases of the samples, such as in recycled concrete, different properties of ITZs and mortars [40,41,43]. The E-modulus of various hydrated phases has been determined using different indentation techniques [44]. The microhardness tests were used to study the bulk properties of cement paste with a maximum penetration depth at the level of 10^{-5} m [46]. As the

area of the indenter is larger than the size of homogenous regions of single hydrates [16,47,48], micro-indentation can only deliver data on hydrate assemblages in cement paste, for which an E-modulus in the range of 10–30 GPa were found [16,47,48]. With the significant advances in the conventional Vickers microhardness technique, a novel micro indentation method was developed to investigate the elastic modulus and the micro-strength of ITZ in reinforced concrete [46–48].

7.3 **Scope of the work**

As stated above, a number of techniques have been developed in the past, aiming to assess AAR-induced deterioration in concrete. However, there are no established correlations between the expansion development and *microscopic/macroscopic* distress of AAR-affected SCMs-made concrete. Furthermore, there is currently limited information in the literature appraising the overall features (i.e., stiffness, chemical composition, etc.) of AAR reaction products on damage generation and propagation of affected concrete. Particularly coupling the influence of different types or natures of reactive aggregates and supplementary cementing materials in the AAR reaction products feature and damage development. This research presents the results of a multi-level assessment of the global AAR damage evolution of SCMs-made concrete specimens as a function of induced expansion (i.e., 0.00%, 0.05%, 0.12%, 0.20% and 0.30%). The evaluation laid on the analysis of distinct concrete mixtures made of a wide range of type/nature reactive aggregates and SCMs (i.e., Slag, Fly Ash, Silica Fume, and Metakaolin) and maintained under laboratory conditions enabling AAR development. At the selected expansion levels, microscopic (i.e., Damage Rating Index) and mechanical (i.e., Stiffness Damage Test, Modulus of Elasticity, Shear Strength and Compressive Strength) analyses were conducted and a comprehensive evaluation of the impact of SCMs on ASR-induced deterioration was performed. Moreover, scanning electron microscopy, energy-dispersive X-ray spectroscopy, and micro-indentation were performed in the AAR-affected specimens to evaluate the mechanical features of the reaction products at distinct locations (i.e., aggregate particles, ITZ and cement paste). The latter is expected to aid in understanding the material's deterioration as a function of AAR development.

7.4 Experimental program

7.4.1 Materials

A conventional Portland cement (GU type, equivalent to ASTM Type I), four different types of supplementary cementing materials (blast furnace slag – SG, fly ash class F – FA, silica fume – SF and metakaolin – MK) and five different reactive aggregate types/natures were selected for this study to manufacture nineteen concrete mixtures. The coarse aggregates ranged from 5 to 20 mm in size. Moreover, non-reactive fine (NF) and coarse (NC) aggregates were used and combined with the reactive aggregate materials for concrete manufacturing. Table 7.1 provides information on the different aggregates used in this study; the chemical and physical properties of the selected binder materials are provided in Table 7.2.

Table 7.1: Reactive (ASR/ACR) and non-reactive (NR) aggregates used in the research.

Aggregate		Reactivity	Rock Type	Specific gravity	Absorption (%)	AMBT[a)] (%)
Coarse	SPH	ASR	Greywacke	2.71	0.70	0.33
	SPT	ASR	Siliceous limestone	2.70	0.62	0.31
	SUD	ASR	Mixed mineralogy gravel	2.59	0.60	0.23
	KING	ACR	Dolomitic argillaceous limestone	2.68	0.57	0.12
	LC	NR	Crushed limestone	2.78	0.42	0.02
Fine	TX	ASR	Polymictic sand	2.60	0.89	0.81
	NF	NR	Natural derived from granite	2.60	0.82	0.08

[a)] Results at 14 days of curing of the AMBT (ASTM C 1260) carried out on the aggregates selected

Table 7.2: Chemical composition of the binder materials.

	PC	Slag	FA	SF	MK
SiO_2 (%)	20.10	36.64	56.31	92.86	52.48
Al_2O_3 (%)	5.03	11.14	23.27	0.05	44.35
CaO (%)	61.93	37.32	10.29	0.62	0.12
Fe_2O_3 (%)	3.80	0.40	3.57	0.12	0.61
SO_3 (%)	3.38	0.37	0.19	0.07	0.04
MgO (%)	2.42	12.15	1.07	0.19	0.08
Na_2O_{eq} (%)	0.91	0.63	3.17	0.52	0.38
C_3S (%)	43.24	-	-	-	-
C_2S (%)	25.02	-	-	-	-
C_3A (%)	6.90	-	-	-	-
C_4AF (%)	11.56	-	-	-	-
Specific Gravity	3.12	2.91	2.01	2.20	2.29
Lost on Ignition (%)	2.91	0.49	0.98	5.05	0.69

7.4.2 **Mix-proportions and manufacture of the concrete specimens**

A total of three hundred and eighty concrete cylinders (twenty samples per each of the 19 mixtures), 100 by 200 mm in size, were investigated in this study. Table 6.2 summarizes the concrete mix designs employed in this work. It is worth mentioning that no chemicals (i.e., water reducers, air-entrained, etc.) were used in this research. Moreover, all nineteen concrete mixtures were mix-proportioned as per ASTM C1293 to present the same water to binder ratio (w/b of 0.45) and amount of binder materials (420 $\pm$ 10 kg/m^3). However, adjustments in the volumes of non-reactive aggregates were made in the mixtures to maintain an equal and constant volume of reactive aggregates.

Table 7.3: Concrete mix proportions.

Mixture	w/b = 0.45		Aggregates (kg/m^3)		SCMs (kg/m^3)			
	Water (kg/m^3)	Cement (kg/m^3)	Fine	Coarse	SG	FA	SF	MK
SPH-Control	189	420	836	938				
SPH-SG50		210	822		210			
SPH-FA15		357	806			63		
SPH-FA30		294	776			126		
SPH-SF5		399	828				21	
SPH-SF10		378	821				42	
SPH-MK7.5		389	829					32
SPH-MK15		357	822					63
TX-Control	189	420	765	1020				
TX-SG50		210		1005	210			
TX-FA15		357		988		63		
TX-FA30		294		957		126		
TX-SF5		399		1012			21	
TX-SF10		378		1004			42	
TX-MK7.5		389		1012				32
TX-MK15		357		1005				63
SPT	189	420	771	1000				
SUD			749	982				
KING			733	1030				

Twenty-four hours after casting, the samples were demoulded, and small holes (i.e., 5 mm in diameter by 15 mm deep) were drilled at the two flat ends of the samples. Steel gauge studs were glued in place with a fast-setting cement slurry for longitudinal expansion measurements. Afterwards, the samples were left to harden at 20 °C and 100% RH over 24 hours (totalizing 2 days since casting) before the zero reading was taken. Next, all samples were finally placed in sealed plastic buckets lined with a damp cloth and stored at 38 °C, and 100% RH. The AAR-affected cylinders were monitored for length variations until they reached different expansion levels (i.e., 0.00%, 0.05%, 0.12%, 0.20% and 0.30%).

As per ASTM C 1293, the buckets were cooled down to 23 °C for 16 ± 4 h prior to the periodic measurements. Then, when the cylinders reached the specified expansion levels, they were wrapped in plastic film and kept under 12 °C to inhibit further AAR deterioration until all tests were conducted (due to testing capacity issues). In order to perform each test selected (i.e., mechanical, microscopy and porosity), all concrete specimens were reconditioned in the moist curing room for two days (enabling the samples rewetting and therefore reducing the test's variability) as per CSA23.2-14C [49] and Sanchez et al. [50].

7.4.3 **Assessment of the ASR development in the concrete**

7.4.3.1 **Damage Rating Index (DRI)**

A semi-quantitative petrographic analysis, using the DRI, was performed on one specimen from each concrete mixture at the specific expansion levels, according to the method described by Sanchez et al. [3,23]. The samples were cut in half axially, polished by a hand polishing device, which uses diamond-impregnated rubber disks (nº. 50-coarse, 100, 400, 800, 1500 to 3000-very fine), and 1cm^2 grids were drawn on the surface of the polished sections. Then, a stereomicroscope (16× magnification) was used to perform the test. The DRI final number presented hereafter is the normalized 100 cm^2 value.

7.4.3.2 **Compressive Strength**

Compressive strength was measured through two different approaches with different and specific goals. First, to characterize all mixtures at 28 days, the samples were wrapped and placed at 12 °C, since some of the specimens contained highly reactive aggregates, and ASTM C39 method could not be followed as they could develop some AAR. Then, the cylinders were maintained at 12 °C for 47 days, according to the maturity concept as by ASTM C 1074. Moreover, considering the use of SCMs and the later strength gain, three extra measurements were taken after 93, 150 and 300 days (maturity equivalent to 56, 90 and 180 days, respectively) from all mixtures. Moreover, it is worth mentioning that no strength gain was observed after 300 days under the above storage conditions. Thus, the compressive strength evolution profiles over time were then traced for each concrete mixture, which helped identify the correct CS of sound concrete wherever the time was necessary to achieve the pre-determined expansion levels of the ASR-affected concrete specimens. Likewise, to determine the SDT loading level (i.e., 40% of the maturity equivalent CS). Second, the compressive strength measurements were carried out on two specimens from each concrete mixture after being subjected to

SDT to verify the compressive strength loss of the material as ASR develops. This procedure was adopted and considered valid after Sanchez et al. [3,23] confirmed the essentially non-destructive character of the SDT.

7.4.3.3 Stiffness Damage Test (SDT)

The SDT procedure was performed following Sanchez et al. publications [3,34,35], i.e. using five loading/unloading cycles at a controlled loading rate of 0.10MPa/s with a maximum load corresponding to 40% of the maturity equivalent concrete strength, as mentioned in 7.4.3.2. Furthermore, one verifies that once the ASR-affected specimens yielded one of the studied expansion levels, the samples were wrapped in plastic film and kept under 12 °C to inhibit further AAR deterioration until all tests are conducted (due to testing capacity issues). Thus, before the test procedure, the samples were reconditioned/prepared under 100% RH for 48 hours [50], and the test was conducted. The results obtained hereafter is an average value from three different specimens tested at each expansion level.

7.4.3.4 Direct Shear Test

The direct shear test was performed according to the method and setup proposed by Barr and Hasso [51] and adapted for damaged concrete as per De Souza et al. [6]. The same approach considering the maturity concept was used to characterize the sound concrete values for all concrete mixtures at equivalent 28, 56, 90, and 180 days. After the specimens achieved the expected expansion levels, two samples from each concrete mixture were selected; however, different from the CS, the stiffness damage test was not performed on the samples before the direct shear test. Before testing, all samples were carefully ground so that a circumferential notch was created [6,51]. The notch depth was adopted as about 20 mm ± 3 mm to ensure a shear-type failure without leaving a too-small area of the sample to be tested.

7.4.4 Assessment of the chemo-mechanical properties of AAR reaction products

7.4.4.1 Micro-Indentation

The remaining half of the samples from DRI tests were carefully inspected through the stereomicroscope to localize the most damaged locations with the presence of ASR-gel. Afterwards,

the samples were carefully cut (two samples of 2x2 cm in size per expansion level) and polished using oil and diamond-impregnated rubber disks (nº. 50-coarse, 100, 400, 800, 1500, 3000 to 10000-very fine), without previous drying or any impregnation. The indentation was conducted at a maximum of 48 h after polishing using a diamond indenter for Vickers indentations (Struers Duramin Machine). To evaluate the mechanical properties of AAR reaction products observed within the cracks, either within the aggregate particles or cement paste, a load of 0.09807 N (98 mN) was selected as per [44,52] at expansion levels of 0.12% (for cracks in the aggregate particles) and 0.20% for measures cracks over the aggregate and cement paste. One verifies that the expansion levels of 0.05% and 0.30% were not used to measure the features of AAR reaction products for two main reasons: first, specimens with 0.05% of expansion were not selected due to the difficulties to localize repeatable areas for testing; second, 0.30% expansion was not used due to comparable reasons (i.e., only a few concrete mixtures yielded this expansion). A dwell time of 15 seconds and a minimum of 5 points were measured to obtain the Vickers micro-hardness average values to cover statistics. Figure 7.1 illustrate an example of a polished sample placed for micro-indentation test equipment (Figure 7.1a); in b) an example of ASR-damaged sample with ASR-gel filling the cracks and visual representation of the indent print in the surface of a polished aggregate in c) and ASR-gel in d) under the microscope of Struers Duramin Machine.

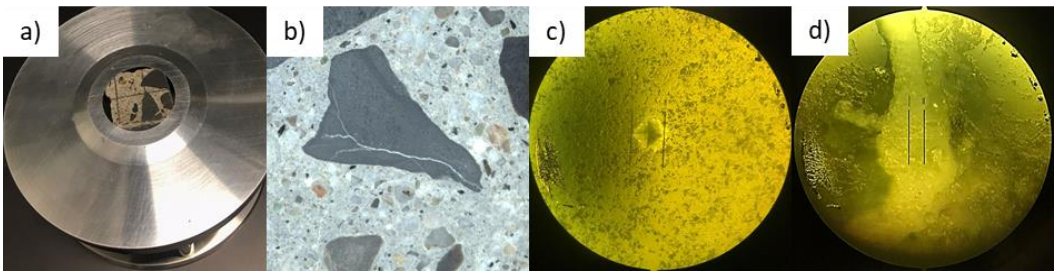

Figure 7.1: a) Example of a polished sample placed for the micro-indentation test; b) example of ASR-damaged sample with ASR-gel filling the cracks; a visual representation of the indent print in the surface of a polished aggregate c) and ASR-gel d) under the microscope of Struers Duramin Machine.

7.4.4.2 Scanning electron microscopy (SEM) & energy dispersive spectroscopy (EDS)

The Scanning electron microscopy (SEM) & energy dispersive spectroscopy (EDS) were performed in the same specimens subjected to micro-indentation analysis; yet, before SEM observations, the

concrete specimens were gently dried for 24 h at 50 °C. Afterwards, they were placed in an EVO MA-10, Carl Zeiss AG equipment in the high-vacuum mode, set at 15 kV, using secondary electron imaging and energy-dispersive X-ray spectroscopy (EDS). Backscattered electron (BSE) images were taken at different magnifications (i.e., x300, x500, x1000 and x3000); however, the main focus of the analysis was to identify the chemical composition of the AAR reaction products found in cracks either within the aggregate particles or cement paste.

7.5 **Results**

7.5.1 **ASR Kinetics**

This section presents ASR expansion kinetics and amplitude results for all mixtures developed in the laboratory. Figure 7.2a displays the expansion results obtained from the mixtures incorporating the five different types/natures of reactive aggregates, while Figure 7.2b illustrates their respective mass variation. Moreover, Figure 4.2c and Figure 4.2d show the expansion amplitudes for the different binder compositions combined with SPH reactive coarse and TX reactive fine aggregates, respectively. The results demonstrate that a wide range of expansion kinetics was obtained as a function of the reactive aggregates and different binder compositions tested. Globally, KING mixtures developed faster reaction kinetics (i.e., yielding 0.30% in 49 days). This mixture involves an extremely reactive coarse dolomitic argillaceous limestone aggregate from the Pittsburgh quarry located in Kingston (Canada). This aggregate is well known to be susceptible to the development of the so-called alkali-carbonate reaction (ACR). On the other hand, for the alkali-silica reactive aggregates (i.e., SPH, SPT, SUD and TX), TX fine displayed faster ASR-kinetics (0.30% in 70 days) and was followed by SPH (0.30% in 132 days), SPT (0.20% in 224 days) and SUD (0.12% in 357 days). In general, the mass gain ranged from 0.43% to 0.86% at maximum expansion levels, and it follows a similar trend as observed for expansion rate.

The replacement of PC by the different types of SCMs significantly altered ASR kinetics of both SPH and TX mixtures. The concrete mixtures MK15 displayed the slower expansion rate throughout evaluation (i.e., 0.02% for SPH and 0.04% for TX) and was closely followed by SF10, achieving 0.03% (SPH-SF10) and 0.06% (TX-SF10) of expansion after 270 days. Overall, aside from the two mentioned mixtures, FA30 presented the lowest expansion, followed by SG50, MK7.5, FA15 and SF5.

Similar trends were observed for both reactive aggregates (SPH and TX), yet TX mixtures yielded higher expansion amplitudes.

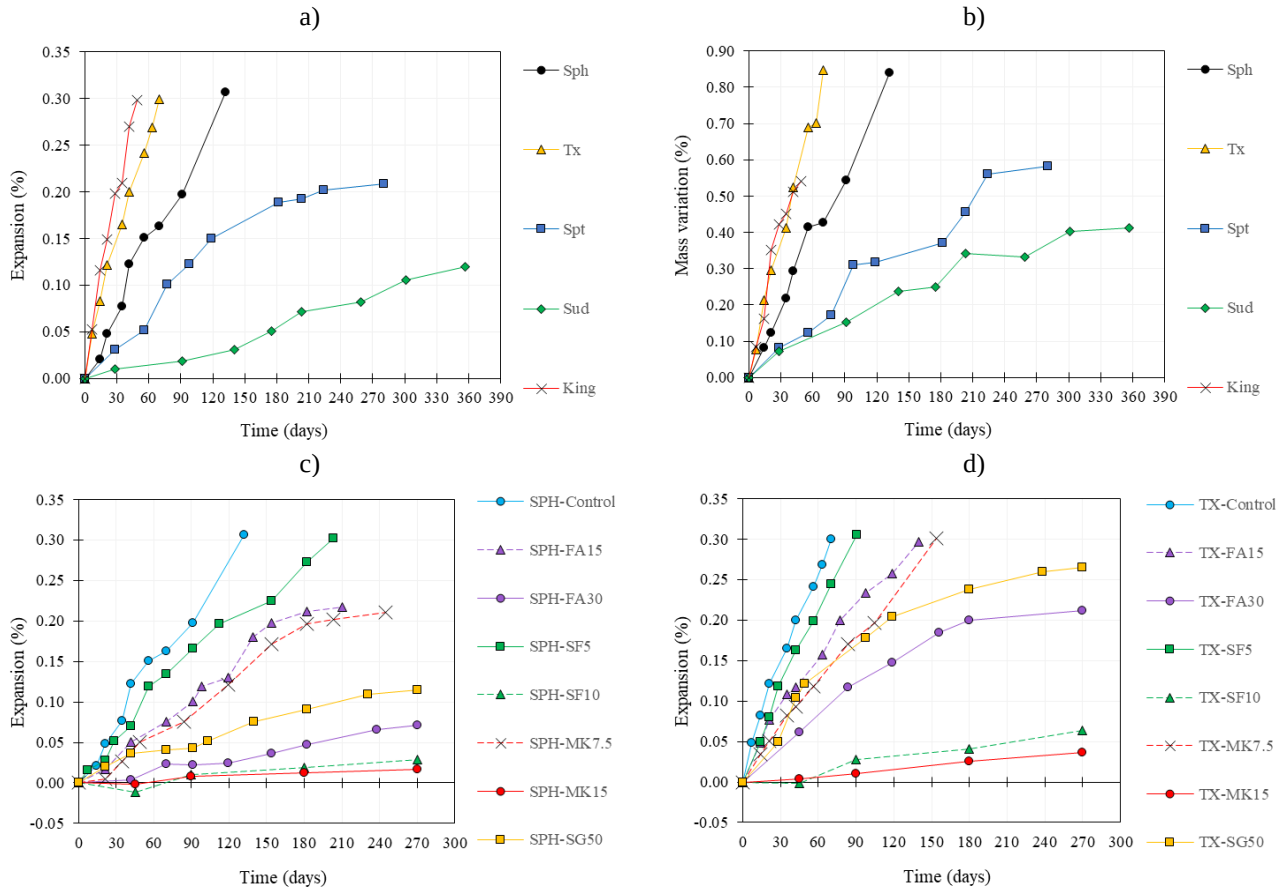

Figure 7.2: AAR development over time: a) expansion and b) mass gain regarding the different reactive aggregates mixtures; c) expansion for different binder compositions made with SPH coarse aggregate; and d) TX fine.

7.5.2 **Damage rating index (DRI)**

Figure 7.3 presents the DRI numbers obtained from the AAR-affected concrete specimens. A complete description of the microscopic features over the AAR development of the SCMs-made concrete and the different types of reactive aggregates is given in the discussion section. Globally, all DRI numbers increase as a function of the specimens' expansions. Furthermore, the ASR-reactive aggregates (i.e., SPH, TX, SPT and SUD) displayed somewhat similar values of DRI (Figure 7.3a). In contrast, the KING mixture gathered considerably higher DRI numbers over the expansion levels. The mixtures incorporating SCMs as binder materials (Figure 7.3b) developed a close trend than ASR control mixtures. Yet, it is clear that higher levels of PC replacement imply an overall lower DRI number for

each expansion degree (i.e. SPH-MK15 at 0.05%, TX-SG50, SPH-SG50 and TX-FA30 at 0.12%, and TX-SG50 and TX-FA30 at 0.20%).

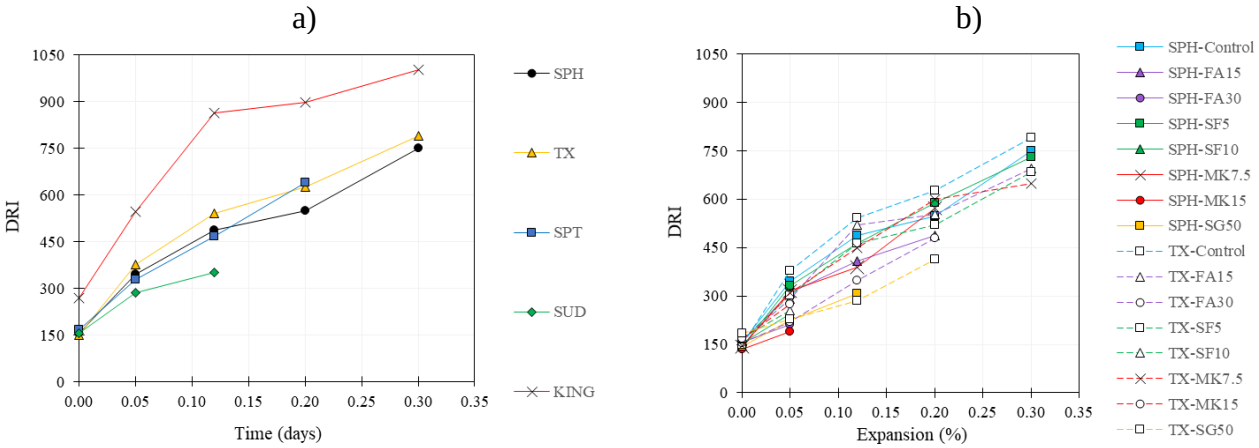

Figure 7.3: Damage Rating Index vs. expansion levels: a) for the different aggregates and b) for mixtures incorporating different types of SCMs.

7.5.3 **Compressive strength (CS)**

Figure 7.4 illustrates the compressive strength reductions for the different concrete mixtures investigated and obtained at each selected "free" expansion level. In general, the CS was found to decrease somewhat modestly compared to the other mechanical properties tested, presented in the following sections. As displayed in Figure 7.4a, the CS losses for samples with low expansion levels (i.e., 0.05%) ranged from 0.01 to 0.10, with which SPT mixtures presented the lowest value and KING, the highest. Moreover, higher expansion levels indicate higher losses in CS. At 0.12% of expansion, the CS reduction values ranged from 0.09 and 0.21, while for 0.20% and 0.30%, it was obtained 0.14-0.26 and 0.22-0.31, respectively. For SCMs-made concrete mixtures (Figure 7.4b), a higher range of values was found of each pre-defined expansion level; yet the global trend in CS reduction is quite similar to Figure 7.4a. The values of CS variations obtained ranged from -0.11 to 0.12 at 0.05% of expansion, from 0.01 to 0.21 at 0.12%, from 0.05-0.23 and 0.17-0.34 at 0.20% and 0.30%, respectively.

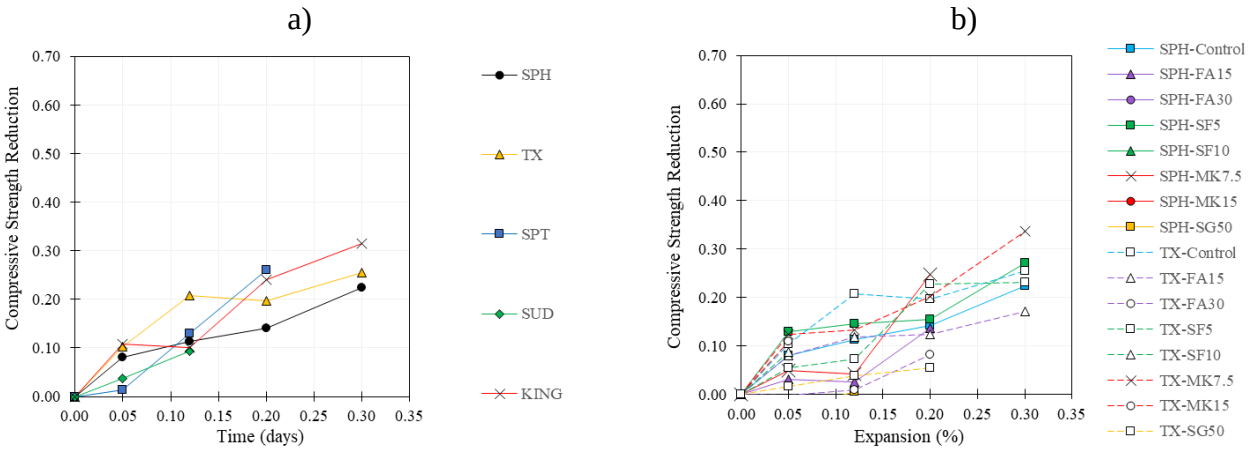

Figure 7.4: Compressive strength reduction vs. expansion levels: a) for the different aggregates and b) for mixtures incorporating different types of SCMs.

7.5.4 **Stiffness damage index (SDI)**

Figure 7.5 illustrates the SDI obtained in this work through the *stiffness damage test* (SDT) method as per Sanchez et al. [3,34,35] of the distinct concrete mixtures investigated. By incorporating different reactive aggregates, the SDI values range from about 0.09 at 0.00% of expansion to 0.31 at 0.30%. Moreover, the overall behaviour of the specimens displays a concave-shaped trend over the AAR development, either for Figure 7.5a or Figure 7.5b. It is worth noting that comparing the mechanical data gathered in this work, SDI displayed the lowest variation between the distinct mixtures at each expansion level. In general, the range of values observed in Figure 7.5a were 0.09-0.14 (at 0.00%), 0.11-0.15 (0.05%), 0.15-0.21 (0.12%), 0.20-0.27 (0.20%), and 0.26-0.31 at 0.30%. Furthermore, comparable values were found for SCMs-made concrete mixtures (Figure 7.5b). The only exception was at 0.00% of expansion, where the results were slightly lower, ranging from 0.06-0.12.

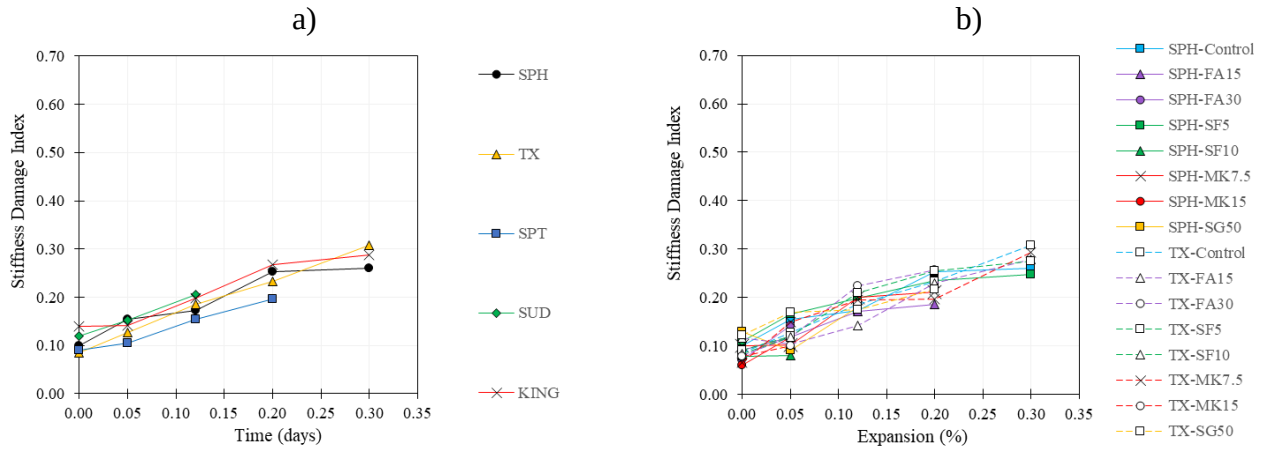

Figure 7.5: Stiffness Damage Index vs. expansion levels: a) for the different aggregates and b) for mixtures incorporating different types of SCMs.

7.5.5 **Modulus of Elasticity (ME)**

Figure 7.6 displays the ME reductions for concrete mixtures a) incorporating the five reactive aggregates and b) combining the different SCMs with SPH and TX aggregates. Even though the different mixtures gathered a wide range of ME loss; the values indicate in both graphs Figure 7.6a and b a concave trend towards AAR-induced development. In general, incorporating different reactive aggregates resulted in a range of values between 0.10-0.26, 0.29-0.38, 0.42-0.59 and 0.51-0.65 at 0.05%, 0.12%, 0.20% and 0.30% of expansion, respectively. The mixtures containing SCMs displayed a much widely variation in ME loss, at 0.05%, 0.12%, 0.20% and 0.30% of induced free expansion, the values were from 0.03-0.34, 0.27-0.45, 0.38-0.59 and 0.55-0.65, respectively.

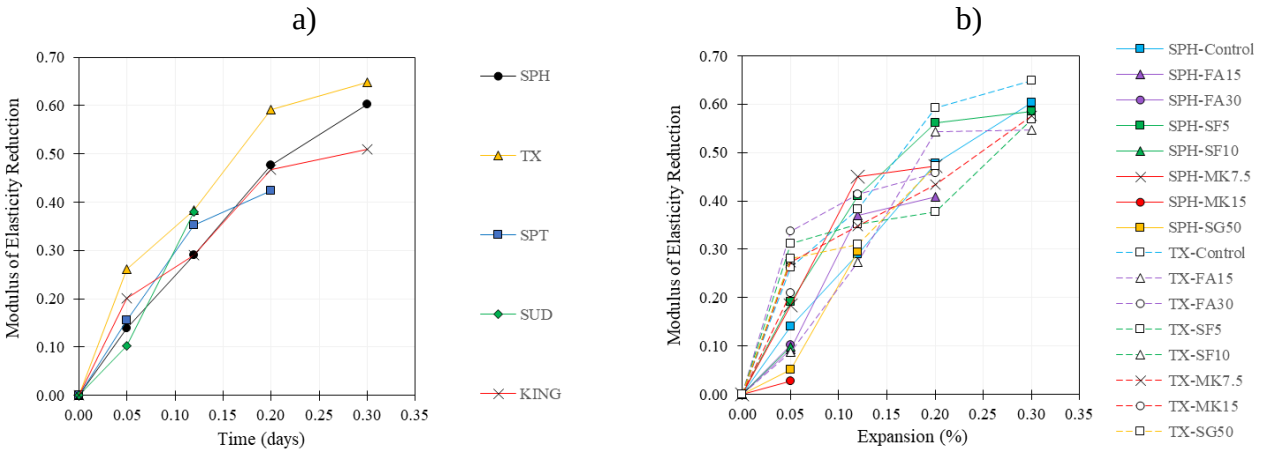

Figure 7.6: Modulus of Elasticity reduction vs. expansion levels: a) for the different aggregates and b) for mixtures incorporating different types of SCMs.

7.5.6 **Direct shear strength (DSS)**

In the direct shear strength (DSS) results of the affected samples, all mixtures displayed shear strength reduction in function of ASR reaction degree as illustrated in Figure 7.7a and Figure 7.7b. Moreover, there is a similar reduction for the distinct mixtures comprising different reactive aggregates and binder compositions. Examining both plots, one may notice that the higher the expansion level, the higher the DSS reduction. Yet, there is "only" a slight difference from damage degree of 0.20% and 0.30%, which displays a somewhat "concave" shape regarding the DSS losses trend. The only exception was seen for the KING mixture that presented a significant variation from 0.20% to 0.30% of the expansion. Overall, the DSS of concrete mixtures without SCMs (Figure 7.7a) ranged from 0.09-0.33, 0.21-0.39, 0.29-0.49 and 0.45-0.53 for 0.05%, 0.12%, 0.20% and 0.30% of expansion, respectively. Likewise, Figure 7.7b indicates similar losses, by replacing the PC by the SCMs the DSS reduction values obtained were from 0.06-0.38, 0.24-0.54, 0.35-0.50 and from 0.47-0.58 for 0.05%, 0.12%, 0.20% and 0.30%, respectively.

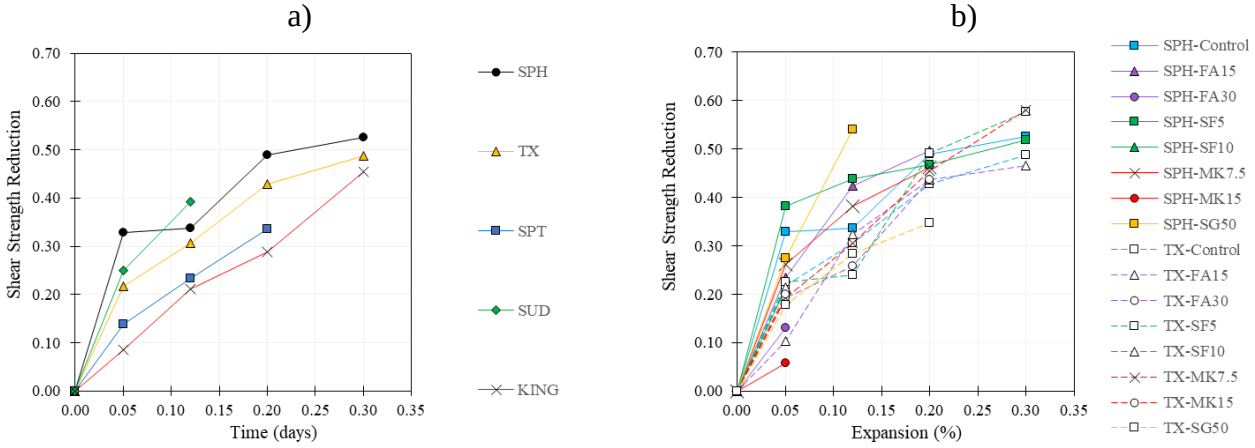

Figure 7.7: Direct shear strength reduction vs. expansion levels: a) for the different aggregates and b) for mixtures incorporating different types of SCMs.

7.5.7 **Assessment of the chemo-mechanical properties of AAR reaction products**

7.5.7.1 **Micro-indentation**

The Vickers hardness average values are displayed in Figure 7.8. Figure 7.8a illustrates the results performed on opened cracks (i.e., crack width average of 120 $\pm$ 20 μm) and filled with AAR rection products, observed in specimens that reached 0.12% of expansion (to comprise all specimens with

similar expansion level). It is worth mentioning that these cracks were not in contact with the cement paste, at least in the visible polished surface. The results indicate the product found within the KING (ACR aggregate) particles had 63.6 HV, the highest among all samples. Regarding the ASR aggregates, TX displayed the higher values (46.6 HV), as was followed by SPT (29.8 HV), SPH (20.2 HV) and SUD (17.5 HV). Figure 7.8b, on the other hand, illustrates the measurements taken on the ASR-gel from the mixtures containing different binder compositions and made of SPH or TX. However, this time the cracks were evaluated in distinct specimen regions, i.e., within the aggregate particle, in the edge of the aggregate and binder paste. It is important to mention that the expansion level of 0.20% was selected to comprise the higher number of specimens with the same expansion. The only exception is the mixture SPH-SG50, in which the expansion of the sample was 0.12%. Globally, the Vickers hardness taken within the aggregate particles was the lowest comparing the different regions. For SPH-made mixtures, the values ranged from 17.0 HV (SPH-SG50) to 25.1 HV (SPH-FA15) and for TX from 13.6 HV (TX-SG50) to 44.1 HV (Control). At the same time, the measurement in the paste matrix ranged from 86.8 HV (SPH-SG50) to 138.6 HV (Control) for SPH mixtures and TX from 67.5 HV (TX-FA30) to 135.9 HV (Control). Finally, the values obtained in edge the aggregate, the averagely highest values by region, ranged from 89.4 HV (SPH-SG50) to 198.6 HV (SPH-SF5) for SPH concrete mixtures and from 74.1 HV (TX-FA30) to 156.6 HV (Control) for TX mixtures.

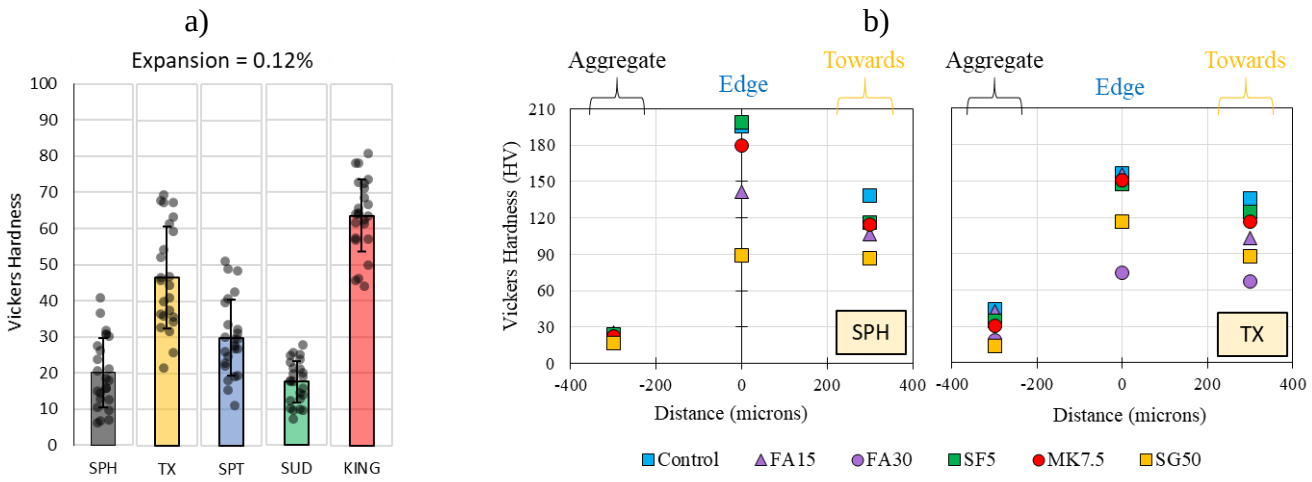

Figure 7.8: Vickers micro-hardness profile: a) taken in the AAR reaction products within the aggregate particles; and c) in ASR-gel within the aggregates/ASR-gel at edge of aggregate/ASR-gel in the paste matrix.

7.5.7.2 Scanning electron microscopy (SEM) & energy dispersive spectroscopy (EDS)

Figure 7.9a and b illustrate the typical microstructure of cracks filled with AAR reaction products (ASR in Figure 7.9a and ACR in Figure 7.9b). One verifies that the visible microcracks observed in the reaction products were perhaps caused by drying shrinkage occurring during the drying step (24 h at 50 °C). As previously mentioned, SEM and EDS analysis were performed in all different reactive aggregates (i.e., SPH, TX, SPT, SUD, and KING) and SPH and TX concrete mixtures that yielded at least 0.20% of the expansion. A summary of the chemical compositions of the particular AAR reaction products found in opened cracks within the reactive aggregates is displayed in Table 7.4. Likewise, Table 7.5 presents the data gathered in cracks filled with ASR-gel over the aggregate, interfacial transition zone (ITZ), and cement paste for SPH and TX control mixtures. Finally, Table 7.6 displays only the chemical composition of the ASR-gel obtained in the cement paste of concrete mixtures incorporating different binder compositions. Overall, the composition of the reaction products shows little variation from one aggregate to another (Table 7.4). The only exception is the KING aggregate, which reveals a lower amount of silica (Si) while higher calcium content (Ca), thus higher Ca/Si-ratio (i.e., 0.51, while the average for SPH, TX, SPT, and SUD was 0.25). On the other hand, the data gathered from different regions in the specimens demonstrate expressive variation in the ASR-gel composition once the cracks achieve the cement paste. On average, from within the aggregate particle to ITZ and cement paste, the Si content decreased 57% in values gathered in the ITZ and 64% in the cement paste. Moreover, the amount of calcium increased 191% and 142% in the ITZ and cement paste, respectively; thus, rising Ca/Si-ratio and dropping (Na + k)/Ca-ratio (Table 7.5). Finally, the different compositions of the binder material in the mixtures seem to influence the composition of the ASR-gel found within the cracks in the cement paste. Globally, the higher the PC's replacement level by the SCMs, the lower the calcium content in the ASR-gel; consequently, the lower the Ca/Si-ratio. The mixtures SG50 and FA30 achieved the lowest Ca/Si-ratios (i.e., 0.77 and 0.82, respectively), whereas FA15, SF5 and MK7.5 were found to have 1.07, 1.17 and 1.20, respectively (Table 7.6).

a)

b)

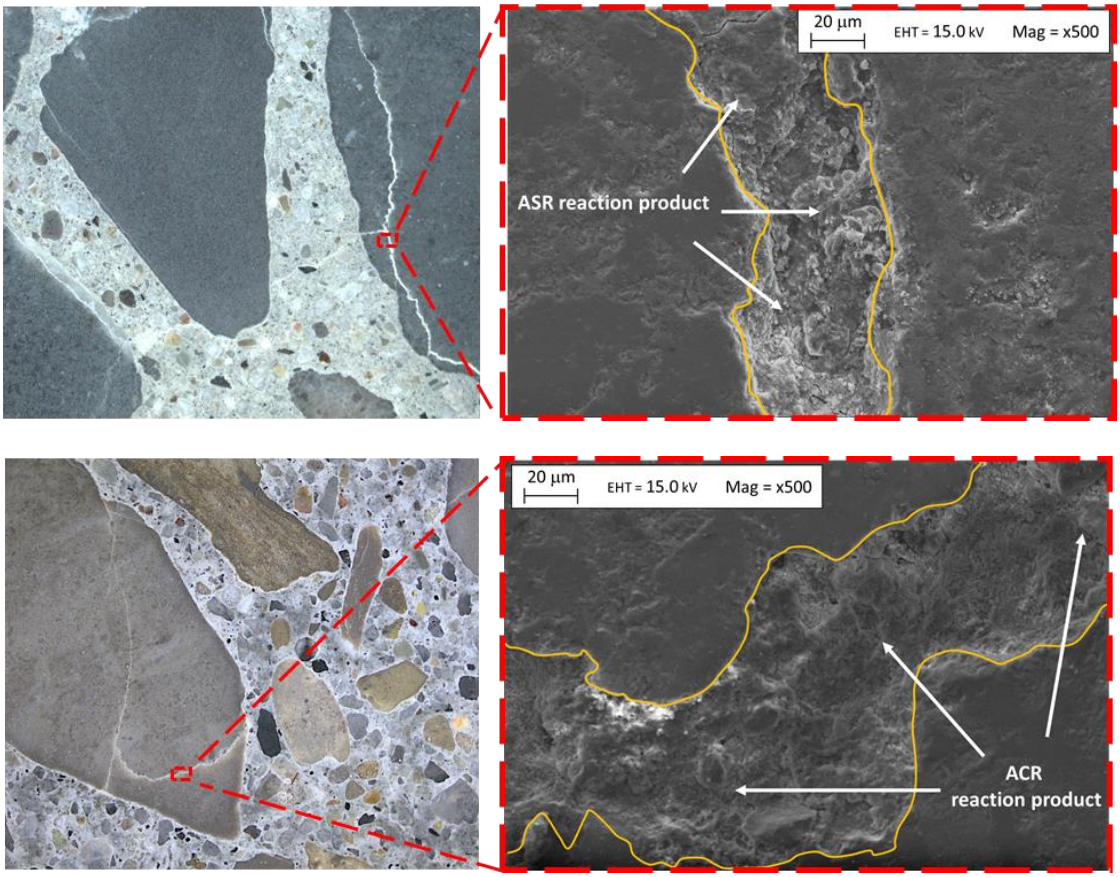

Figure 7.9: Illustration of SEM-image of the studied AAR products: a) taken from SPH reactive aggregate (ASR); and b) from KING reactive coarse aggregate (ACR).

Table 7.4: Composition of the reaction products in five different reactive aggregates, SPH, TX, SPT, SUD and KING.

Element in mol-%	Aggregate					
	SPH	TX	SPT	SUD	KING	
O	46.12 + 1.84	45.43 + 1.81	46.21 + 1.83	45.21 + 1.78	43.07 + 1.74	
Na	1.77 + 0.53	2.37 + 0.71	2.08 + 0.62	2.75 + 0.75	4.42 + 1.31	
Mg	0.14 + 0.04	0.41 + 0.12	0.32 + 0.09	0.46 + 0.12	2.49 + 0.75	
Al	0.18 + 0.05	1.70 + 0.51	1.18 + 0.35	1.69 + 1.45	1.57 + 0.47	
Si	35.51 + 1.39	32.62 + 1.31	34.49 + 1.36	31.97 + 1.15	27.22 + 1.07	
K	8.75 + 0.86	6.98 + 0.69	7.02 + 0.70	6.35 + 0.57	5.39 + 0.54	
Ca	7.54 + 0.74	9.33 + 0.94	7.84 + 0.77	8.45 + 0.77	13.84 + 1.39	
Fe	0.00 + 0.00	1.15 + 0.34	0.86 + 0.26	3.12 + 1.44	2.00 + 0.60	
Ca/Si	0.21 + 0.03	0.29 + 0.04	0.23 + 0.04	0.26 + 0.03	0.51 + 0.05	
(Na + K)/Si	0.30 + 0.09	0.29 + 0.08	0.26 + 0.08	0.28 + 0.08	0.36 + 0.1	
(Na + K)/Ca	1.39 + 0.1	1.00 + 0.14	1.16 + 0.13	1.08 + 0.09	0.71 + 0.14	
Na/K	0.20 + 0.06	0.34 + 0.1	0.30 + 0.06	0.43 + 0.17	0.82 + 0.21	
Num. of Spectrums	87	62	37	26	29	

Table 7.5: Composition of the reaction products in different regions of the concrete specimens 300 µm from ITZ within the aggregate, ITZ, and cement paste.

Element in mol-%	300 microns						Edge of the aggregate						Cement paste					
	SPH			TX			SPH			TX			SPH			TX		
O	45.34	+	1.81	45.08	+	1.77	40.73	+	1.63	38.72	+	1.54	39.98	+	1.58	41.31	+	1.64
Na	1.85	+	0.74	1.39	+	0.55	1.62	+	0.64	2.79	+	1.10	1.30	+	0.51	2.15	+	0.86
Mg	0.35	+	0.21	0.25	+	0.15	0.85	+	0.50	0.45	+	0.26	0.77	+	0.46	0.78	+	0.46
Al	0.49	+	0.30	0.16	+	0.09	4.95	+	2.96	2.68	+	1.62	3.76	+	2.21	1.80	+	1.07
Si	33.59	+	1.32	33.37	+	1.31	19.81	+	0.79	18.46	+	0.74	19.05	+	0.76	23.56	+	0.94
K	8.25	+	0.82	8.30	+	0.82	0.96	+	0.10	4.12	+	0.41	1.87	+	0.19	2.91	+	0.29
Ca	9.28	+	0.91	11.22	+	1.13	30.24	+	2.99	29.37	+	2.89	23.40	+	2.36	26.21	+	2.57
Fe	0.84	+	0.08	0.23	+	0.02	0.84	+	0.09	3.41	+	0.34	9.87	+	0.98	1.28	+	0.13
Ca/Si	0.28	+	0.03	0.34	+	0.04	1.53	+	0.18	1.59	+	0.19	1.23	+	0.15	1.11	+	0.13
(Na + K)/Si	0.30	+	0.04	0.29	+	0.03	0.13	+	0.02	0.37	+	0.04	0.17	+	0.02	0.21	+	0.03
(Na + K)/Ca	1.09	+	0.13	0.86	+	0.10	0.09	+	0.01	0.24	+	0.03	0.14	+	0.02	0.19	+	0.02
Na/K	0.22	+	0.03	0.17	+	0.02	1.69	+	0.20	0.68	+	0.08	0.70	+	0.08	0.74	+	0.09
Num. of Spectrums	26			31			31			28			35			39		

Table 7.6: Composition of the reaction products found in the paste matrix of different concrete mixtures, FA15, FA30, SF5, MK7.5, and SG50.

Element in mol-%	FA15		FA30	SF5		MK7.5		SG50	
	SPH	TX	TX	SPH	TX	SPH	TX	SPH	TX
O	41.12	40.83	40.77	40.70	39.87	42.19	40.70	41.63	41.20
Na	3.80	1.94	3.83	1.22	4.12	0.94	1.43	1.95	3.80
Mg	0.09	1.64	0.84	0.47	0.69	1.83	2.03	1.22	0.74
Al	3.77	3.62	4.15	0.47	2.86	5.70	6.66	4.48	4.38
Si	22.20	21.08	22.48	23.43	21.33	21.61	18.59	22.61	22.71
K	3.06	3.16	8.26	3.33	6.71	0.87	2.99	5.24	6.58
Ca	22.56	23.56	18.40	28.99	23.59	24.99	23.20	16.15	18.87
Fe	3.39	4.18	1.26	1.40	0.84	1.87	4.39	6.71	1.73
Ca/Si	1.02	1.12	0.82	1.24	1.11	1.16	1.25	0.71	0.83
(Na + K)/Si	0.31	0.24	0.54	0.19	0.51	0.08	0.24	0.32	0.46
(Na + K)/Ca	0.30	0.22	0.66	0.16	0.46	0.07	0.19	0.45	0.55
Na/K	1.24	0.62	0.46	0.37	0.61	1.08	0.48	0.37	0.58
Num. of Spectrums	37	35	29	28	38	38	32	31	25

7.6 Discussions

7.6.1 Overall distress of concrete under "free" AAR-induced expansion

AAR-induced damage development is often directly correlated with the level of expansion triggered by the concrete under this physicochemical mechanism. Yet, in the last decade, important progress has been made to better understand and explain the development of mechanical and microscopical distress due to AAR in concrete. As widely studied by Sanchez et al. [5,23,24] for conventional concrete with strengths of 25, 35 and 45 MPa and without supplementary cementing materials (SCMs), ASR-induced damage progress starts with cracks being formed within the reactive aggregate particles (i.e. at expansion level of 0.05%). At this point, a notable increase in DRI number (Figure 7.3a) and SDI (Figure 7.5a) are verified; likewise, the stiffness of the ASR-affected concrete significantly drops (losses from 10% to 26%), which is somewhat expected once the modulus of elasticity is governed by the aggregate particles for conventional concrete [53]. Moreover, one verifies that cracks within the aggregate particles considerably impact the "aggregate interlock", thus reflecting in the shear strength, which achieved losses from 15% to 33% for ASR aggregates. On the other hand, the compressive strength is much less affected (up to 10% in loss).

As the expansion levels rise (i.e. 0.12%), more cracks are formed; nevertheless, the pre-existing cracks keep increasing in length and width, reaching the cement paste [5,23,24]. At this moderate level of expansion, there are significant increases in the total DRI number (351 to 542) and SDI (0.15 to 0.20); besides, the drops in modulus of elasticity and shear strength were more heightened, reaching values in between 29% and 38% (ME loss) 23% and 39% (DSS loss). One interesting observation made during the microscopic analysis of concrete mixtures fabricated with SPT and SPH reactive (ASR) coarse aggregates is that two different trends were found between the overall crack formation and propagation of concrete made with these two aggregates. For SPT, it was found much more frequently onion skin/echelon type of crack, crack type B as described by [24], whereas in SPH-made concrete it was more common the sharp type of cracks (Type A of cracks as [24]) passing almost through the aggregate particle (Figure 7.10). These diverse types of distress features between both aggregates may explain the distinct losses in shear strength obtained; hence the "aggregate interlock" is affected differently. Nevertheless, as mentioned above, the cracks start propagating over the paste matrix at moderate

expansion levels; thus, distinguished losses in the compressive strength were detected (i.e., losses from 10% to 21%).

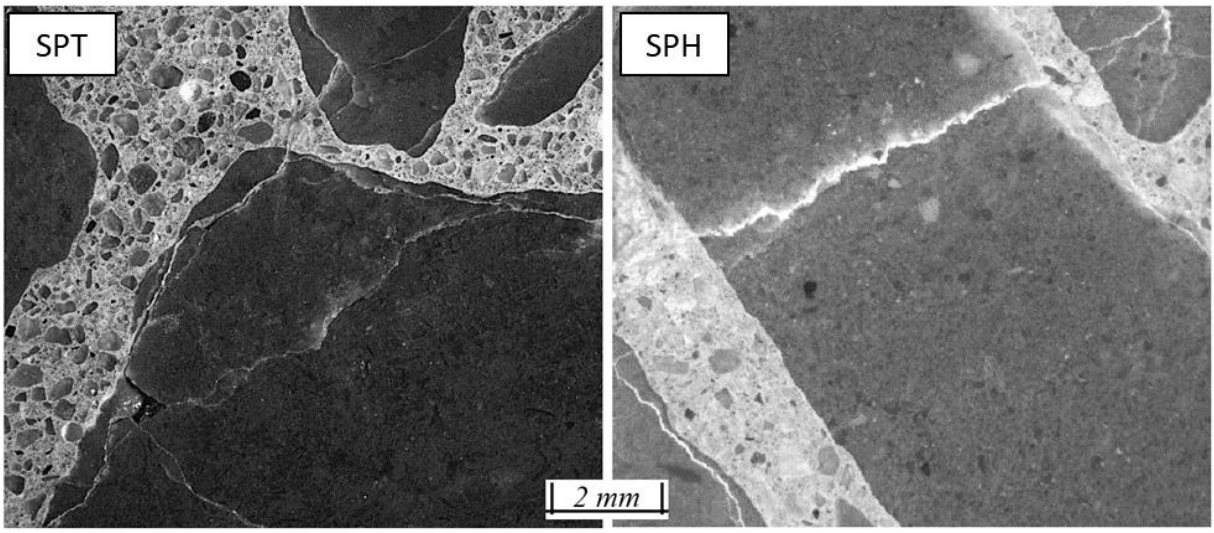

Figure 7.10: Typical cracking features in the concrete incorporating siliceous limestone (SPT) and greywacke (SPH), both reactive coarse aggregate

At a higher level of expansion (i.e. 0.20%), several cracks are found to have crossed the entire particle of the reactive aggregate, and the vast majority of the cracks generated within the aggregate have propagated through the cement paste [5,23,24]. Thus, resulting in a substantial increase in SDI (0.20-0.26) and total DRI numbers (i.e., from 548 to 639); moreover, ME, shear and compressive strengths keeps dropping, achieving losses of 42% to 59% for ME, 34% to 49% for DSS and 14% to 26% for CS. Finally, at about 0.30% of expansion, the cracks start to connect, forming a high crack networking considerably compromising all the mechanical properties of the affected concrete [23,24].

On the other hand, ACR-induced expansion and damage features propagation displayed a particular mechanism of deterioration (i.e., cracks generation and propagation). Besides the notably fast reaction kinetics observed by the concrete made of KING, it was also observed that at lower expansion levels (i.e., 0.05%), several cracks in the cement paste, a few of them partially filled by reaction products. Moreover, the overall loss in compressive strength seems to develop much earlier. One verifies that once cracks reach the cement paste at low and moderate expansion levels, the total DRI number obtained was higher than the ASR-affected concrete mixtures. On the other hand, the DSS loss seems to be slightly less affected over the expansion development. Therefore, it is worth noting that besides

some similarities between ACR and ASR, the distress mechanism appears to be significantly different between them and causing a distinct impact on the mechanical response of the affected materials.

7.6.2 **Distress development of ASR-induced expansion on SCMs-made concrete**

The extensive testing conducted allowed some characteristics of the influence of supplementary cementing materials on the overall behaviour of ASR-affected concrete. In general, ASR damage development of the SCMs-made concrete mixtures follows similar distress characteristics than concrete made only with Portland cement as the binder material. Yet, distinguishing features were noticed, evidencing that SCMs-made concrete should be considered distinctly. One may notice that although SCMs significantly modify ASR-kinetics as emphasized in the literature and results section [11,20,54–56], one of the main objectives of this study was to verify if the distress of SCMs-made concrete is analogous to "conventional concrete" once they both reach similar expansion levels.

The study of Sanchez et al. [5] presents a very suitable description of the ASR distress development characteristics. Moreover, the authors elaborated a table to help practical engineers classify the damage degree of ASR-affected concrete, which correlates the reference expansion level with mechanical and microscopical features. In general, both control mixtures (SPH and TX) fit in the ranges proposed by the authors. Furthermore, besides minor variations, all SCMs-made concrete presented in this research had their stiffness losses and SDI values within the proposed ranges in all evaluated expansion levels. Moreover, the losses in shear strength obtained were quite like the Control mixes, indicating a lower influence of the SCMs in this property. Yet, the petrographic features (Figure 7.11) and the rate of compressive strength loss were notably affected by replacing the PC for the SCMs. In general, the higher the PC replacement level, the lower the CS losses and total DRI number at each expansion amplitude. The microscopic features for concrete mixtures incorporating the different types of SCMs are illustrated in Figure 7.11, taking into account the weighting factors [24], while Figure 7.12 (relative features in %) and Figure 7.13 (crack density) are presented disregarding the weighting factors. The results obtained give a more comprehensive assessment of the ASR-damaged concrete specimens, and the following discussion can be drawn.

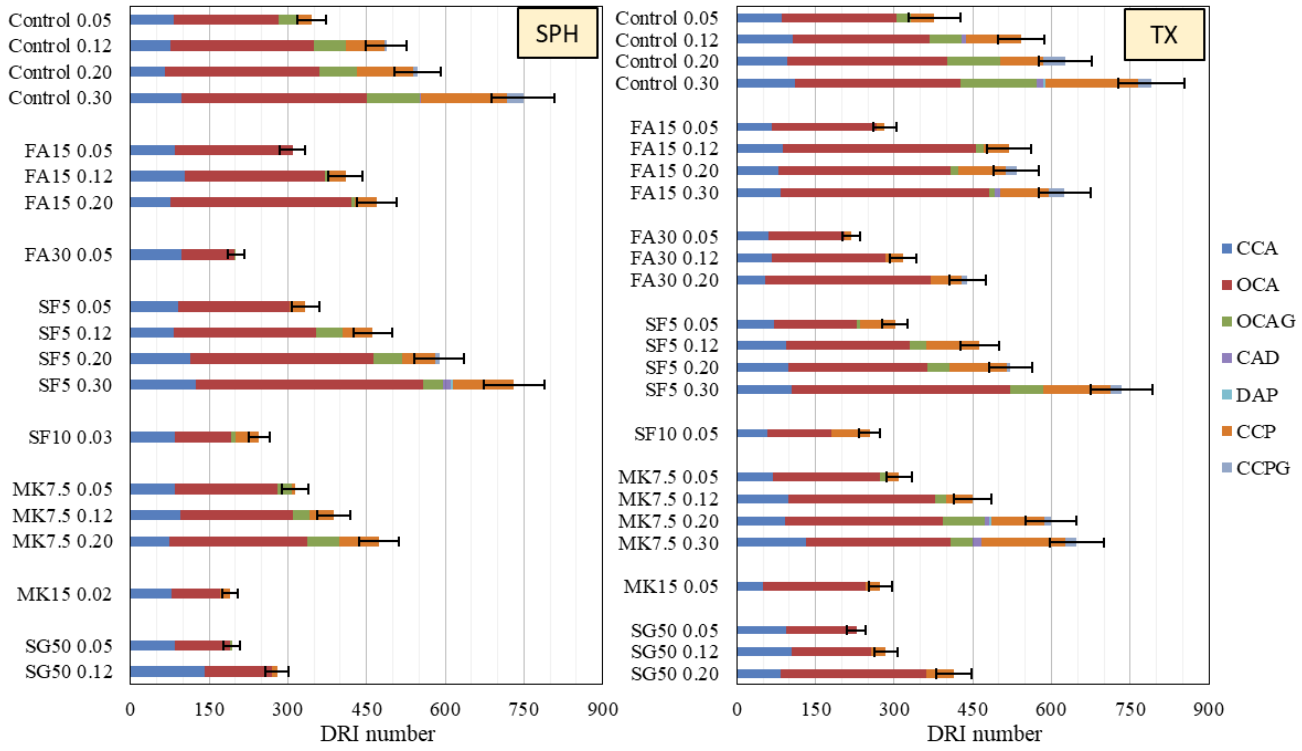

Figure 7.11: Petrographic features for concrete mixtures incorporating different SCMs with SPH and TX aggregates.

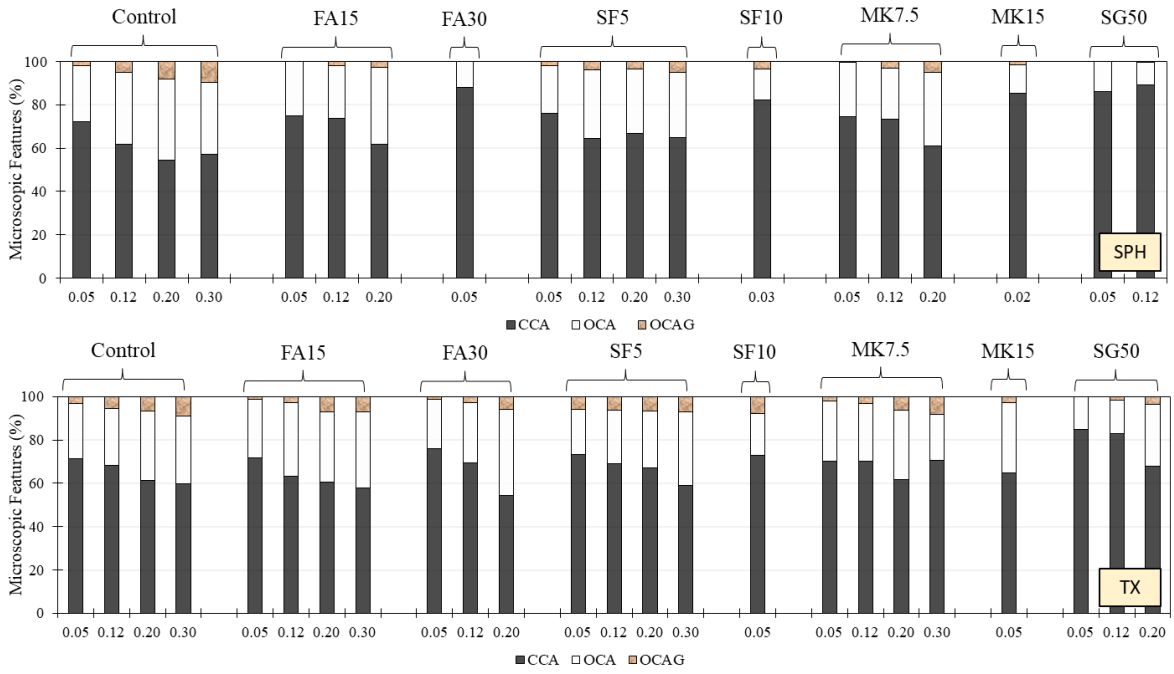

Figure 7.12: Percentage of microscopic features (disregarding weighting factors) in SCMs-made concrete mixtures

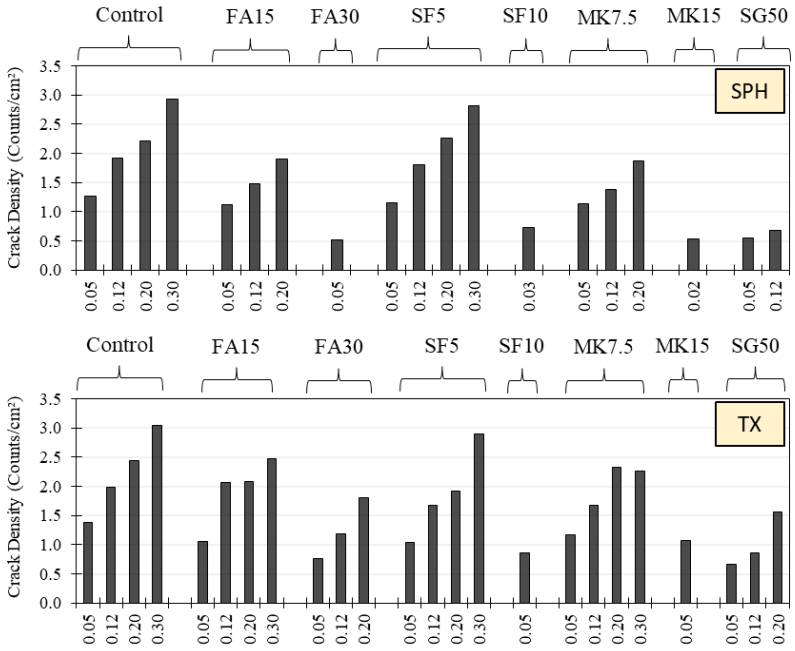

Figure 7.13: Crack density (counts/cm^2) of SCMs-made concrete mixtures.

First, it is worth mentioning that the mixtures SPH-SF10 and SPH-MK15 did not reach 0.05% of expansion. Yet, they were tested at the maximum expansion found during the evaluated period (i.e., 0.03% and 0.02%, respectively). In both mixtures, the presence of closed cracks in the aggregate particles (CCA), corresponding to 83% (SPH-SF10) and 86% (SPH-MK15) of the cracks, probably as a result of the aggregate processing operations, as well as initiation of ASR were identified. Moreover, it was detected randomly spread thin cracks in the paste matrix (very difficult to localize under magnification of 15-16x), which could result from a different mechanism, such as shrinkage, improper consolidation, etc. However, the mechanical properties losses were negligible, and for compressive strength, both mixtures had negative variations, indicating a gain of CS.

At marginal expansion levels (i.e., 0.05%), mixtures containing low replacement levels of PC (i.e., FA15, SF5 and MK7.5) tend to behave similarly to the control specimens. Although SPH-FA15 did not show cracks in the paste matrix, the crack density (CD) displayed was close to SPH-Control (i.e., 1.12 for FA15 against 1.27 for Control), similar CD was also found for SPH-SF5 (1.16) and SPH-MK7.5 (1.14). On the other hand, for TX mixtures, the CD obtained was slightly lower than the control specimens. Otherwise, higher PC replacement levels (i.e., FA30 and SG50) significantly decrease the specimens' overall number of cracks and DRI numbers. Likewise, the CD were considerably smaller than control specimens, achieving 0.52, 0.54, 0.77 and 0.67 for SPH-FA30, SPH-SG50, TX-FA30 and

TX-SG50. Furthermore, there were no cracks in the paste matrix for these mixtures; the only exception was TX-FA30, which likely explains the compressive strength behaviour that these samples presented over ASR development, i.e., negligible variation.

At moderate expansion levels (i.e., 0.12%), the mixtures with lower PC's replacement levels remain behaving similarly to control specimens; the exception was SPH-FA15 that showed slightly lower DRI number and CS loss. On the other hand, FA30 and SG50 displayed significantly lower DRI numbers than control specimens, which may result from the difficulty to localize cracks in the paste matrix of these mixtures. The overall counts of cracks per cm^2 of these specimens were more than 50% lower than SPH and TX control, i.e., SPH- SG50 displayed CD of 0.67 and TX-FA30 and TX- SG50, 1.19 and 1.01. Yet, a slightly higher incidence of crack formation within the aggregate particles (Figure 4.11 and Figure 4.12) was noticed, which likely explains the losses in ME, DSS, and the SDI values that remained averagely close to control specimens. In contrast, CS losses were relatively lower than initially expected (0.01 for SPH-SG50 and 0.01 and 0.04 for TX-FA30 and TX-SG50).

The high and very high expansion levels (i.e., 0.20% and 0.30%) will be discussed together once the concrete mixtures made of higher PC's replacement levels did not reach 0.30% of expansion, plus, incorporating SPH aggregate FA30, and SG50 did not even reach 0.20% of expansion. Moreover, those mixtures with lower replacement levels that yielded 0.30% of expansion displayed similar behaviour to those of the control specimens. Thus, one verifies that it was quite challenging to find ASR-gel in the specimens made of high PC's replacement levels even at high expansion levels. However, this does not necessarily mean that they produced less ASR-gel than other mixtures. Since SCMs can modify the mechanical and chemical properties of the ASR-gel, they could be more easily lost during the cutting and polishing process of sample preparation. Both TX-FA30 and TX-SG50 displayed a notably lower number of cracks at 0.20% of expansion, with CD of 1.81 and 1.57, while TX-control reached 2.45. Once again, a relatively lower amount of cracks were found in the paste matrix (at least under magnification of 15-16x). This trend significantly impacted the CS losses, which achieved a maximum of 8% and 5% losses for FA30 and SG50, respectively.

Globally, higher PC's replacement levels seem to delay the crack development in the binder paste, while they slightly increase the concentration of cracks within the aggregate particles (Figure 7.14), at least for evaluation at a magnification of 15-16x. These results reinforce the importance of a complete

campaign with different and powerful tools and technics to assess and further classify the overall "distress degree" of ASR-affected concrete, i.e. as proposed by Sanchez et al. [33,57–59].

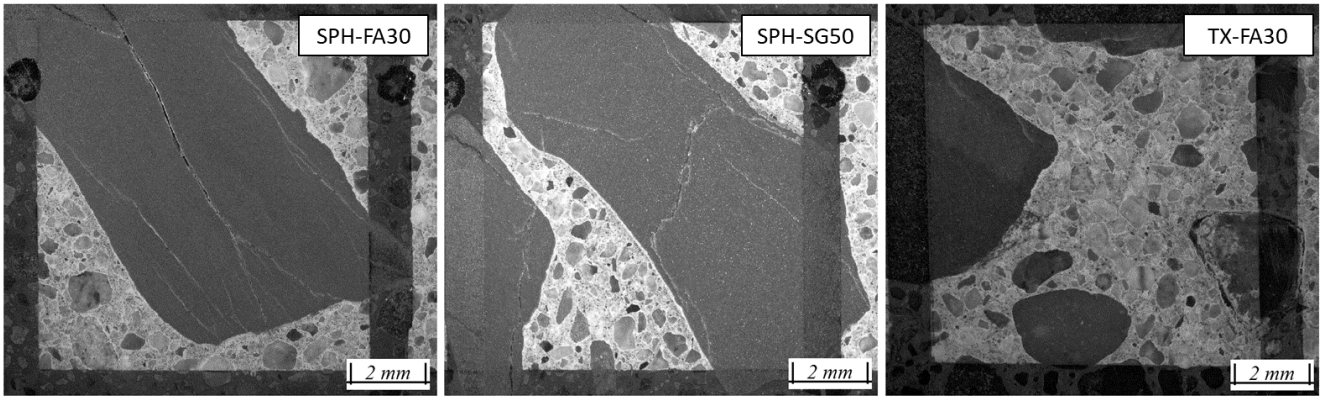

Figure 7.14: Typical cracking features in the concrete incorporating high content of fly ash and slag for SPH and TX aggregates.

7.6.3 Assessment of the chemo-mechanical properties of the AAR reaction products

The surface hardness of the AAR reaction products measured through the micro-indentation on the polished and undried samples was presented in Figure 7.8. In general, the Vickers' hardness values for crystalline reaction products located in the center of different reactive aggregates ranged from 17.5 HV to 63.6 HV (Figure 7.8a), where KING aggregate (ACR) displayed the highest HV values among all reactive aggregates. Thus, one verifies that the Vickers hardness is almost linearly linked to the E-modulus of the tested material (i.e., AAR reaction product) as showed in the literature [44,52], likewise, viscosity [60,61]. In general, the higher the Vickers hardness, the higher E-modulus values and viscosity. The so-called alkali-carbonate reaction (ARC) is constantly debated in the scientific community; different studies have indicated that ACR is just a variant of ASR. Indeed, results found in the literature suggest that the leading cause of distress in ACR-affected concrete is the formation of ASR-gel from unstable and cryptocrystalline SiO_2 particles found in ACR-aggregates [1,62,63].

Moreover, in the present study, EDS analysis indicates a formation of ASR-gel on KING aggregates (Table 7.4). However, comparing the values obtained for ASR-aggregate (i.e., SPH, TX, SPT, and SUD), the concentration of calcium in the gel found within KING was significantly higher, i.e., the ratio of Ca/Si found was 0.51 $\pm$ 0.05 for KING and average of 0.25 $\pm$ 0.04 for SPH, TX, SPT, and SUD. Thus, although the obtained ratios agreed with the literature [1,44,52,62,63], it seems common to

find higher Ca/Si ratios in "ASR-gel" present within ACR-aggregates than in the ASR ones. Nevertheless, this increase in the calcium content in the gel of ACR-particles may explain the differences in the surface hardness observed. Furthermore, this behaviour could justify the further development of distress features obtained by Sanchez et al. [5,24]. Yet, it is worth mentioning that further research needs to be developed and better understand the mechanical and physical properties of the ACR reaction products.

Regarding ASR-aggregates, the Vickers Hardness values ranged from 17.5 to 46.6 HV, in which TX samples displayed the higher average value, yet with a considerable deviation. One verifies that the quantity of ASR-gel in TX mixtures was visually higher than the other mixtures. However, it was pretty tricky to localized "good" regions to test the concrete made with this aggregate. Overall, the smaller the size of the reactive particle, the higher the chance of the cement paste influence in the results for inside the aggregate. Moreover, the coarser particles in TX are somewhat more porous, facilitating the diffusion of Ca^{2+} ions from the paste matrix. The chemical composition of the ASR products displayed in Table 7.4 reinforces this statement; hence TX mixtures exhibited the highest Ca/Si-ratio among the ASR reactive aggregate (i.e., 0.29 against 0.21, 0.23, and 0.26 for SPH, SPT, and SUD, respectively). The HV values for SPH, SPT and SUD aggregates were somewhat similar, with a general average of 22.5 HV.

Through the aggregate particles (SPH and TX) towards the cement paste, the structure of the ASR-gel changes its properties (Figure 4.8b) in the function of the increase in calcium content in the gel composition (Table 4.5) significantly, regardless of the concrete mixture. However, it is well known that the use of SCMs trends enhances the microstructure of the concrete and decreases the portlandite content in the hydrated paste. Overall, the higher the replacement level, the lower the $Ca(OH)_2$ content [19,64,65]. Comparing the data gathered from SCMs-made concrete specimens with control mixtures, it became clear that within the aggregate particle, the distinct binder mixtures did not significantly modify both the HV values and the Ca/Si-ratios of ASR-gel. Conversely, the mechanical and chemical properties of ASR-gel found in cracks close to the edge of aggregates and towards binder paste were significantly affected by SCMs in the concrete mixture. Globally, the higher the replacement levels of PC by the SCMs, the lower the HV values in the edge of aggregates and towards binder paste. Likewise, an expressive decrease on Ca/Si-ratios of the ASR-gel was found on SCMs-made concrete specimens.

Finally, there is still a debate in the scientific community about how the chemical composition of ASR-gel influences its swelling properties. Yet, it is somewhat agreed that SCMs-made concrete develops ASR reactions products with lower swelling properties and lower viscosity [66,67]. This behaviour might clarify that the concrete specimens with high SCMs levels, which developed cracks in the cement paste (i.e., FA30 and SG50), were significantly thinner than the control specimens. Moreover, further analysis needs to be performed to better understand the influence of SCMs on the rheological, swelling properties, alkalinity, and osmotic pressure of the ASR-gel. Since these parameters likely govern the overall expansive behaviour and damage of ASR-affected concrete.

7.7 Conclusions

The main objective of this research program was to better understand the ASR distress mechanism in concrete specimens made with a wide range of supplementary cementing materials (SCMs) and different types/natures of reactive aggregates. Moreover, an important emphasis was given to understanding the induced damage at distinct locations of the affected concrete, including the analysis of ASR-gel features. From the results obtained in this study, the following conclusions may be drawn:

- Overall, the higher the Portland cement replacement level by the different types of SCMs, the slower the ASR-induced development (i.e., kinetics). However, once the specimens reach similar (and pre-determined) expansion levels, the mechanical outcomes of affected concrete (i.e., stiffness damage index, losses in modulus of elasticity and shear strength) are quite similar to conventional concrete, regardless of the binder composition of the mixture.
- The microscopic investigations showed that the development of ASR distress results in the formation of cracks within the reactive aggregate particles that propagate to the cement paste at advanced expansion levels. Yet, the results indicate that higher levels of PC replacement had smaller crack density and developed fewer cracks in the cement paste under "free expansion conditions", at moderate and higher levels of expansion. Nonetheless, the number of cracks found within the aggregate particles slightly increased in comparison to control specimens. In

other words, agreed with the rate of mechanical properties loss (i.e., stiffness and shear strength losses). On the other hand, the lower formation of cracks in the binder paste of SCMs-made concrete lessened the compressive strength losses. In general, the higher the replacement level, the slower the rate of CS loss.

- The evaluation of ASR-gel through micro-indentation indicates that whenever within the aggregates, ASR-gel presents lower Vickers hardness values, lower than the values found when the gel is in contact with the cement paste. However, at the interface aggregate/ITZ, the highest HV values were found. Moreover, the calcium content obtained through EDS analysis seems to be the main reason for this variation in the surface hardness. This behaviour highlights the importance of understanding ASR-gel features for assessing damage and developing models to predict ASR-induced distress development. Nevertheless, PC replacement impacts the micro indentation results; in general, the higher the replacement level, the lower the Vickers hardness of the ASR-gel towards the paste matrix.
- Finally, the evaluation of the AAR reaction products (ASR vs. ACR) through micro-indentation revealed that, in general, the properties (i.e., mechanical and chemical) of the gel found within the ASR reactive particles are somewhat similar between the different types/natures of the aggregates. However, HV values and the Ca/Si ratios of the ACR reaction products were 123% and 77% higher than the ASR-aggregates, respectively; this could explain the fasted reaction kinetics and distinct distress development displayed by KING mixtures. Yet, further research needs to be developed to better understand the mechanical and physical properties of the ACR reaction products.

7.8 Acknowledgment

The authors would like to thank Dr. Gamal Elnabelsya and Dr. Muslim Majeed, technical officers of Materials and Structures Laboratory in the Department of Civil Engineering at the University of Ottawa. As well as De Souza benefits from the University of Ottawa Excellence Scholarship, Collaborative Research & Development by NSERC (Natural Science and Engineering Research Council of Canada), and the prestigious Vanier CGS scholarship, also financed by the NSERC.

7.9 References

[1] T. Katayama, The so-called alkali-carbonate reaction (ACR) - Its mineralogical and geochemical details, with special reference to ASR, Cem. Concr. Res. 40 (2010) 643–675. doi:10.1016/j.cemconres.2009.09.020.

[2] J. Lindgård, Ö. Andiç-Çakir, I. Fernandes, T.F. Rønning, M.D.A. Thomas, Alkali-silica reactions (ASR): Literature review on parameters influencing laboratory performance testing, Cem. Concr. Res. 42 (2012) 223–243. doi:10.1016/j.cemconres.2011.10.004.

[3] L.F.M. Sanchez, Contribution to the assessment of damage in aging concrete infrastructures affected by alkali-aggregate reaction, (2014) 341.

[4] B. Fournier, M.-A. Bérubé, Alkali-aggregate reaction in concrete: a review of basic concepts and engineering implications, Can. J. Civ. Eng. 27 (2000) 167–191. doi:10.1139/cjce-27-2-167.

[5] L.F.M. Sanchez, B. Fournier, M. Jolin, D. Mitchell, J. Bastien, Overall assessment of Alkali-Aggregate Reaction (AAR) in concretes presenting different strengths and incorporating a wide range of reactive aggregate types and natures, Cem. Concr. Res. 93 (2017) 17–31. doi:10.1016/j.cemconres.2016.12.001.

[6] DJ De Souza, L.F.M. Sanchez, M.T. De Grazia, Evaluation of a direct shear test setup to quantify AAR-induced expansion and damage in concrete, Constr. Build. Mater. 229 (2019). doi:10.1016/j.conbuildmat.2019.116806.

[7] V.E. Saouma, M.A. Hariri-Ardebili, Y. Le Pape, R. Balaji, Effect of alkali–silica reaction on the shear strength of reinforced concrete structural members. A numerical and statistical study, Nucl. Eng. Des. 310 (2016) 295–310. doi:10.1016/j.nucengdes.2016.10.012.

[8] J.W. Schmidt, S.G. Hansen, R.A. Barbosa, A. Henriksen, Novel shear capacity testing of ASR damaged full scale concrete bridge, Eng. Struct. 79 (2014) 365–374.

doi:10.1016/j.engstruct.2014.08.027.

[9] M. Thomas, The effect of supplementary cementing materials on alkali-silica reaction: A review, Cem. Concr. Res. 41 (2011) 1224–1231. doi:10.1016/j.cemconres.2010.11.003.

[10] DJ De Souza, L.F.M. Sanchez, M.T. De Grazia, Evaluation of a direct shear test setup to quantify AAR-induced expansion and damage in concrete, Constr. Build. Mater. 229 (2019) 116806. doi:10.1016/j.conbuildmat.2019.116806.

[11] Z. Shi, C. Shi, J. Zhang, S. Wan, Z. Zhang, Z. Ou, Alkali-silica reaction in waterglass-activated slag mortars incorporating fly ash and metakaolin, Cem. Concr. Res. 108 (2018) 10–19. doi:10.1016/j.cemconres.2018.03.002.

[12] J. Duchesne, M.-A. Bérubé, The Effectiveness Of Supplementary Cementing Materials In Suppressing Expansion Due To Asr: Another Look At The Reaction Mechanisms Part 1: Concrete Expansion And Portlandi'ie Depletion, Cem. Concr. Res. 24 (1994) 221–230.

[13] Y. Kawabata, K. Yamada, The mechanism of limited inhibition by fly ash on expansion due to alkali–silica reaction at the pessimum proportion, Cem. Concr. Res. 92 (2017) 1–15. doi:10.1016/j.cemconres.2016.11.002.

[14] A.M. Boddy, R.D. Hooton, M.D.A. Thomas, The effect of the silica content of silica fume on its ability to control alkali-silica reaction, Cem. Concr. Res. 33 (2003) 1263–1268. doi:10.1016/S0008-8846(03)00058-9.

[15] M.C.G. Juenger, C.P. Ostertag, Alkali-silica reactivity of large silica fume-derived particles, Cem. Concr. Res. 34 (2004) 1389–1402. doi:10.1016/j.cemconres.2004.01.001.

[16] A. Leemann, L. Bernard, S. Alahrache, F. Winnefeld, ASR prevention - Effect of aluminum and lithium ions on the reaction products, Cem. Concr. Res. 76 (2015) 192–201. doi:10.1016/j.cemconres.2015.06.002.

[17] J. Wei, B. Gencturk, A. Jain, M. Hanifehzadeh, Mitigating alkali-silica reaction induced concrete degradation through cement substitution by metakaolin and bentonite, Appl. Clay Sci. 182 (2019) 105257. doi:10.1016/j.clay.2019.105257.

[18] P. Lawrence, M. Cyr, E. Ringot, Mineral admixtures in mortars, Cem. Concr. Res. 33 (2003) 1939–1947. doi:10.1016/S0008-8846(03)00183-2.

[19] B. Lothenbach, K. Scrivener, R.D. Hooton, Supplementary cementitious materials, Cem. Concr. Res. 41 (2011) 1244–1256. doi:10.1016/j.cemconres.2010.12.001.

[20] A.K. Saha, M.N.N. Khan, P.K. Sarker, F.A. Shaikh, A. Pramanik, The ASR mechanism of reactive aggregates in concrete and its mitigation by fly ash: A critical review, Constr. Build.

Mater. 171 (2018) 743–758. doi:10.1016/j.conbuildmat.2018.03.183.

[21] P. Fecteau, B. Fournier, G. Engineering, Use of SCMs on ACR-affected concrete: expansion and damage evaluation through the damage rating index, 15th Int. Conf. Alkali-Aggregate React. (2016).

[22] B. Fournier, R. Chevrier, A. Bilodeau, P.P.C. Nkinamubanzi, N. Bouzoubaa, R. Chevrier, Comparative field and laboratory investigations on the use of supplementary cementing materials (SCMs) to control alkali-silica reaction (ASR) in concrete, in: 15th Int. Conf. Alkali-Aggregate React., Bernardes, H.M & Hasparyk, N.P., São Paulo, 2016.

[23] L.F.M. Sanchez, B. Fournier, M. Jolin, M.A.B. Bedoya, J. Bastien, J. Duchesne, Use of Damage Rating Index to quantify alkali-silica reaction damage in concrete: Fine versus coarse aggregate, ACI Mater. J. 113 (2016) 395–407. doi:10.14359/51688983.

[24] L.F.M. Sanchez, B. Fournier, M. Jolin, J. Duchesne, Reliable quantification of AAR damage through assessment of the Damage Rating Index (DRI), Cem. Concr. Res. 67 (2015) 74–92. doi:10.1016/j.cemconres.2014.08.002.

[25] M. Beyene, A. Snyder, R.J. Lee, M. Blaszkiewicz, Alkali Silica Reaction (ASR) as a root cause of distress in a concrete made from Alkali Carbonate Reaction (ACR) potentially susceptible aggregates, Cem. Concr. Res. 51 (2013) 85–95. doi:10.1016/j.cemconres.2013.04.014.

[26] M.D.A. Thomas, K.J. Folliard, Concrete aggregates and the durability of concrete, Durab. Concr. Cem. Compos. (2007) 247–281. doi:10.1533/9781845693398.247.

[27] P. Fecteau, B. Fournier, M. Choquette, J. Duchesne, Contribution To the Understanding of the So-Called Alkali-Carbonate Reaction (Acr), 14th Int. Conf. Alkali Aggreg. React. (2012).

[28] T. Katayama, V. Jensen, C.A. Rogers, The enigma of the 'so-called' alkali-carbonate reaction, Proc. Inst. Civ. Eng. Constr. Mater. (2016). doi:10.1680/jcoma.15.00071.

[29] T. Katayama, P.E. Grattan-Bellew, Petrography of the Kingston experimental sidewalk at age 22 years--ASR as the cause of deleteriously expansive, socalled alkali-carbonate reaction, in: Proc. 14th Int. Conf. Alkali-Aggregate React. Concr. Austin, Texas, USA, 2012: p. 10.

[30] V. Villeneuve, B. Fournier, Determination of the damage in concrete affected by ASR–the damage rating index (DRI), in: 14th Int. Conf. Alkali-Aggregate React. Concr., Austin (Texas), 2012: p. electronic.

[31] J.B. Walsh, The effect of cracks on the uniaxial elastic compression of rocks, J. Geophys. Res. 70 (1965) 399–411. doi:10.1029/JZ070i002p00399.

[32] R.S. Crouch, Specification for the determination of stiffness damage parameters from the low

cyclic uniaxial compression of plain concrete cores, 1987.

[33] L.F.M. Sanchez, B. Fournier, M. Jolin, J. Bastien, Evaluation of the stiffness damage test (SDT) as a tool for assessing damage in concrete due to ASR: Test loading and output responses for concretes incorporating fine or coarse reactive aggregates, Cem. Concr. Res. 56 (2014) 213–229. doi:10.1016/j.cemconres.2013.11.003.

[34] L.F.M. Sanchez, B. Fournier, M. Jolin, J. Bastien, Evaluation of the Stiffness Damage Test (SDT) as a tool for assessing damage in concrete due to alkali-silica reaction (ASR): Input parameters and variability of the test responses, Constr. Build. Mater. 77 (2015) 20–32. doi:10.1016/j.conbuildmat.2014.11.071.

[35] L.F.M. Sanchez, T. Drimalas, B. Fournier, D. Mitchell, J. Bastien, Comprehensive damage assessment in concrete affected by different internal swelling reaction (ISR) mechanisms, Cem. Concr. Res. 107 (2018) 284–303. doi:10.1016/j.cemconres.2018.02.017.

[36] M. Haskett, D.J. Oehlers, M.S. Mohamed Ali, S.K. Sharma, Evaluating the shear-friction resistance across sliding planes in concrete, Eng. Struct. 33 (2011) 1357–1364. doi:10.1016/j.engstruct.2011.01.013.

[37] L. Banks-Sills, M. Arcan, An edge-cracked Mode II fracture specimen., Exp. Mech. 23 (1983) 257–261.

[38] D.F. Adams, D.E. Walrath, Current status of the Iosipescu shear test method., J. Compos. Mater. 21 (1987) 494–507.

[39] H.A. Richard, A new compact shear specimen, Int. J. Fract. 17 (1981) 5–7.

[40] D.J. Shuman, A.L.M. Costa, M.S. Andrade, Calculating the elastic modulus from nanoindentation and microindentation reload curves, Mater. Charact. 58 (2007) 380–389. doi:10.1016/j.matchar.2006.06.005.

[41] B. Lu, C. Shi, Z. Cao, M. Guo, J. Zheng, Effect of carbonated coarse recycled concrete aggregate on the properties and microstructure of recycled concrete, J. Clean. Prod. 233 (2019) 421–428. doi:10.1016/j.jclepro.2019.05.350.

[42] W. Wu, R. Wang, C. Zhu, Q. Meng, The effect of fly ash and silica fume on mechanical properties and durability of coral aggregate concrete, Constr. Build. Mater. 185 (2018) 69–78. doi:10.1016/j.conbuildmat.2018.06.097.

[43] A. Nastic, A. Merati, M. Bielawski, M. Bolduc, O. Fakolujo, M. Nganbe, Instrumented and Vickers Indentation for the Characterization of Stiffness, Hardness and Toughness of Zirconia Toughened Al2O3 and SiC Armor, J. Mater. Sci. Technol. 31 (2015) 773–783.

doi:10.1016/j.jmst.2015.06.005.

[44] A. Leemann, P. Lura, E-modulus of the alkali-silica-reaction product determined by micro-indentation, Constr. Build. Mater. 44 (2013) 221–227. doi:10.1016/j.conbuildmat.2013.03.018.

[45] J.H. Kim, T. Tabaru, H. Hirai, Evaluation technique of the hardness and elastic modulus of materials with fine microstructures, Mater. Trans. 44 (2003) 673–676. doi:10.2320/matertrans.44.673.

[46] H. Liu, X. Ren, J. Li, Indentation tests based multi-scale random media modeling of concrete, Constr. Build. Mater. 168 (2018) 209–220. doi:10.1016/j.conbuildmat.2018.02.050.

[47] P. Lura, P. Trtik, B. Münch, Validity of recent approaches for statistical nanoindentation of cement pastes, Cem. Concr. Compos. 33 (2011) 457–465. doi:10.1016/j.cemconcomp.2011.01.006.

[48] W. Zhu, P.J.M. Bartos, Application of depth-sensing microindentation testing to study of interfacial transition zone in reinforced concrete, Cem. Concr. Res. 30 (2000) 1299–1304. doi:10.1016/S0008-8846(00)00322-7.

[49] Standard counsil of Canada, CSA23.2-14C: Obtaining and testing drilled cores for compressive strength testing, in: CSA A23.119/CSA A23.219 Natl. Stand. Canada, 2019: pp. 774–778.

[50] L.F.M. Sanchez, B. Fournier, M. Jolin, J. Bastien, Evaluation of the Stiffness Damage Test (SDT) as a tool for assessing damage in concrete due to alkali-silica reaction (ASR): Input parameters and variability of the test responses, Constr. Build. Mater. 77 (2015) 20–32. doi:10.1016/j.conbuildmat.2014.11.071.

[51] B. Barr, E.B.D. Hasso, development of a compact cylindrical shear test specimen, J. Mater. Sci. Lett. 5 (1986) 1305–1308.

[52] C. Zhang, L. Sorelli, B. Fournier, J. Duchesne, J. Bastien, Z. Chen, Stress-relaxation of crystalline alkali-silica reaction products: Characterization by micro- and nanoindentation and simplified modeling, Constr. Build. Mater. 148 (2017) 455–464. doi:10.1016/j.conbuildmat.2017.05.069.

[53] P.K. Mehta, P.J.M. Monteiro, Concrete: Microstructure, Properties, and Materials, 3rd Edition, 2013. doi:10.1036/0071462899.

[54] R.B. Figueira, R. Sousa, L. Coelho, M. Azenha, J.M. de Almeida, P.A.S. Jorge, C.J.R. Silva, Alkali-silica reaction in concrete: Mechanisms, mitigation and test methods, Constr. Build. Mater. 222 (2019) 903–931. doi:10.1016/j.conbuildmat.2019.07.230.

[55] H. Maraghechi, F. Rajabipour, C.G. Pantano, W.D. Burgos, Effect of calcium on dissolution and

precipitation reactions of amorphous silica at high alkalinity, Cem. Concr. Res. 87 (2016) 1–13. doi:10.1016/j.cemconres.2016.05.004.

[56] B. Fournier, R. Chevrier, A. Bilodeau, P.C. Nkinamubanzi, N. Bouzoubaa, Comparative field and laboratory investigations on the use of supplementary cementing materials (SCMs) to control alkali-silica reaction (ASR) in concrete, in: 15th Int. Conf. Alkali-Aggregate React., Bernardes, H.M & Hasparyk, N.P., São Paulo, 2016.

[57] L.F.M. Sanchez, T. Drimalas, B. Fournier, D. Mitchell, J. Bastien, Comprehensive damage assessment in concrete affected by different internal swelling reaction (ISR) mechanisms, Cem. Concr. Res. 107 (2018) 284–303. doi:10.1016/j.cemconres.2018.02.017.

[58] DJ De Souza, L.F.M. Sanchez, M.T. De Grazia, Evaluation of a direct shear test setup to quantify AAR-induced expansion and damage in concrete, Constr. Build. Mater. 229 (2019) 116806. doi:10.1016/j.conbuildmat.2019.116806.

[59] L.F.M. Sanchez, B. Fournier, M. Jolin, J. Duchesne, Reliable quantification of AAR damage through assessment of the Damage Rating Index (DRI), Cem. Concr. Res. 67 (2015) 74–92. doi:10.1016/j.cemconres.2014.08.002.

[60] C. Bernard, V. Keryvin, J.C. Sangleboeuf, T. Rouxel, Indentation creep of window glass around glass transition, Mech. Mater. 42 (2010) 196–206. doi:10.1016/j.mechmat.2009.11.008.

[61] T. Rouxel, H. Ji, J.P. Guin, F. Augereau, B. Ruffĺ, Indentation deformation mechanism in glass: Densification versus shear flow, J. Appl. Phys. 107 (2010). doi:10.1063/1.3407559.

[62] M. Beyene, A. Snyder, R.J. Lee, M. Blaszkiewicz, Alkali Silica Reaction (ASR) as a root cause of distress in a concrete made from Alkali Carbonate Reaction (ACR) potentially susceptible aggregates, Cem. Concr. Res. 51 (2013) 85–95. doi:10.1016/j.cemconres.2013.04.014.

[63] P.E. Grattan-Bellew, L.D. Mitchell, J. Margeson, D. Min, Is alkali-carbonate reaction just a variant of alkali-silica reaction ACR = ASR?, Cem. Concr. Res. 40 (2010) 556–562. doi:10.1016/j.cemconres.2009.09.002.

[64] J. Duchesne, M.A. Bérubé, Long-term effectiveness of supplementary cementing materials against alkali-silica reaction, Cem. Concr. Res. 31 (2001) 1057–1063. doi:10.1016/S0008-8846(01)00538-5.

[65] Y. Scholz, C. Hübert, K.-J. Hünger, The Influence of Supplementary Cementing Materials on the Dissolution of Aggregates in Alkaline Solutions, in: NP. Bernardes, H. M. & Hasparyk (Ed.), 15th Int. Conf. Alkali-Aggregate React., São Paulo, 2016.

[66] F. Rajabipour, E. Giannini, C. Dunant, J.H. Ideker, M.D.A. Thomas, Alkali-silica reaction:

Current understanding of the reaction mechanisms and the knowledge gaps, Cem. Concr. Res. 76 (2015) 130–146. doi:10.1016/j.cemconres.2015.05.024.

[67] A. Gholizadeh Vayghan, F. Rajabipour, J.L. Rosenberger, Composition-rheology relationships in alkali-silica reaction gels and the impact on the Gel's deleterious behavior, Cem. Concr. Res. 83 (2016) 45–56. doi:10.1016/j.cemconres.2016.01.011.

Chapter Eight: The use of self-healing technology combined with supplementary cementing materials to mitigate the Alkali-Silica Reaction distress.

Diego J. De Souza[1], Leandro F. M. Sanchez[1]

[1]Department of Civil Engineering, University of Ottawa, Ottawa, Canada.

Abstract

Alkali-Silica Reaction (ASR) is one of the most harmful distress mechanisms affecting the durability and serviceability of concrete infrastructure worldwide. Over the past decades, several engineers and researchers around the globe have tried to develop preventive measures in the laboratory and in the field to avoid, cease or at least mitigate ASR development rate and damage. It has been shown that ASR-induced expansion and distress could be reduced or delayed by the appropriate use of supplementary cementing materials (SCMs). Moreover, it has been verified that some products, such as crystalline admixtures, could enhance concrete's healing properties, thus presenting an interesting "physical" solution for durability-related distress due to ASR. In this context, this paper aims to evaluate different concrete mixes presenting two different types of highly reactive aggregates (i.e., Springhill Coarse and Texas fine aggregate), incorporating a wide range of binder compositions (i.e., GU-type cement, silica fume, fly ash, slag and Metakaolin) and using distinct types of chemical admixtures, such as crystalline self-healing and lithium nitrate. The samples were fabricated, exposed to ASR development, and monitored over time. Mechanical (i.e., compressive and shear strength, modulus of elasticity and stiffness damage test) and microscopic (damage rating index) techniques were then selected for further analysis of the distinct mixtures appraised performance. Finally, comparisons among the results are made, and further discussions and recommendations on the reliability of adopting self-healing products modified with SCMs to suppress ASR are conducted.

Keywords: Alkali-silica reaction mitigation, the durability of concrete, self-healing, crystalline admixtures.

8.1 Introduction

One of the main damage mechanisms affecting the durability and long-term performance of concrete structures is alkali-silica reaction (ASR). ASR generates secondary products that induce swelling pressures within the reacting aggregate material(s) and the adjacent cement paste while moisture uptake [1–3] and its development leads to microcracking, loss of material's integrity and functionality of the affected structure. Over the past decades, several approaches and recommendations have been developed to assess the efficiency of preventive measures (i.e. supplementary cementing materials – SCMs, such as fly ash, silica fume, blast furnace slag, natural pozzolans, etc.) to mitigate ASR in the field [3–6]. Although it has been found that ASR-induced expansion and distress may be prevented by the appropriate use of SCMs [2,4,7], recent studies are now finding that the deterioration is "only" delayed and does not entirely prevent ASR occurrence [8]. Moreover, once ASR starts in the field, onerous human intervention becomes necessary.

Artificially triggering healing agents have been studied in the past years [9–12], and one of the most innovative materials used is the so-called crystalline admixtures (CA), a permeability-reducing admixture with hydrophilic nature [13]. Results suggest that CA-concrete significantly decreases water penetration depth [14,15], enhances the resistance to chloride penetration [14,16,17] and almost fully recover mechanical properties of distressed concrete [18–20]. Moreover, the combination of CA and SCMs (e.g., Blast Furnace Slag [21], fly ash [9,19,22,23] and silica fume [12]) can expressively enhance the self-healing efficiency of damaged concrete. Yet, although its overall behaviour under critical development of physicochemical mechanism is still relatively unknown, there is a potential strategy to use SH products to either prevent (in combination with SCMs) or mitigate the distress of ASR-induced development. However, there are no current studies indicating the efficiency of CA to prevent/mitigate ASR-affected concrete, especially combined with supplementary cementing materials (SCMs) forming binary/ternary/quaternary mixtures aiming to enhance the physicochemical properties of the concrete against ASR development, which emphasizes the need for investigations in the area.

8.2 Background

8.2.1 Influence of supplementary cementitious materials (SCMs) on ASR

Preventive measures, including the use of supplementary cementing materials (SCMs) such as fly ash (FA) [5,24,25], granulated blast-furnace slag (GBFS) [26,27], silica fume (SF) [28,29] and metakaolin [5–7], have been widely studied to decrease the likelihood of ASR. SCMs can control ASR-induced development mainly by their capacity of reducing the alkalinity available in the system, thus limiting their availability to react with the aggregates [2,4,25]. Furthermore, it has been reported that the ability of SCMs to bind alkalis and hydroxyls ions seems to be strongly related to the CaO/SiO_2 ratio of the SCMs; i.e., the higher this ratio, the lower its binding capacity [4]. Chemically, SCMs can dilute the alkalis available from the clinker and change de properties of the ASR-gel by consuming $Ca(OH)_2$ from the pore solution [2,4,25]. Furthermore, these materials are able to enhance concrete microstructure, affecting the mobility of ions and slowing the reaction rate [25,30,31]. Yet, each different type of SCMs has a particular behaviour against ASR development.

It has been discussed that *Ground/granulated blast furnace slag (GBFS)* as an SCM in concrete just delays the effect of ASR by temporarily modifying the gel composition [32]. At the same time, it does not significantly affect the amount and composition of the ASR-gel formed at the early stages of ASR development [33]. In general, effective amounts of slag to suppress ASR development typically range from 25-50% or more, depending on the reactivity of the aggregate and exposure conditions [34]; yet, no threshold values have been established to mitigate the ASR efficiently. Results demonstrated that replacing 50% of PC by GBFS decreases the expansion rate to lower values than low-alkali PC concrete [35]. Likewise, concrete mixtures made with different portions of GBFS (i.e., 35%, 50% and 65%) and various types of reactive aggregates have shown negligible expansion levels after 15 years of exposure to field conditions; the only exception was the 35% of PC replacement incorporating highly reactive aggregates [36].

The effectiveness of concrete made of *fly ash (FA)* against ASR depends on the overall FA properties and calcium content (i.e., class F containing less than 15% of CaO, class CL for CaO content ranging from 15% to 20%, and class CH containing more than 20% of CaO) [37]. Besides both types of FA displayed some efficiency to prevent ASR development, FA class F has demonstrated better results [4],

which is likely explained by the different CaO/SiO_2 ratios of FAs. In general, the lower the CaO/SiO_2 ratio, the higher its efficiency [35] to suppress ASR. Moreover, it is agreed that the replacement level of PC by FA ranges from 15% to 40% for FA with CaO content lower than 20%. In contrast, for FA with CaO higher than 20%, the results are quite variable, and its use is recommended only after testing their effectiveness per standards, i.e., [38,39].

In general, the use of *Silica Fume (SF)* to mitigate ASR in concrete is recommended; yet its mitigation mechanism is still not entirely understood [2,28]. Overall, SF particles rapidly bind alkalis, decreasing the alkalinity of the concrete pore solution [2,28]. However, at later ages, alkalis can eventually be released and re-increase alkali concentration [27,35]. In other words, SF can mitigate ASR at "safe" levels, yet a long exposure period can be challenging. For instance, results have demonstrated that moderately and highly reactive aggregates combined with 7.5% to 12.5% of SF in concrete contributed to keeping expansion levels at safe levels after 10 years of exposure to ASR development. Conversely, concrete made of SF and highly reactive aggregates barely keep the expansion amplitudes under the above expansion level after 15 years of field exposure [35,36].

Different studies [6,40,41] have discussed the efficiency of the metakaolin (MK) to suppress ASR in concrete; yet, no threshold values have been defined. However, results suggest that mortar bars incorporating 10% MK by cement mass lessened ASR-induced expansion by about 70% [6,7], whereas 15% of PC replacement resulted in values up to 85% lower [40,42,43]. The mechanism of ASR mitigation by MK usage is commonly attributed to the increased aluminum content into the concrete pore solution, which is absorbed on reactive SiO_2 surfaces, slowing down its dissolution [6,40,41] to values close to zero [44]. Yet, decelerating the dissolution of reactive SiO_2 did not modify the chemical composition and morphology of the ASR-gel [6]. Furthermore, it is unlikely that the swelling potential of ASR products in cementitious materials incorporating MK is lessened [6].

8.2.2 **Using crystalline admixture (CA) to enhance the self-healing of concrete**

One of the smartest materials used for self-healing applications in concrete is the so-called crystalline admixtures (CA). These materials are permeability-reducing admixtures with a hydrophilic nature that easily react with water and can effectively serve as self-healing engineered admixtures [13]. Sisomphon and co-workers [45] demonstrated that by adding 1.5% and 4% (by PC mass) of CA in cement paste

mixtures, cracks with a width of 250 to 400 µm were fully closed. Combining 0.3% of CA, expansive additive and PVA fibres fully recover the mechanical properties (e.g., flexural strength, stiffness and deflection capacity) [46]. Likewise, healing ratios of 0.98 for cracks up to 400 µm were obtained after 42 days of healing by adding 4% CA (by PC mass) [22]; as well as complete sealing of crack with widths below 300 µm [16]; 95% of strength regaining capacity [20]; 50% lower water penetration, and 30% lower chloride diffusivity [14]. Moreover, it has been recently demonstrated that the combination of CA and SCMs (Blast Furnace Slag [21], Fly Ash [9,19,22,23] and silica fume [12] can even reach higher values of self-healing ratios, in general, efficiency between 90% to 105%; yet depending on the exposure condition [19]. It is worth mentioning that there is a relative agreement in the literature in which cementitious composites soaked in water solution trends to achieved higher self-healing ratios and faster healing rates, followed by wet/dry cycles, water contact and air exposure, respectively [12,14,16,18,19,22,47]. Finally, recent studies suggest that CA-made mortar bars may mitigate ASR expansion development by about 70%, likely due to the lower permeability of the exposed mortar bars, delaying the diffusion of alkali ions from the external solution. However, these findings still need further validation, particularly for concrete specimens exposed to ASR-induced development.

8.3 **Scope of the work**

As stated above, several techniques, supplementary cementing materials, and chemical admixtures have been used in the past, aiming to assess, prevent, and mitigate ASR development in the field. However, there is very little research (if any) on the use of self-healing products combined and or modified with SCMs; hence, forming a binary/ternary/quaternary chemical-physical treatment leaves room for major developments in this area. The current research aims to evaluate the combination of a wide range of binder materials (i.e., GU-type cement, silica fume, fly ash, slag and metakaolin) and crystalline admixtures (i.e., modified and conventional products) to prevent and/or mitigate (i.e., physically, chemically or both) concrete deterioration caused by ASR-induced development. The concrete specimens were fabricated incorporating two ASR highly reactive aggregate types (e.g., Greywacke coarse aggregate and natural Polymictic sand) and stored under controlled environmental conditions enabling ASR development. The specimens were continuously monitored over time and at the selected exposure periods, microscopic (i.e., Damage Rating Index) and mechanical (i.e., Stiffness Damage Test, Modulus of Elasticity, Shear Strength and Compressive Strength) analyses were conducted, and a

comprehensive evaluation of the impact of the self-healing on ASR-induced deterioration was performed.

8.4 Experimental program

8.4.1 Materials

A conventional Portland cement (i.e., GU type, equivalent to ASTM Type I), four different types of supplementary cementing materials (i.e., blast furnace slag – SG, fly ash class F – FA, silica fume – SF and metakaolin – MK), four commercially available hydrophilic permeability reducer admixtures (or Crystalline Admixture – CA1, CA2, CA3 and CA4), four chemically modified versions of CA, two different chemical admixtures (lithium nitrate – $LiNO_3$ and nano-silica – NS), and two different reactive aggregate types/natures (i.e., coarse and fine reactive aggregates) were selected for this study to manufacture forty-two concrete mixtures. One may notice that neither water reducers nor air-entrained admixtures were used in this research. The coarse aggregates ranged from 5 to 20 mm in size. Non-reactive fine (NF) and coarse (NC) aggregates were combined with the reactive aggregate materials for concrete manufacturing. Table 7.1 provides information on the different aggregates used in this study, and the chemical and physical properties of the selected binder materials are provided in Table 8.2.

Table 8.1: Reactive (ASR) and non-reactive (NR) aggregates used in the research.

Aggregate		Reactivity	Rock Type	Specific gravity	Absorption (%)	AMBT[a] (%)
Coarse	SPH	ASR	Greywacke	2.71	0.70	0.33
	LC	NR	Crushed limestone	2.78	0.42	0.02
Fine	TX	ASR	Polymictic sand	2.60	0.89	0.81
	NF	NR	Natural derived from granite	2.60	0.82	0.08

[a)] Results at 14 days of curing of the AMBT (ASTM C 1260) carried out on the aggregates selected

Table 8.2: Chemical composition of the binder materials.

	PC	Slag	FA	SF	MK
SiO_2 (%)	20.10	36.64	56.31	92.86	52.48
Al_2O_3 (%)	5.03	11.14	23.27	0.05	44.35
CaO (%)	61.93	37.32	10.29	0.62	0.12
Fe_2O_3 (%)	3.80	0.40	3.57	0.12	0.61
SO_3 (%)	3.38	0.37	0.19	0.07	0.04
MgO (%)	2.42	12.15	1.07	0.19	0.08
Na_2O_{eq} (%)	0.91	0.63	3.17	0.52	0.38
C_3S (%)	43.24	-	-	-	-
C_2S (%)	25.02	-	-	-	-
C_3A (%)	6.90	-	-	-	-
C_4AF (%)	11.56	-	-	-	-
Specific Gravity	3.12	2.91	2.01	2.20	2.29
Lost on Ignition (%)	2.91	0.49	0.98	5.05	0.69

8.4.2 **Mix-proportions and manufacture of the concrete specimens**

A total of thirteen-hundred and forty-four cylinders (thirty-two samples per each of the forty-two mixtures), 100 by 200 mm in size, were investigated in this study. Table 6.2 summarizes the concrete mix designs employed in this work. All forty-two concrete mixtures were mix-proportioned as per ASTM C1293 to present the same water to binder ratio (w/b of 0.45) and amount of binder materials (420 $\pm$ 10 kg/m^3). However, adjustments were made in the volume of non-reactive aggregates to maintain the volume of reactive aggregate constant in all mixtures: i.e., non-reactive fine aggregates ranged from 776 to 836 kg/m^3, while reactive coarse aggregate was fixed at 938 kg/m^3; likewise, the non-reactive coarse aggregates ranged from 957 to 1019 kg/m^3, while the reactive fine aggregate was set at 765 kg/m^3. The amounts of $LiNO_3$, NS, CA1, CA2, CA3 and CA4 were fixed per the manufacturers' recommendation and according to what is used in field applications. Based on the CA1 and CA2 usage recommendations, the same amount was also fixed for CA1MK2 (i.e., CA1 + coarse MK), CAWRP (i.e., CA1 + WRP) and CA2MK (i.e., CA2 + MK). It is worth mentioning that for CA1MK2, the metakaolin powder was sieved, and only fractions above 40 µm were used. The dosage of SCMs chosen in this study was selected based on CSA A23.2-27A; the rationale behind this selection was not to design the concrete mixtures able to prevent ASR entirely, yet, proportioning mixtures with the highest amount of SCMs possible but developing some measurable ASR. Thus, understanding the influence of the crystalline admixtures in the different systems and their potential to modify ASR development.

Twenty-four hours after casting, the samples were demoulded and stored in a moist curing room for another 24 h. Then, small holes (5 mm in diameter by 15 mm deep) were drilled at the two flat ends of

the samples, in which steel gauge studs were glued in place with a fast-setting cement slurry for longitudinal expansion measurements. Afterwards, the samples were taken for the zero reading, being finally placed in sealed plastic buckets lined with a damp cloth and stored at 38 °C and 100% RH. The AAR-affected cylinders were monitored for length changes over time for a total period of two years. As per ASTM C1293, the buckets were cooled to 23 °C for 16 ± 4 h before the periodic measurements.

Table 8.3: Concrete mix proportions.

Mixture[a)]	w/b = 0.45		SCMs (kg/m³)				Chemical Admixtures[b)]					
	Water (kg/m³)	Cement (kg/m³)	SG	FA	SF	MK	CA1	CA2	CA3/4	CA_{mod}[c)]	NS	$LiNO_3$ [d)]
Control	189	420										
LTM		420										0.74
Sg		210	210									
FA		294		126								
SF		378			43							
MK		357				63						
CA1		420					8					
CA2		420						8				
CA3		420							8			
CA4		420							8			
CA1+CA2		420					4	4				
CA1MK2		420								8		
CA2MK		420								8		
CAWRP		420								8		
CA1-Sg		210	210				8					
CA1-FA		294		126			8					
CA1-SF		378			43		8					
CA1-MK		357				63	8					
CA1-NS		399					8				21	
CA1-NS-MK		353				50	8				17	
CA1-NS-SF-MK		349			21	42	8				8	

[a)] Mixtures indicates the "binder paste composition", to indicate the type of reactive aggregate used in the concrete mixtures it will be added SPH (Greywacke coarse) and TX (polymictic fine) abbreviations in the form of the name of the cement/binder paste mixture (i.e., SPH-Control, SPH-LTM, etc.).

[b)] CA1/2/3/4, CA_{mod} and $LiNO_3$ were added into the mixtures; they do not replace the cement content, yet, for $LiNO_3$ solution, the total amount of water was corrected once the material has water in its composition. For NS mixtures, the cement was replaced as indicated in the mixture.

[c)] All CA_{mod} materials were produced in the lab by modifying the chemical composition of the original CA with metakaolin (MK) and water repellent (CAWRP), at a replacement level of 25% by mass of CA.

[d)] LTM – Lithium Nitrate ($LiNO_3$) admixture – the ratio Li/Na_2O_{eq} was kept constant as 0.74

8.4.3 **Assessment of the ASR development in the concrete**

8.4.3.1 **Damage Rating Index (DRI)**

A semi-quantitative petrographic analysis, using the DRI, was performed on one specimen from each concrete mixture after 90, 180, 360, 720 days of exposure, according to the method described by Sanchez [48,49]. First, the samples were cut in half axially, polished by a hand polishing device, which uses diamond-impregnated rubber disks (nº. 50-coarse, 100, 400, 800, 1500 to 3000-very fine), and 1cm^2 grids were drawn on the surface of the polished sections. Then a stereomicroscope (16× magnification) was used to perform the test. The DRI final number presented hereafter is the normalized 100 cm^2 value.

8.4.3.2 **Compressive Strength**

Compressive strength was measured through two different approaches with different and specific goals. First, to characterize all mixtures at 28, 56, 90, and 180 days, the samples were wrapped and placed at 12 °C, since some of the specimens contained highly reactive aggregates and ASTM C39 method could not be followed as they could develop some AAR. Cylinders of all mixtures were maintained at 12 °C for 47-, 93-, 150- and 300-days periods (maturity equivalent to 28, 56, 90 and 180 days, respectively), according to the maturity concept as by ASTM C 1074. Moreover, it is worth noting that no strength gain was observed after 300 days under the above storage conditions. Thus, the compressive strength of sound concrete after 360 and 720 days were considered as the values measured at 180 days. Likewise, to determine the SDT loading level, the 40% of CS used were the values obtained at each specific age of the concrete (i.e., 90 and 180, while for 360 and 720, it was considered the CS found at 180 days). Second, the compressive strength measurements were carried out on two specimens from each concrete mixture after being subjected to SDT to verify the compressive strength loss of the material as ASR develops. This procedure was adopted and considered valid after Sanchez et al. [49,50] confirmed the largely non-destructive character of the SDT.

8.4.3.3 **Stiffness Damage Test (SDT)**

The SDT procedure was performed following Sanchez et al. publications [51–54], i.e., using five loading/unloading cycles at a controlled loading rate of 0.10MPa/s with a maximum load corresponding to 40% of the maturity equivalent concrete strength over time (i.e. 90, 180, 360, and 720

days), as mentioned in 8.4.3.2. It is worth noting that once the ASR affected specimens reach one of the specified periods of evaluation (i.e., 90, 180, 360, and 720 days), the samples were wrapped in plastic film and kept under 12 °C to inhibit further AAR deterioration until all tests are conducted (due to testing capacity issues). Thus, before the test procedure, the samples were re-conditioned/prepared under 100% RH for 48 hours [55], and the test was conducted. The results obtained hereafter is an average value from three different specimens tested at each expansion level.

8.4.4 **Direct Shear Test**

The direct shear test was performed according to the method and setup proposed by Barr and Hasso [56] and adapted for damaged concrete as per De Souza et al. [57]. The same approach considering the maturity concept was used to characterize the sound concrete values for all concrete mixtures at equivalent 28, 90, and 180 days. Three samples from each concrete mixture were selected after the specimens achieved the expected curing periods; however, differently from CS, the stiffness damage test was not performed on the samples previous to the direct shear test. Before testing, all samples were carefully ground so that a circumferential notch was created [56,57]. The notch depth was adopted as about 20 mm ± 3 mm to ensure a shear-type failure without leaving a too-small area of the sample to be tested.

8.5 **Results**

8.5.1 **ASR Kinetics**

This section presents ASR expansion kinetics and amplitude results for all mixtures developed in the laboratory. Figure 7.2 displays the expansion results obtained by incorporating a wide range of binder materials/compositions and two different types/natures of reactive aggregates. Figure 7.2a and b illustrate the expansion development and mass variation of concrete mixtures made of SPH reactive coarse, whereas Figure 7.2c and d display the results with reactive fine TX.

A wide range of expansion amplitudes was obtained from the reactive aggregate and different binder materials/compositions tested. In general, the mixtures containing the reactive fine TX presented faster reactivity than those incorporating reactive coarse SPH aggregate. Moreover, all mixtures comprising both SCMs and chemical admixtures developed lower expansion than the control specimens for both SPH and TX mixtures. After 720 days of ASR development, the control specimens SPH-Control and

TX-Control reached 0.49% and 0.89% of expansion, respectively. Moreover, adding lithium nitrate in the concrete mixtures decreased the expansion amplitude to 0.07% (SPH-LTM) and 0.14% (TX-LTM). The specimens containing only crystalline admixtures either conventional or chemically modified (i.e., CA1, CA2, CA1+CA2, CA3, CA4, CA1MK2, CAWRP and CA2MK) presented faster reactivity than mixtures made with SCMs or lithium nitrate, reaching expansion values that ranged from 0.33% (SPH-CA1MK2) and 0.46% (SPH-CA3) for SPH (32.7% and 6.1% lower than SPH-Control, respectively). Involving the extremely reactive TX, CA mixtures results ranged from 0.52% (CA1 and CA1MK2) and 0.78% (CA2), representing values 41.6% and 12.4% lower than TX-Control, respectively.

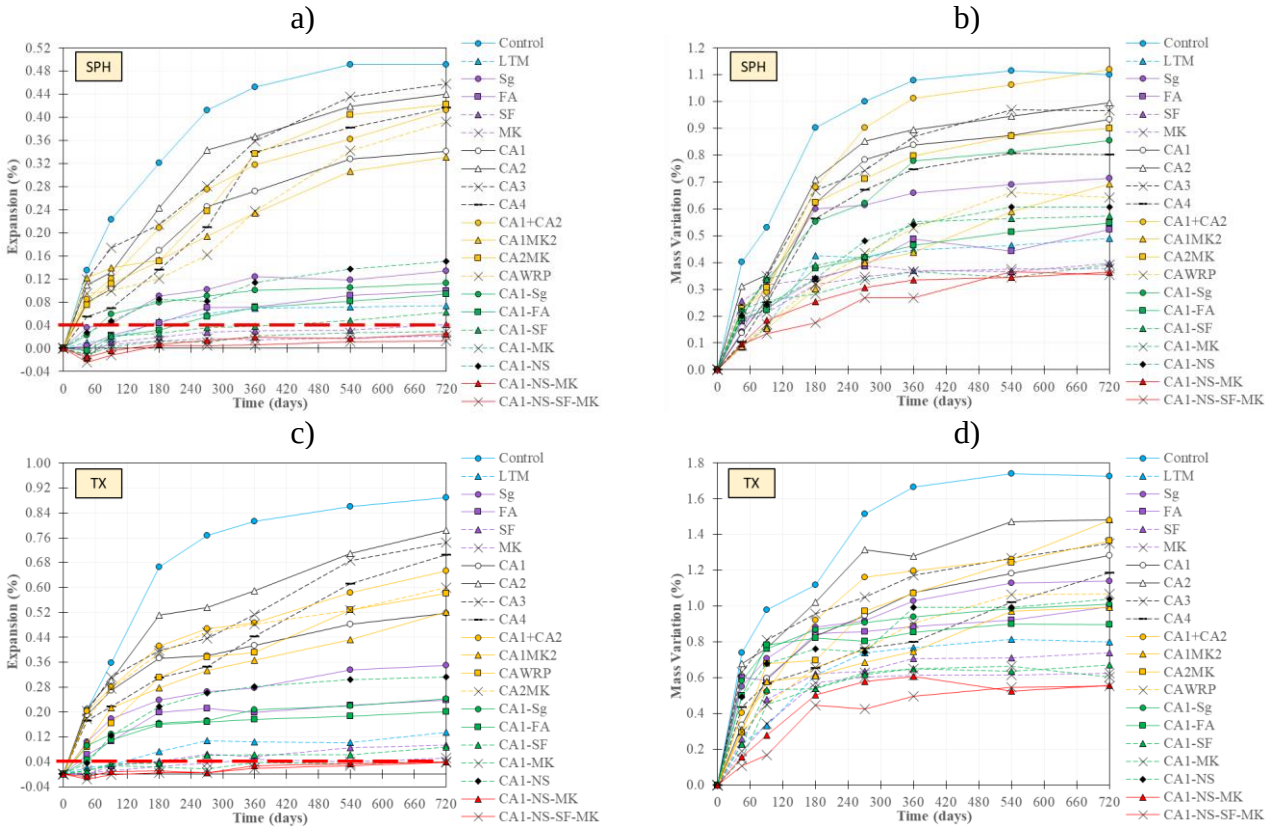

Figure 8.1: ASR-kinetics over time: a) expansion and b) mass gain for concrete mixtures made of SPH coarse aggregate and c) expansion and d) mass gain for concrete mixtures made of TX fine aggregate.

The use of supplementary cementing materials (SCMs), either combined or not with CA1, was able to modify ASR kinetics significantly. The values ranged from 0.01% (SPH-CA1-NS-SF-MK) to 0.15% (SPH-CA1-NS) for SPH-made concrete mixtures and from 0.04% (TX-CA1-NS-SF-MK) and 0.35% (TX-SG). In general, the mixtures combining CA1 and the different types of SCMs showed lower results than those incorporating only SCMs; i.e., for SPH specimens, SG, FA, SF and MK, the

expansion levels measured were 0.13%, 0.10%, 0.04% and 0.02%, respectively, whereas CA1-SG, CA1-FA, CA1-SF and CA1-MK showed 0.11%, 0.09%, 0.06% and 0.03%. Incorporating the fine TX aggregate, all groups containing CA1 plus SCMs displayed lower values than SCMs only. The most efficient mixtures to mitigate ASR-induced expansion were SPH-SF, SPH-MK, SPH-CA1-MK, SPH-CA1-NS-MK, SPH-CA1-NS-SF-MK, TX-CA1-MK, TX-CA1-NS-MK, TX-CA1-NS-SF-MK, all showing ASR-induced expansion minor or equal to 0.04% at 720 days of exposure. Finally, the mass gain of the concrete specimens somewhat followed the trend seen for induced expansion; the higher the expansion level, the higher the mass gain. Moreover, the values ranged from 0.35% to 1.12% for SPH mixtures and from 0.55% to 1.73% for TX mixtures.

8.5.2 **Damage rating index (DRI)**

Figure 7.3 gives the plots of the DRI numbers obtained from the ASR-affected concrete specimens. A complete description of the microscopic features over the ASR development of the different concrete mixtures is given in the discussion section. Globally, it is possible to see that all DRI numbers obtained for the different mixtures and aggregate types increase as a function of the specimens' expansions. Moreover, at equivalent expansion levels, the overall behaviour of the various aggregates is somewhat similar, although TX mixtures reached slightly higher values. Greater DRI numbers were found in control specimens (1091 for SPH-Control and 1177 for TX-Control at the maximum expansion measured), followed by CA3 and CA4 for both aggregates. One may notice that the concrete mixtures incorporating SCMs averagely presented lower DRI numbers (about 15%) at similar expansion levels than the Control and LTM mixtures. Likely, the addition of crystalline admixtures increased this difference to 22% lower results; on average, the exceptions were CA3 and CA4 mixtures.

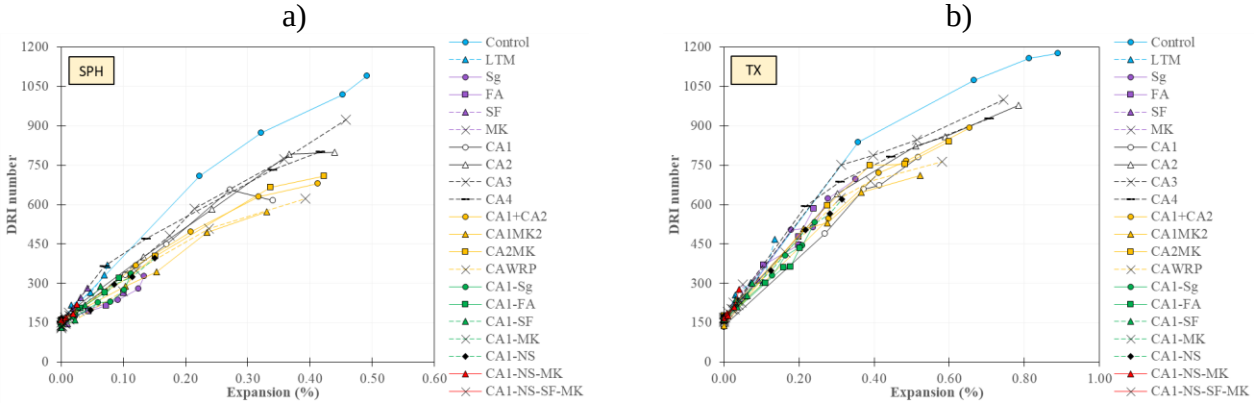

Figure 8.2: Damage Rating Index vs. expansion levels: a) for the different aggregates and b) for mixtures incorporating different types of SCMs.

8.5.3 **Mechanical properties assessment**

This section evaluates the stiffness damage index (SDI) and the losses in modulus of elasticity (ME), direct shear strength (DSS) and compressive strength (CS) of the various concrete mixtures investigated. The mechanical data presented hereafter displays the ratio of values obtained from an ASR-induced expansion at 90, 180, 360, and 720 days over the values gathered on sound concrete specimens presenting "equivalent maturity" than the damaged samples as previously discussed in 0. Moreover, one may notice that the mentioned mechanical ratios are displayed as a function of their respective expansion amplitudes to better visualize the mitigative behaviour of the binder compositions after ASR has already started.

8.5.3.1 **Compressive strength (CS)**

Figure 7.4a and b (SPH and TX concrete mixtures) illustrate the compressive strength reductions for the different concrete mixtures investigated. In general, the CS was found to decrease in function of the expansion level; the higher the expansion level, the higher the CS loss. At each period of evaluation, SPH-Control reached 0.22%, 0.32%, 0.45% and 0.49% of expansion resulting in 22%, 28%, 35.1% and 34.6% of CS loss. Moreover, the faster ASR-kinetics of TX attained to higher expansion values (i.e., 0.36%, 0.67%, 0.81% and 0.89%), thus the losses in CS were proportionally higher (i.e., 28%, 36%, 40% and 43%). Globally, the mixtures containing SCMs, chemical admixtures or both, lowered CS losses for comparable expansion levels than Control specimens, particularly for expansion levels higher than 0.20% (averagely 47% lower CS loss for SPH mixtures and 36% for TX). Nevertheless, this behaviour was more notable for concrete mixtures incorporating crystalline admixtures. Yet, a few exceptions were observed, such as CA3 and CA4 mixtures, which demonstrated somewhat similar behaviour to SPH and TX Control. Moreover, mixtures that developed lower expansion amplitudes (i.e., <0.05%) after 720 days of ASR-induced development trend to display CS variation between -5% to 3% (negative values indicate an increase in CS comparing to values obtained on sound concrete specimens).

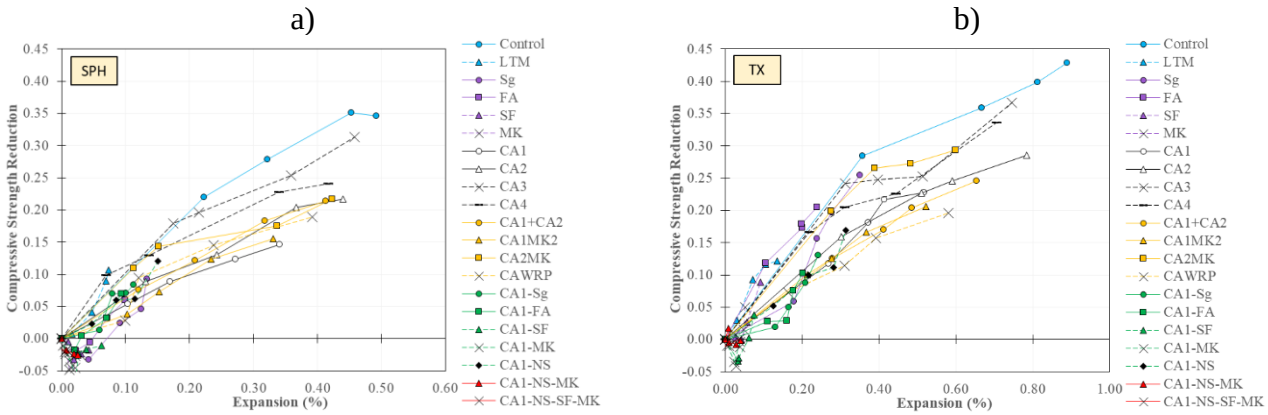

Figure 8.3: Compressive strength reduction vs. expansion levels: a) SPH coarse aggregate mixtures and b) TX fine aggregate mixtures.

8.5.3.2 Stiffness damage index (SDI)

Figure 7.5 illustrates the SDI values for the different concrete mixtures investigated and obtained at each "free" expansion level yielded by the distinct concrete mixtures after 90, 180, 360 and 720 days of ASR development. Globally, SDI values increased towards ASR development for all mixtures; moreover, the higher the expansion amplitudes, the higher the SDI. By incorporating different reactive aggregates, supplementary cementing materials and chemical admixtures, SDI was found to range from about 0.05 (CA1-NS-MK) at 0.00% of expansion to 0.40 (Control) at 0.49% for SPH mixtures and from about 0.04 (CA1-NS-SF-MK) at 0.00% to 0.47 (Control) at 0.81% for TX. Furthermore, besides SHP-CA3 and SPH-CA4 showed closer behaviour than the Control specimens, the mixtures containing SCMs, chemical admixtures or both, displayed overall lower SDI values than Control specimens for similar expansion levels (20.2% lower SDI for SPH mixtures and 13.4% for TX).

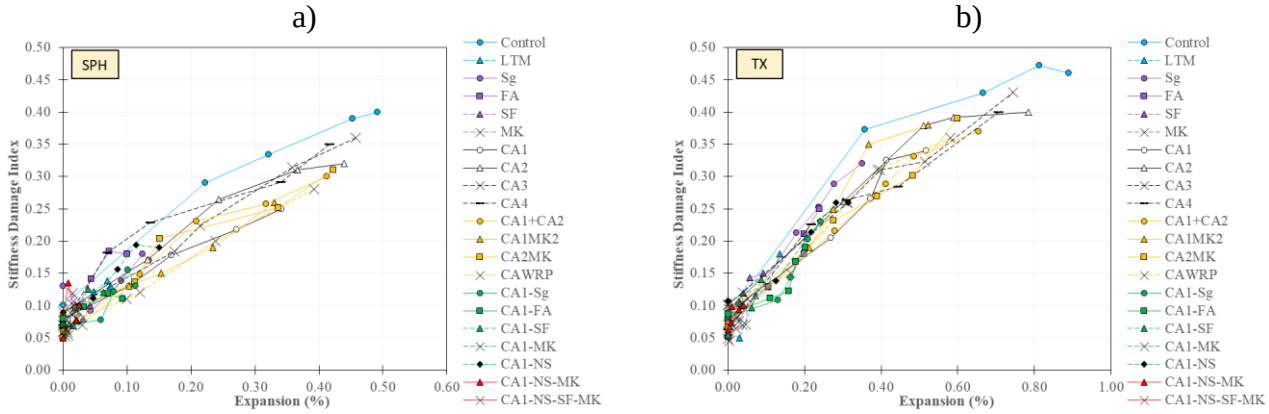

Figure 8.4: Stiffness Damage Index vs. expansion levels: a) SPH coarse aggregate mixtures and b) TX fine aggregate mixtures.

8.5.3.3 **Modulus of Elasticity (ME)**

The modulus of elasticity (ME) results of the affected samples are displayed in Figure 7.6a (SPH mixtures) and Figure 7.6b (TX mixtures). Even though the different mixtures gathered a wide range of ME losses, the values indicated in both plots (Figure 7.6a and b) a concave trend towards AAR development. Globally, at equivalent expansion levels, regardless of the binder composition of the concrete mixtures, the loss in ME was somewhat similar. Yet, TX mixtures reached higher ME losses since these mixtures achieved higher expansion levels; the maximum losses measured for SPH-made mixtures were 62% for Control specimens at 0.49% of expansion. In comparison, for TX the maximum loss was 69% at 0.89% of expansion for Control specimens. At lower expansion levels (≤0.05%), specimens containing SCMs, either combined with crystalline admixtures or not, presented relatively lower losses in ME than those only made with PC as binder materials. On the other hand, lithium-made concrete mixtures (SPH-LTM and TX-LTM) displayed a slightly higher ME loss at similar expansion levels.

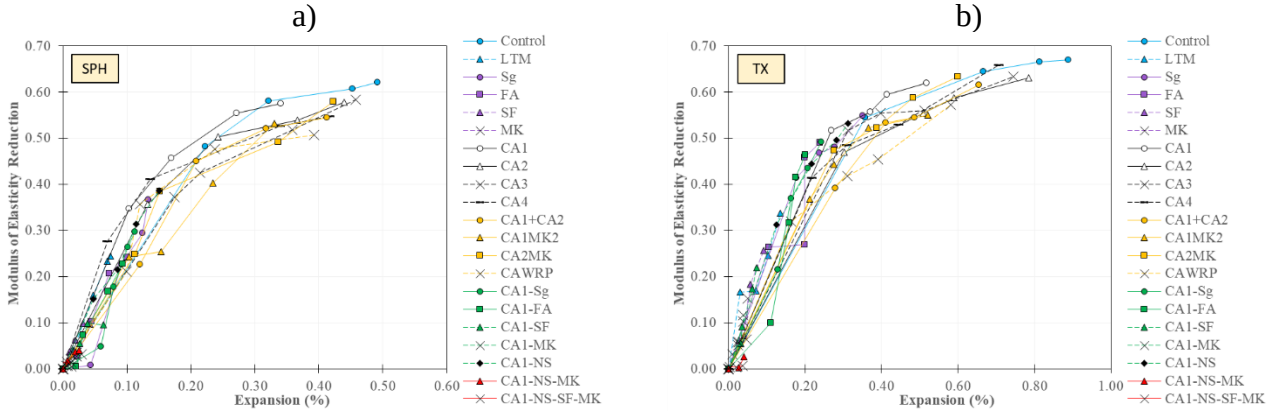

Figure 8.5: Modulus of Elasticity reduction vs. expansion levels: a) SPH coarse aggregate mixtures and b) TX fine aggregate mixtures.

8.5.3.4 **Direct shear strength (DSS)**

The direct shear strength (DSS) results of the affected samples are illustrated in Figure 7.7a (SPH mixtures) and Figure 7.7b (TX mixtures). All mixtures present a shear strength decrease as a function of ASR-induced expansion. At equivalent expansion levels, samples made of SPH aggregate showed slightly higher DSS loss, and besides a few exceptions, the overall behaviour of the concrete mixtures is quite similar. Yet, a higher range of variation in the results is observed among TX mixtures. Evaluating both plots, one may notice that the higher the expansion level, the higher the DSS reduction;

yet there is "only" a slight difference from damage degree above and beyond 0.20% of expansion. Globally, DSS loss ranged from 15% to 51% for moderate expansion levels (about 0.12%) and from 25% to 61% for high expansion levels (≥0.20%).

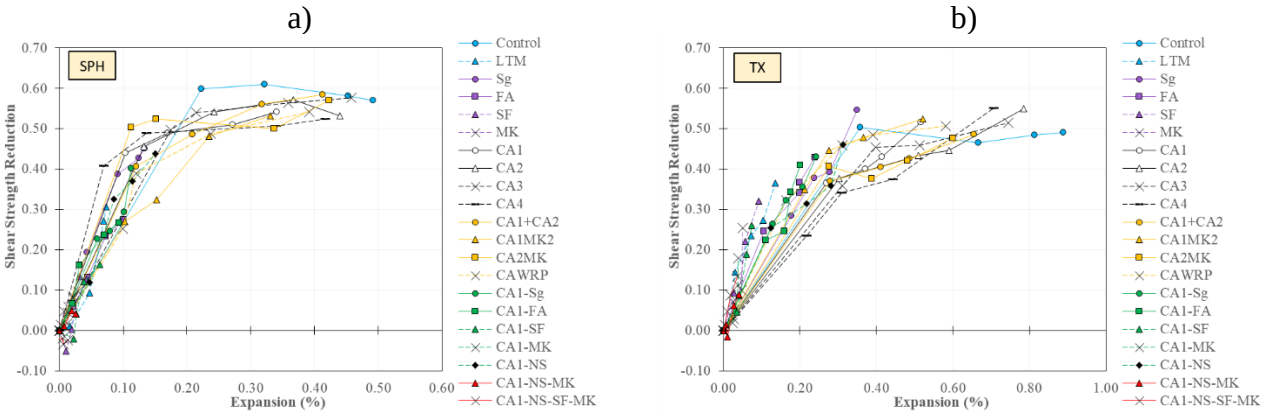

Figure 8.6: Shear strength reduction vs. expansion levels: a) SPH coarse aggregate mixtures and b) TX fine aggregate mixtures.

8.6 Discussions

8.6.1 ASR kinetics development

ASR damage development is often directly correlated to the level of expansion triggered by the concrete under this physicochemical mechanism. Based on the results above, it is clear that concrete mixtures made of TX fine aggregate had faster ASR kinetics. This is because the material has a generally lower particle size than the TX, which increases the surface contact area between the reactive particles and the alkali solution. Moreover, all mixtures, whether incorporating SCMs, chemical admixtures or both, could change ASR-kinetics lowering the expansion amplitudes. In general, SPH-Control and TX-Control specimens exhibited substantial deceleration in the rate of expansion and mass gain after about 270 days of curing. Moreover, the expansion and mass gain of both mixtures trend to flatten in between 540 and 720 days, suggesting that the reactive aggregates reached their maximum reactivity and expansion at the test conditions used in this study (i.e., 0.49% and 0.89% of expansion for SPH and TX Control, respectively). Likewise, similar behaviour was seen for most concrete mixtures, indicating different expansion amplitudes at the end of 720 days.

Lithium nitrate is a well-known powerful admixture to mitigate the ASR in concrete (considering the used ratio of 0.74 of Li/Na_2O_{eq}). However, besides both lithium-based concrete mixtures (i.e., SPH-

LTM and TX-LTM) significantly changed ASR kinetics and lessened the ultimate expansion amplitudes, they could not maintain the expansion bellow 0.04% at 2 years of curing as per [39]. Nevertheless, it is worth noting that both SPH and TX can be classified as extremely ASR reactive aggregates.

8.6.1.1 Influence of the crystalline admixtures on ASR-induced expansion development.

The use of crystalline admixtures (CAs) in the concrete mixtures showed promising evidence that, besides the CAs mixtures displayed high expansion values after 720 days of curing, they significantly modify ASR-kinetics. On average, CA mixtures lessened ASR expansion by 33% for concrete made of SPH and 31% for TX over all periods. Among the four different commercially sold crystalline admixtures (i.e., CA1, CA2, CA3 and CA4), CA1 demonstrated the lowest expansion values over 720 days (0.34% for SPH and 0.52% for TX concrete) and was followed by CA4 (0.42% for SPH and 0.71% for TX), CA2 (0.44% for SPH and 0.78% for TX) and CA3 (0.46% for SPH and 0.75% for TX). As demonstrated by [58], autonomous or autogenous healing processes could partially self-heal cracks and recover the mechanical properties. Yet, the behaviour was studied mainly in cracks formed in the paste matrix. Moreover, pre-existent and generated cracks within the aggregates' particles were not even partially healed [58]. In other words, these materials may create a physical barrier delaying the continuous cracking development through the paste matrix and further ASR-gel deposition, which can explain the change in the reaction kinetics. Furthermore, the bigger impact in the expansion amplitudes occurs mainly after about 0.07%-0.10% of expansion (when crack generated by ASR would start to reach the paste matrix [48,51]).

Based on the results of CA1, CA2, CA3 and CA4, also by those obtained in [58], the modified versions of CAs were developed. The results demonstrated that comparing to SPH and TX Control specimens, the modified versions of CA lessen, on average, 39% (SPH) and 33% (TX) the expansion amplitudes along the 720 days. However, up to 360 days of curing, it was pretty clear that the modified versions significantly changed ASR-kinetics by delaying the expansion development. In this regard, CA1MK2 and CAWRP were both found to have 12% smaller expansion values than SPH-CA1. Both mixtures had 23% lower values than TX-CA1 up to 360 days of curing. Likewise, CA2 enhanced with CA1 (CA1+CA2 mixtures), and CA2MK was found to have 16% and 25% lower expansion than SPH-CA2 and 12% and 16% lower than TX-CA2 up to the end of the first year. The coarser particles of MK2

provided by the modified CA1MK2 are SiO_2 and Al_2O_3 rich. Coarser particles tend to have slower pozzolanic reactivity, which could decelerate the release of SiO_2 and Al_2O_3 to be combined with $Ca(OH)_2$. Thus, delaying further C-S-H precipitating in pores and cracks, improving the self-healing. On the other hand, the WRP added in CAWRP difficult the permeability of water and delays ASR kinetics.

8.6.1.2 Influence of crystalline admixtures to enhance the ability of SCMs to suppress ASR-induced expansion.

Replacing the PC with the distinct SCMs displayed different behaviour on the ASR development. Although all mixtures containing SCMs mitigated ASR in the proportions used, it is worth mentioning that SG, FA, and SF mixtures were found to have expansion values equal to or higher than 0.04% for both reactive aggregates at 720 days of curing. These results were somewhat expected once the mixtures were designed to modify ASR kinetics but not "fully" prevent it. On the other hand, designed to mitigate ASR to "safe" levels (≤0.04% of expansion at 720 days), concrete mixtures made incorporating MK at 15% of PC replacement reached 0.02% (SPH-MK) and 0.05% (TX-MK) at the end of the tests. Metakaolin is a well-known material with high pozzolanic reactivity. Thus, 15% of PC's replacement can expressively consume the Portlandite from the hydrated paste and change ASR-kinetics and the properties of the ASR-gel. Moreover, high aluminum content into the concrete pore solution can be absorbed on reactive SiO_2 surfaces, slowing down its dissolution aluminum content into the concrete pore solution absorbed on reactive SiO_2 surfaces, slowing down its dissolution [6,40,41] to values close to zero [44].

Combining crystalline admixtures with SCMs in binary or ternary mixtures showed promising changes in the deleterious reaction kinetics. First, comparing the binary concrete mixtures made of SCMs with CA+SCMs ones, it was quite interesting that SCMs-made concrete mixtures with a maximum expansion of about 0.08% without CAs did not show substantial changes in the ASR-kinetics and expansion amplitudes when combined with CAs. However, SPH-SG, TX-SG and TX-FA, which reached 0.13%, 0.35% and 0.24% of expansion, when combined with CAs, significantly had their expansion amplitudes decreased (i.e., SPH-CA1-SG, TX-CA1-SG and TX-CA1-FA reached 0.10%, 0.24% and 0.19%). This interesting behaviour may indicate that the CAs-made concrete can modify ASR-kinetics once cracks reach the paste matrix. Thus, quaternary and higher blends could mitigate ASR to "safe" levels up to 2 years of curing to expansion under 0.04%.

8.6.2 **Micro-mechanical coupling analysis of the distinct concrete mixtures.**

The data obtained with microscopy analysis (i.e., DRI) agreed with the compressive and shear strength, SDI and modulus of elasticity results. Furthermore, assessing the extension of damage of the ASR-affected mixtures through microscopical and mechanical analyses indicates results in agreement with the expansion levels obtained. Overall, the higher the expansion levels, the higher the DRI number and mechanical properties losses for all mixtures; thus, the different kinetics of the aggregates and binder mixtures displayed an essential role in the extension of damage after 720 days of curing.

In general, concrete mixtures fabricated with TX fine aggregate developed presented higher expansion levels due to the available lower particle size of the TX, as previously explained. However, SPH-made concrete specimens exhibit slightly higher "measured damage" (i.e., microscopical features and mechanical losses) than TX-made concrete mixtures at equivalent expansion levels. The present research results demonstrate that while the SDI values of all SPH concrete specimens were 5.1% higher than TX for equivalent expansion levels (between the variation range of the test). On the other hand, ME losses were significantly higher for concrete mixtures incorporating reactive SPH coarse aggregate. The modulus of elasticity of ordinary concrete is primarily governed by the mechanical properties of the aggregates, especially the coarse aggregate [62]. Therefore, this phenomenon is likely responsible for the significant decrease in ME of ASR-affected mixtures. Likewise, the average DSS found for SPH-made concrete was 25.8% higher than concrete mixtures incorporating reactive TX fine. One verifies that the development of cracks within the aggregate particles considerably impacts the "aggregate interlock", thus facilitating the propagation of cracks during the test and reflecting in drops in shear strength. On the other hand, TX developed higher losses in compressive strength, which is likely explained by the fact that concrete made of TX demonstrated a higher amount of cracks in the cement paste.

The mechanical and microscopical distress development due to ASR in concrete has been widely studied by Sanchez et al. [51]. The authors described that for "conventional concrete" specimens (without SCMs or chemical admixtures), at the beginning of the physicochemical reaction (i.e., at expansion levels up to 0.05%), ASR-induced damage progress starts with cracks being formed within the reactive aggregate particles. As the expansion levels rise (i.e., 0.12%), more cracks are formed. Nevertheless, the pre-existing cracks keep increasing in length and width, reaching the cement paste; at a higher level of expansion (i.e., 0.20%), the vast majority of the cracks generated within the aggregate

considerably propagated through the cement paste. Finally, in about 0.30% of expansion, the cracks start to connect, forming a high crack networking considerably compromising all the mechanical properties of the affected concrete [48,49]. However, the propagation of cracks due to ASR development was modified by the SCMs, CAs or their combination (Figure 8.7); thus, impacting not only on the total amount of crack and crack patterns but also on the mechanical properties' losses. Incorporating the different types of SCMs, CAs, or the combination of both decreased the total DRI number by 20.4% (SCMs mixtures), 21.3% (CAs mixtures) and 22.9% (SCMs + CAs mixtures) comparing to Control specimens (Control and LTM mixtures). The global impact of the distinct concrete mixtures on microscopical and mechanical distress is discussed as follows.

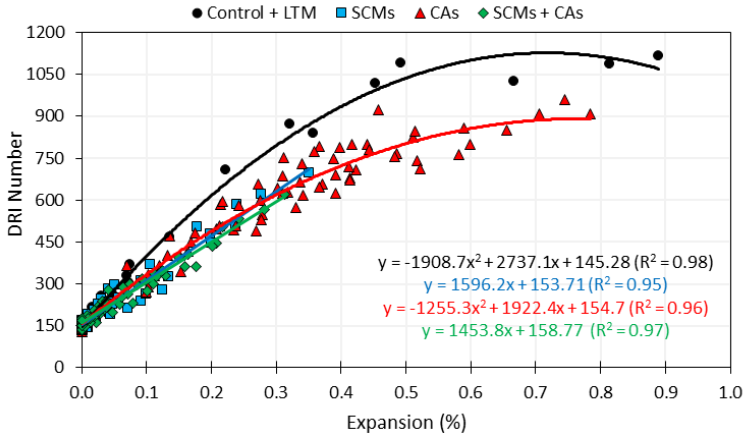

Figure 8.7: DRI behaviour comparison between the groups of mixtures (Control + LTM, SCMs, CAs and SCMs + CAs) for both reactive aggregates (SPH and TX).

8.6.2.1 Influence of the crystalline admixtures on ASR distress development.

Among the commercially available CA formulas (i.e., CA1, CA2, CA3 and CA4), the CA1 concrete mixture displayed higher efficiency to decrease the DRI number (23.5% lower than control), followed by CA2 (17.3%), CA4 (13.8%) and CA3 (13.3%). Moreover, the modified versions were able to enhance this performance slightly. Therefore, one verifies that ASR-induced damage progress starts with cracks formed within the reactive aggregate particles and further propagated towards the cement paste at an advanced level of damage. Thus, it is worth highlighting that until the point in which the internal crack of the aggregates reaches the cement paste, it is unlike that self-healing processes can modify the development of those cracks, as demonstrated by De Souza and Sanchez [58]. To clarify this statement, Figure 8.8 was developed to display, separately, the petrographic features of the DRI analysis (CCA, OCA and OCAG in Figure 8.8a, and CCP and CCPG in Figure 8.8b, as per [48]).

Overall, while CAs mixtures displayed a 6.1% (CAs) lower amount of cracks within the aggregate particles than control mixtures, the value is 47.8% smaller in the cement paste.

a) b)

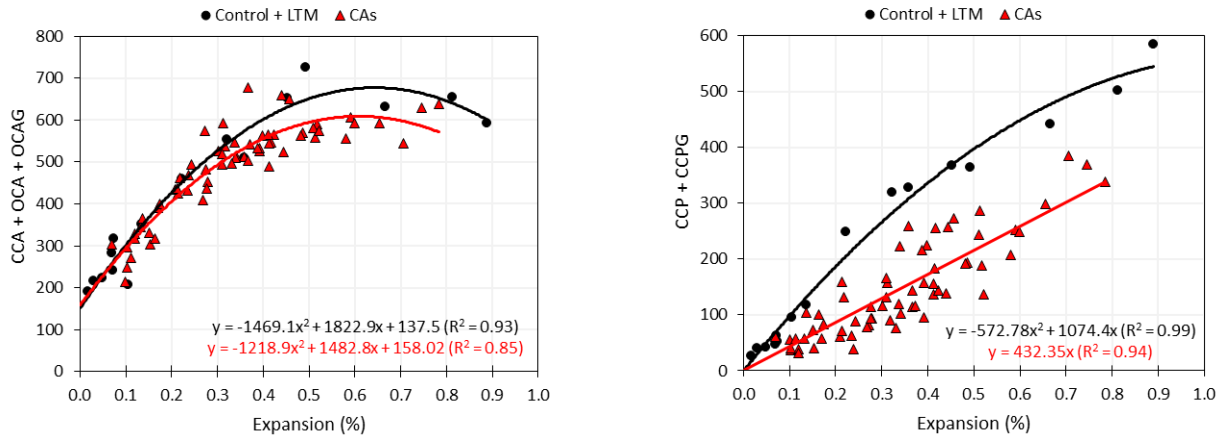

Figure 8.8: Comparison of a) the number of cracks formed within the aggregate particles and b) cement paste among the groups of mixtures (Control + LTM and CAs) for both reactive aggregates (SPH and TX).

Evaluating only the amount of cracks found in the cement paste (CCP and CCPG as per [48]), CA1MK2 displayed the highest decrease among all CA mixtures; on average, CA1MK2 specimens lowered 65.9% of CCP and CCPG combined. The coarser particles of MK2 provided by the modified CA1MK2 are SiO_2 and Al_2O_3 rich and trends to demonstrate slower pozzolanic reactivity, decelerating the release of SiO_2 and Al_2O_3 from MK2 grains to combined with $Ca(OH)_2$ and further forming C-S-H. Thus, later precipitating in pores and cracks and improving the self-healing. Moreover, regardless of CA3 and CA4, which lessened the number of cracks in the cement paste by 29.5% and 29.2%, all the other mixtures exhibit numbers higher than 50% (i.e., 64.3%, 53.1%, 60.8%, 60.7% and 52.2% for CA1, CA2, CA1+CA2, CAWRP and CA2MK mixtures). These promising results show that these materials may create a physical barrier that delays the continuous cracking development through the paste matrix and further ASR-gel deposition modifying the reaction kinetics, as illustrated in Figure 7.2. Moreover, this particular behaviour was highlighted when the expansion amplitudes overcome values between 0.07%-0.10%.

The influence mentioned above of the crystalline admixtures in the development mechanism of ASR is supported by the mechanical properties analysis. For instance, the compressive strength of conventional concrete is a mechanical property known to be governed by the cement paste (CP) properties. Thus,

any concrete mixture able to delay the damage development in the CP can also modify the rate of CS loss. Moreover, although CA mixtures exhibit relatively high expansion amplitudes and expressive CS losses, comparing the CAs results with Control mixtures, they significantly decreased the CS losses at similar expansion levels (Figure 8.9a). On average, considering the data from both types of reactive aggregates and all CAs mixtures (commercially or modified versions), incorporating 1.91% of CAs (by mass of PC) in the concrete could reduce CS losses by 32.6% over the 720 days of curing. Likewise, adding crystalline admixtures on concrete drops, SDI results in 14.9% over ASR development (Figure 8.9b). Otherwise, CAs-made concrete mixtures do not significantly influence the modulus of elasticity and shear strength loss for unrestrained ASR development (Figure 8.9c and Figure 8.9d, respectively). Naturally, the different CA mixtures modified the kinetics of ASR and changed the rate of ME and DSS losses over time, though once the specimens reached a specific expansion level, the loss among different mixtures are averagely similar with control specimens.

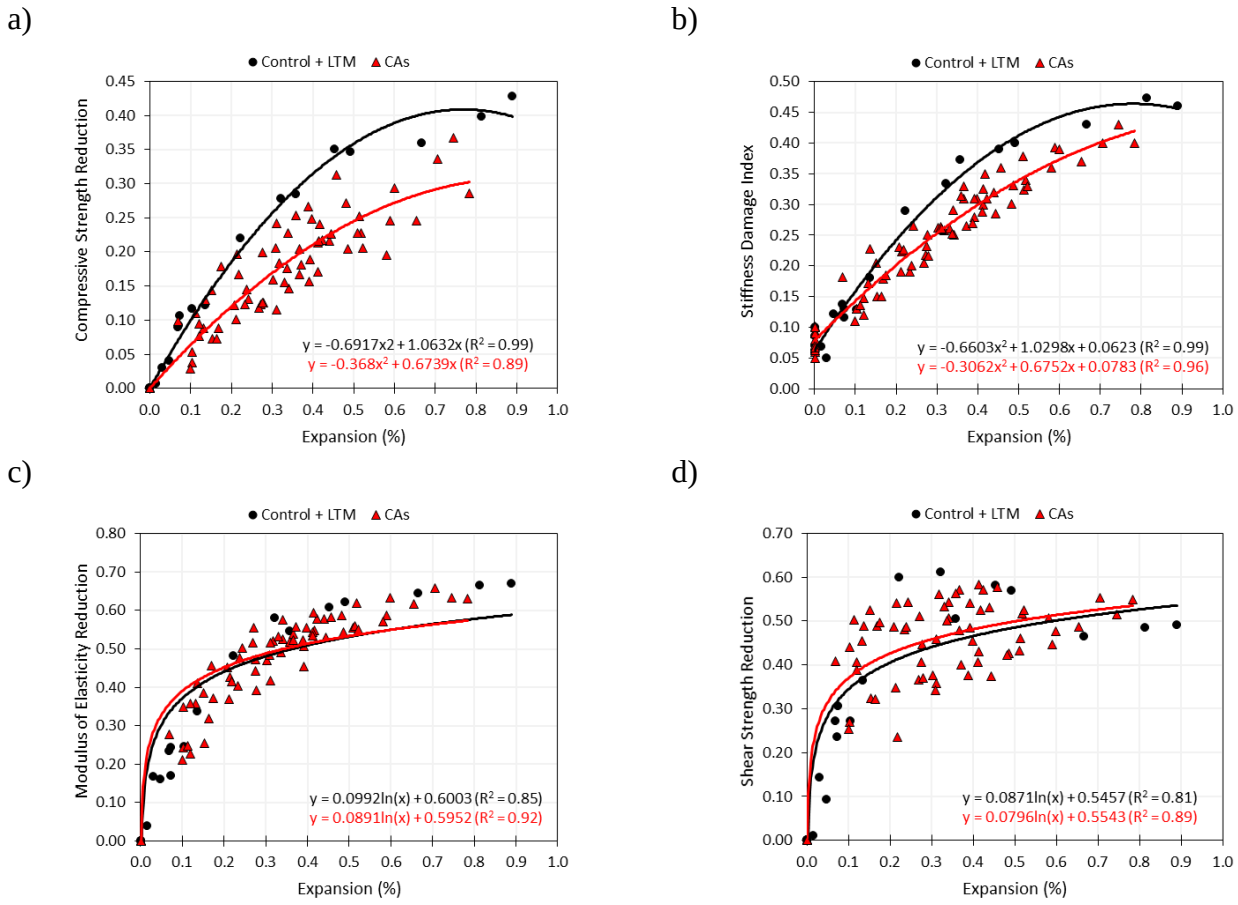

Figure 8.9: Mechanical properties comparison between the groups of mixtures (Control + LTM and CAs) for both reactive aggregates (SPH and TX): a) compressive strength loss; b) stiffness damage index; c) modulus of elasticity loss; d) direct shear strength loss.

The induced expansion, compressive strength loss and stiffness damage index suggest that among the commercially available crystalline admixtures, CA1 seems to have the higher ability of self-healing and followed by CA2, CA3 and CA4. Regarding the modified versions of CAs, the only mixtures which displayed worsen results than the major CA used in the mixture was CA2MK. On the other hand, altering CA1 with coarse MK2 particles reached the best results of CA mixtures for both CS loss and SDI. This behaviour can be explained by the fact that coarser MK particles have significantly slower reactivity than finer ones, enhancing the further formation of hydrates collaborating to close formed cracks. However, it is worth mentioning that the overall stiffness of a concrete specimen is sensitive to cracks formed in both the cement paste or within the aggregate particles, which might explain the lower differences obtained between the CAs mixtures and compared to control specimens.

8.6.2.2 Influence of crystalline admixtures to enhance the ability of SCMs to suppress ASR distress development.

De Souza and Sanchez [60] suggested that a high volume of PC replacement by SCMs lessens the developed cracks in the binder paste of the concrete under "free expansion conditions" at moderate and higher levels of expansion. This behaviour could result from the enhancement of the natural healing process due to the higher volume of SCMs. In the present study, the mixtures SG, FA, SF, and MK, averagely lessened the total DRI numbers by 25.0%, 22.8%, 4.7% and 3.6%, respectively, at equivalent expansion levels than the control mixtures (Control and LTM). Moreover, combining SCMs with crystalline admixtures trends to improve even more the ability of the concrete mixtures to lower the crack development in the cement paste. In general, SCMs + CAs mixtures displayed 21.8% lower DRI numbers than control specimens, the highest values among all groups of binder composition (Figure 8.10).

Moreover, directly comparing SG, FA, SF and MK mixtures with CA1-SG, CA1-FA, CA1-SF and CA1-MK, the addition of CA1 lessened the number of cracks found in the cement paste by 12.4%, 15.8%, 18.8% and 36.2%. However, it is worth mentioning that SF, MK, CA1-SF and CA1-MK developed negligible to marginal expansion levels, with the highest values equal to 0.09% for the TX-SF mixture. Thus, it is unlike that crack formed within the aggregate particles has significantly propagated through the paste matrix. Furthermore, the CCPs detected in these mixtures were randomly spread in the paste matrix (very difficult to localize under magnification of 15-16x), which could result from a different mechanism, such as shrinkage, improper consolidation, etc. Thus, the differences of

18.8% (between SF and CA1-SF) and 36.2% (between MK and CA1-MK) could enhance the overall microstructure of concrete specimens, providing a good preventive preventive preventive measure to delay the initiation of ASR or different damage mechanism.

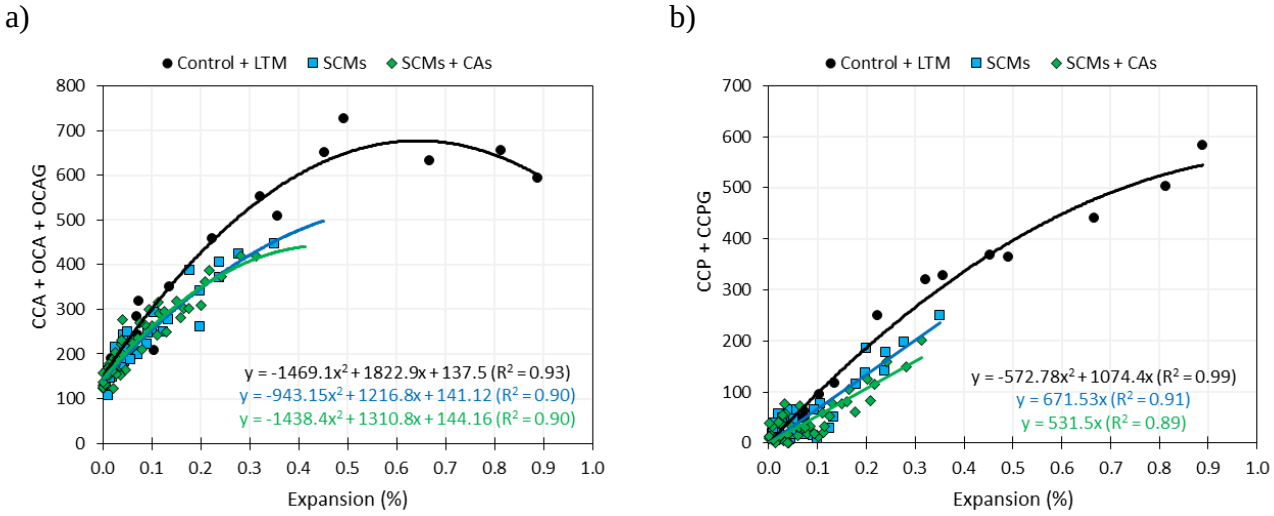

Figure 8.10: Comparison of a) the amount of cracks formed within the aggregate particles and b) cement paste among the groups of mixtures (Control + LTM, SCMs, and SCMs+CAs) for both reactive aggregates (SPH and TX).

Concrete specimens made by the combination of SCMs and CA1 had, in their majority, negligible to marginal expansion levels. Besides that, the group of mixtures SCMs + CAs displayed the lower losses in CS in the function of the expansion level (Figure 8.11a); on average, 54%, 36.7% and 29.3% less than control, SCMs and CAs specimens, respectively. For SDI values, concrete mixtures made only by replacing the PC with the different SCMs reduced SDI values by 7.1%, compared to control specimens (Control and LTM mixtures) for similar expansion levels. Furthermore, combining SCMs and CAs achieved even lower numbers, an average of 17.2% lower than control specimens. It is worth noting that SCMs can modify the mechanical and chemical properties of the ASR-gel, significantly changing the reaction kinetics; moreover, several researchers [19,60,61,63–65] have reported that high volume of SCMs can improve autogenous healing of the concrete. Likewise, crystalline admixtures enhance the artificial/autonomous healing; moreover, combining with SCMs, CA can further "activate" unhydrated SCMs and PC's particles, developing a microstructure with better quality and enhancing the self-healing of the concrete. Yet, mechanical properties governed by the inner quality of the aggregates (i.e., ME and DSS), once again, were minor affected by the use of SCMs and SCMs+CAs, besides the fact that these mixtures change ASR kinetics.

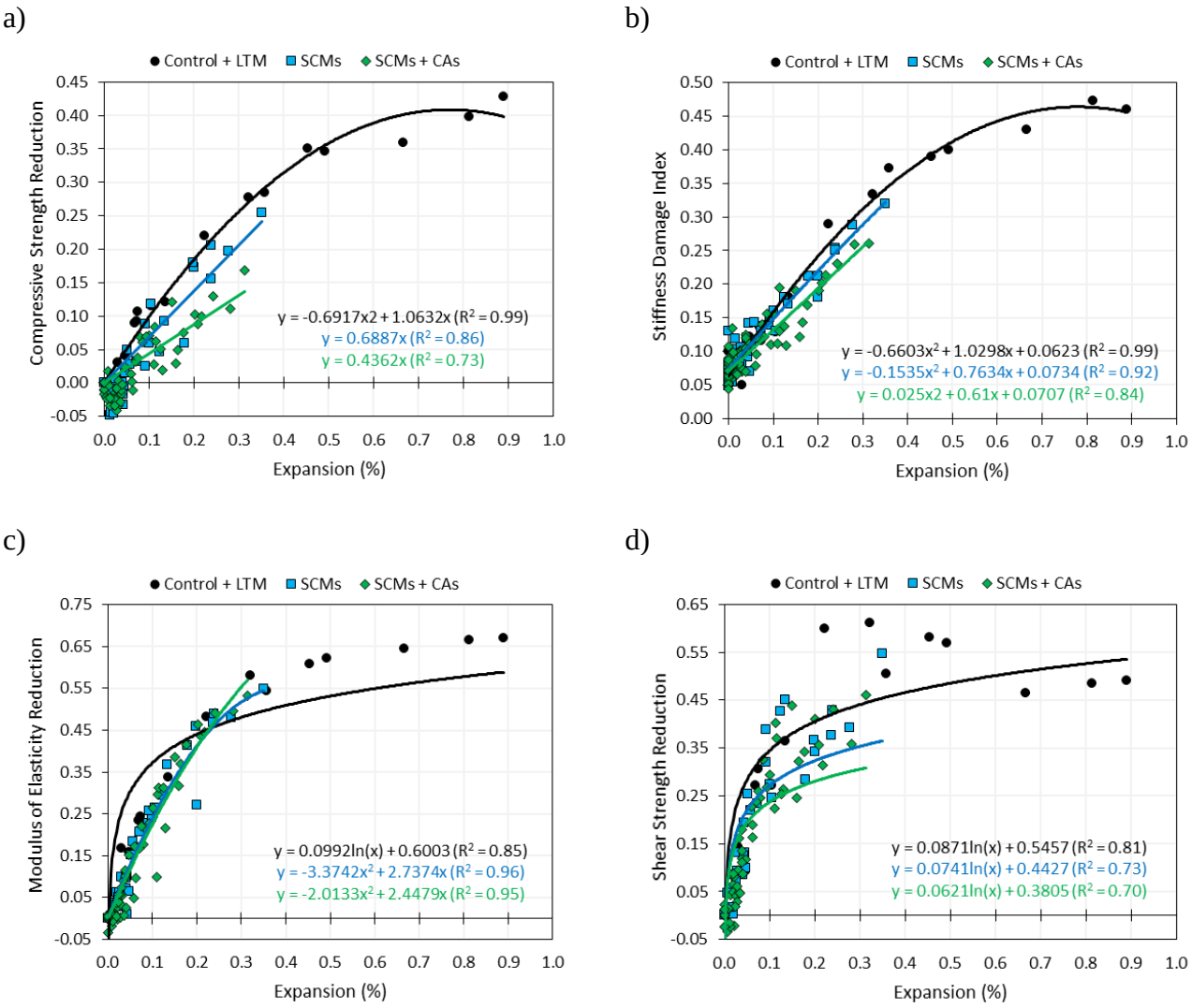

Figure 8.11: Mechanical properties comparison between the groups of mixtures (Control + LTM, SCMs, and SCMs + CAs) for both reactive aggregates (SPH and TX): a) compressive strength loss; b) stiffness damage index; c) modulus of elasticity loss; d) direct shear strength loss.

Finally, concrete mixtures CA1-NS-MK and CA1-NS-SF-MK developed negligible expansion levels after 720 days of curing, primarily due to their chemical composition and pozzolanic reactivity. Thus, it is unlike that the crystalline admixture significantly influences CA1-NS-MK and CA1-NS-SF-MK mixtures, yet CA1 can enhance the microstructure, helping to prevent ASR development. Moreover, this material can be an essential tool to modify ASR-kinetics once the reaction starts to damage the binder paste, delaying the deterioration and giving extra time to intervene and reinforce affected structures.

8.7 Conclusions

The primary objective of this research program was to evaluate different concrete mixes presenting two different types of reactive aggregates (i.e., Greywacke Coarse and Polymictic Fine aggregates), incorporating a wide range of binder compositions (i.e., GU cement, slag, fly ash class F, silica fume and metakaolin) and using different types of admixtures (i.e., crystalline, nano-silica, water repellent and lithium-based products). From the results obtained in this study (after 720 days of exposure), the following conclusions may be drawn:

- ASR kinetics, mechanical properties and microscopic changes are dependent on the aggregate's type (i.e., fine vs coarse aggregate). Samples incorporating the highly reactive Tx sand were more damaged than SPH samples. Moreover, samples containing Tx have developed more cracks in shorter periods due to their faster ASR-induced kinetics.
- The use of crystalline admixtures (CA), either commercially available or modified versions, could change ASR kinetics and distress for both reactive aggregates used. It is believed that the CAs can start healing cracks and modify ASR kinetics and further deterioration only when the cracks reach the cement paste.
- The most effective crystalline admixtures in decrease the number of cracks in the cement paste of the affected concrete specimens was CA1MK2, CA1WRP and CA1. The latter is the commercially available formula of CA, and the first two are the modified versions incorporation coarse metakaolin particles (CA1MK2) and water repellent in powder (CA1WRP).
- The combined use of different SCMs and crystalline admixtures was highly effective in mitigating ASR, either changing ASR-kinetics or damage development. Although the chemical composition of the SCMs plays a major role in the development of ASR, the use of CA enhanced the healing properties of the SCMs-made concrete favouring the slower damage development.

- The use of metakaolin in combination with crystalline admixtures, nano-silica and silica fume (i.e., CA1-MK, CA1-NS-MK, and CA1-NS-SF-MK mixtures) yielded the best results, even better than the samples containing Lithium Nitrate in the proportion of 0.74 Li/Na. However, it is unlike that the crystalline admixture has a significant influence in these mixtures, yet CA can enhance the microstructure helping to prevent ASR development. Moreover, this material can be an important tool to modify ASR-kinetics once the reaction starts to damage the paste matrix, delaying the deterioration and giving extra time to intervene and reinforce affected structures.

8.8 Acknowledgment

The authors would like to thank Dr. Gamal Elnabelsya and Dr. Muslim Majeed, technical officers of Materials and Structures Laboratory in the Department of Civil Engineering at the University of Ottawa. Likewise, the authors would like to express their sincere gratitude and appreciation to Kryton International, Mr. Alireza Biparva, Mary Grace Rosalin, Dr. Pejman Azarsa. As well as De Souza benefits from the University of Ottawa Excellence Scholarship, Collaborative Research & Development by NSERC (Natural Science and Engineering Research Council of Canada), and the prestigious Vanier CGS scholarship, also financed by the NSERC.

8.9 References

[1] T. Katayama, The so-called alkali-carbonate reaction (ACR) - Its mineralogical and geochemical details, with special reference to ASR, Cem. Concr. Res. 40 (2010) 643–675. doi:10.1016/j.cemconres.2009.09.020.

[2] J. Lindgård, Ö. Andiç-Çakir, I. Fernandes, T.F. Rønning, M.D.A. Thomas, Alkali-silica reactions (ASR): Literature review on parameters influencing laboratory performance testing, Cem. Concr. Res. 42 (2012) 223–243. doi:10.1016/j.cemconres.2011.10.004.

[3] B. Fournier, M.A. Bérubé, Alkali-aggregate reaction in concrete: A review of basic concepts and engineering implications, Can. J. Civ. Eng. 27 (2000) 167–191. doi:10.1139/l99-072.

[4] M. Thomas, The effect of supplementary cementing materials on alkali-silica reaction: A review, Cem. Concr. Res. 41 (2011) 1224–1231. doi:10.1016/j.cemconres.2010.11.003.

[5] Z. Shi, C. Shi, J. Zhang, S. Wan, Z. Zhang, Z. Ou, Alkali-silica reaction in waterglass-activated slag mortars incorporating fly ash and metakaolin, Cem. Concr. Res. 108 (2018) 10–19. doi:10.1016/j.cemconres.2018.03.002.

[6] A. Leemann, L. Bernard, S. Alahrache, F. Winnefeld, ASR prevention - Effect of aluminum and lithium ions on the reaction products, Cem. Concr. Res. 76 (2015) 192–201. doi:10.1016/j.cemconres.2015.06.002.

[7] J. Wei, B. Gencturk, A. Jain, M. Hanifehzadeh, Mitigating alkali-silica reaction induced concrete degradation through cement substitution by metakaolin and bentonite, Appl. Clay Sci. 182 (2019) 105257. doi:10.1016/j.clay.2019.105257.

[8] B. Fournier, R. Chevrier, A. Bilodeau, P.P.C. Nkinamubanzi, N. Bouzoubaa, R. Chevrier, Comparative field and laboratory investigations on the use of supplementary cementing materials (SCMs) to control alkali-silica reaction (ASR) in concrete, in: 15th Int. Conf. Alkali-Aggregate React., Bernardes, H.M & Hasparyk, N.P., São Paulo, 2016.

[9] B. Park, Y.C. Choi, Self-healing capability of cementitious materials with crystalline admixtures and super absorbent polymers (SAPs), Constr. Build. Mater. 189 (2018) 1054–1066. doi:10.1016/j.conbuildmat.2018.09.061.

[10] H. Huang, G. Ye, C. Qian, E. Schlangen, Self-healing in cementitious materials: Materials, methods and service conditions, Mater. Des. 92 (2016) 499–511. doi:10.1016/j.matdes.2015.12.091.

[11] P. Escoffres, C. Desmettre, J.P. Charron, Effect of a crystalline admixture on the self-healing capability of high-performance fiber reinforced concretes in service conditions, Constr. Build. Mater. 173 (2018) 763–774. doi:10.1016/j.conbuildmat.2018.04.003.

[12] TCS. Reddy, A. Ravitheja, C. Sashidhar, Micromechanical Properties of Self-Healing Concrete with Crystalline Admixture and Silica Fume, ACI Mater. J. 117 (2020) 63–74. doi:10.14359/51722395.

[13] ACI 212.3R, ACI 212 . 3R-10 Report on Chemical Admixtures for Concrete, American Concrete Institute, 2015.

[14] P. Azarsa, R. Gupta, A. Biparva, Assessment of self-healing and durability parameters of concretes incorporating crystalline admixtures and Portland Limestone Cement, Cem. Concr. Compos. 99 (2019) 17–31. doi:10.1016/j.cemconcomp.2019.02.017.

[15] H. Ma, S. Qian, Z. Zhang, Effect of self-healing on water permeability and mechanical property of Medium-Early-Strength Engineered Cementitious Composites, Constr. Build. Mater. 68 (2014) 92–101. doi:10.1016/j.conbuildmat.2014.05.065.

[16] E. Cuenca, A. Tejedor, L. Ferrara, A methodology to assess crack-sealing effectiveness of crystalline admixtures under repeated cracking-healing cycles, Constr. Build. Mater. 179 (2018) 619–632. doi:10.1016/j.conbuildmat.2018.05.261.

[17] H. Liu, Q. Zhang, C. Gu, H. Su, V. Li, Self-healing of microcracks in Engineered Cementitious Composites under sulfate and chloride environment, Constr. Build. Mater. 153 (2017) 948–956. doi:10.1016/j.conbuildmat.2017.07.126.

[18] L. Ferrara, V. Krelani, M. Carsana, A "fracture testing" based approach to assess crack healing of concrete with and without crystalline admixtures, Constr. Build. Mater. 68 (2014) 535–551. doi:10.1016/j.conbuildmat.2014.07.008.

[19] TCSR Reddy, A.R. Theja, C. Sashidhar, Self-Healing Ability of High-Strength Fibre-Reinforced Concrete with Fly Ash and Crystalline Admixture, Civ. Eng. J. 4 (2018) 971. doi:10.28991/cej-0309149.

[20] TCS. Reddy, A. Ravitheja, Macro mechanical properties of self healing concrete with crystalline admixture under different environments, Ain Shams Eng. J. 10 (2019) 23–32. doi:10.1016/j.asej.2018.01.005.

[21] G. Li, S. Liu, M. Niu, Q. Liu, X. Yang, M. Deng, Effect of granulated blast furnace slag on the self-healing capability of mortar incorporating crystalline admixture, Constr. Build. Mater. 239 (2020) 117818. doi:10.1016/j.conbuildmat.2019.117818.

[22] M. Roig-Flores, F. Pirritano, P. Serna, L. Ferrara, Effect of crystalline admixtures on the self-healing capability of early-age concrete studied by means of permeability and crack closing tests, Constr. Build. Mater. 114 (2016) 447–457. doi:10.1016/j.conbuildmat.2016.03.196.

[23] T. Chandra Sekhara Reddy, A. Ravitheja, Macro mechanical properties of self healing concrete with crystalline admixture under different environments, Ain Shams Eng. J. 10 (2019) 23–32. doi:10.1016/j.asej.2018.01.005.

[24] Y. Kawabata, K. Yamada, The mechanism of limited inhibition by fly ash on expansion due to alkali–silica reaction at the pessimum proportion, Cem. Concr. Res. 92 (2017) 1–15. doi:10.1016/j.cemconres.2016.11.002.

[25] A.K. Saha, M.N.N. Khan, P.K. Sarker, F.A. Shaikh, A. Pramanik, The ASR mechanism of reactive aggregates in concrete and its mitigation by fly ash: A critical review, Constr. Build.

Mater. 171 (2018) 743–758. doi:10.1016/j.conbuildmat.2018.03.183.

[26] D. Hester, C. McNally, M. Richardson, A study of the influence of slag alkali level on the alkali-silica reactivity of slag concrete, Constr. Build. Mater. 19 (2005) 661–665. doi:10.1016/j.conbuildmat.2005.02.016.

[27] M.C.G. Juenger, R. Siddique, Recent advances in understanding the role of supplementary cementitious materials in concrete, Cem. Concr. Res. (2015). doi:10.1016/j.cemconres.2015.03.018.

[28] M.H. Shehata, M.D.A. Thomas, Use of ternary blends containing silica fume and fly ash to suppress expansion due to alkali-silica reaction in concrete, Cem. Concr. Res. 32 (2002) 341–349. doi:10.1016/S0008-8846(01)00680-9.

[29] T. Nochaiya, W. Wongkeo, A. Chaipanich, Utilization of fly ash with silica fume and properties of Portland cement-fly ash-silica fume concrete, Fuel. 89 (2010) 768–774. doi:10.1016/j.fuel.2009.10.003.

[30] P. Lawrence, M. Cyr, E. Ringot, Mineral admixtures in mortars, Cem. Concr. Res. 33 (2003) 1939–1947. doi:10.1016/S0008-8846(03)00183-2.

[31] B. Lothenbach, K. Scrivener, R.D. Hooton, Supplementary cementitious materials, Cem. Concr. Res. 41 (2011) 1244–1256. doi:10.1016/j.cemconres.2010.12.001.

[32] Q. Zhao, J. Stark, E. Freyburg, M. Zhou, The Mechanism of Gbfs Preventing AAR: a Discussion, in: 13th Int. Conf. Alkali-Aggregate React. Concr., Trondheim, Norway, 2008.

[33] N. Arano, M. Kawamura, Comparative consideration on the mechanism of ASR suppression due to different mineral admixtures., in: BD. M.A. Bérubé, B. Fournier (Ed.), 11th Int. Conf. Alkali–Aggregate React. Concr. (ICAAR)., Quebéc, 2000: pp. 553–562.

[34] V.M. Malhotra, B. Fournier, Overview of Research on Alkali-Aggregate Reactions., in: Int. Work. Alkali-Aggregate React. Concr., Nova Scotia, 1995: pp. 1–45.

[35] J. Duchesne, M.A. Bérubé, Long-term effectiveness of supplementary cementing materials against alkali-silica reaction, Cem. Concr. Res. 31 (2001) 1057–1063. doi:10.1016/S0008-8846(01)00538-5.

[36] B. Fournier, R. Chevrier, A. Bilodeau, P.C. Nkinamubanzi, N. Bouzoubaa, Comparative field and laboratory investigations on the use of supplementary cementing materials (SCMs) to control alkali-silica reaction (ASR) in concrete, in: 15th Int. Conf. Alkali-Aggregate React., Bernardes, H.M & Hasparyk, N.P., São Paulo, 2016.

[37] CSA A23.1-14, Concrete materials and methods of concrete construction, Can. Stand. Assoc.

(2019).

[38] ASTM C1293, Standard test method for determination of length change of concrete due to alkali-silica reaction, Annu. B. ASTM Stand. (2015) 1–7. doi:10.1520/C1293-08B.2.

[39] CSA A23.2-28A, Standard Practice for Laboratory Testing to Demonstrate the Effectiveness of Supplementary Cementing Materials and Chemical Admixtures to Prevent ASR in Concrete, Can. Stand. Assoc. (2009).

[40] T. Chappex, K.L. Scrivener, The influence of aluminium on the dissolution of amorphous silica and its relation to alkali silica reaction, Cem. Concr. Res. 42 (2012) 1645–1649. doi:10.1016/j.cemconres.2012.09.009.

[41] T. Chappex, K. Scrivener, Alkali fixation of C-S-H in blended cement pastes and its relation to alkali silica reaction, Cem. Concr. Res. 42 (2012) 1049–1054. doi:10.1016/j.cemconres.2012.03.010.

[42] A. Mirdamadi, H. Layssi, M.H. Eftekhar, M. Shekarchi, Comparative Study of Metakaolin and Silica Fume To Prevent Alkali-Silica Reaction in Concrete, in: NP. Bernardes, H. M. & Hasparyk (Ed.), 13th Int. Conf. Alkali-Aggregate React. Concr., 2008.

[43] FA.. Munhoz, Y. Kihara, M.A. Cincotto, Effect of Mineral Admixtures on To the Mitigation of Alkali-Silica Reaction in Concrete, in: 13th Int. Conf. Alkali-Aggregate React. Concr., Trondheim, Norway, 2008.

[44] K.-J. Huenger, M. Kositz, M. Huenger, J. Krey, M. Muehlstaedt, Surface Coating of Siliceous Parts of Aggregate Grains By Alumina Containing Scm`S in Alkaline Solutions, in: N.P. Bernardes, H. M. & Hasparyk (Ed.), 15th Int. Conf. Alkali-Aggregate React., São Paulo, 2016.

[45] K. Sisomphon, O. Copuroglu, E.A.B. Koenders, Self-healing of surface cracks in mortars with expansive additive and crystalline additive, Cem. Concr. Compos. 34 (2012) 566–574. doi:10.1016/j.cemconcomp.2012.01.005.

[46] K. Sisomphon, O. Copuroglu, E.A.B. Koenders, Effect of exposure conditions on self healing behavior of strain hardening cementitious composites incorporating various cementitious materials, Constr. Build. Mater. 42 (2013) 217–224. doi:10.1016/j.conbuildmat.2013.01.012.

[47] S. Guzlena, G. Sakale, Self-healing concrete with crystalline admixture - A review, IOP Conf. Ser. Mater. Sci. Eng. 660 (2019). doi:10.1088/1757-899X/660/1/012057.

[48] L.F.M. Sanchez, B. Fournier, M. Jolin, J. Duchesne, Reliable quantification of AAR damage through assessment of the Damage Rating Index (DRI), Cem. Concr. Res. 67 (2015) 74–92. doi:10.1016/j.cemconres.2014.08.002.

[49] L.F.M. Sanchez, B. Fournier, M. Jolin, M.A.B. Bedoya, J. Bastien, J. Duchesne, Use of Damage Rating Index to quantify alkali-silica reaction damage in concrete: Fine versus coarse aggregate, ACI Mater. J. 113 (2016) 395–407. doi:10.14359/51688983.

[50] L.F.M. Sanchez, Contribution to the assessment of damage in aging concrete infrastructures affected by alkali-aggregate reaction, (2014) 341.

[51] L.F.M. Sanchez, B. Fournier, M. Jolin, D. Mitchell, J. Bastien, Overall assessment of Alkali-Aggregate Reaction (AAR) in concretes presenting different strengths and incorporating a wide range of reactive aggregate types and natures, Cem. Concr. Res. 93 (2017) 17–31. doi:10.1016/j.cemconres.2016.12.001.

[52] L. Sanchez, Contribution to the assessment of damage in aging concrete infrastructures affected by alkali-aggregate reaction, UNIVERSITE LAVAL, 2014.

[53] L.F.M. Sanchez, B. Fournier, M. Jolin, J. Bastien, Evaluation of the stiffness damage test (SDT) as a tool for assessing damage in concrete due to ASR: Test loading and output responses for concretes incorporating fine or coarse reactive aggregates, Cem. Concr. Res. 56 (2014) 213–229. doi:10.1016/j.cemconres.2013.11.003.

[54] L.F.M. Sanchez, B. Fournier, M. Jolin, J. Bastien, D. Mitchell, Practical use of the Stiffness Damage Test (SDT) for assessing damage in concrete infrastructure affected by alkali-silica reaction, Constr. Build. Mater. 125 (2016) 1178–1188. doi:10.1016/j.conbuildmat.2016.08.101.

[55] L.F.M. Sanchez, B. Fournier, M. Jolin, J. Bastien, Evaluation of the Stiffness Damage Test (SDT) as a tool for assessing damage in concrete due to alkali-silica reaction (ASR): Input parameters and variability of the test responses, Constr. Build. Mater. 77 (2015) 20–32. doi:10.1016/j.conbuildmat.2014.11.071.

[56] B. Barr, E.B.D. Hasso, development of a compact cylindrical shear test specimen, J. Mater. Sci. Lett. 5 (1986) 1305–1308.

[57] DJ De Souza, L.F.M. Sanchez, M.T. De Grazia, Evaluation of a direct shear test setup to quantify AAR-induced expansion and damage in concrete, Constr. Build. Mater. 229 (2019). doi:10.1016/j.conbuildmat.2019.116806.

[58] DJ De Souza, L.F.M. Sanchez, Multi-level assessment of physical and mechanical properties recovery of self-healed concrete., Under Publ. (2021).

[59] D.J. Souza, L.Y. Yamashita, F. Dranka, M.H.F. Medeiros, R.A. Medeiros-Junior, Repair Mortars Incorporating Multiwalled Carbon Nanotubes: Shrinkage and Sodium Sulfate Attack, J. Mater. Civ. Eng. 29 (2017) 1–12. doi:10.1061/(ASCE)MT.1943-5533.0002105.

[60] DJ De Souza, L.F.M. Sanchez, Multi-level assessment of the AAR-affected concrete including Vickers' hardness in concrete., Under Publ. (2021).

[61] M. Şahmaran, SB Keskin, G. Ozerkan, I.O. Yaman, Self-healing of mechanically-loaded self consolidating concretes with high volumes of fly ash, Cem. Concr. Compos. 30 (2008) 872–879. doi:10.1016/j.cemconcomp.2008.07.001.

[62] P.K. Mehta, P.J.M. Monteiro, Concrete: Microstructure, Properties, and Materials, 3rd Edition, 2013. doi:10.1036/0071462899.

[63] K. Van Tittelboom, E. Gruyaert, H. Rahier, N. De Belie, Influence of mix composition on the extent of autogenous crack healing by continued hydration or calcium carbonate formation, Constr. Build. Mater. 37 (2012) 349–359. doi:10.1016/j.conbuildmat.2012.07.026.

[64] D. Jaroenratanapirom, R. Sahamitmongkol, Effects of Different Mineral Additives and Cracking Ages on Self-Healing Performance of Mortar, in: Annu. Concr. Conf. 6, Thailand Concrete Association, 2010: pp. 551–556.

[65] K. Van Tittelboom, N. De Belie, Self-healing in cementitious materials-a review, 2013. doi:10.3390/ma6062182.

Chapter Nine: Evaluation of the efficiency of distinct surface treatments to mitigate alkali-silica reaction induced expansion and deterioration.

Diego J. De Souza[1], Leandro F. M. Sanchez[1]

[1]Department of Civil Engineering, University of Ottawa, Ottawa, Canada.

Abstract

One of the main distress mechanisms of aging concrete structures is alkali-silica reaction (ASR). Its development leads to microcracking, loss of material integrity and functionality of the affected structure. Moreover, once ASR takes place, there is no consensus on the most efficient method(s) nor when they should be implemented to mitigate/rehabilitate ASR-affected concrete structures/structural members. Although various waterproofing materials have demonstrated promising results, their efficiency is immediately compromised by the progression of ASR and new cracks formation. Recently, waterproofing materials with self-healing properties have been introduced in the market, yet their behaviour under critical development of physicochemical distress mechanism is relatively unknown. Thus, this research aims to appraise the ability of waterproofing self-healing coating mixtures to mitigate (i.e., physically, chemically, or both) concrete deterioration caused by ASR in its initial, moderate, and advanced phases. Moreover, comparisons with other systems such as silane/siloxane, rigid coating and lithium-based are also performed, and the efficiency of those different systems to mitigate ASR is multi-level assessed (i.e., mechanically and microscopically). The results indicate that the surface treatments significantly changed ASR-kinetics and the mechanical properties loss and microscopic features likely follow the induced expansion results obtained. Finally, qualitative charts were developed to provide interesting data to help in the "decision making" for engineers to better select different types of coating and sealers and the most appropriate "time" to apply them in ASR-affected concrete.

Keywords: alkali-silica reaction, the durability of concrete, self-healing, surface treatment of aging concrete.

9.1 Introduction

Alkali silica reaction (ASR) is one of the main processes affecting the durability, serviceability and performance of concrete infrastructure worldwide [1]. ASR generates secondary products that induce swelling pressures within the reacting aggregate material(s) and the adjacent cement paste while moisture uptake [1,2]. Its development leads to microcracking, loss of material integrity and functionality of the affected structure.

Over the years, specifications have been implemented to reduce significantly or eliminate ASR in newly constructed structures [3]. Yet, many structures built before these specifications were in place; thus, many of them are currently showing signs of distress or are expected to in the coming years [4]. Moreover, once ASR takes place, there is no consensus on the most efficient method(s), nor when they should be implemented, mitigate/rehabilitate ASR-affected concrete structures/structural members [1,4–6]. Overall, studies suggest that to reduce ASR-induced expansion and associated damage in aging structures, the most important strategy is lessening moisture uptake from the surrounding environment [1,7,8]. Although various waterproofing materials are available in the market, their efficiency is immediately compromised by the progressing of ASR and the formation of new cracks since the internal moisture of concrete can further develop the reaction [4,9–11]. Likewise, cracks formation from different physical or chemical-related mechanisms.

Crystalline admixtures (CA) have been successfully used for a wide variety of waterproofing applications and have demonstrated improvement in the self-sealing capability of concrete [12–14]. CAs are hydrophilic materials by nature, and they can be added while mixing concrete or combined with cementing materials and used as surface coatings. These materials generate pore-blocking deposits resisting water penetration, yet with breathable properties [13,15–17]. Furthermore, the reaction can also undergo a delayed activation whenever the material comes back into contact with water and/or environment moisture, which enhances the self-healing of concrete at later ages [18]. Yet, their behaviour under critical development of physicochemical distress mechanisms such as ASR is quite unknown. Thus, this research aims to appraise the ability of self-healing coating mixtures to mitigate (i.e., physically, chemically, or both) concrete deterioration caused by ASR in its initial, moderate, and advanced phases. Moreover, comparisons with other systems such as silane/siloxane, rigid coating and lithium-based are also performed, and the efficiency of those different systems to mitigate ASR is evaluated.

9.2 Background

ASR *microscopic/macroscopic* distress degree and features depend upon the type (i.e., fine and coarse aggregate) and reactivity of the aggregates used, the amount of alkalis of the concrete, temperature and relative humidity of the environment, along with the exposure and confinement (i.e., reinforcement ratio, etc.) conditions of a given structure/structural member. Moreover, three conditions are simultaneously necessary for the development of ASR in concrete: the presence of reactive aggregates, high alkalis concentration, and high humidity conditions [2].

It is worth reinforcing that once ASR starts in the field, there is no consensus about different solutions that should be applied in various cases, and each situation should be evaluated as "unique". Thus, multiple types of treatments, primarily aiming to "physically" stop/reduce the ingress of moisture and/or to provide confinement of the affected members (e.g., silane/siloxane water repellents, coatings, lithium-based treatments, prestress confinement, etc.), have been tested and have shown quite promising results. However, many contradictory data were also obtained [4,6,9–11,19–26], reflecting the current lack of consensus in the area.

9.2.1 Minimizing ASR development in aging concrete

The relative humidity (RH) impacts significantly on ASR-kinetics and damage since high RH is one of the key requirements for ASR occurrence. Generally, the relative humidity should be greater than 80% to cause significant ASR development and damage in the concrete [1,8,27]. In contrast, studies demonstrated that RH lower than 60% could lessen ASR development to negligible and marginal values [8]. However, at a given alkali loading, the RH threshold is dependent on temperature and the reactive form of silica present within the aggregate [7]. Globally, water plays two crucial roles in ASR reaction: first, as transport medium of the ions involved in ASR; second, as a reactant (water is included in the amorphous gel formed). Thus, preventing the ingress of airborne moisture is critical to preventing and mitigating ASR expansion.

9.2.1.1 Limiting moisture uptake through hydrophobic impregnations treatment

Hydrophobic impregnations and coatings have been used in various forms in the construction industry to help prevent water and chloride ingress, and their benefits are well documented [28–33]. Breathable coating and sealants composed of siloxanes or silanes have shown promising results in reducing ASR-

induced expansion [34,35]. Evidences from numerous studies demonstrate that the application of silanes significantly reduces water uptake [36,37], lowering ASR-induced expansion values by 40% [4] to 60% [38]. The removal of internal moisture prevents or slows the ASR-induced expansion, and the water-repelling ability of silane prevents additional moisture from reaching the gel [9]. However, their performance is affected by surface imperfections, wetting and drying cycles, application technique and precision, surface preparation, application rates and local environmental conditions at the time of application [6]. In general, silane treatments are more effective if pre-wetting periods are lengthened [4]. Moreover, to effectively mitigate ASR-induced development, it has been demonstrated that more extended pre-curing periods will permit the formation of strong oxygen bridging bonds between silane molecules and the substrate, which provides a surface with stable hydrophobic character [38].

9.2.1.2 External strengthening of concrete to suppress ASR development

Different authors, however, have studied the influence of several external strengthening techniques to mitigate ASR development, such as fibre-reinforced polymer (FRP) sheets [19,39,40] and fibre-reinforced concrete jacketing [41,42]. Moreover, such materials could also protect concrete members against weathering conditions, recover the mechanical properties of the damaged concrete elements [19], improving compressive strength and modulus of elasticity [43–45]. Conversely, the inferior performance of external strengthening was also reported [46]. Furthermore, besides applying FRPs and fibre-reinforced concrete jacketing have demonstrated promising results in decreased ASR expansion development, these materials do not chemically modify ASR or limit moisture uptake [26].

9.2.1.3 Surface chemical treatment (lithium-based materials) to mitigate ASR development

Regarding the chemical suppression of ASR, the use of lithium salts appears as a potential technique to mitigate ASR distress in concrete [47–49]. Among the different types of lithium compounds that demonstrate a good response in modifying the reaction kinetics, lithium nitrate (i.e., $LiNO_3$) stands out for good solubility. In addition, it slightly alters the pH of concrete pore solution [48,50]. The exact nature of the role of lithium ions in controlling ASR is still not clearly understood, yet different mechanisms have been proposed, including (1) formation of a physical barrier by insoluble silicon–lithium (Si–Li) reaction products [48,51], (2) formation of less expansive Si–Li reaction products, Li–

Ca–Na–Si gel [48,51]; and (3) increased chemical stability of reactive silica exposed to pore solution [48,50,52]. However, the efficiency of lithium salts to suppress ASR is somewhat limited to their addition during the concrete mixture. Thus, contradictory results have been found in the literature once Li products are applied to aging concrete [48,51,53]. The key factor of the high variability in the results is the overall application procedure. In that regard, the US Federal Highway Administration manual suggests three different methods: 1) Sprinkling on the concrete surface, 2) Applying 40V voltage [54], and 3) Vacuum injection [55]. Nevertheless, the penetration depth of the lithium ions is limited to the first layers of the concrete, reaching depths of 5 mm to 50 mm, which significantly limits their effectiveness; thus, poor results can be found in the literature [54,56–58].

Overall, once ASR starts in the field, there is no efficient solution to fully mitigate the residual expansion and damage. However, it is somewhat clear that limiting moisture uptake demonstrates better results to modify the reaction kinetics. Furthermore, in the past decades, it has been verified that some crystalline waterproofing coating materials can provide concrete with interesting self-healing properties besides waterproofing, which may present an interesting "physical" solution for durability-related distress in concrete [59–61].

9.2.2 **Cement-based crystalline waterproofing (CCW) coatings**

Over the past decade, researchers have studied the benefits of adding crystalline admixtures (CAs) in cement-based systems, either internally or externally combined with cementitious coating material [13,16,62,63]. Regardless of their application, crystalline materials are permeability-reducing admixtures with a hydrophilic nature that reacts easily with water and can effectively serve as self-healing engineered admixtures [15]. The active ingredients from CCW coatings can penetrate the cement matrix and react with hydration products to form crystalline or gelatinous substances that fill the capillary pores and micro-cracks [59]. It has been found that the healing products formed in the cracks display large calcium carbonate and ettringite contents, although C-S-H gel was also found [59,64]. Studies suggest that the penetration depths of CCW can reach values between 33–80 mm, decreasing gas permeability values 11 times lower [59], lessening in 70% the water absorption [65] and at least 90 % chloride ions penetration [66], improve the resistance to freeze-thaw damage in about 50% [67]. However, these values seem to depend on the microstructure of the treated concrete and the number of coarse aggregates close to the surface [66,67]. Finally, it can be addressed that there are no current studies indicating the efficiency of CCW coatings to prevent/mitigate ASR-affected concrete,

particularly its influence in different phases of ASR development (i.e., initial, moderate and advanced), leaving room for major developments in this area.

9.3 Scope of the work

As stated above, several techniques have been used in the past, aiming to prevent and/or mitigate the development of ASR in the field. However, there is very few research (if any) linking the effectiveness of sealers and coating materials with the previous damage degree of the ASR-affected concrete. Moreover, recent research programs have introduced new coating products in the market aiming to produce waterproofing concrete structures with enhanced self-healing ability. The current research aims to evaluate different surface treatments and techniques (i.e., water repellent, external strengthening, lithium-based products, crystalline waterproofing coatings, etc.) to stop and/or mitigate further ASR-induced development in its initial, moderate, and advanced phases. In order to achieve the above objective, specimens were manufactures in the laboratory incorporating two types/nature of reactive aggregates (i.e., Greywacke coarse and Polymictic fine) and maintained under conditions enabling the development of ASR in the laboratory. At selected "unrestrained" expansion levels (i.e., 0.00%, 0.05%, 0.12%, 0.20%, and 0.30%) first, the mechanical properties and the microscopic features of the concrete mixtures were assessed, then different surface treatments and techniques were applied. Finally, the influence of the distinct surface treatments on the residual expansion and deterioration due to ASR were monitored (i.e., mechanically and microscopically) over 24 months conditioned at 38 ^{o}C and 100% of RH.

9.4 Experimental program

9.4.1 Materials for concrete production

A conventional Portland cement (GU type, equivalent to ASTM Type I) and two different reactive aggregate types/natures were selected for this study to manufacture two 35 MPa concrete mixtures (i.e., one per reactive aggregate type). The coarse aggregates ranged from 5 to 20 mm in size. Non-reactive fine (NF) and coarse (NC) aggregates were combined with the reactive aggregate materials for concrete manufacturing. Table 9.1 provides information on the different aggregates used in this study, and the chemical and physical properties of the selected binder materials are provided in Table 9.2.

Table 9.1: Reactive (ASR) and non-reactive (NR) aggregates used in the research.

Aggregate		Reactivity	Rock Type	Specific gravity	Absorption (%)	AMBT[a] (%)
Coarse	SPH	ASR	Greywacke	2.71	0.70	0.33
	LC	NR	Crushed limestone	2.78	0.42	0.02
Fine	TX	ASR	Polymictic sand	2.60	0.89	0.81
	NF	NR	Natural derived from granite	2.60	0.82	0.08

[a)] Results at 14 days of curing of the AMBT (ASTM C 1260) carried out on the aggregates selected

Table 9.2: Chemical composition of the binder materials.

Chemical Composition	Cement	Mineralogical Phases	
SiO_2 (%)	20.10	C_3S (%)	43.24
Al_2O_3 (%)	5.03	C_2S (%)	25.02
CaO (%)	61.93	C_3A (%)	6.90
Fe_2O_3 (%)	3.80	C_4AF (%)	11.56
SO_3 (%)	3.38		
MgO (%)	2.42		
Na_2O_{eq} (%)	0.91		
LOI (%)	2.91		

9.4.2 **Mix-proportions and manufacture of the concrete specimens**

A total of one thousand, three hundred and twenty concrete specimens (sixty samples per each of the twenty-two groups of surface treatment), 100 by 200 mm in size, were investigated in this study. Table 9.3 summarizes the concrete mix designs employed in this work. The two concrete mixtures were mix-proportioned as per ASTM C1293 to present the same water to binder ratio (w/b of 0.45) and amount of binder materials (420 kg/m^3).

Table 9.3: Concrete mix proportions.

Mixture	w/b = 0.45		Aggregates (kg/m^3)	
	Water (kg/m^3)	Cement (kg/m^3)	Fine	Coarse
SPH	189	420	836	938
TX	189	420	765	1020

Twenty-four hours after casting, the samples were demoulded, and small holes (5 mm in diameter by 15 mm deep) were drilled at the two flat ends of the samples, in which steel gauge studs were glued in place with a fast-setting cement slurry for longitudinal expansion measurements. Afterwards, the specimens were left to harden at 20 °C and 100% RH over 24 hours (totalizing 2 days after casting) before the zero reading was taken. Next, one hundred and thirty-two specimens per mixture were randomly selected and separated for surface treatment and application of coating materials, as described in the following section. The remaining samples were finally placed in sealed plastic buckets lined with a damp cloth and stored at 38 °C and 100% RH. The specimens were monitored for length variations until they reached different expansion levels (i.e., 0.05%, 0.12%, 0.20% and 0.30%). As per

ASTM C1293, the buckets were cooled down to 23 °C for 16 ± 4 h before the periodic measurements. Then, when the cylinders reached the specified expansion levels, they were taken for surface treatment and further application of coating materials.

9.4.3 **Surface treatment and coating materials**

It is worth noting that the application of coated materials requires a surface treatment of concrete for better adherence and achieve better performance. The overall surface treatment used in this study can be divided into three main steps: a) surface preparation, b) drying the specimens, c) coating application. The first two were implemented on all specimens, even for control specimens in which any coating material was applied. The third was determined accordingly with the specification of each material used. After achieving the pre-determined expansion levels, i.e., 0.00%, 0.05%, 0.12%, 0.20% and 0.30%, twelve specimens per group of coating materials (Table 9.4) and for each concrete mixture were taken and fully wrapped with sponges saturated with a low acid solution (98% of distilled water and 2% of acetic acid) for 24 hours at 12 ^{o}C. It is worth mentioning that to avoid further evaporation and changes in acid concentration, the covered specimens were also wrapped in plastic film and placed in sealed buckets. Next, the specimens were unwrapped, and the surface was gently scrubbed with a wire bristle brush to increase rugosity and enhance the adherence of the coating materials, then cleaned with a nylon brush and water (Figure 9.1). Afterwards, the samples were placed at 12 ^{o}C, and 60% RH yet kept unwrapped out of the sealed buckets for 120 hours. The coating mixtures Sil, CA and PCB were applied following each specification of the commercially available materials and following what is used in field applications. Moreover, the combined/modified formulas developed in this research (i.e., CA+Fib, CA+Sil, CACBS, CALTM, CAWRP and CANS) followed the original formula's recommendation Crystalline Surface Waterproofing (CA). It is worth noting that just before applying the coating materials, clear water was gently spayed at the surface of the concrete specimens to achieve better adherence. The only exception was the Sp LTM mixture, in which $LiNO_3$ solution was sprayed ten times on the concrete surface. Finally, the specimens were placed back within sealed buckets and left for 14 days at 12 ^{o}C and 60% RH for hardening purposes and to provides a surface with stable hydrophobic character. Afterwards, the specimens were stored at 38 °C and 100% RH. As per ASTM C1293, the buckets were cooled down to 23 °C for 16 ± 4 h prior to the periodic length measurements (i.e., 45, 90, 180, 360, and 720 days). Moreover, mechanical and microscopical tests were performed at 360 and 720 days as per the following section.

Table 9.4: Coating mixtures applied on the treated surface of the concrete specimens.

Group	"Coating" Material	Modification
Control	Any	Any
Sp LTM	Sprayed Lithium (LiNO3 solution)	Any
Sil	High-performance penetrating silane/siloxane	Any
CA	Crystalline Surface Waterproofing	Any
PCB	Polymer-Modified Cement-Based Compound	Any
CA + Fib[a)]	Crystalline Surface Waterproofing	Addition of Acrylic fibers
CA + Sil[b)]		High-performance penetrating silane/siloxane
CACBS		Cementitious based materials
CALTM[c)]		CA mixed with LiNO3
CAWRP		Powder water repellent
CANS		Nano silica

[a)] Acrylic fibres were added to the original powder of CA (0.25%, by mass of CA)
[b)] After the conventional application of CA, high-performance penetrating silane/siloxane was further applied to the surface of the specimens.
[c)] Instead of using pure water in the CA mixture, LiNO3 solution was used to mix CA

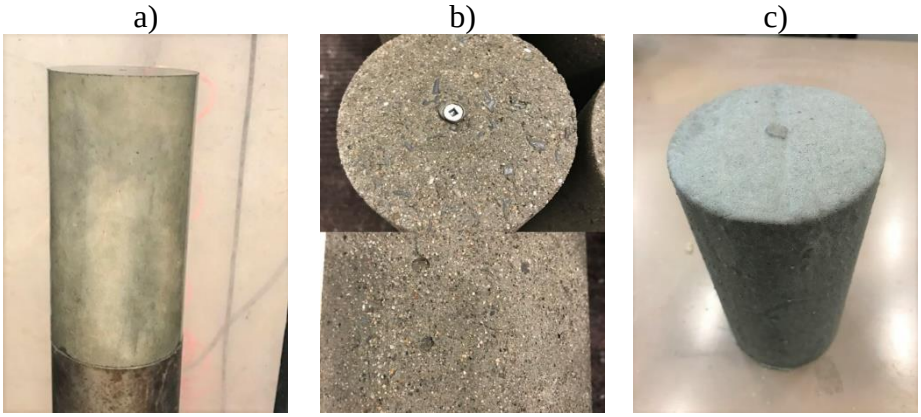

Figure 9.1: Illustration of the different concrete surface profiles: a) before surface treatment, b) after surface treatment, and c) after applying the coating material.

9.4.4 Assessment of the ASR development in the concrete

9.4.4.1 Damage Rating Index (DRI)

A semi-quantitative petrographic analysis, using the DRI, was performed on one specimen from each concrete mixture at the specific expansion levels, according to the method described by Sanchez et al. [68,69]. The samples were cut in half axially, polished by a hand polishing device, which uses diamond-impregnated rubber disks (n°. 50-coarse, 100, 400, 800, 1500 to 3000-very fine), and 1cm^2 grids were drawn on the surface of the polished sections. Then a stereomicroscope (16× magnification)

was used to perform the test. The DRI final number presented hereafter is the normalized 100 cm^2 value.

9.4.4.2 Compressive Strength

Compressive strength was measured through two different approaches with different and specific goals. First, to characterize all mixtures at 28 days compressive strength, samples were wrapped just after demoulding and placed at 12 °C, since some of the specimens contained highly reactive aggregates and ASTM C39 method could not be followed as they could develop some ASR. The cylinders were maintained at 12 °C for 47 days, according to the maturity concept as by ASTM C 1074. Second, the compressive strength measurements were carried out on two specimens from each concrete mixture after being subjected to SDT (explained below) to verify the compressive strength loss of the material as ASR develops. This procedure was adopted and considered valid after Sanchez et al. [69,70] confirmed the largely non-destructive character of the SDT.

9.4.4.3 Stiffness Damage Test (SDT)

The SDT procedure was performed following Sanchez et al. publications [70–73], i.e. using five loading/unloading cycles at a controlled loading rate of 0.10MPa/s with a maximum load corresponding to 40% of the 180-days compressive strength. In addition, it is worth mentioning that the 180 days compressive strength of the sound concrete was obtained following the maturity concepts as per ASTM C1074. Finally, the test was conducted, and the results obtained are an average value from three different specimens tested at each curing period.

9.4.4.4 Direct Shear Test

The direct shear test was performed according to the method and setup proposed by Barr and Hasso [74] and adapted for damaged concrete as per De Souza et al. [75]. The same approach considering the maturity concept was used to characterize the “zero” reading for all concrete mixtures at equivalent 28-days. After the specimens achieved the expected exposure periods (i.e., 360 and 720 days), three samples from each concrete mixture were selected. However, the stiffness damage test was not performed on the samples previous to the direct shear test differently from CS. Before testing, all samples were carefully ground so that a circumferential notch was created [74,75]. The notch depth

was adopted as about 20 mm ± 3 mm to ensure a shear-type failure without leaving a too-small area of the sample to be tested.

9.5 **Results**

9.5.1 **ASR Kinetics**

This section presents ASR expansion kinetics and amplitude results for all mixtures developed in the laboratory. Figure 7.2 displays the expansion results obtained by incorporating a wide range of coating materials applied on two different concrete mixtures made of two different types/natures of reactive aggregates. Figure 7.2a illustrates the expansion progress of concrete mixtures made incorporating SPH reactive coarse aggregate and further developments after applying the different coating materials at 0.00%, 0.05%, 0.12%, 0.20% and 0.30% of expansion indicated. In comparison, Figure 7.2b displays the results with reactive TX fine. In general, the mixtures containing the reactive TX presented faster reactivity than those incorporating reactive SPH coarse aggregate. Moreover, all coated specimens developed lower expansion than the control samples for both SPH and TX; the only exception was sprayed lithium samples (Sp LTM) which demonstrate equivalent values to control SPH and TX. At 720 days of ASR development after treating the surface of the concrete cylinders, the control specimens SPH-Control and TX-Control reached, on average, 0.53% and 0.85% of expansion, respectively. However, SPH-concrete samples treated with CAWRP, CA+Fib, CA+Sil, CACBS, CALTM, PCB, CA, Sil, CANS and Sp LTM lessened, on average, the final expansion in 44%, 40%, 39%, 32%, 30%, 29%, 28%, 23%, 19% and 6%, respectively. Involving the extremely reactive TX, it was found that the “efficiency” of the surface treatments decreased in 28%, CAWRP, CA+Fib, CA+Sil, CACBS, PCB, CALTM, CA, Sil, CANS and Sp LTM achieved 40%, 34%, 34%, 28%, 18%, 17%, 12%, 12%, 11% and 2% lower values than TX-Control, respectively. It is worth highlighting that CAWRP displayed averagely lower expansion results for both aggregates. Moreover, combining CA and polypropylene fibres (i.e., CA+Fib) showed the lowest rate of expansion until one year, yet the higher between one and two years, especially when applied at lower expansion levels (i.e., 0.00% and 0.05%).

a)

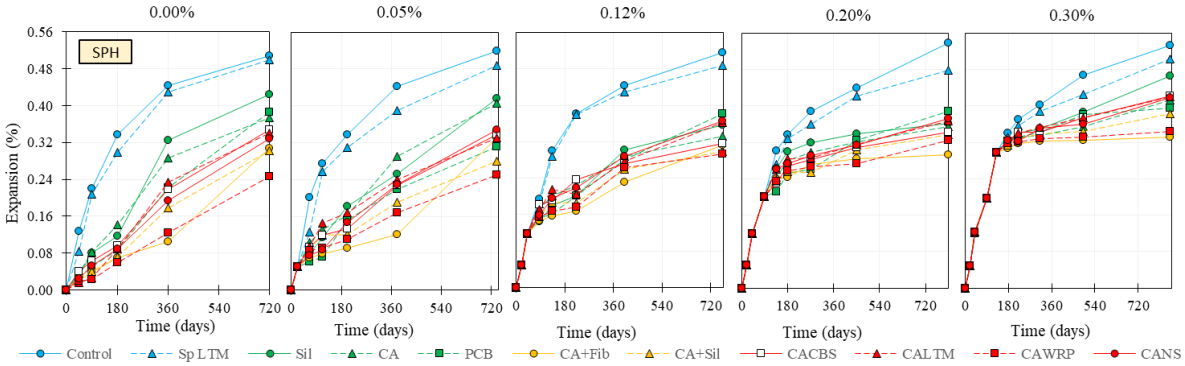

b)

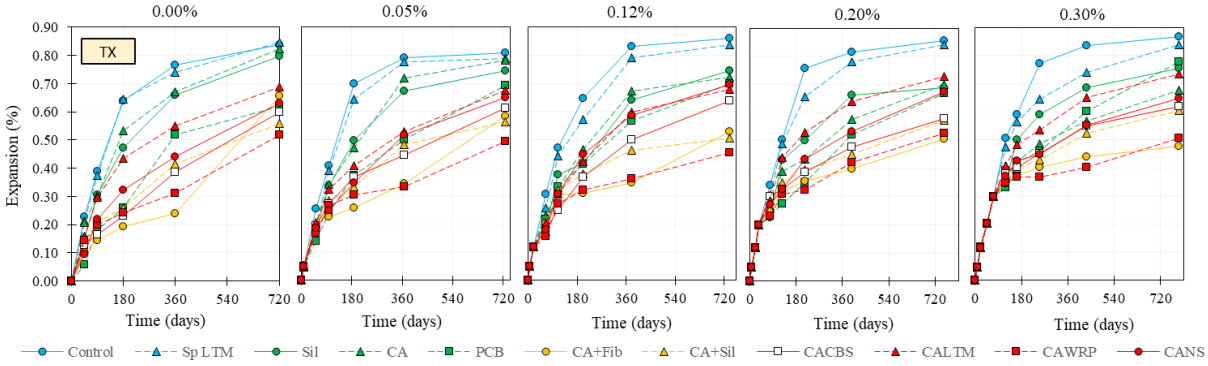

Figure 9.2: ASR-kinetics over time for the different surface treatments applied at 0.00%, 0.05%, 0.12%, 0.20% and 0.30% of expansion for: a) SPH-concrete specimens, and b) TX-concrete specimens.

9.5.2 **Damage rating index (DRI)**

Figure 7.3 gives the plots with the total DRI numbers obtained from the ASR-affected concrete specimens. Globally, it is possible to observe that all DRI numbers obtained increase as a function of the specimens' expansions. Moreover, at equivalent expansion levels, the overall behaviour of the mixtures made with different aggregates is somewhat similar, although TX mixtures reached higher values. Greater DRI numbers were found in control specimens, i.e., 1200 for SPH-Control at 0.54% of expansion and 1199 for TX-Control at 0.86% of expansion. However, besides CA+Fib treatment decreased ASR expansion along two years of exposure, the mixture increases DRI numbers when applied at lower expansion levels (i.e., 0.00%, 0.05%, and 0.12%), which agreed with the mechanical tests data.

a)

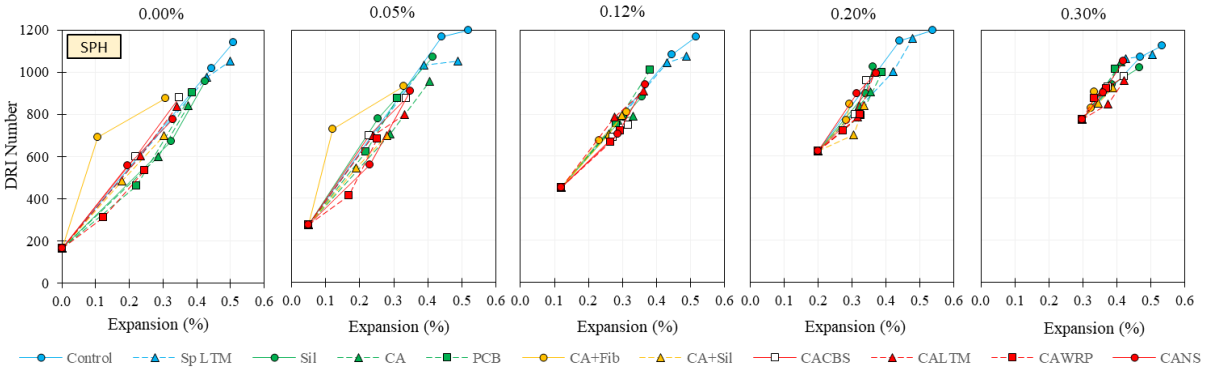

b)

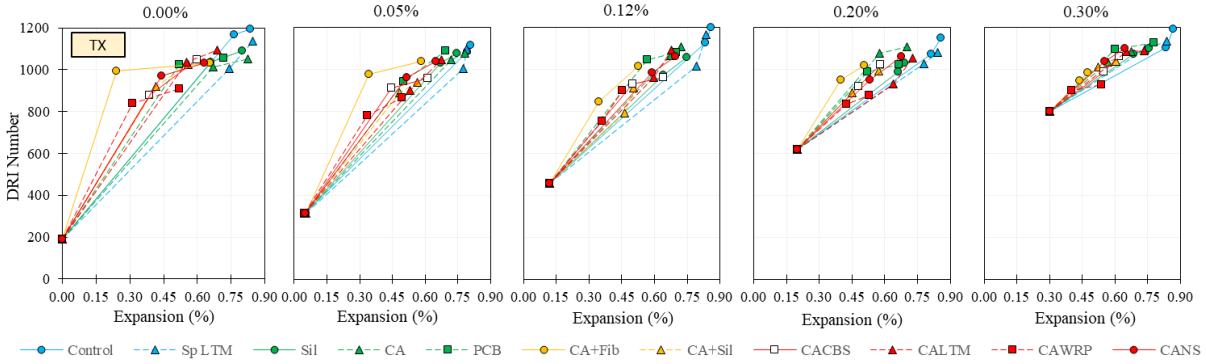

Figure 9.3: Damage Rating Index vs. expansion levels: a) for the different aggregates and b) for mixtures incorporating different types of SCMs.

9.5.3 **Mechanical properties assessment**

This section evaluates the stiffness damage index (SDI) and the losses in modulus of elasticity (ME), direct shear strength (DSS) and compressive strength (CS) of the various concrete mixtures investigated. The mechanical data (ME, DSS and CS) presented hereafter displays the ratio of values obtained from an ASR-induced expansion at the pre-determined expansion levels (i.e., 0.00%, 0.05%, 0.12%, 0.20% and 0.30%) and after 360 and 720 days of exposure over the values gathered on sound concrete specimens presenting “equivalent maturity” than the damaged samples as previously discussed in 0. Moreover, one may notice that the mentioned mechanical ratios are displayed in the function of their respective expansion amplitudes to better visualize the possible mitigative behaviour of the coating treatments after.

9.5.3.1 **Compressive strength (CS)**

Figure 7.4a and b (SPH and TX concrete mixtures, respectively) illustrate the compressive strength reductions for the different coating mixtures investigated. In general, compressive strength (CS) was found to decrease somewhat modestly compared to the other mechanical properties tested, yet the higher the expansion level, the higher the CS loss. For instance, the lowest CS loss found after applying the coating materials on the surface of the concrete specimens was 0.06 at 0.12% of expansion for the SPH-CAWRP mixture, one year after applying the material at 0.00% of expansion. On the other hand, SPH-control reached CS loss of 0.35 at 0.54% of expansion, the highest among SPH-concrete specimens. Overall, TX-concrete attained higher expansion values; thus, the losses in CS were proportionally higher than SPH mixtures. The CS loss of TX-control was found to range from 0.11 at 0.05% of expansion to 0.45 at 0.86% of expansion, the higher value among all specimens studied. Moreover, for SPH or TX reactive aggregate, the different surface treatments displayed similar CS loss behaviour. The only exception was CA-Fib mixtures, which demonstrated the higher losses once applied at lower expansion levels (i.e., 0.00%, 0.05% and 0.12%), whereas equivalent to lower losses when applied at higher expansion levels (i.e., 0.20% and 0.30%).

a)

b)

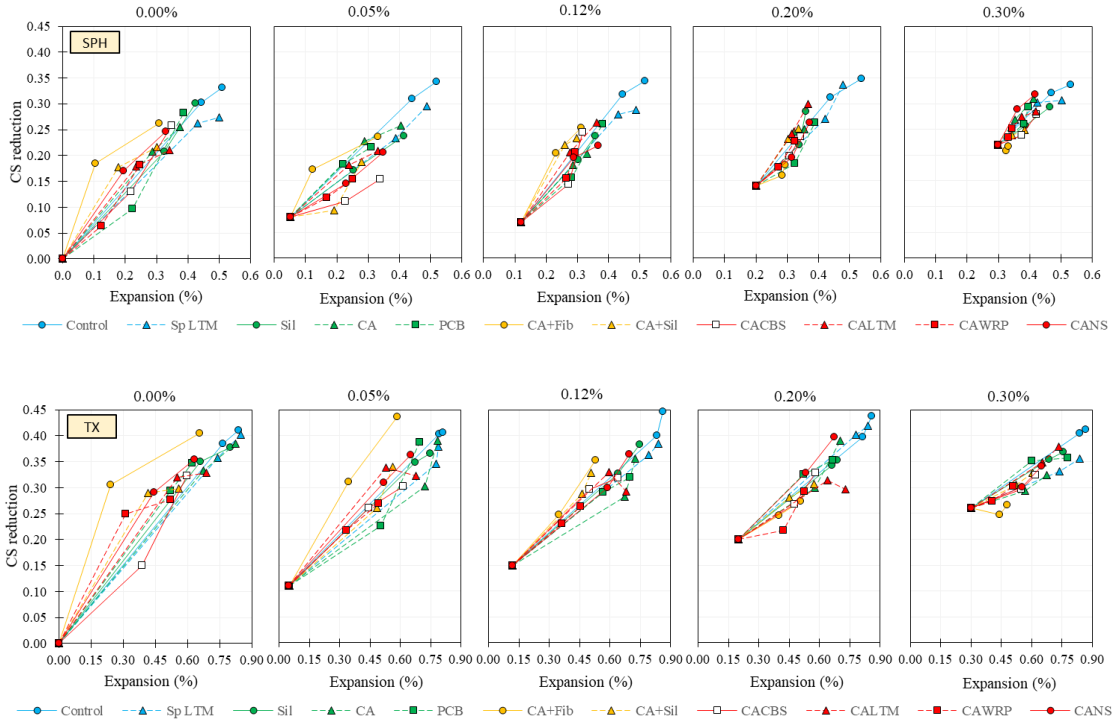

Figure 9.4: Compressive strength reduction vs. expansion levels: a) SPH coarse aggregate mixtures and b) TX fine aggregate mixtures.

9.5.3.2 **Stiffness damage index (SDI)**

Figure 7.5 illustrates the SDI values for the different concrete mixtures and surface treatments investigated, in a) incorporating the SPH reactive coarse aggregate, whereas in b) the TX fine aggregate. By combining various reactive aggregates and different surface treatments, SDI was found to range from about 0.09 (SPH-Control) at 0.00% of expansion to 0.39 (SPH-Control) at 0.53% for SPH mixtures, and from about 0.10 (TX-Control) at 0.00% to 0.45 (TX-Control) at 0.87% for TX. Furthermore, besides SHP-CA3 and SPH-CA4 showed closer behaviour than the Control specimens, the mixtures containing SCMs, chemical admixtures or both, displayed overall lower SDI values than Control specimens for similar expansion levels (20.2% lower SDI for SPH mixtures and 13.4% for TX). Overall, SDI values increased towards ASR development for all mixtures; moreover, the higher the expansion amplitudes, the higher the SDI. Thus, once the different materials applied could change ASR-kinetics, SDI values followed the same trend. Yet, CA+Fib specimens displayed somewhat higher SDI values than all groups of samples, especially when applied at 0.00%, 0.05% and 0.12% of expansion.

a)

b)

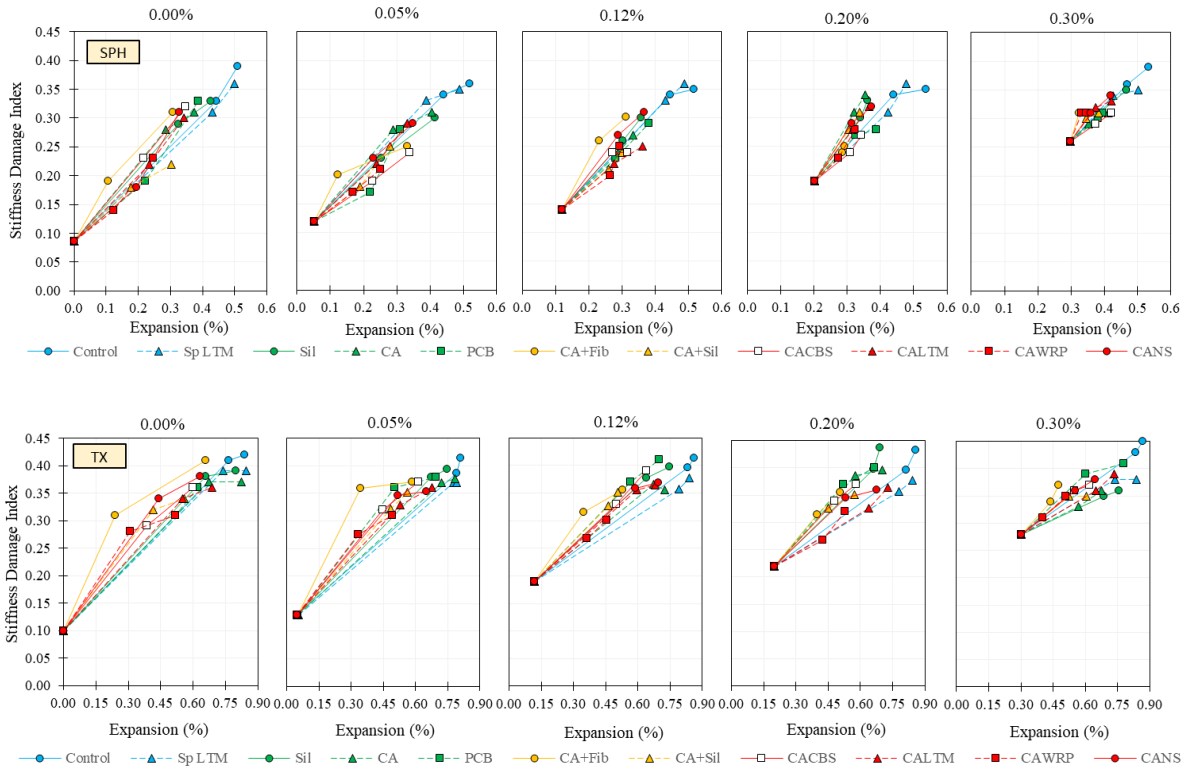

Figure 9.5: Stiffness Damage Index vs. expansion levels: a) SPH coarse aggregate mixtures and b) TX fine aggregate mixtures.

9.5.3.3 **Modulus of Elasticity (ME)**

The modulus of elasticity (ME) results of the affected samples are displayed in Figure 7.6a (SPH mixtures) and Figure 7.6b (TX mixtures). Globally, TX mixtures reached higher ME losses once these mixtures achieved higher expansion levels. The maximum losses measured for SPH-made mixtures were 0.65 for Control specimens at 0.53% of expansion, while for TX, the maximum loss was 0.70 at 0.73% of expansion for CALTM (applied at 0.30%) specimens. In general, at equivalent expansion levels, regardless of the concrete mixtures or surface treatment, the loss in ME was somewhat higher for SPH-made concrete. Moreover, CA-Fib displayed significantly higher ME loss at equivalent expansion levels than the other mixtures.

a)

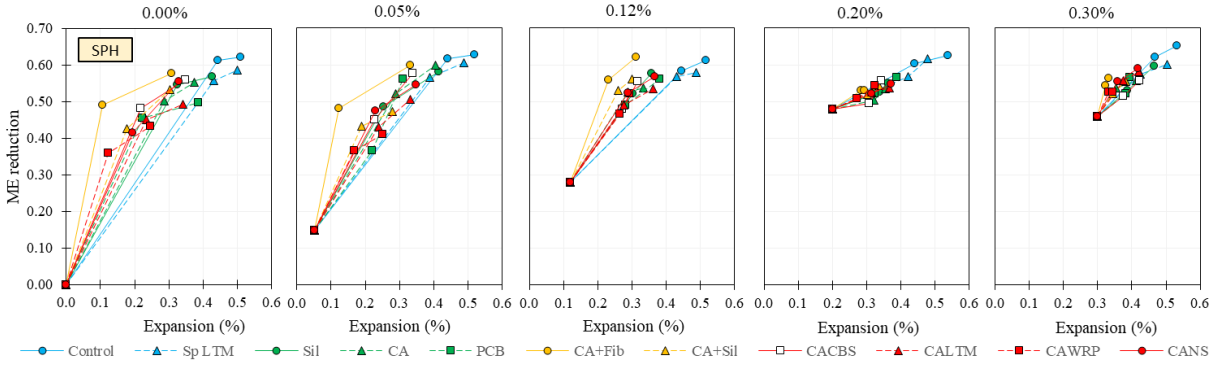

b)

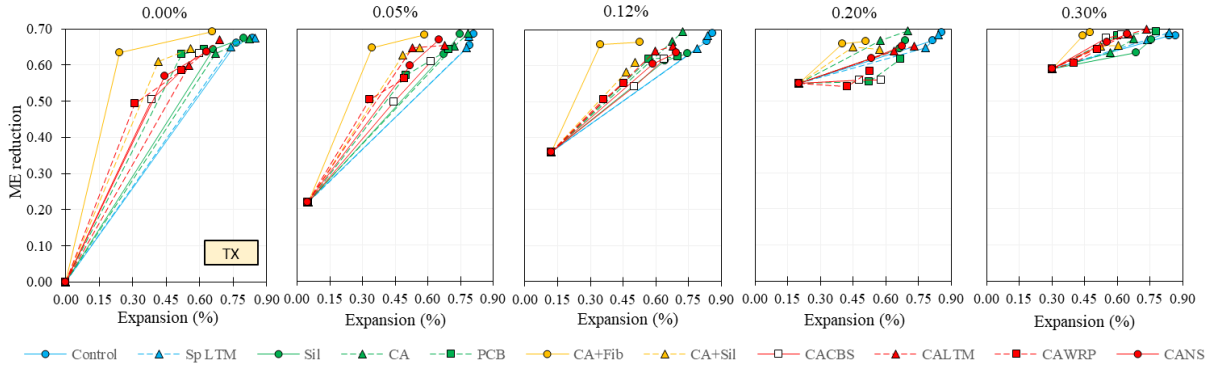

Figure 9.6: Modulus of Elasticity reduction vs. expansion levels: a) SPH coarse aggregate mixtures and b) TX fine aggregate mixtures.

9.5.3.4 **Direct shear strength (DSS)**

The direct shear strength (DSS) results of the affected samples are illustrated in Figure 7.7a (SPH mixtures) and Figure 7.7b (TX mixtures). All mixtures present a shear strength decrease as a function

of ASR-induced expansion; one may notice that the higher the expansion level, the higher the DSS reduction. However, at equivalent expansion levels, samples made of SPH aggregate showed slightly higher DSS loss. Besides a few exceptions, the overall behaviour of the surface-treated samples was quite similar. Shear strength loss ranged from 0.23 at 0.05% of expansion to 0.60 at 0.57% of expansion for SPH-Control specimens and from 0.19 at 0.05% of expansion for TX-control to 0.64 at 0.64% of expansion for TX-CA+Fib coating applied at 0.00%. Moreover, TX-CA+Fib also achieved a DSS loss of 0.64 at 0.35% for application at 0.12%. Globally, the CA+Fib mixture trend to display higher DSS losses for both aggregates at compared expansion levels than other mixtures. Finally, it is worth mentioning that SPH-CAWRP, SPH-CALTM and SPH-CANS applied at 0.20%. Also, SPH-CA applied at 0.30% showed a small decrease in DSS loss, which could indicate a "regain" of shear strength, yet it can be a result of the variation of the test once those trends were not constant.

a)

b)

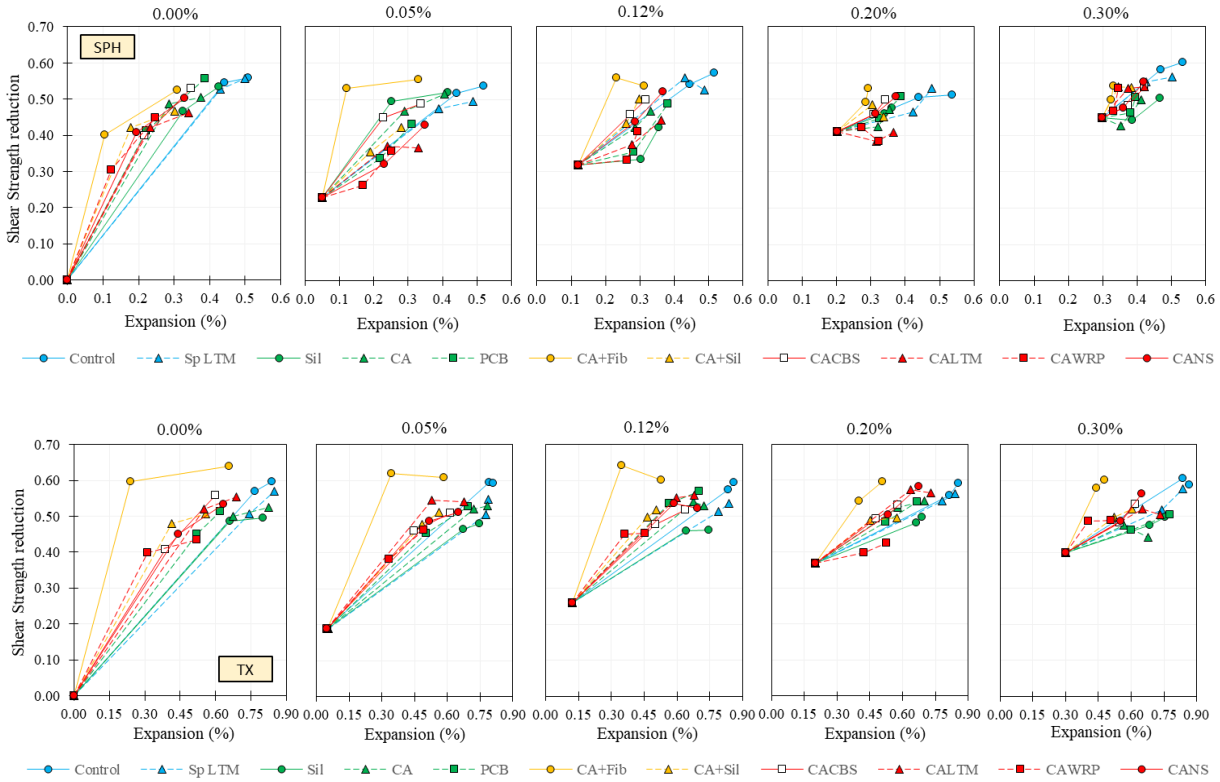

Figure 9.7: Shear strength reduction vs. expansion levels: a) SPH coarse aggregate mixtures and b) TX fine aggregate mixtures.

9.6 Discussions

9.6.1 ASR kinetics development

The results demonstrated that concrete mixtures made of TX fine aggregate presented faster ASR kinetics (i.e., 2.35 times faster, on average, to achieve 0.05%, 0.12%, 0.20%, and 0.30% of expansion). This behaviour is likely linked to TX's general lower particle size, which increases the surface contact area between the reactive particles and the alkali solution. Moreover, the ultimate expansion gathered by TX-Control specimens was 1.63 times higher than SPH-Control samples (i.e., 0.85% and 0.52%, respectively) after the evaluation period. Overall, the application of coating and sealers on the surface of the concrete specimens showed promising evidence that, besides the different materials displayed high expansion values after 720 days of exposure, they significantly modify ASR-kinetics. Moreover, the efficiency of the employed materials likely changes over the selected deterioration degree in which they were applied (i.e., 0.00%, 0.05%, 0.12%, 0.20%, and 0.30%). Globally, it was observed that the higher ASR damage degree before the application of the surface treatments, the higher their respective efficiency in decrease the “residual” expansion amplitudes. Figure 6.8a (for concrete made of SPH) and Figure 6.8b (for concrete made of TX) were developed to better visualize this trend. One verifies that the efficiency displayed in the y axis was obtained from the differences in expansion at 720 days between the control specimens and each coating material. However, for applications 0.05%, 0.12%, 0.20%, and 0.30%, the initial expansion, before the treatment, was deducted: e.g., after coating the SPH-concrete with CA+Fib at 0.30% of expansion and exposure for more 720 days, the expansion measured was 0.33% (0.03% of variation), whereas SPH-control varied from 0.30% to 0.53% (0.23% of variation). Thus, the efficiency of SPH-CA+Fib was calculated as 87% (i.e., 1 - 0.03/0.23).

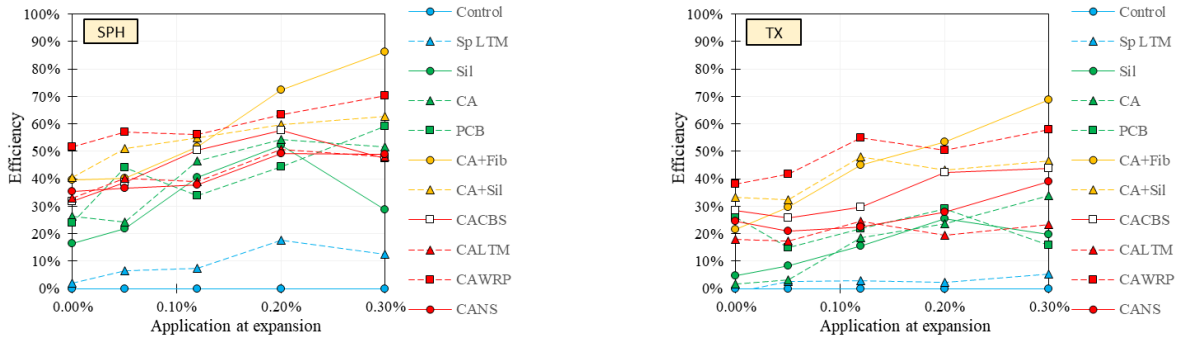

Figure 9.8: Efficiency of the coatings and sealers to mitigate ASR expansion development for a) SPH and b) TX aggregates.

Among the mixtures incorporating primary materials without mixing different products or modifying their formula (i.e., Sp LTM, Sil, CA, and PCB), Sp LTM displayed the highest expansion amplitudes, an average of 0.49% (SPH-Sp LTM) and 0.83% (TX-Sp LTM). Although lithium nitrate is a well-known admixture able to suppress ASR when added in the bulk concrete, the results were statistically similar to Control specimens (Figure 9.9) for surface application. On the other hand, Sil, CA and PCB demonstrated notable efficiency to modify ASR-kinetics, achieving expansion averages of 0.40% and 0.75% (SPH-Sil and TX-Sil), 0.38% and 0.74% (SPH-CA and TX-CA), 0.37% and 0.69% (SPH-PCB and TX-PCB). Yet, their performance significantly changed over the different "damage degrees" when they were applied. The efficiency of silane sealer in reducing ASR expansion varied from 16% (SPH-Sil at 0.00%) to 52% (SPH-Sil 0.20%). In contrast, lower numbers were obtained for TX concrete specimens, with an efficiency of 5% at 0.00% and 26% at 0.20%. Similar trends are seen for CA and PCB coatings; the efficiency of CA coating ranged from 24% at 0.05% to 54% at 0.20% for SPH-CA and from 2% at 0.00% to 34% at 0.30% for TX-CA mixtures. Likewise, for PCB coating the values ranged from 24% at 0.00% to 59% at 0.30% for SPH-CA and from 14% at 0.00% to 29% at 0.20% for TX-CA mixtures. It is worth mentioning that either TX-Sil at 0.00% or TX-CA at 0.00% and 0.05% or TX-CA displayed statistically similar results to TX-Control specimens (Figure 9.9b).

a)

b)

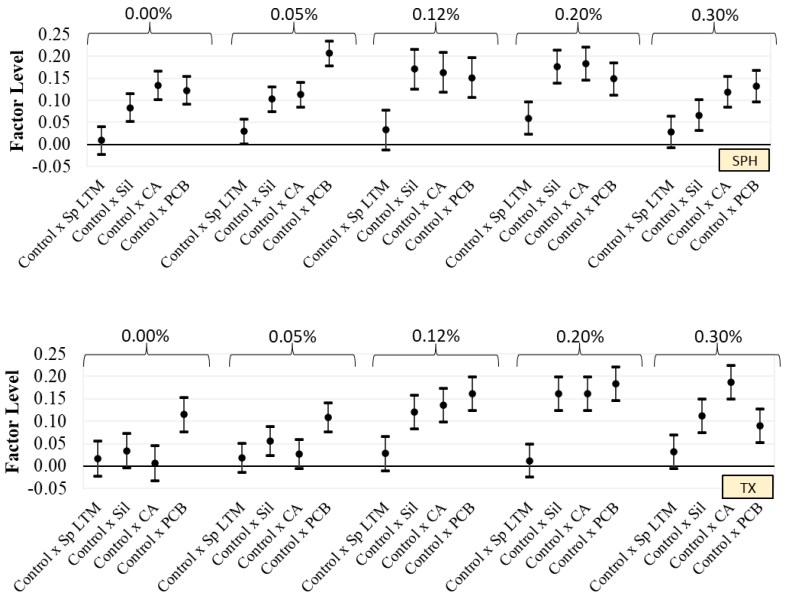

Figure 9.9: Comparative analysis (Tukey test for a significance level of 5%) between the average expansion of Control, Sp LTM, CA, and PCB mixtures for a) SPH and b) TX reactive aggregates.

The coating treatments made by combining different materials or techniques (i.e., CA+Fib and CA+Sil) achieved expansion averages of 0.32% (SPH-CA+Fib and SPH-CA+Sil), 0.55% (TX-CA+Fib), and 0.56% (TX-CA+Sil) after 720 days of exposure. Although reaching similar expansion averages, both mixtures had distinct behaviour to applications at different expansion levels. While CA+Fib efficiency ranged from 39% and 22% (for SPH and TX at 0.00%) to impressive 86% and 69% (for SPH and TX at 0.30%), the highest variation among all tested mixtures, CA+Sil ranged from 41% at 0.00% to 63% at 0.30% for SPH-concrete and from 32% at 0.05% to 48% at 0.12% for TX-concrete mixture. Moreover, it is worth highlighting that CA+Fib applied at 0.00%, 0.05%, and 0.12% for either SPH or TX, demonstrated the lowest expansion development up to 360 days of exposure. Yet, in between 360 and 720 days, the faster "kinetics", thus the higher variation in the expansion amplitudes. This interesting behaviour is likely believed to be caused by two main reasons: first, since no chemical modifications were made on CA, it is believed that the ASR-kinetics should be similar to SPH-CA and TX-CA; second, the confinement effect proportioned by the use of the fibres. Although, once the internal stresses induced by ASR development overcome the strength of the coating fibres, the coating layer starts to crack and the confinement effect decreases, consequently releasing the confined "energy" and accelerating the expansion kinetics. The combination of both waterproofing coating and breathable silane sealer (i.e., CA+Sil), on the other hand, demonstrate much more "stable" behaviour and displayed expressive performance for all applied expansion levels, moreover, showing as one of the most efficient coating materials used in this research to lessen ASR expansion amplitudes. One verifies that both CA+Fib and CA+Sil did not demonstrate statistical similarities with CA and Sil mixtures, as illustrated in the comparative analysis between the expansion averages (Tukey test for a significance level of 5%) displayed in Figure 9.10.

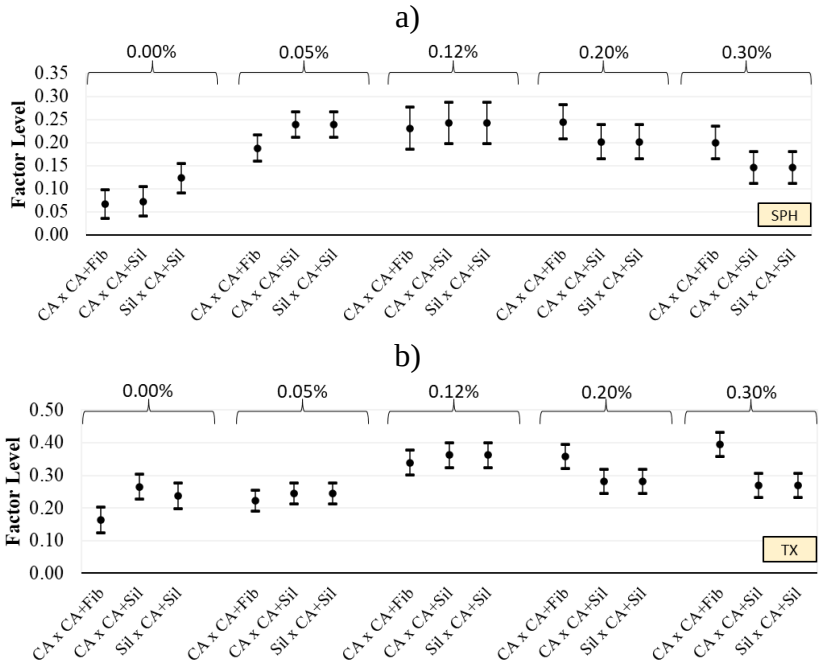

Figure 9.10: Comparative analysis (Tukey test for a significance level of 5%) between the average expansion of CA, CA+Fib, CA+Sil, and Sil mixtures for a) SPH and b) TX reactive aggregates.

The modified versions of CA coating (i.e., CALTM, CAWRP, CACBS, and CANS) reached average expansion amplitudes of 0.36% (SPH-CALTM), 0.30% (SPH-CAWRP), 0.35% (SPH-CACBS), 0.37% (SPH-CANS), 0.70% (TX-CALTM), 0.51% (TX-CAWRP), 0.61% (TX-CACBS), and 0.66% (TX-CANS). CALTM demonstrates the lower performance to mitigate ASR expansion development (i.e., 31% considering both reactive aggregates). The efficiency of CALTM ranged from 33% at 0.00% to 51% at 0.20% for concrete made of SPH and from 17% at 0.05% to 24% at 0.12% for TX-concrete. Interestingly, combining CA coating with lithium nitrate enhanced the performance of CA when applied at lower expansion levels (i.e., 0.00% and 0.05%), yet worsen values were obtained at 0.20% and 0.30%. Similar trends were observed for SPH-CANS specimens, better performance for application at lower expansion levels and worse for higher expansions compared with CA only. It is worth mentioning that the same behaviour was not observed for concrete made of TX; in this case, CANS displayed higher performance at all expansion levels of application. The efficiency of SPH-CANS to decelerate ASR expansion ranged from 35% at 0.00% to 49% at 0.20% for SPH-concrete and from 21% at 0.05% to 39% at 0.30% for TX-concrete.

The combination of CA and nano-silica developed the lower variation among the application at different damage degrees of the aging specimens, which indicate that the mixtures demonstrate

promising efficiency to delay ASR development regardless of the damage degree of the aging concrete. The results gathered with CACBS coating were slightly higher than CA for concrete made of SPH coarse aggregate (i.e., 5% higher than SPH-CA), yet for TX-concrete specimens, CACBS demonstrate efficiency 18% higher than TX-CA. The most efficient coating to mitigate ASR expansion development was CAWRP, combined effect of the crystalline admixture and the water repellency. The later displayed efficiency average of 60% (from 52% at 0.00% to 70% at 0.30%) and 49% (38% at 0.00% to 58% at 0.30%) for SPH and TX concrete mixtures, respectively. Finally, the comparative analysis between the expansion averages (Figure 9.11) indicates that modifying the CA waterproofing coating material significantly modified the results gathered. The exceptions were SPH-CALTM and SPH-CACBS, which displayed statistically similar results than SPH-CA coating at 0.00% of expansion (Figure 9.11a).

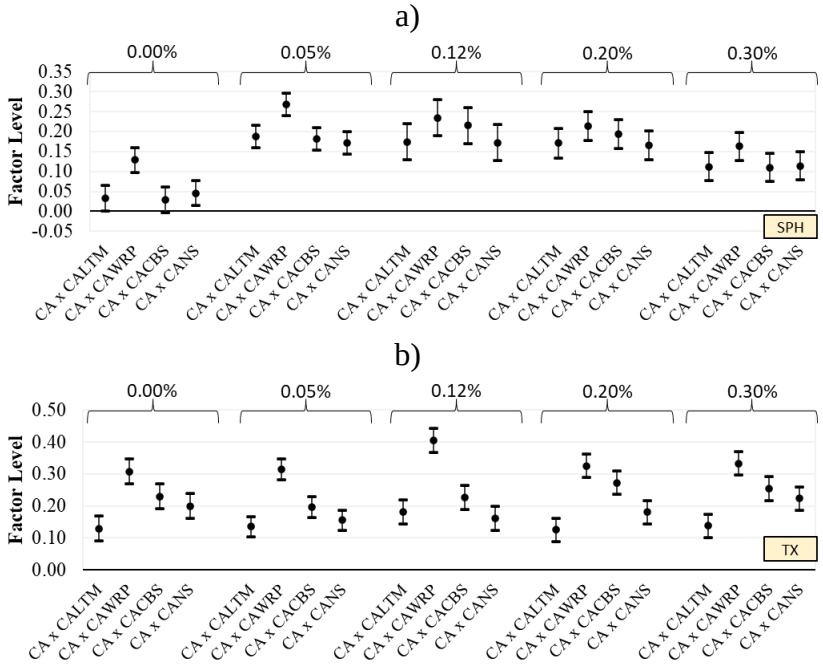

Figure 9.11: Comparative analysis (Tukey test for a significance level of 5%) between the average expansion of CA, CALTM, CAWRP, CACBS, and CANS mixtures for a) SPH and b) TX reactive aggregates.

9.6.2 **Microscopic assessment of ASR affected specimens**

Overall, the data obtained with the DRI are in agreement with the compressive and shear strength, SDI and modulus of elasticity results. ASR distress development has been widely studied and described by Sanchez et al. [76,77]. At the beginning of the physicochemical reaction (i.e., 0.05%), cracks are

formed within the aggregate particles; with the progressive development of ASR, new cracks are generated, yet pre-existing cracks keep increasing length and width, starting to extend to the cement paste at (i.e., 0.12% of expansion). At high expansion levels (i.e., 0.20%), cracks keep propagating through the aggregate particles and cement paste, likely following the "minimum energy law", they start to connect, forming a high crack networking (i.e., at 0.30% of expansion) compromising the mechanical properties of the affected concrete [76,77]. Besides minor exceptions, the global distress development noticed in the concrete specimens monitored in this research followed the model proposed by Sanchez et al. [76,77]. Moreover, the higher the expansion level displayed by the specimens, the higher the DRI number for all mixtures; yet the different kinetics of the aggregates displayed an important role in the damage features developed over the 720 days of exposure (Figure 9.12).

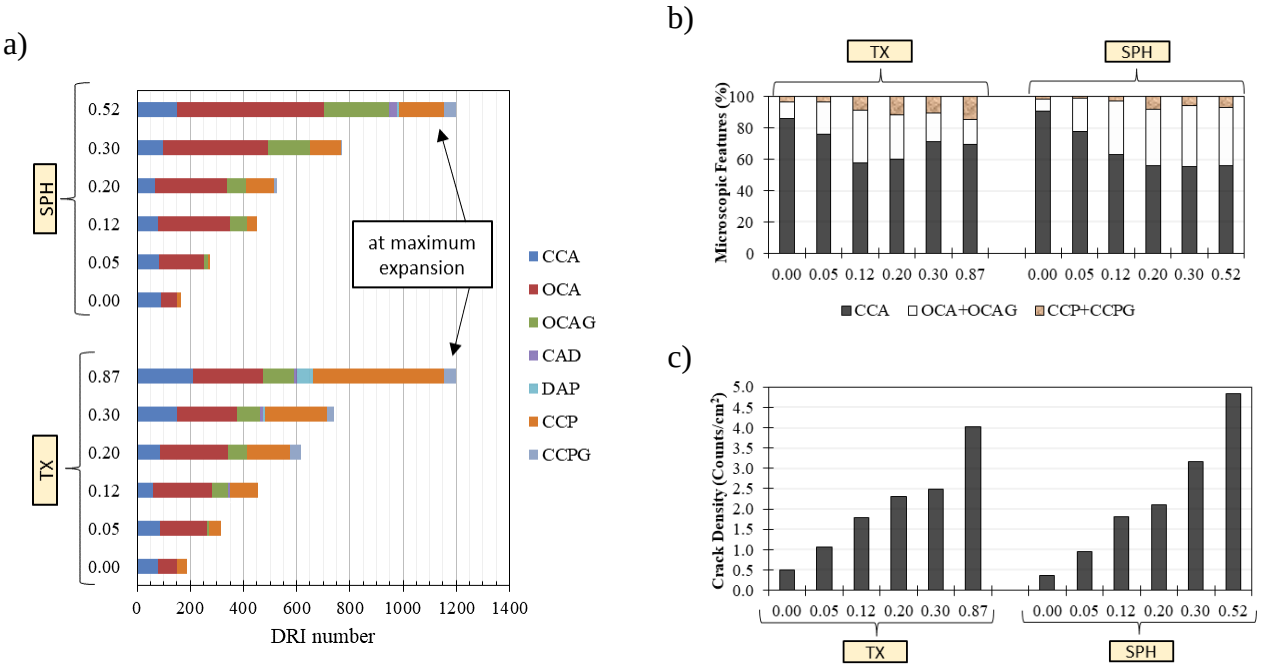

Figure 9.12: Crack development through Control mixtures incorporating SPH and TX aggregates: a) Petrographic features, b) Percentage of microscopic features (disregarding weighting factors), c) Crack density (counts/cm^2).

Concrete mixtures made by the incorporation of TX reactive fine displayed somewhat higher DRI numbers (i.e., 7.2%) than SPH-concrete specimens for the same expansion amplitudes (i.e., 0.05%, 0.12%, 0.20%, and 0.30%). In general, under examination of the polished samples at 15-16x magnification, it was found that besides the close DRI numbers and crack density between TX and SPH concrete mixtures. The petrographic features (Figure 9.12a and Figure 9.12b) reveal a faster and

more intense crack development in the cement paste for TX-made concrete. In contrast, the SPH coarse aggregate mixtures were more "concentrated" within the reactive coarse aggregate particles. Moreover, the petrographic observations revealed an increase in the proportion of closed cracks in non-reactive aggregate particles with the increase of expansion (e.g., 0.30% or higher) in either TX of SPH made concrete. However, this behaviour was clearer for TX mixtures (Figure 9.12b), in which the non-reactive limestone particles were able to even developed opened cracks through the progress of the expansion in the test specimens, increasing the percentage of CCA at 0.30% and 0.87% of expansion.

Furthermore, the crack density of the TX-concrete was 15% higher than SPH until 0.20% of expansion (Figure 9.12b), while at higher levels of expansion (i.e., 0.30% and higher), SPH specimens demonstrated 19% higher crack density than TX, which is linked to the higher formation of CCA in non-reactive particles seen at 0.30% and 0.87% of expansion, once the crack density takes into account the sum of opened cracks in the aggregate particles and cracks in the cement paste, with and without reaction products over the surface examined. The expansive ASR stresses generated by a large number of TX reactive particles likely follow the "minimum energy law", which is not only restricted to cracks formed by ASR but also through flaws or pre-existing cracks within the particles generated over crushing/weathering processes. For instance, Figure 9.13a and Figure 9.13b illustrate the crack development of the different mixtures (i.e., SPH and TX-made concrete). It is pretty interesting that the cracks initially formed within the reactive particles advanced towards the cement paste and sharply crossed through the non-reactive aggregates (heightened by the red circles). Moreover, it was noticed that concrete specimens made of TX fine displayed a significantly higher amount of ASR-gel as indicated by the yellow circle in Figure 9.13b; this was seen in most of the TX specimens, either with or without surface treatment.

a) b)

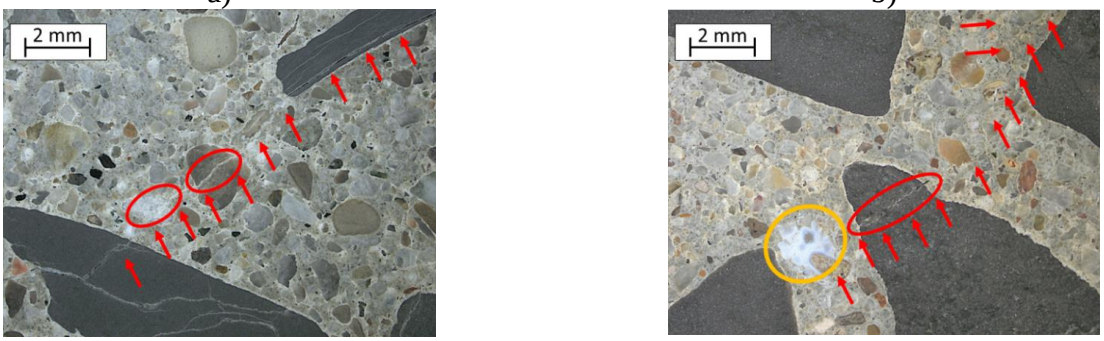

Figure 9.13: Open crack in non-reactive aggregate particles of the concrete mixtures incorporating a) Springhill coarse aggregate b) Texas sand.

The global crack development of the coated specimens follows the model proposed by Sanchez et al. [76,77] as seen for the control specimens. Moreover, the total DRI numbers and crack density were quite well linked with the expansion level of each different surface treatment. In other words, regardless of the CA+Fib treatment, the sealers and coating materials could not modify the ASR distress development mechanism. Yet, they altered ASR-kinetics slowing and delaying the overall progress of the damage. To exemplify these findings, Figure 9.14 displays the correlation between the efficiency of the coating materials to slower the increase in the total DRI number and expansion amplitudes after 720 days of exposure for both reactive aggregates (i.e., SPH and TX). The efficiency to "decrease" the total DRI number was calculated as demonstrated previously for the expansion amplitudes: i.e., the difference between control specimens and each coating and sealer treatment. Moreover, it is worth mentioning that the cracks formed previously to the coating application were deducted from the total value. Therefore, it was considered only the cracks formed after the surface treatment. The DRI values were found to increase almost linearly with increasing expansion, as observed by Sanchez et al. [76,77], therefore is quite reliable that the correlation between the efficiency to reduce DRI values and expansion follows a linear trend; in this case, the coefficient of determination found was equal to 0.92. Nevertheless, a few observations were made during the microscopic evaluation of the specimens and are addressed as follows.

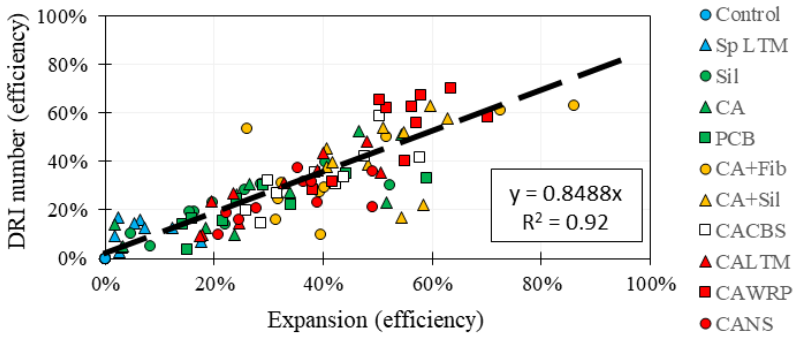

Figure 9.14: Correlation between the efficiency of the coating materials (at all applied expansions) to slow the development of the DRI number and expansion amplitudes after 720 days of exposure for both reactive aggregates.

Differently from the behaviour noticed for the expansion development, surface treated concrete specimens made of SPH coarse aggregate did not display a clear change in the efficiency to reduce the DRI numbers for application at different expansion levels (Figure 9.15a). However, except for SPH-Sp LTM and SPH-CANS, which lessened the efficiency with the increase of damage degree of the aging

concrete, the other mixtures either kept their performance constant or slightly increased it as highest the initial expansion. The only exception was CA+Fib coating which significantly enhanced the efficiency from 27.1% when applied at 0.00% to 63.2% at 0.30%. Yet, on average, SPH-CA+Fib was found to lessen the total DRI number in 46.1%, whereas SPH-CAWRP and SPH-Sil 61.8% and 54.4%, respectively, followed by CACBS (40.9%), CALTM (38.1%), CA (36.2%), CANS (31.5%), PCB (29.9%), Sil (26.7%), and Sp LTM (11.5%). For surface treated concrete specimens made of TX, besides exhibiting lower efficiency averages (i.e., 46.6%, 31.1%, 27%, 26.2%, 17.7%, 17.2%, 16.7%, 15.9%, 13.7%, and 8.8% for CAWRP, CA+Sil, CA+Fib, CACBS, CANS, Sil, CALTM, PCB, CA, and Sp LTM), all coatings and sealers demonstrated substantial increases in the efficiency to develop lower DRI number with the increase of the damage degree when coating and sealers where applied (Figure 9.15b).

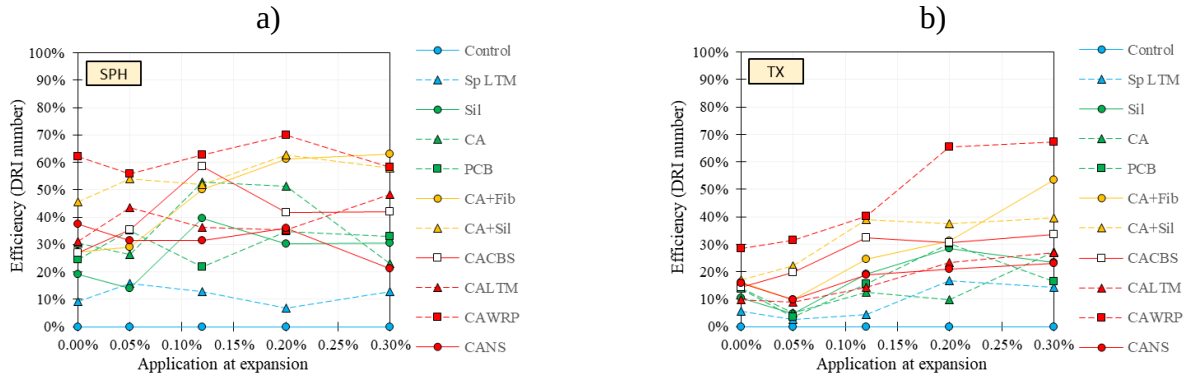

Figure 9.15: Efficiency of the coatings and sealers to mitigate the development of internal crack in concrete specimens made of a) SPH and b) TX aggregates.

The microscopic observations also revealed that although displaying similar DRI numbers, the specimens treated at lower expansion levels (i.e., 0.00% and 0.05%), developed wider OCAs than specimens treated at 0.20% and 0.30% after 720 days (Figure 9.16a and Figure 9.16b). Likewise, the specimens also displayed evidences of higher accumulation of ASR-gel in the wider cracks and pores, as indicated by the red arrows in Figure 9.16a. Although specimens with 0.20% and 0.30% of initial expansion also reveal OCAG, more spread in thinner cracks (yellow arrow in Figure 9.16b) through the polished samples. It is worth mentioning that both Figure 9.16a and Figure 9.16b were taken from SPH specimens with CANS applied at 0.05% and 0.20% and cured for 720 days, respectively. Moreover, the final expansion of both specimens was found as 0.35% (SPH-CANS at 0.05%) and 0.37% (SPH-CANS at 0.20%). Therefore, the inner damage observed during the microscopic evaluation likely contributed

to the overall deterioration found on the external samples' surface. Although not quantified, the visual inspection of the specimens indicates the lower formation of cracks on the surface of specimens coated at 0.00% and 0.05% of expansion (Figure 9.16c), yet significantly thicker than specimens coated at higher expansion levels (Figure 9.16d). Conversely to the "internal" evaluation, the latter displayed evidence of higher accumulation of ASR-gel on the external surface of the specimens, as highlighted by the red arrow in Figure 9.16d.

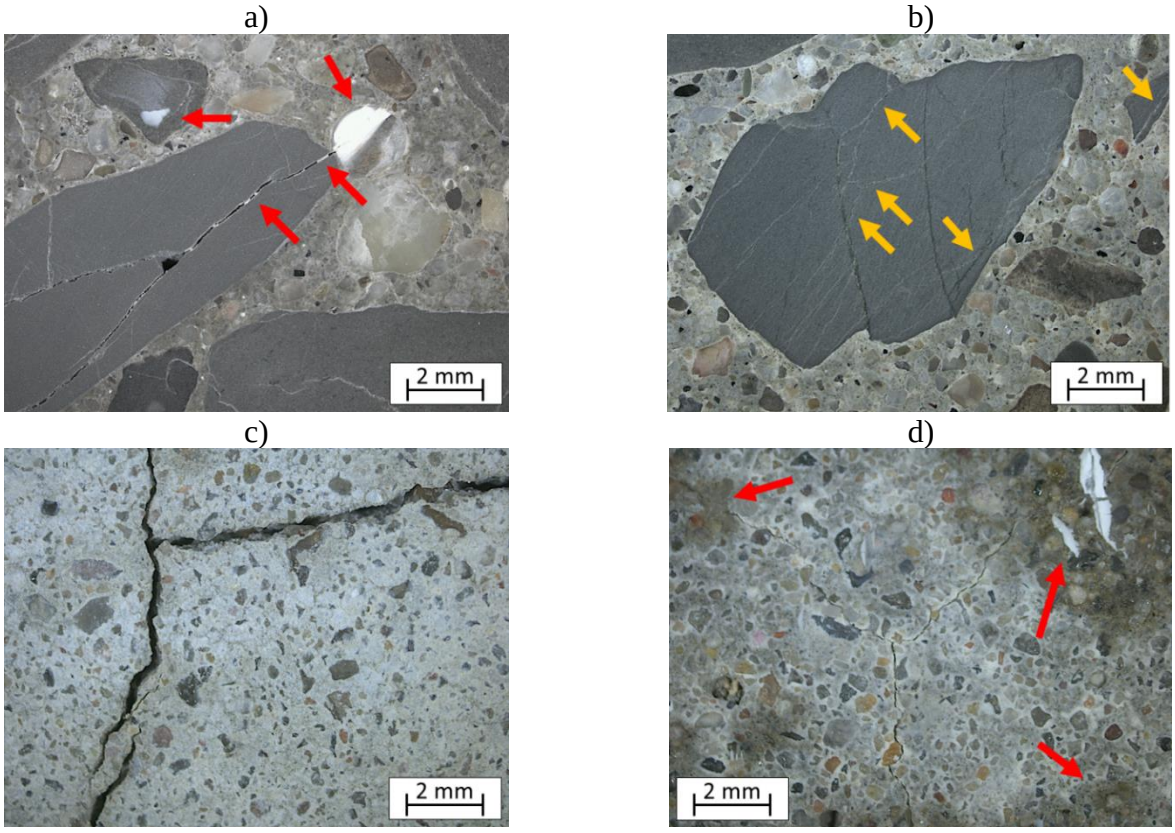

Figure 9.16: Pictures captured during the DRI analysis after 720 days of exposure: from SPH-CANS specimens applied at a) 0.05%, and b) at 0.20%; and from TX-Sil specimens applied at c) 0.05%, and d) at 0.30%.

Among the different coatings and sealers applied on the surface of the concrete specimens, CA+Fib displayed the most expressive differences in the data gathered. Although slowing the expansion development, the inner damage and crack development did not follow a similar trend. One year after the application of CA+Fib at lower expansion levels (i.e., 0.00% and 0.05%), SPH-CA-Fib specimens exhibited expansions of about 0.11%, yet the overall DRI numbers and crack density revealed greater values than SPH-control samples with high expansion levels, such as 0.20% (Figure 9.17). Moreover,

the three-dimensional confinement effect proportioned by the CA-Fib coating modified the distribution of cracks and the proportions of the microscopic features. For instance, comparing the data gathered after one year of storage for CA-Fib applied at 0.00% and 0.05% with the SPH-control at 0.12%, all specimens displayed similar expansion amplitudes. However, at 0.00% and 0.05%, CA-Fib exhibited 81.5% and 82.6% of closed cracks within the aggregate particles (CCA). In contrast, the control specimens with similar expansion displayed 63.1%, thus a significantly higher amount of OCA and OCAG. Furthermore, it is worth highlighting that after two years of exposure, both specimens (CA-Fib at 0.00% and 0.05%) showed expansion of 0.31% and 0.33%, and their microscopic features are somewhat similarly distributed as found for SPH-control 0.30%. However, the total DRI number was found to be higher. Moreover, for CA+Fib applied at 0.12%, a somewhat similar behaviour was also seen, i.e., an increase in the number of CCA after one year of exposure, followed by a decrease after two years of exposure. This behaviour is likely explained by the fact that the internal stresses induced by the ASR expansion development overcome the strength of the coating fibres, which fails (as indicated by the yellow arrows in Figure 9.18), thus releasing the confined "energy", and accelerating the expansion kinetics.

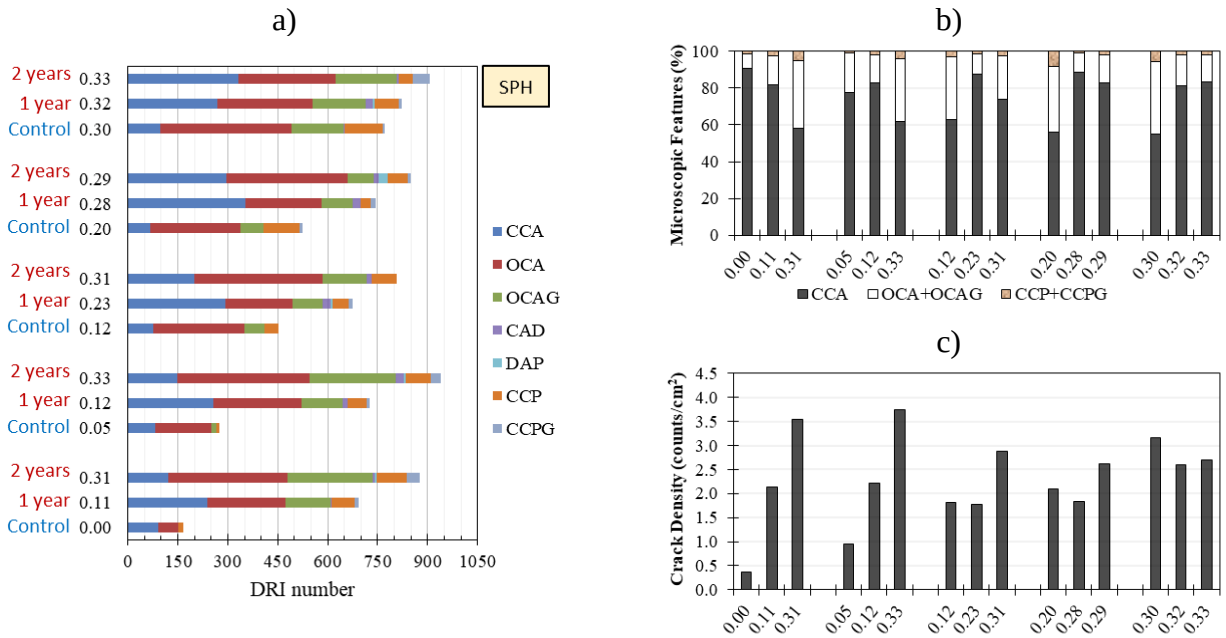

Figure 9.17: Crack development through SPH-CA+Fib mixtures: a) Petrographic features, b) Percentage of microscopic features (disregarding weighting factors), c) Crack density (counts/cm^2).

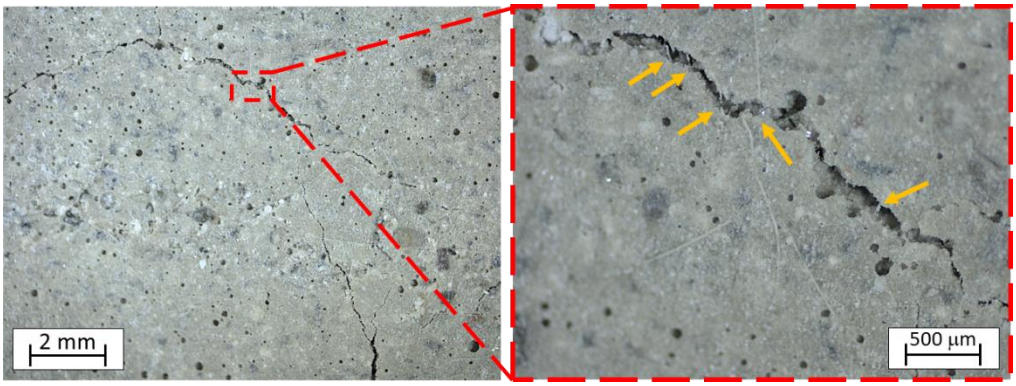

Figure 9.18: Pictures captured on the surface of an SPH-CA+Fib (720 days after application at 0.00%) with stereomicroscope at x16 and x64 magnification.

Differently from CA+Fib applied at lower expansion, at moderate (i.e., 0.12%) and higher levels (i.e., 0.20% and 0.30%), the amount of OCA and OCAG remain similar or slightly decreased after one year of exposure, whereas CCA significantly increased (Figure 9.17). These findings revealed that besides the continued ASR development and formation of new cracks, previously formed open cracks might close towards the increase in the internal stresses caused by the combination of ASR development and the confinement effect. Moreover, for CA+Fib applied at 0.20% and 0.30% expansion, even the total amount of CCP decreased, supporting the previous statement. Likewise, the microscopic analysis also revealed that the overall crack distribution pattern of the CA+Fib specimens changed, while the free expansion of the control specimens developed a much more random and distributed crack pattern, i.e., map-cracking like (Figure 9.19a and b), the specimens coated with CA+Fib displayed patterns with a higher concentration of cracks in the "external" layers of the specimen (Figure 9.19c and d). Furthermore, the cracks trend predominantly oriented parallelly to the exposed surface of the sample. Finally, it is worth noting that the heating map (Figure 9.19b and Figure 9.19d) are the DRI number of each square centimetre of the polished concrete specimens displayed in Figure 9.19a and Figure 9.19c (orientation of cracks obtained through image analysis).

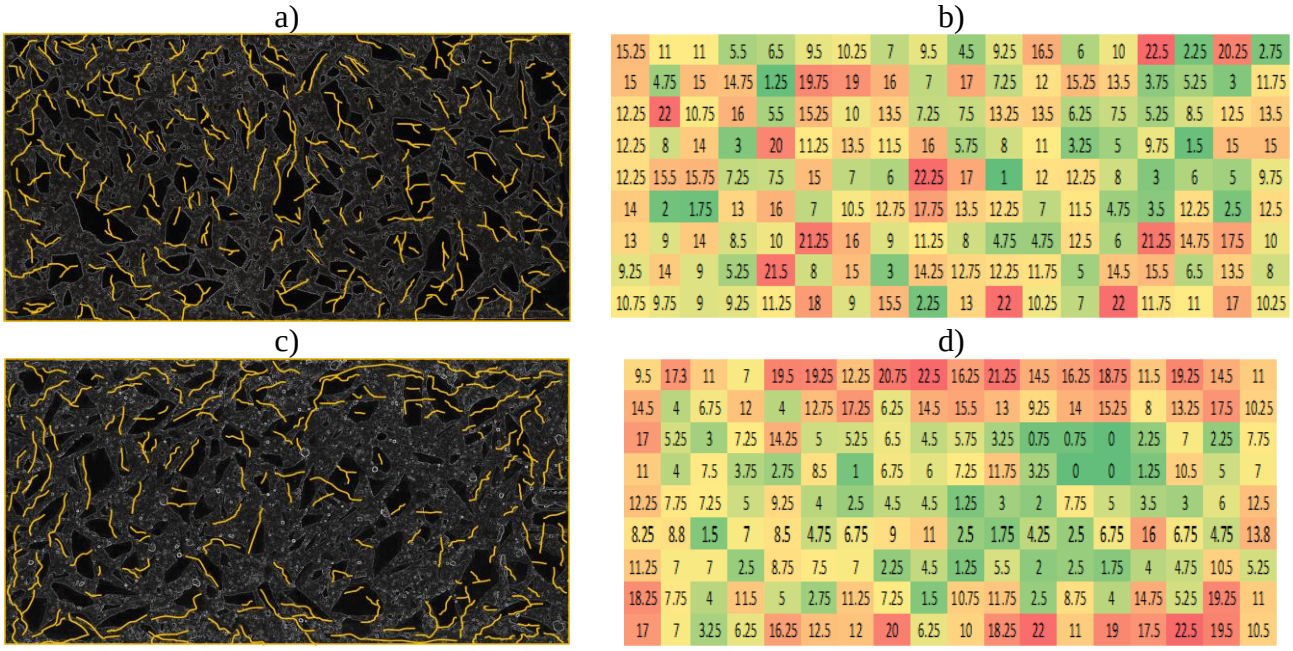

Figure 9.19: ASR-induced crack orientation obtained through image analysis (IA) and damage rating index (DRI): a) IA and b) DRI of SPH-Control specimens; c) IA, and d) DRI of SPH-CA+Fib specimens.

Finally, Figure 9.20 displays crack development through TX-CA+Fib mixtures, petrographic features (Figure 9.20a), percentage of microscopic features (Figure 9.20b), and crack density (Figure 9.20c). Overall, the results revealed similar trends as discussed for SPH-CA+Fib. Yet, it is worth mentioning that a significant amount of cracks, either CCA and OCA, were found in non-reactive aggregate particles, which contributed to raising the total CCA and OCA of the specimens. Moreover, TX specimens displayed an expressive reduction of CCP over the expansion development on CA+Fib samples. For instance, TX-CA+Fib applied at 0.30% of expansion decreased in 47% and 40% lower amount of CCP and CCPG after one and two years of exposure compared with the TX specimens' initial damage at 0.30% of expansion.

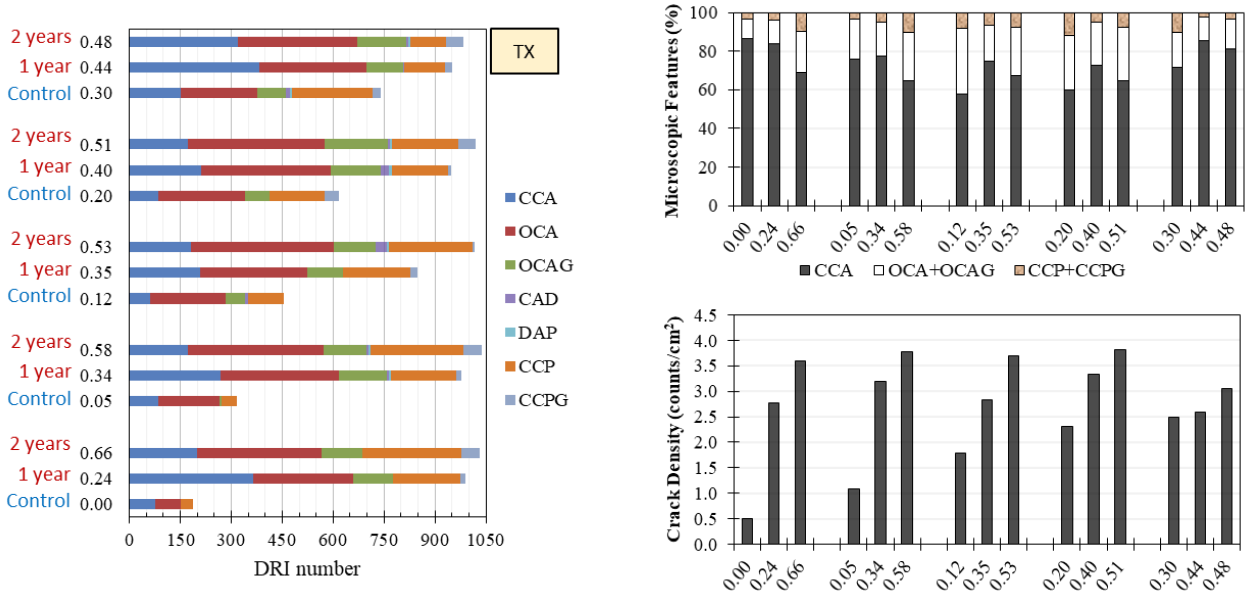

Figure 9.20: Crack development through TX-CA+Fib mixtures: a) Petrographic features, b) Percentage of microscopic features (disregarding weighting factors), c) Crack density (counts/cm^2).

9.6.3 **Mechanical assessment of ASR affected specimens**

The assessment of the extension of damage of the ASR-affected mixtures through mechanical analyses indicates results in agreement with the expansion levels and microscopic data gathered. Overall, the higher the expansion level and DRI numbers, the higher the SDI values and losses in modulus of elasticity, shear and compressive strength. However, the different kinetics of the aggregates displayed an essential role in the distressing development. Concrete specimens made of TX fine aggregate developed significantly higher expansion amplitudes than SPH mixtures. However, at similar expansion levels, the global mechanical property losses, particularly the modulus of elasticity, were higher for concrete mixtures made of SPH coarse aggregate. This behaviour was reasonably expected, though, since coarse aggregates influence the concrete mechanical properties, particularly on the stiffness or modulus of elasticity. Moreover, the DRI results displayed in Figure 9.12 showed cracks in the aggregates for SPH coarse aggregate specimens compared to TX-concrete samples. This distinction in the cracking pattern explains the higher loss of modulus of elasticity obtained for SPH mixtures and confirms the mechanical results obtained. On the other hand, the higher amount of cracks in the cement paste exhibited by the TX-concrete specimens likely explains the higher losses of compressive strength than concrete made of SPH coarse aggregate.

The surface-treated specimens could not modify the ASR distress development mechanism, yet they altered ASR-kinetics slowing and delaying the overall progress of the damage. Figure 9.21 exhibits a linear correlation (R^2 of 0.89) between the efficiency of the coating materials to slower the average mechanical properties loss (considering SDI, ME, DSS, CS) and expansion amplitudes after 720 days of exposure for both reactive aggregates (i.e., SPH and TX).

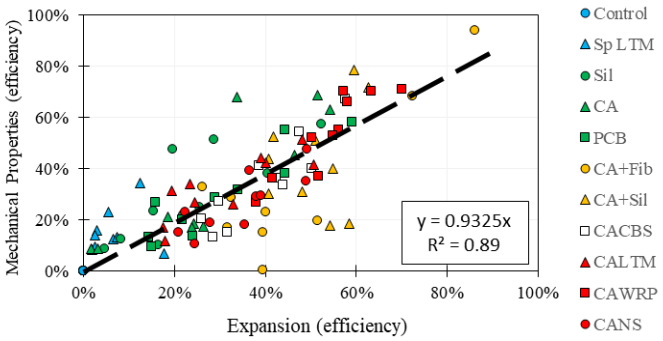

Figure 9.21: Correlation between the efficiency of the coating materials (at all applied expansions) to slow mechanical properties loss and expansion amplitudes after 720 days of exposure for both reactive aggregates.

The SDI values displayed in Figure 7.5 demonstrated a somewhat linear correlation with the expansion amplitudes, suggesting an overall straight increase in the inner cracks or physical integrity importance (i.e., number vs width of cracks) as a function of ASR-induced expansion. The mixtures that displayed the slowest gain in SDI were CAWRP and CA+Sil, agreeing with the expansion amplitudes and DRI numbers. Moreover, regardless of the the CA+Fib specimens (which will be discussed later), the SDI values did not vary significantly as per the distinct mixtures studied at equivalent expansion levels. This behaviour indicates that the importance of inner cracking remains roughly the same except for the aggregate type as a function of ASR expansion. As previously mentioned, the compounds of the concrete mixture (i.e., aggregate type, fine vs coarse) govern the crack locations, which affect the mechanical properties of the specimens differently. For instance, the higher concentration of cracks found in SPH-concrete samples increased ME losses at equivalent expansions than concrete made of TX. Likewise, the surface-treated specimens follow a similar trend.

The direct shear strength decreases as a function of ASR-induced expansion. The shear reduction is expected due to “shear friction or aggregate interlock loss” caused by ASR-induced development; the latter seems to depend on the aggregate’s type (i.e., fine vs coarse aggregate). In samples incorporating SPH aggregate, the shear strength losses were more sensitive for equivalent expansion levels.

Moreover, except for the CA+Fib, which demonstrated expressive shear strength losses, the application of the distinct coating and sealers did not vary DSS values.

The compressive strength was found to decrease somewhat modestly compared to the other mechanical properties tested. Moreover, it is verified that the compressive strength of concrete is governed by the cement paste (CP) properties. Consequently, the higher amount of CCP and CCPG found for concrete specimens made of TX likely explain the higher losses obtained for these mixtures. Furthermore, the coating materials containing crystalline admixtures (i.e., enhanced healing properties) did not modify the distress mechanism of ASR. However, a few cracks were found to be self-healed close to the external layer of the specimens.

It is clear that, besides a few particularities, the global mechanical properties loss of the coated specimens likely follows the overall development of the expansion of the concrete samples. Thus, the waterproofing ability of the coatings and sealers seems to play a major role in the distress development of the specimens. Moreover, it is quite interesting that the efficiency or performance of the applied materials to delay expansion development and crack development increases over the initial deterioration; likewise, similar trends were found for mechanical properties Figure 9.22. It is worth mentioning that the efficiency displayed in Figure 9.22a (SPH-concrete specimens) and Figure 9.22b (TX-concrete samples) were calculated as previously explained. Yet, Figure 9.22 illustrates the average values of SDI, ME, DSS, and CS, once the overall efficiency behaviour of each property was somewhat similar. The data gathered from concrete made of SPH aggregate shows much higher variation, yet the higher the expansion before treating the surface of the concrete, the higher the efficiency of the coatings and sealers. Likewise, TX-concrete specimens displayed a clear efficiency enhancement over the initial expansion, although lower values than SPH samples. The coating mixtures CAWRP and CA+Sil displayed the higher efficiency, on average, while Sp-LTM, the lowest. Moreover, CA-Fib demonstrated the greater increase in efficiency from applications at 0.00% and 0.30%, from 15% to 93% for SPH-concrete, and from -1% to 33% for concrete made of TX. The “negative” efficiency obtained for TX-CA+Fib at 0.00% suggest that, overall, the mechanical properties loss after 720 days of exposure were higher than TX-control specimens.

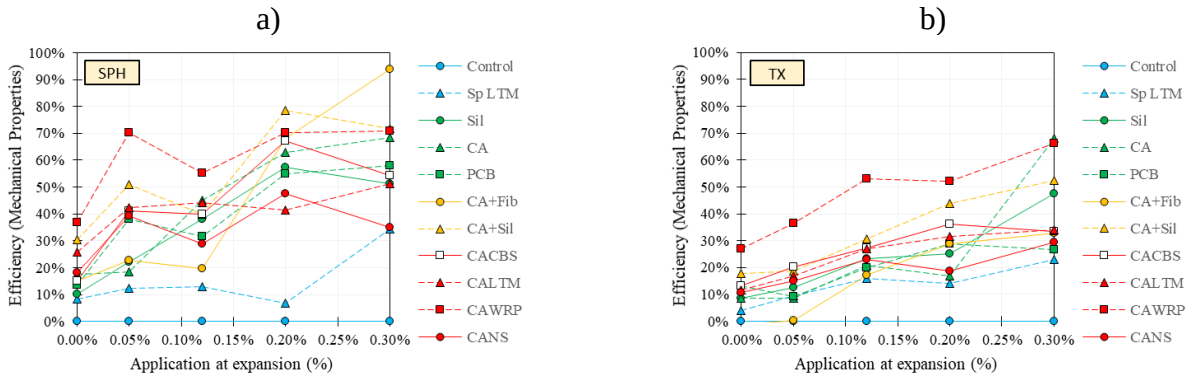

Figure 9.22: Efficiency of the coatings and sealers to mitigate the mechanical properties loss in concrete specimens made of a) SPH coarse aggregate and b) TX sand.

Among the distinct coating and sealers, CA+Fib exhibits the higher differences in the mechanical properties results. The confinement effect caused by the use of fibres plays a major role in the data gathered. Overall, SPH-CA+Fib samples treated at lower and moderate expansion levels (i.e., 0.00%, 0.05%, and 0.12%) developed the most distinguished losses in all mechanical properties; however, at higher levels (i.e., 0.20% and 0.30%), even some gain the properties were observed (e.g., SDI at 0.20% and ME, DSS, and CS at 0.30%). On the other hand, TX-CA+Fib specimens did not demonstrate the same behaviour at higher expansion levels. The only exception was for CS at 0.30%, in which it was found that the initial CS loss of 0.25 was maintained after one year of exposure and increased to 0.27 after two years of exposure. The higher losses achieved by CA+Fib mixtures "disagreed" with the expansion levels obtained for the samples; although slowing the expansion development, the inner damage did not follow a similar trend. For instance, SPH-CA+Fib treated at 0.00% of expansion displayed after one year of exposure 0.11% of expansion. Yet, the SDI found was equal to 0.25 and ME, DSS, and CS losses of 0.49, 0.40, and 0.18, values comparable to SPH-control specimens that achieved 0.20% or higher expansion levels. Likewise, similar trends were also obtained for TX-CA+Fib mixtures. However, it is worth mentioning that expansion development of the TX-CA+Fib samples increased the number of cracks formed within the non-reactive coarse aggregate after one and two days of exposure, thus increasing the losses in SDI and mainly in ME and DSS. This behaviour may also explain why the TX specimens reached higher SDI numbers and ME and DSS losses for surface treatment at higher expansion levels. Finally, the "gain" of SDI, ME, and DSS obtained for SPH-CA+Fib may be linked to the decrease of crack density (Figure 9.12) and the amount of OCA and OCAG obtained in the microscopy analysis. Likewise, the decrease of CCP and CCPG supports the slight recovery of CS for SPH-CA+Fib and TX-CA+Fib applied at 0.30% of expansion.

9.6.4 **Global analysis of the ASR distress of the surface-treated concrete specimens**

Overall, cases of ASR have become widespread in critical concrete infrastructure worldwide. Over the years, specifications have been implemented to reduce significantly or eliminate ASR in newly constructed transportation structures. Yet, there are many structures built before these specifications were in place, and many of these structures are currently showing signs of distress or are expected to in the coming years. Therefore, besides several studies that have been developed to mitigate ASR development after the reaction has already started, the engineering practice still demands information in this regard. Yet, not only on the performance of each distinct employed material but also the appropriate time to applied them.

The extensive testing performed in this study demonstrated that the ASR damage degree of the aging concrete before the surface treatment significantly influences in the efficiency of the surface applied materials. Globally, the higher the initial expansion level, the higher the efficiency displayed by the studied coatings and sealers (Figure 9.8, Figure 9.15, and Figure 9.22). Sanchez et al. [76,77] described that the ASR distress development begins forming cracks within the reactive aggregate particles (i.e., at about 0.05% of expansion), which progressively increase the length and width and extending to the cement paste (i.e., 0.12%). Finally, a large number of cracks are already found in the cement paste (i.e., 0.20%) until they connect, forming a high crack networking (i.e., 0.30%). Therefore, it is expected the higher amount of cracks in the cement paste facilitate the drying process of the concrete. Consequently, increasing the efficiency of the surface-treated specimens to mitigate ASR. Moreover, the higher the initial expansion of the concrete specimens, the lower the “residual expansion”. Comparing the values obtained for concrete made of SPH and TX reactive aggregates revealed that all coatings and sealers had higher efficiency over SPH-made concrete. Yet, one verifies that the ultimate expansion of SPH-bearing concrete was about 0.53%, whereas TX-concrete was 0.87%; these values suggest that the residual expansion of the concrete samples after the surface treatment may play an important role in the efficiency of the materials.

However, the increase in the efficiency of the surface treatments over the initial expansion does not mean that the best option is to treat concrete structures at a higher damage degree. The overall performance of the concrete may be so affected by ASR that even the most effective surface treatment will not benefit from delaying the lifespan of the aging structure. To present the results in a more straight-forward and practical way, Figure 9.23 illustrates the average performance losses of each

studied material after one year of exposure (Figure 9.23a and Figure 9.23b for SPH and TX made concrete mixtures) and after two years of exposure (Figure 9.23c and Figure 9.23d for SPH and TX made concrete mixtures). It is worth mentioning that the "performance loss" displayed in Figure 9.23 is the average of all properties measured in this study: i.e., ME, DSS, and CS are simply the values exhibited in Figure 7.6, Figure 7.7, and Figure 7.4, whereas the "performance loss" of length variation, DRI, and SDI, are the individual values obtained over the maximum value of the control specimens after two years of exposure. The initial performance loss, indicated by the black dashed line in the plots, refers to the properties' losses of the concrete specimens at each pre-determined expansion level (i.e., 0.00%, 0.05%, 0.12%, 0.20%, and 0.30%) before the surface treatment be implemented. Whereas the coloured markers refer to the results after the mentioned exposure period of each material applied at each initial expansion.

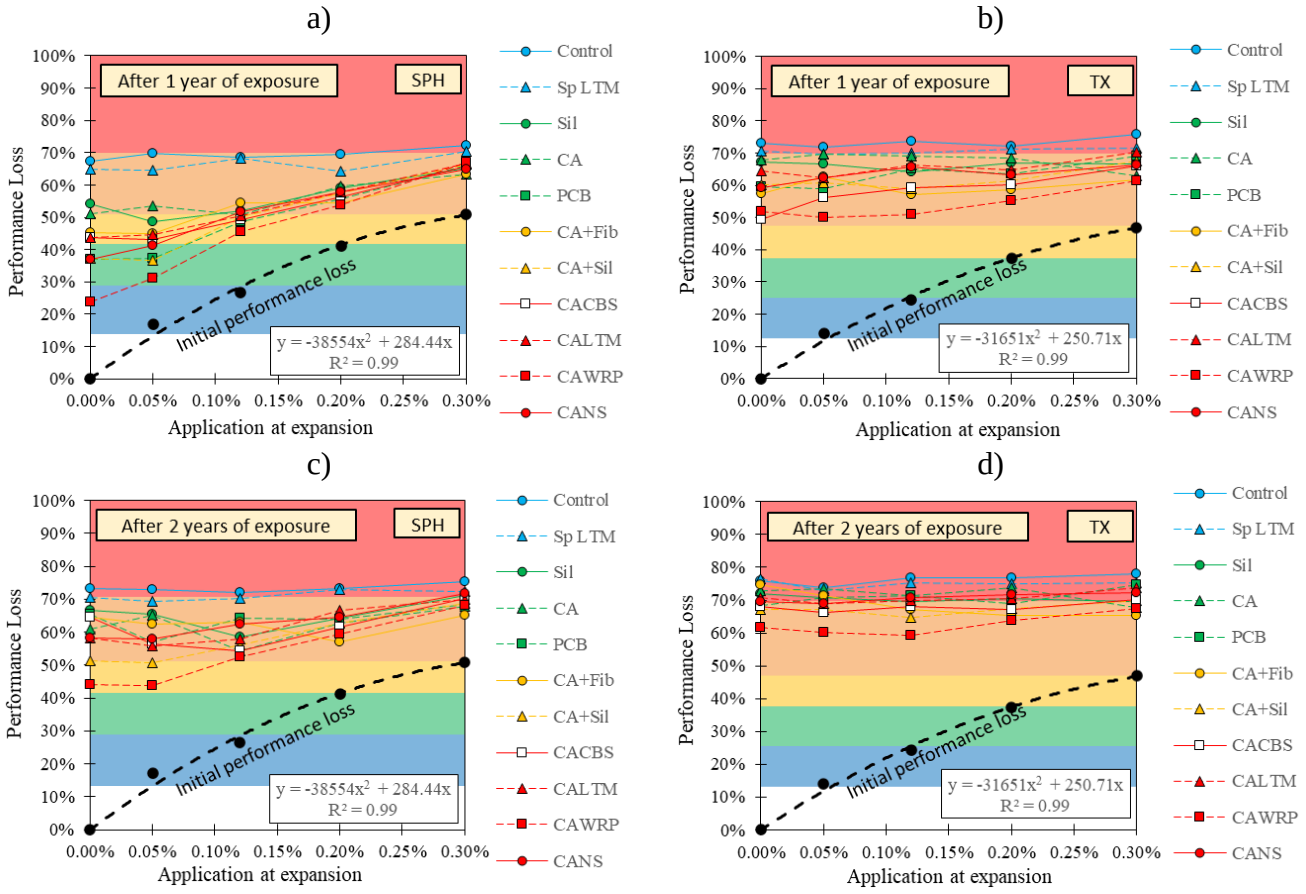

Figure 9.23: Performance losses of the surface-treated specimens after one year of exposure for a) SPH-concrete and b) TX-concrete, and after two years of exposure for c) SPH-concrete and d) TX-concrete.

The goal of using these graphs is to provide interesting data to help in the "decision making" for engineers to better select different types of coating and sealers and the most appropriate "time" to apply them. Likewise, to help in the prognosis of further distress of ASR progress after applying the distinct coatings and sealers effectively. Interestingly, although the overall efficiency of the surface treatments increases over the initial damage degree, the performance losses suggest that the early the detection and treatment of concrete, the lower the performance loss over time. At very high levels of initial expansion (i.e., 0.30%), on the other hand, the data gathered revealed that even the different materials demonstrated different efficiency, the performance loss after their application slightly changed after two years of exposure. Moreover, the different reactive aggregates used and their respective "residual expansion" play an essential role in the ability of the coatings and sealers to maintain the losses in performance at smaller values. For instance, the coating CAWRP applied in SPH-concrete specimens with 0.00% of expansion lost 23.8% of its overall performance after one year of the accelerated test, whereas for concrete made of TX, the obtained value was 51.9%. Furthermore, after two years of exposure, the losses significantly increase to 44.2% and 61.8% for SPH and TX-made concrete mixtures. This difference between one and two years may highlight the importance of maintenance of the coating materials to keep its efficiency at higher levels; however, further investigation is needed to confirm this statement. One verifies that without any surface treatment, the initial performance loss should keep increasing until reach the numbers obtained by the control specimens at one and two years of exposure (i.e., over 70% of losses). Overall, the coating CAWRP and CA-Sil displayed the best performance against ASR development, yet increasing the initial damage degree, the performance losses of the CAWRP and CA-Sil concrete specimens decreased, as aforementioned. However, not all surface mixtures demonstrated the same behaviour. For instance, the lower performance losses obtained by SPH-Sil, SPH-CA, and SPH-CACBS were achieved when applied at 0.12% of expansion, whereas SPH-CA+Fib and TX-CA+Fib achieved the best performances once applied at 0.20% of expansion and after two years of exposure.

The results gathered in this research, although acquired from concrete specimens under "free expansion conditions", highlights the importance of two aspects for exposed field concrete structures, such as: first, the correct diagnosis and classification of the damage degree in an ASR-affected aging concrete, e.g., as per Sanchez et al. [78]; second, an assessment of the residual expansion potential of concrete from structures damaged by ASR [79,80]. Finally, the evaluation of the different coating and sealers deemed crucial further development on field exposed specimens (i.e., cubes, blocks, etc.). Hence, to

consider a critical aspect for waterproofing and repellent materials, the wet and drying cycles can significantly enhance their efficiency to maintain the relative humidity of the concrete at lower levels, thus increasing their performance against ASR development.

9.7 Conclusions

The main objective of the current comprehensive experimental campaign was to understand the influence of different surface treatments and techniques (i.e., water repellent, rigid coating based, lithium-based products, crystalline waterproofing coatings, etc.) to mitigate further ASR-induced development in its initial, moderate, and advanced phases. From the results obtained in this study, over 720 days of accelerated ASR development, the following conclusions may be drawn:

- ASR kinetics, mechanical properties and microscopic changes are dependent on the aggregate's type (i.e., fine vs coarse aggregate). Concrete mixtures containing Tx developed faster ASR kinetics and higher ultimate expansion amplitudes (e.g., 0.85% for TX-Control against 0.52% for SPH-Control). Moreover, the residual expansion (i.e., the difference between ultimate expansion and the initial expansion before the surface treatment) plays an important role in the efficiency of the coating and sealers to mitigate further ASR development. Globally, the higher the residual expansion, the lower the treatment efficiency.
- Overall, the application of coating and sealers on the surface of the concrete specimens showed promising evidence that, besides the different materials displayed high expansion values after 720 days of exposure, they significantly modify ASR-kinetics. Furthermore, the statistical analysis (Tukey's test) confirmed the significance of the surface treatments. The only exception was spraying lithium on the surface, which displays similar results to control samples. On the other hand, the coating containing crystalline waterproofing and water repellent (i.e., CAWRP) demonstrated the higher efficiency to mitigate ASR, followed by CA+Sil (i.e., crystalline

waterproofing plus silane treatment), and CA-Fib (i.e., crystalline waterproofing mixed with acrylic fibres).

- The microscopic observations revealed that the total DRI numbers were quite well linked with the expansion level of each different surface treatment. The sealers and coating materials could not modify the ASR distress development mechanism, yet they altered ASR-kinetics slowing and delaying the overall progress of the damage. The only exception was the coating CA-Fib, which slowed the expansion development, yet the inner damage and crack development found in CA-Fib specimens were significantly higher, comparable to specimens that achieved expansions 1.5 to 3 times higher. Moreover, the three-dimensional confinement effect proportioned by the CA-Fib coating modified the distribution of cracks and the proportions of the microscopic features.
- The use of crystalline waterproofing coatings, which contain artificial triggering healing agents, did not modify the distress mechanism of ASR or recovered mechanical properties of the affected concrete specimens. Although a few cracks were found to be self-healed close to the external layer of the specimens.
- Finally, four qualitative charts were developed to provide interesting data to help in the "decision making" for engineers to better select different types of coating and sealers and the most appropriate "time" to apply them. Globally, the coating and sealers demonstrated higher efficiency as higher the initial damage degree due to ASR. However, the performance loss plots indicate that as earlier the surface treatment is applied, the lower the performance loss of the concrete cylinders. Moreover, the analysis indicates that at higher initial damage degree (i.e., 0.20% and 0.30%), the performance losses of the treated concrete were somewhat similar among each surface treatment and control group.

9.8 Acknowledgment

The authors would like to thank Dr. Gamal Elnabelsya and Dr. Muslim Majeed, technical officers of Materials and Structures Laboratory in the Department of Civil Engineering at the University of Ottawa. Likewise, the authors would like to express their sincere gratitude and appreciation to Kryton International, Mr. Alireza Biparva, Mary Grace Rosalin, Dr. Pejman Azarsa. As well as De Souza benefits from the University of Ottawa Excellence Scholarship, Collaborative Research & Development by NSERC (Natural Science and Engineering Research Council of Canada), and the prestigious Vanier CGS scholarship, also financed by the NSERC.

9.9 References

[1] B. Fournier, M.-A. Bérubé, Alkali-aggregate reaction in concrete: a review of basic concepts and engineering implications, Can. J. Civ. Eng. 27 (2000) 167–191. doi:10.1139/cjce-27-2-167.

[2] J. Lindgård, Ö. Andiç-Çakir, I. Fernandes, T.F. Rønning, M.D.A. Thomas, Alkali-silica reactions (ASR): Literature review on parameters influencing laboratory performance testing, Cem. Concr. Res. 42 (2012) 223–243. doi:10.1016/j.cemconres.2011.10.004.

[3] CSA A23.2-27A, Standard practice to identify degree of alkali-reactivity of aggregates and to identify measures to avoid deleterious expansion in concrete, Can. Stand. Assoc. (2019) 439–451. doi:10.1520/C0618-15.2.

[4] R.D. Lute, K.J. Folliard, T. Drimalas, C.K. Rust, Coatings and sealers for mitigation of alkali-silica reaction and/or delayed ettringite formation, in: H.M. Bernardes, N.P. Hasparyk (Eds.), 15th Int. Conf. Alkali-Aggregate React., São Paulo, 2016.

[5] R.B. Figueira, R. Sousa, L. Coelho, M. Azenha, J.M. de Almeida, P.A.S. Jorge, C.J.R. Silva, Alkali-silica reaction in concrete: Mechanisms, mitigation and test methods, Constr. Build. Mater. 222 (2019) 903–931. doi:10.1016/j.conbuildmat.2019.07.230.

[6] C. Christodoulou, C.I. Goodier, S.A. Austin, J. Webb, G.K. Glass, Long-term performance of surface impregnation of reinforced concrete structures with silane, Constr. Build. Mater. 48 (2013) 708–716. doi:10.1016/j.conbuildmat.2013.07.038.

[7] R.A. Deschenes, E.R. Giannini, T. Drimalas, B. Fournier, W.M. Hale, Effects of moisture, temperature, and freezing and thawing on Alkali-Silica reaction, ACI Mater. J. 115 (2018) 575–584. doi:10.14359/5170219.

[8] S. Poyet, A. Sellier, B. Capra, G. Thè-venin-Foray, J.M. Torrenti, H. Tournier-Cognon, E. Bourdarot, Influence of water on alkali-silica reaction: Experimental study and numerical simulations, J. Mater. Civ. Eng. 18 (2006) 588–596. doi:10.1061/(ASCE)0899-1561(2006)18:4(588).

[9] C.D. Murray, R.A. Deschenes, W.M. Hale, Durability of silane sealer in highly alkaline environment, ACI Mater. J. 113 (2016) 387–393. doi:10.14359/51688982.

[10] R. Deschenes, M. Waidner, W.H. Hale, Mitigation of Alkali-Silica Reaction in Concrete Pavements By Silane Treatment, in: NP. Bernardes, H.M. & Hasparyk (Ed.), 15th Int. Conf. Alkali-Aggregate React., São Paulo, 2016.

[11] CMS. Rua, N.P. Hasparyk, P.J.M. Monteiro, D. Dal Molin, L. Eiger, Study of silane compositions to mitigate alkali-silica reaction, in: H.M. Bernardes, N.P. Hasparyk (Eds.), 15th Int. Conf. Alkali-Aggregate React., São Paulo, 2016.

[12] G. Li, S. Liu, M. Niu, Q. Liu, X. Yang, M. Deng, Effect of granulated blast furnace slag on the self-healing capability of mortar incorporating crystalline admixture, Constr. Build. Mater. 239 (2020) 117818. doi:10.1016/j.conbuildmat.2019.117818.

[13] P. Azarsa, R. Gupta, A. Biparva, Assessment of self-healing and durability parameters of concretes incorporating crystalline admixtures and Portland Limestone Cement, Cem. Concr. Compos. 99 (2019) 17–31. doi:10.1016/j.cemconcomp.2019.02.017.

[14] K. Sisomphon, O. Copuroglu, E.A.B. Koenders, Self-healing of surface cracks in mortars with expansive additive and crystalline additive, Cem. Concr. Compos. 34 (2012) 566–574. doi:10.1016/j.cemconcomp.2012.01.005.

[15] ACI 212.3R, ACI 212 . 3R-10 Report on Chemical Admixtures for Concrete, American Concrete Institute, 2015.

[16] S. Guzlena, G. Sakale, Self-healing concrete with crystalline admixture - A review, IOP Conf. Ser. Mater. Sci. Eng. 660 (2019). doi:10.1088/1757-899X/660/1/012057.

[17] H. Ma, S. Qian, Z. Zhang, Effect of self-healing on water permeability and mechanical property of Medium-Early-Strength Engineered Cementitious Composites, Constr. Build. Mater. 68 (2014) 92–101. doi:10.1016/j.conbuildmat.2014.05.065.

[18] L. Ferrara, V. Krelani, M. Carsana, A “fracture testing” based approach to assess crack healing of concrete with and without crystalline admixtures, Constr. Build. Mater. 68 (2014) 535–551. doi:10.1016/j.conbuildmat.2014.07.008.

[19] S.H. Diab, A.M. Soliman, M.R. Nokken, Feasibility of basalt and glass FRP mesh for

strengthening and confinement concrete damage due to ASR-expansion, Constr. Build. Mater. 266 (2021) 120893. doi:10.1016/j.conbuildmat.2020.120893.

[20] K.J. Folliard, R. Barborak, T. Drimalas, L. Du, S. Garber, J. Ideker, T. Ley, S. Williams, M. Juenger, B. Fournier, M.D.A. Thomas, Preventing ASR/DEF in new concrete:final report., Austin (Texas), 2006.

[21] D.P. Johnston, R. Surdahl, D.P. Stokes, A Case Study of a Lithium-Based Treatment of an ASR-Affected Pavement., in: BD. M.A. Berube, B. Fournier (Ed.), 11th Int. Conf. Alkali- Aggreg. React., Quebéc, 2000: pp. 1149–1158.

[22] E.F. Carneiro, J.C. Pinfari, T.P.A. Cappi, M.H.L. Covre, Maintenance and Repairs on the Water Intake of Jaguari Hydropowerplant Affected By Aar, in: NP. Bernardes, H.M. & Hasparyk (Ed.), 15th Int. Conf. Alkali-Aggregate React., São Paulo, 2016.

[23] G.M. Ahlstrom, J. Mullarky, F. Faridazar, U. States, G. Consulting, F. Highway, the United States Federal Highway Administration ' S Efforts To Eliminate Alkali-Silica Reaction in, in: 13th Int. Conf. Alkali-Aggregate React. Concr., 2008.

[24] V. Corinaldesi, G. Moriconi, V.B. Bianche, Alkali-Aggregate Reaction : From Prognosis To Intervention, in: 13th Int. Conf. Alkali-Aggregate React. Concr., 2008.

[25] S. Matsumoto, T. Miyagawa, Y. Yamaguchi, Y. Hisari, T. Goto, Impregnation depth of silane penetrant system and its effect on ASR expansion, in: 13th Int. Conf. Alkali-Aggregate React. Concr., 2008.

[26] S.H. Diab, A.M. Soliman, M. Nokken, Exterior strengthening for ASR damaged concrete: A comparative study of carbon and basalt FRP, Constr. Build. Mater. 235 (2020) 117435. doi:10.1016/j.conbuildmat.2019.117435.

[27] S. Poyet, A. Sellier, B. Capra, G. Foray, J.M. Torrenti, H. Cognon, E. Bourdarot, Chemical modelling of Alkali Silica reaction: Influence of the reactive aggregate size distribution, Mater. Struct. Constr. 40 (2007) 229–239. doi:10.1617/s11527-006-9139-3.

[28] T. Bader, R. Lackner, Acrylic surface treatment applied to architectural High-Performance Concrete (HPC): Identification of potential pitfalls on the way to long-lasting protection, Constr. Build. Mater. 237 (2020) 117415. doi:10.1016/j.conbuildmat.2019.117415.

[29] S. Weisheit, S.H. Unterberger, T. Bader, R. Lackner, Assessment of test methods for characterizing the hydrophobic nature of surface-treated High Performance Concrete, Constr. Build. Mater. 110 (2016) 145–153. doi:10.1016/j.conbuildmat.2016.02.010.

[30] PAM Basheer, L. Basheer, D.J. Cleland, A.E. Long, Surface treatments for concrete:

Assessment methods and reported performance, Constr. Build. Mater. 11 (1997) 413–429. doi:10.1016/S0950-0618(97)00019-6.

[31] Z. Liu, W. Hansen, Effect of hydrophobic surface treatment on freeze-thaw durability of concrete, Cem. Concr. Compos. 69 (2016) 49–60. doi:10.1016/j.cemconcomp.2016.03.001.

[32] S.R.C. Madduru, K.S. Shaik, R. Velivela, V.K. Karri, Hydrophilic and hydrophobic chemicals as self curing agents in self compacting concrete, J. Build. Eng. 28 (2020) 101008. doi:10.1016/j.jobe.2019.101008.

[33] A.A. Almusallam, F.M. Khan, S.U. Dulaijan, O.S.B. Al-Amoudi, Effectiveness of surface coatings in improving concrete durability, Cem. Concr. Compos. 25 (2003) 473–481. doi:10.1016/S0958-9465(02)00087-2.

[34] M.. Berube, B. Fournier, Influence of Wetting-Drying and Freezing-Thawing Cycles, and Effectiveness of Sealers on ASR, in: Ahmad Sheyan (Ed.), 10th Int. Conf. Alkali-Aggregate React. Concr., Melbourne, 1996: pp. 1056–1063.

[35] D. Stark, The moisture condition of field concrete exhibiting alkali-silica reactivity, in: 2nd Int. Conf. Durab. Concr., ACI Publication SP, 1991: pp. 973–987.

[36] M.H.F. Medeiros, P. Helene, Surface treatment of reinforced concrete in marine environment: Influence on chloride diffusion coefficient and capillary water absorption, Constr. Build. Mater. 23 (2009) 1476–1484. doi:10.1016/j.conbuildmat.2008.06.013.

[37] R.S.C. Woo, H. Zhu, M.M.K. Chow, C.K.Y. Leung, J.K. Kim, Barrier performance of silane-clay nanocomposite coatings on concrete structure, Compos. Sci. Technol. 68 (2008) 2828–2836. doi:10.1016/j.compscitech.2007.10.028.

[38] K. Tosun, B. Felekoglu, B. Baradan, Effectiveness of alkyl alkoxy silane treatment in mitigating alkali-silica reaction, ACI Mater. J. 105 (2008) 20–27. doi:10.14359/19203.

[39] I. Mohamed, L. Curtil, S. Ronel-Idrissi, P. Hamelin, Influence of composite materials confinement on alkali aggregate expansion, Mater. Struct. Constr. 38 (2005) 387–394. doi:10.1617/14158.

[40] G. Jen, R. Hay, C.P. Ostertag, Multi-scale evaluation of hybrid fiber restraint of alkali-silica reaction expansion in concrete, Constr. Build. Mater. 211 (2019) 1117–1126. doi:10.1016/j.conbuildmat.2019.03.102.

[41] L. Curtis, E. Ferrier, S. Ronel-Idrissi, P. Hamelin, Composite materials contribution in strengthening concrete structures affected by alkali–aggregate reaction, Int. J. Mater. Prod. Technol. 19 (2003) 68.

[42] J. Li, MNS. Hadi, behaviour of externally confined high-strength concrete columns under eccentric loading, Compos. Struct. 62 (2003) 145–153. doi:10.1016/S0263-8223(03)00109-0.

[43] I. Mohamed, S. Ronel, L. Curtil, Influence of composite materials confinement on alkali-aggregate mechanical behaviour, Mater. Struct. Constr. 39 (2006) 479–490. doi:10.1617/s11527-005-9019-2.

[44] L. Lam, J.G. Teng, C.H. Cheung, Y. Xiao, FRP-confined concrete under axial cyclic compression, Cem. Concr. Compos. 28 (2006) 949–958. doi:10.1016/j.cemconcomp.2006.07.007.

[45] S.H. Diab, A.M. Soliman, M. Nokken, Exterior strengthening for ASR damaged concrete: A comparative study of carbon and basalt FRP, Constr. Build. Mater. 235 (2020) 117435. doi:10.1016/j.conbuildmat.2019.117435.

[46] S. Abdullah, R. Al-Mahaidi, A. Shayan, CFRP confinement of RC columns damaged by alkali aggregate reaction, in: 5th Civ. Eng. Conf. Asian Reg. Australas. Struct. Eng. Conf., 2010: p. 773.

[47] T. Kim, J. Olek, The effects of lithium ions on chemical sequence of alkali-silica reaction, Cem. Concr. Res. 79 (2016) 159–168. doi:10.1016/j.cemconres.2015.09.013.

[48] X. Feng, M.D.A. Thomas, T.W. Bremner, K.J. Folliard, B. Fournier, New observations on the mechanism of lithium nitrate against alkali silica reaction (ASR), Cem. Concr. Res. 40 (2010) 94–101. doi:10.1016/j.cemconres.2009.07.017.

[49] A. Leemann, L. Bernard, S. Alahrache, F. Winnefeld, ASR prevention - Effect of aluminum and lithium ions on the reaction products, Cem. Concr. Res. 76 (2015) 192–201. doi:10.1016/j.cemconres.2015.06.002.

[50] C. Tremblay, M.A. Bérubé, B. Fournier, M.D. Thomas, K.J. Folliard, Experimental investigation of the mechanisms by which LiNO3 is effective against ASR, Cem. Concr. Res. 40 (2010) 583–597. doi:10.1016/j.cemconres.2009.09.022.

[51] A. Leemann, L. Lörtscher, L. Bernard, G. Le Saout, B. Lothenbach, R.M. Espinosa-Marzal, Mitigation of ASR by the use of LiNO3 - Characterization of the reaction products, Cem. Concr. Res. 59 (2014) 73–86. doi:10.1016/j.cemconres.2014.02.003.

[52] C.L. Collins, J.H. Ideker, G.S. Willis, K.E. Kurtis, Examination of the effects of LiOH, LiCl, and LiNO3 on alkali-silica reaction, Cem. Concr. Res. 34 (2004) 1403–1415. doi:10.1016/j.cemconres.2004.01.011.

[53] X. Mo, B. Fournier, Investigation of structural properties associated with alkali-silica reaction by

means of macro- and micro-structural analysis, Mater. Charact. 58 (2007) 179–189. doi:10.1016/j.matchar.2006.04.018.

[54] LMS. Souza, R.B. Polder, O. Çopuroğlu, Lithium migration in a two-chamber setup as treatment against expansion due to alkali–silica reaction, Constr. Build. Mater. 134 (2017) 324–335. doi:10.1016/j.conbuildmat.2016.12.052.

[55] M.D.A. Thomas, B. Fournier, K.J. Folliard, J.H. Ideker, Y. Resendez, The Use of Lithium To Prevent or Mitigate Alkali-Silica Reaction in Concrete Pavements and Structures., Washington, DC, 2007.

[56] M. Kawamura, T. Kodera, Effects of externally supplied lithium on the suppression of ASR expansion in mortars, Cem. Concr. Res. 35 (2005) 494–498. doi:10.1016/j.cemconres.2004.04.032.

[57] S. Ekolu, G. Rakgosi, D. Hooton, Long-term mitigating effect of lithium nitrate on delayed ettringite formation and ASR in concrete – Microscopic analysis, Mater. Charact. 133 (2017) 165–175. doi:10.1016/j.matchar.2017.09.025.

[58] K. Kobayashi, Y. Takagi, Penetration of pressure-injected lithium nitrite in concrete and ASR mitigating effect, Cem. Concr. Compos. 114 (2020) 103709. doi:10.1016/j.cemconcomp.2020.103709.

[59] Y. Zhang, L. Zuo, J. Yang, X. Cai, Y. Zhao, X. Zeng, Effect of cementitious capillary crystalline waterproofing coating on the gas permeability of mortar, Struct. Concr. 20 (2019) 1763–1770. doi:10.1002/suco.201900016.

[60] Y. Zhang, X. Du, Y. Li, F. Yang, Z. Li, Research on cementitious capillary crystalline waterproofing coating for underground concrete works, Adv. Mater. Res. 450–451 (2012) 286–290. doi:10.4028/www.scientific.net/AMR.450-451.286.

[61] G. Lu, W. Zhao, D. Dai, Study on Preparation of cementitious capillary crystalline waterproofing coating, Proc. 3rd Int. Conf. Mechatronics, Robot. Autom. 15 (2015) 79–84. doi:10.2991/icmra-15.2015.16.

[62] E. Cuenca, A. Tejedor, L. Ferrara, A methodology to assess crack-sealing effectiveness of crystalline admixtures under repeated cracking-healing cycles, Constr. Build. Mater. 179 (2018) 619–632. doi:10.1016/j.conbuildmat.2018.05.261.

[63] TCS. Reddy, A. Ravitheja, C. Sashidhar, Micromechanical Properties of Self-Healing Concrete with Crystalline Admixture and Silica Fume, ACI Mater. J. 117 (2020) 63–74. doi:10.14359/51722395.

[64] G. Li, X. Huang, J. Lin, X. Jiang, X. Zhang, Activated chemicals of cementitious capillary crystalline waterproofing materials and their self-healing behaviour, Constr. Build. Mater. 200 (2019) 36–45. doi:10.1016/j.conbuildmat.2018.12.093.

[65] M.J. Al-Kheetan, M.M. Rahman, D.A. Chamberlain, Moisture evaluation of concrete pavement treated with hydrophobic surface impregnants, Int. J. Pavement Eng. 21 (2020) 1746–1754. doi:10.1080/10298436.2019.1567917.

[66] R. Al-Rashed, M. Al-Jabari, Concrete protection by combined hygroscopic and hydrophilic crystallization waterproofing applied to fresh concrete, Case Stud. Constr. Mater. 15 (2021) e00635. doi:10.1016/j.cscm.2021.e00635.

[67] R. Al-Rashed, M. Jabari, Dual-crystallization waterproofing technology for topical treatment of concrete, Case Stud. Constr. Mater. 13 (2020) e00408. doi:10.1016/j.cscm.2020.e00408.

[68] L.F.M. Sanchez, B. Fournier, M. Jolin, J. Duchesne, Reliable quantification of AAR damage through assessment of the Damage Rating Index (DRI), Cem. Concr. Res. 67 (2015) 74–92. doi:10.1016/j.cemconres.2014.08.002.

[69] L.F.M. Sanchez, B. Fournier, M. Jolin, M.A.B. Bedoya, J. Bastien, J. Duchesne, Use of Damage Rating Index to quantify alkali-silica reaction damage in concrete: Fine versus coarse aggregate, ACI Mater. J. 113 (2016) 395–407. doi:10.14359/51688983.

[70] L. Sanchez, Contribution to the assessment of damage in aging concrete infrastructures affected by alkali-aggregate reaction, UNIVERSITE LAVAL, 2014.

[71] L.F.M. Sanchez, B. Fournier, M. Jolin, D. Mitchell, J. Bastien, Overall assessment of Alkali-Aggregate Reaction (AAR) in concretes presenting different strengths and incorporating a wide range of reactive aggregate types and natures, Cem. Concr. Res. 93 (2017) 17–31. doi:10.1016/j.cemconres.2016.12.001.

[72] L.F.M. Sanchez, B. Fournier, M. Jolin, J. Bastien, Evaluation of the stiffness damage test (SDT) as a tool for assessing damage in concrete due to ASR: Test loading and output responses for concretes incorporating fine or coarse reactive aggregates, Cem. Concr. Res. 56 (2014) 213–229. doi:10.1016/j.cemconres.2013.11.003.

[73] L.F.M. Sanchez, B. Fournier, M. Jolin, J. Bastien, D. Mitchell, Practical use of the Stiffness Damage Test (SDT) for assessing damage in concrete infrastructure affected by alkali-silica reaction, Constr. Build. Mater. 125 (2016) 1178–1188. doi:10.1016/j.conbuildmat.2016.08.101.

[74] B. Barr, E.B.D. Hasso, development of a compact cylindrical shear test specimen, J. Mater. Sci. Lett. 5 (1986) 1305–1308.

[75] DJ De Souza, L.F.M. Sanchez, M.T. De Grazia, Evaluation of a direct shear test setup to quantify AAR-induced expansion and damage in concrete, Constr. Build. Mater. 229 (2019). doi:10.1016/j.conbuildmat.2019.116806.

[76] L.F.M. Sanchez, B. Fournier, M. Jolin, J. Duchesne, Reliable quantification of AAR damage through assessment of the Damage Rating Index (DRI), Cem. Concr. Res. 67 (2015) 74–92. doi:10.1016/j.cemconres.2014.08.002.

[77] L.F.M. Sanchez, B. Fournier, M. Jolin, M.A.B. Bedoya, J. Bastien, J. Duchesne, Use of Damage Rating Index to quantify alkali-silica reaction damage in concrete: Fine versus coarse aggregate, ACI Mater. J. 113 (2016) 395–407. doi:10.14359/51688983.

[78] L.F.M. Sanchez, B. Fournier, M. Jolin, D. Mitchell, J. Bastien, Overall assessment of Alkali-Aggregate Reaction (AAR) in concretes presenting different strengths and incorporating a wide range of reactive aggregate types and natures, Cem. Concr. Res. 93 (2017) 17–31. doi:10.1016/j.cemconres.2016.12.001.

[79] S. Multon, F.-X. Barin, B. Godart, F. Toutlemonde, Estimation of the Residual Expansion of Concrete Affected by Alkali Silica Reaction, J. Mater. Civ. Eng. 20 (2008) 54–62. doi:10.1061/(asce)0899-1561(2008)20:1(54).

[80] C. Merz, A. Leemann, Assessment of the residual expansion potential of concrete from structures damaged by AAR, Cem. Concr. Res. 52 (2013) 182–189. doi:10.1016/j.cemconres.2013.07.001.

Chapter Ten: A proposed framework for an optimized selection of raw materials to avoid or mitigate ASR in concrete.

Diego J. De Souza[1], Leandro F. M. Sanchez[1]

[1]Department of Civil Engineering, University of Ottawa, Ottawa, Canada.

Abstract

Alkali-Silica Reaction (ASR) is one of the most harmful distress mechanisms affecting the durability and serviceability of concrete infrastructure worldwide. Over the past decades, different tools and protocols have been developed to assess and mitigate ASR initiation and development in the field. Moreover, the traditional standards/protocols are in constant need of improvement, particularly to optimize the use of materials without losing performance. This study aims to develop a new mix-design approach focused on the chemical composition of the blended binders (i.e., based on the main ternary oxides of binder materials) towards the mitigation of ASR. Thus, developing an interesting tool for mix-designers to appropriate select the different types and quantities of SCMs to prevent damage in concrete. To achieve this goal, the work is divided into three phases: 1) selection and pre-determination of the blended mixtures; 2) assessment of ASR kinetics and expansion development of the distinct mixtures; and 3) mechanical and microscopical evaluation of ASR distress development on the distinct concrete mixtures. The data gathered demonstrate promising results on using the proposed ternary oxides approach and provide interesting data to help in the "decision making" to select the best options (i.e., the combination of different SCMs and quantities) to apply in the concrete structures exposed to ASR development.

Keywords: alkali-silica reaction, the durability of concrete, assessment of ASR-induced expansion, preventive measures.

10.1 **Introduction**

Alkali-Silica Reaction (ASR) is one of the most harmful distress mechanisms affecting the durability and serviceability of concrete infrastructure worldwide. ASR is conventionally defined as a chemical reaction between the alkali hydroxides (i.e. Na^+, K^+ and OH^-) and metastable silica mineral forms present in both natural and synthetic aggregates [1–3]. The reaction generates a secondary product, the so-called *ASR-gel* (alkali-calcium-silicate-hydrate), that induces expansive pressures within the reacting aggregate material(s) and the adjacent cement paste while moisture uptake [4]. Thus, causing microcracking, loss of material integrity (mechanical/durability), and, in some cases, functionality in the affected structure [5].

Over the past decades, several approaches and recommendations have been developed to assess the efficiency of preventive measures (i.e. SCMs such as fly ash, silica fume, blast furnace slag, natural pozzolans, etc.) to mitigate ASR in the field [6–9]. These measures generally include performance approaches based on laboratory tests, following a risk analysis based on type and reactivity of the aggregates, size and exposure condition of the concrete structure, and cementing materials recommended for use [10–15]. However, although it is overall accepted that it is now possible to build new concrete infrastructure with minimum or even calculated/limited risk of ASR, the traditional standards/protocols are in constant need of improvement, particularly to optimize the use of materials without losing performance. Moreover, these protocols currently comprise the replacement of cement by traditional binder materials (i.e., fly ash, blast furnace slag, and silica fume), limiting guidelines or at least a first approach on the level of use of “new” sustainable materials (i.e., rice husk ash, wood ash, calcined clays, metakaolin, glass clays, etc.). Moreover, depletion in the coming years is expected to some of the most common SCMs (e.g., fly ash), making it imperative to find alternative materials able to reduce the embodied energy of concrete and provide mixtures with a low-risk ASR development [1,6]. In this context, advanced concrete mix-design approaches accounting for the “free” selection of the different binder materials aiming to achieve pre-determined “chemical composition” of the blended materials, based on the performance against ASR are highly desirable. Yet, have not been explored in the literature. Thus, leaving room for major developments in this area.

10.2 Background

10.2.1 Preventing ASR development in concrete structures

Preventive measures, including the use of supplementary cementing materials (SCMs) such as fly ash (FA) [7,16,17], granulated blast-furnace slag (GBFS) [18,19], and silica fume (SF) [20,21], have been widely studied to decrease the likelihood of ASR. SCMs can control ASR-induced development mainly by their capacity to reduce the alkalinity available in the system, thus limiting their availability to react with the aggregates [2,6,17]. Furthermore, it has been reported that the ability of SCMs to bind alkalis and hydroxyls ions seems to be strongly related to the CaO/SiO_2 ratio of the SCMs; i.e. the higher this ratio, the lower its binding capacity [6]. Chemically, SCMs can dilute the alkalis available from the clinker and change the properties of the ASR-gel by consuming $Ca(OH)_2$ from the pore solution [2,6,17]. Furthermore, these materials can enhance concrete microstructure, impacting the mobility of ions and possibly slowing the reaction rate [17,22,23].

The threshold values that have been established to mitigate the ASR efficiently are quite variable; they are a function of each different type of SCMs, their corresponding reactivity, and the type/nature of the aggregates. Overall, it has been demonstrated that the effective amounts of the most common SCMs to suppress ASR development can range from 25-65% for granulated blast-furnace slag [18,19,24], 15-50% for fly ashes [7,16,17,24], and 5-15% for silica fume [20,21,24]. Lately, the Canadian Standard Association has developed a performance-based design approach (i.e., CSA A23.2-27A), giving concrete mix-designers a standard practice to identify the degree of alkali-reactivity of aggregates and to identify measures to avoid harmful expansion in concrete [10]. The innovation of the CSA.A23.27A, unique in global scope, presents a step-by-step decision-making procedure according to variables that can influence the development of AAR and that could be present in the application of the structure, making it easier to produce concrete that will present greater resistance to ASR. The step-by-step approach to identify the preventive measures determines four different levels of prevention (i.e., from V to Z). Thus, it is given the minimum quantities (% by mass of total cementitious materials) of each type of SCMs (i.e., slag, fly ashes, and silica fume) per each prevention level [10]. However, besides the three most common types of SCMs, it is only suggested that different types of natural pozzolans should meet the requirements of CSA A3001 and may be used if they effectively control ASR-induced expansion as per CSA A23.2-28A [11]. Yet, any range or minimum values are given for those

materials for testing in accordance with CSA A23.2-28A. Therefore, different approaches that may bring some light in this regard are highly desirable.

10.2.2 The role of CaO, SiO_2 and Al_2O_3 from binder materials on the likelihood of ASR.

Over the years, authors [25–32] have studied the mechanisms that may trigger ASR-induced expansion and damage. Overall, ASR development may be summarized in three steps: (1) interaction of the alkaline environment and dissolution of the metastable siliceous phases from the aggregates; (2) the production of ASR-gel with the increase of alkali concentration within the aggregate particles and; (3) osmotic moisture absorption and gel expansion. The ASR is essentially the "attack" to certain forms of unstable and reactive silica with sodium (Na^+), potassium (K^+), and hydroxyls ions (OH^-). However, the kinetics and magnitude of the reaction development depend on several factors, such as alkali concentration, relative humidity, temperature, etc [1]. Despite that, the three main oxides from the chemical composition of the binder materials play important roles in the whole process and ASR damage development.

Overall, the hydration of Portland cement releases a significant amount of $Ca(OH)_2$, which is further combined with SiO_2 to form C-S-H and with Al_2O_3 forming ettringite and calcium monosulfoaluminate hydrate, decreasing its concentration in the interstitial concrete pore solution. The remaining soluble ions of Ca^{2+}, thus, play two important roles in the ASR development: exchange with alkalis in the reaction products (alkali recycling); and changing the composition and swelling properties of ASR reaction products [26]. Results suggest that the higher the calcium concentration in concrete pore solution, the higher the degree of reactive silica dissolution from aggregates and further ASR damage development [33]. Moreover, calcium increases the ASR-gel's viscosity, yield strength, E-modulus, and swelling behaviour, resulting in larger stress magnitudes within the concrete [26,33,34]. Conversely, increasing SiO_2 and Al_2O_3 contents in the blended binder materials trend to slow down ASR-kinetics and decrease the ultimate expansion amplitudes on the affected concrete. In general, the increase in SiO_2 contribute to bound alkalis, form more C-S-H, and reduce portlandite in the concrete pore solution [19,20]. Nevertheless, the presence of aluminum in the pore solution, either from SCMs or cement, is absorbed on the surface of reactive SiO_2 from aggregates, slowing both the dissolution of SiO_2 and formation of reaction products [8].

The chemical composition of supplementary cementing materials is generally characterized by lower calcium content than Portland cement (Figure 10.1) [23]. Considering the aforementioned influences of CaO, SiO_2 and Al_2O_3 on ASR development, also the overall agreement in the literature in which the higher the replacement level of PC by SCMs, the higher the effectiveness of the concrete mixtures to suppress ASR. Therefore, it is pretty reasonable that locating and mapping different areas with different binder mixtures could indicate the best regions to efficiently mitigate ASR. Yet, this approach for optimizing the selection of raw materials to avoid and or mitigate ASR in concrete has not been explored in the literature, leaving room for further development in the area.

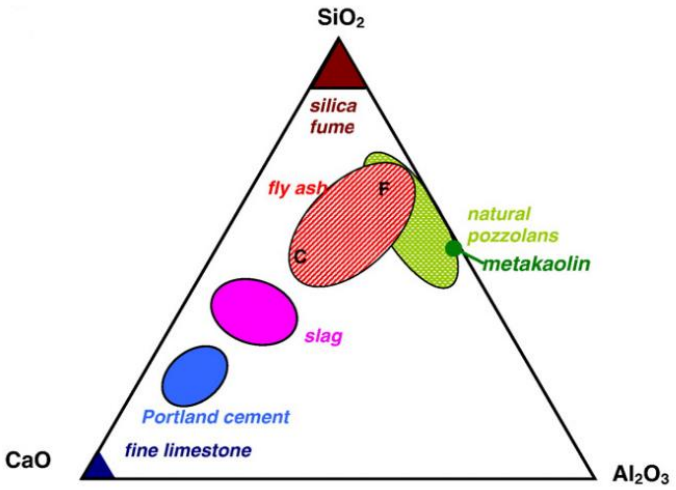

Figure 10.1: CaO–Al2O3–SiO2 ternary plot of cementing materials [23] (*reproduced with permission of Elsevier*).

10.2.3 Assessing ASR-induced expansion and deterioration

10.2.3.1 ASR-induced expansion

Among the various test procedures currently used to identify the potential reactivity of aggregates in concrete, one may mention the accelerated mortar bar test - AMBT [38,39] and the concrete prism test – CPT [40,41]. The AMBT allows the assessment of ASR potential reactivity of coarse or fine aggregates within 16 days. Mortar specimens are manufactured and demoulded after 24 hours, followed by 24 hours curing period in water at 80°C; afterwards, the specimens are immersed in a highly concentrated alkaline solution (i.e., 1M NaOH) at 80°C for further 14 days. Although this method can provide an interesting fast screening of ASR potential reactivity, it has been shown that false negatives and false positives can be found due to the severe conditions of exposure of mortars

[42]. Moreover, there are criticisms regarding the use of SCMs as the exposure period in the test is too short to allow significant pozzolanic reactions [2,42–45]. On the other hand, the CPT (ASTM C1293/ CSA A23.2-14A) often provides more reliable results which are closer to what is experienced in the field. Moreover, it can better classify aggregates' reactivity and more precisely appraise concrete mixtures incorporating a wide variety of binder compositions in the laboratory [2,46,47]. In the CPT method, concrete prisms are moulded and cured in the moist-curing room over 24 hours. They are then demoulded and stored at 38^{o}C and 100 of RH for either one year (in the case of evaluating the reactivity of the aggregate) or two years (while assessing preventive measures). As a result, the total content of binder materials and the water-to-cement (or binder) ratio are roughly fixed (i.e., narrow ranges are provided) in the mix. Furthermore, the amount of alkalis in the system is boosted by adding reagent NaOH grade to the mixing water so that the equivalent alkali content (Na_2O_e) of the cement is raised to 1.25% (by mass).

Even though the CPT is considered the most reliable existing test procedure, one crucial disadvantage of the method is its long testing period (1-2 years). In this regard, trying to solve this issue, accelerated CPT procedures were proposed in the ’90s [48]. Among them, an accelerated CPT version (i.e., ACPT) conducted at 60^{o}C stood out, showing promising results worldwide. It has been found that reliable results might be achieved within either 3-4 months or 6-8 months for evaluating the potential reactivity of aggregates or the efficiency of preventive measures, respectively. This method has been standardized in Europe by RILEM [49]. However, in North America, it is not currently a standard since some issues related to alkalis leaching and essential variability in the test outcomes were observed [50].

10.2.3.2 **ASR-induced deterioration**

Compressive strength (CS)

Compressive strength is commonly used for structural concrete design. Yet, several past studies also aimed to use it to quantify AAR damage and development with more or less success. In AAR-affected concrete, the compressive strength is a mechanical property that is the least affected by the chemical reaction due to AAR microscopic features (i.e., mainly cracks within the aggregate particles). Significant reductions in compressive strength are only observed for high and very high expansion levels (i.e. >0.20%) as by [5,35], which disables its use for diagnostic purposes.

Stiffness Damage Test (SDT)

The Stiffness Damage Test (SDT) was first developed by Walsh (1965) for evaluating the quality of rocks specimens [51], being afterwards adapted for assessing concrete by Crouch [52]. The test procedure is based on a cyclic loading (in compression) of concrete specimens and can quantify the degree of damage or physical integrity of distressed concrete. Both researchers selected the use of fixed loads of either 5.5 or 10 MPa, respectively, at a loading rate of 0.10 MPa. The outcomes of the SDT are the modulus of elasticity, the hysteresis area or the dissipated energy (hysteresis area), the plastic deformation and the non-linearity index (NLI) [53,54].

Details on the test procedure and specific considerations on its application as a diagnostic tool for assessing ASR-affected concrete can be found in Sanchez et al. [53,55]. The method was found very promising for assessing AAR damage and progress in concrete and the authors indicated that 40% of the concrete design strength provided the best correlation between SDT output parameters (Stiffness Damage Index – SDI, Plastic Deformation Index - PDI and Non-Linearity Index - NLI) and the expansion of the ASR-affected concrete. However, since in most practical cases, the 28-day strength of aging concrete structures is unknown. Sanchez [53] suggested that the most suitable approach would be to first determine the compressive strength on cores extracted from locations that are not/less damaged in the structural member under investigation and then use 40% of this value for stiffness damage testing.

Damage Rating Index (DRI)

The Damage Rating Index (DRI) is a semi-quantitative microscopic analysis performed using a stereomicroscope (about 15-16 x magnification) where the petrographic damage features associated with AAR are counted through a grid of 1 cm^2 (i.e., 10 × 10 mm units) drawn on the surface of a polished concrete section [56,57]. The number of counts corresponding to each type of petrographic characteristic is then multiplied by a set of weighting factors, whose purpose is to balance their relative importance towards the distress mechanism. The final DRI value is normalized to an area of 100 cm^2; overall the higher the DRI number, the greater the deterioration of affected concrete [53,56,58]. The DRI is a complementary petrographic tool aiming to quantify the “damage degree” between different members from an affected structure or as a function of time within a specific concrete member.

A complete review of the DRI development and specific considerations on its application are given in Sanchez et al. [53,56,58]. The authors used the DRI to evaluate AAR distress with a wide range of reactive aggregates, different concrete strengths (25-45 MPa) and expansion levels (0.05% to 0.30%). It was found that the DRI is a powerful tool to detect AAR damage/progress in concrete whatever the aggregate type and concrete strength used, mainly when the aggregate particles are analyzed down to 1 mm. Moreover, [53,56,58] proposed the so-called "extended DRI version" in which the microscopic distress features could be presented in absolute values (counts) and relative (%) disregarding the weighting factors, giving a more comprehensive assessment of the damaged concrete specimens.

10.3 **Scope of the work**

As stated above, although a number of techniques, tools, and protocols have been developed in the past to assess and mitigate ASR initiation and development in the field, there is currently a need for improvement and optimization on the use of materials without losing concrete performance. This study aims to propose a framework for optimizing the selection of raw materials towards the prevention and/or mitigation of ASR in concrete. The work is divided into three phases to achieve this goal: First, selection and pre-determination of the blended mixtures through a new proposed framework (ternary main oxides plot). Second, based on the pre-determined blended mixtures, mortar bars and concrete specimens were manufactures in the laboratory incorporating two types/nature of reactive aggregates (i.e., Greywacke coarse and Polymictic fine) and maintained under conditions enabling the development of ASR in the laboratory (i.e., AMBT, ACPT, and CPT). Finally, at selected exposure periods, according to each accelerated method, the length variation, microscopic (i.e., Damage Rating Index) and mechanical (i.e., Stiffness Damage Test, Modulus of Elasticity, and Compressive Strength) analyses were conducted and a comprehensive evaluation of the impact of the distinct binder mixtures on ASR-induced deterioration was performed.

10.4 **Experimental program**

10.4.1 **Materials**

The accelerated mortar bar test (AMBT) as per ASTM C 1567 [59], accelerated concrete prism test (ACPT) as per CSA A23.1-14 (Annex B) [41], and concrete prism test (CPT) as per ASTM C1293 [40]

were conducted incorporating two highly reactive coarse (crushed Springhill) and fine (natural Texas sand) aggregates as described in Table 7.1. One verifies that the coarse aggregates ranged from 5 to 20 mm in size. Moreover, nzzon-reactive fine (NF) and coarse (NC) aggregates were combined with the reactive aggregate materials for concrete manufacturing. Table 10.2 provides information on the chemical composition (obtained through X-Ray Fluorescence) of the different powder materials used in this research: i.e., PC-GU type (equivalent to ASTM type I), blast furnace slag, fly ash class F, silica fume, metakaolin, and calcium hydroxide.

Table 10.1: Reactive (ASR) and non-reactive (NR) aggregates used in the research.

Aggregate		Reactivity	Rock Type	Specific gravity	Absorption (%)	AMBT[a)] (%)
Coarse	SPH	ASR	Greywacke	2.71	0.70	0.31
	LC	NR	Crushed limestone	2.78	0.42	0.02
Fine	TX	ASR	Polymictic sand	2.60	0.89	0.85
	NF	NR	Natural derived from granite	2.60	0.82	0.08

[a)] Results at 14 days of curing of the AMBT (ASTM C 1260) carried out on the aggregates selected

Table 10.2: Chemical composition of the binder materials.

	PC	Slag	FA	SF	MK	$Ca(OH)_2$
SiO_2 (%)	20.10	36.64	56.31	92.86	52.48	0.93
Al_2O_3 (%)	5.03	11.14	23.27	0.05	44.35	0.13
CaO (%)	61.93	37.32	10.29	0.62	0.12	72.73
Fe_2O_3 (%)	3.80	0.40	3.57	0.12	0.61	0.07
SO_3 (%)	3.38	0.37	0.19	0.07	0.04	-
MgO (%)	2.42	12.15	1.07	0.19	0.08	0.45
Na_2O_{eq} (%)	0.91	0.63	3.17	0.52	0.38	0.05
C_3S (%)	43.24	-	-	-	-	-
C_2S (%)	25.02	-	-	-	-	-
C_3A (%)	6.90	-	-	-	-	-
C_4AF (%)	11.56	-	-	-	-	-
Specific Gravity	3.12	2.91	2.01	2.20	2.29	2.23
Lost on Ignition (%)	2.91	0.49	0.98	5.05	0.69	25.54

10.4.2 Mix-proportions and manufacture of the concrete specimens

10.4.2.1 Determination of the distinct binder compositions

The blended binder materials' proportion was pre-determined based on fixed percentages of the three main oxides found in cementing materials (i.e., Portland cement, slag, fly ash, silica fume, metakaolin, and calcium hydroxide). To clarify this goal, Figure 10.2a was developed based on the data gathered from the literature [12,20,35–37]; the plot illustrates different binder mixtures and demonstrates the trend of ASR prevention towards the “chemical proportions” of the main oxides found in cementing materials. One verifies that the legends indicate the overall final expansion of concrete mixtures

incorporating high or highly reactive aggregates, i.e., marginal (about 0.05% or lower), moderate (about 0.12%), high (about 0.20%), and very high (about 0.30% or higher). Likewise, Figure 10.2b displays the ternary plot, yet including ten different points (i.e., control mixture made of Portland cement as only binder material and mixtures from #1 to #9), which will be explored in this study, focusing on mapping regions in the plot with the best behaviour to mitigate ASR. It is worth highlighting that to elaborate the ternary oxides plot, the sum of CaO, SiO_2, and Al_2O_3 is equal to 100%. For instance, the chemical composition of a general use cement displayed in Table 10.2 corresponds to the following point: (71.1%, 23.1%, 5.8%) for CaO, SiO_2, and Al_2O_3, respectively, in the ternary oxides plot. Table 10.3 provides the percentage of each oxide (i.e., CaO, SiO_2, and Al_2O_3) of the pre-selected point and the control mixtures. It is worth noting that the proportions of the binder materials used to achieve all nine points are described in the following sections.

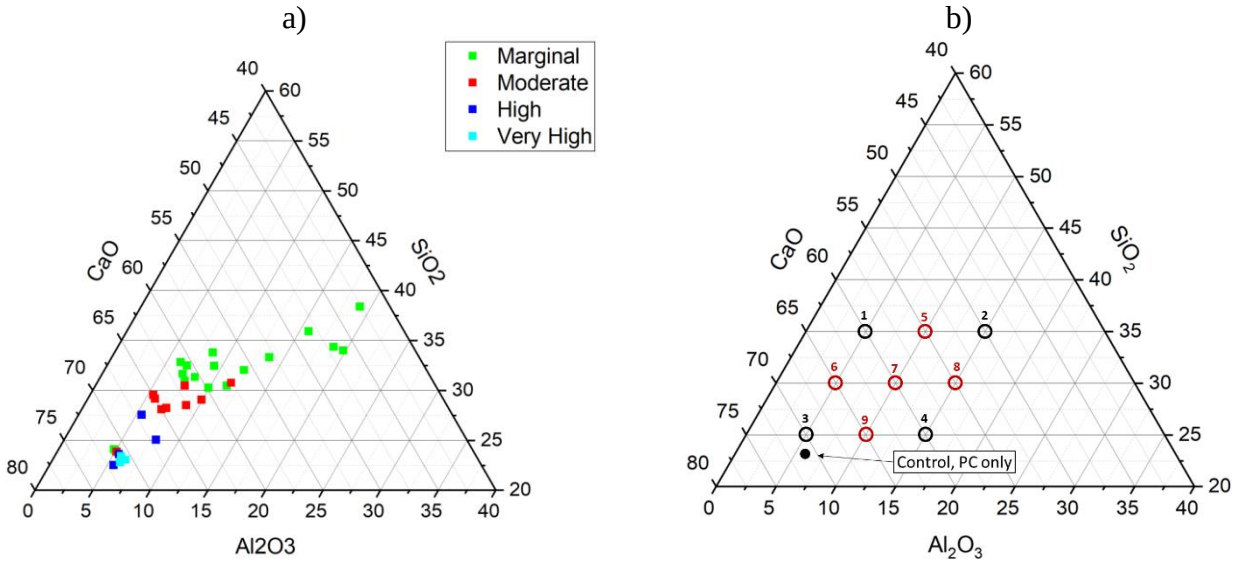

Figure 10.2: Ternary oxides plot of a) data gathered from the literature [12,20,35–37] and b) including the studied points

Table 10.3: Oxides composition for each pre-selected point in the ternary plot.

	Ternary oxides composition (%)									
	Control	**#1**	**#2**	**#3**	**#4**	**#5**	**#6**	**#7**	**#8**	**#9**
CaO	71.1	60	50	70	60	55	65	60	55	65
SiO_2	23.1	35	35	25	25	35	30	30	30	25
Al_2O_3	5.8	5	15	5	15	10	5	10	15	10

10.4.2.2 **Manufacturing of specimens (mortar bars and concrete cylinders)**

The current research was divided into two phases. In the first phase, the expansion behaviour of twenty different mortar bar mixtures, incorporating the two distinct reactive aggregate types (displayed in Table 7.1) and the nine different ternary plot points plus control mixture, was evaluated through the AMBT as per ASTM C 1567 [59] (Table 10.4). One verifies that achieving precisely each of the points mentioned above (Table 10.3) was not an easy task; thus, a maximum variation range of ± 0.5% for each oxide was adopted.

Table 10.4: Mortar mixtures for both reactive aggregates (i.e., crushed SPH and TX), according to ASTM C 1567.

Group ID	Fine materials (g)						Water (g)[a)]	Fine Aggregates
	Cement	Sg	FA	SF	MK	$Ca(OH)_2$		
Control	440	-	-	-	-	-	206.8	990g of Tx or SPH aggregates
#1	374	-	-	66	-	-		
#2	279.4	-	-	15.4	85.8	-		
#3	378.4	-	-	19.8	-	-		
#4	132	-	-	4.4	110	193.6		
#5	347.6	-	-	44	48.4	-		
#6	404.8	-	-	35.2	-	-		
#7	363	-	63.8	-	13.2	-		
#8	347.6	-	-	-	92.4	-		
#9	343.2	-	-	-	48.4	48.4		

[a)] The amount of water of mixture #4 was adjusted based on the contribution of water from $Ca(OH)_2$

In the second phase, a total of two-hundred and eighty cylinders with 100 by 200 mm in size, were fabricated as per ASTM C1293 [62] and investigated in this study through ACPT [41] and CPT [40]. Table 10.5 summarizes the concrete mix designs employed in this work. All twenty concrete mixtures were mix-proportioned as per ASTM C1293 to present the same water to binder ratio (w/b of 0.45) and amount of binder materials (420 ± 10 kg/m^3). Though, adjustments were made in the volume of non-reactive aggregates to maintain the volume of reactive aggregate constant and keep the correct design in 1 cubic meter of concrete. It worth mentioning that due to testing capacity issues, ACPT was not performed for all mixtures as for AMBT and CPT, instead, only the control, #1, #2, #3, and #4 mixtures (black marked points in Figure 10.2b) for both reactive aggregates were exposed to 60 ^{o}C. Moreover, it should be highlighted that the alkali loading of all mixtures were fixed as 1.25% m^3 of the total binder mass, instead of cement mass as suggested by ASTM C1293. Thus, regardless of the materials used or the point selected in the ternary plot, the amount of alkalis is constant.

Table 10.5: Concrete mix proportions.

Mixture	w/b = 0.45		Aggregates (kg/m³)		SCMs (kg/m³)				
	Water (kg/m³)	Cement (kg/m³)	Fine	Coarse	SG	FA	SF	MK	$Ca(OH)_2$ [a)]
SPH-Control	189	420.0	836	938					
SPH-#1		357.0	813				63.0		
SPH-#2		266.7	801		56.7		14.7	81.9	
SPH-#3		361.2	815				18.9		39.9
SPH-#4		126.0	738				4.2	105.0	184.8
SPH-#5		331.8	806				42.0	46.2	
SPH-#6		386.4	824				33.6		
SPH-#7		346.5	803			60.9		12.6	
SPH-#8		331.8	808					88.2	
SPH-#9		327.6	806					46.2	46.2
TX-Control	189	420.0	765	1020					
TX-#1		357.0		996			63.0		
TX-#2		266.7		984	56.7		14.7	81.9	
TX-#3		361.2		998			18.9		39.9
TX-#4		126.0		918			4.2	105.0	184.8
TX-#5		331.8		989			42.0	46.2	
TX-#6		386.4		1007			33.6		
TX-#7		346.5		985		60.9		12.6	
TX-#8		331.8		991				88.2	
TX-#9		327.6		988				46.2	46.2

[a)] The amount of water of mixture #4 was adjusted based on the contribution of water from $Ca(OH)_2$

Twenty-four hours after casting, the samples were demoulded, and small holes (5 mm in diameter by 15 mm deep) were drilled at the two flat ends of the samples, in which steel gauge studs were glued in place with a fast-setting cement slurry for longitudinal expansion measurements. Afterwards, the samples were left to harden at 20 °C and 100% RH over 24 hours (totalizing 2 days since casting) before the zero reading was taken. Next, all samples were finally placed in sealed plastic buckets lined with a damp cloth and stored at 60 °C (ACPT) and 38 °C (CPT), and both at 100% RH. The ASR-affected cylinders were monitored for length variations overtime for 180 days for ACPT and 720 days CPT. As per ASTM C1293, before each periodic measurement, the buckets were cooled to 23 °C for 16 ± 4 h. Then, to perform each test selected (i.e., mechanical, microscopy and porosity), the samples were conditioned/prepared as per the following section.

10.4.3 Assessment of the ASR development in the concrete

The comprehensive investigation program carried out throughout this research on the concrete cylinder was performed after two different periods of exposure for each ACPT (i.e., 90 and 180 days) and CPT

(i.e., 360 and 720 days) method. The multi-level data gathered includes mechanical testing (SDT, elastic modulus, and compressive strength evaluations) and semi-quantitative petrographic analysis (DRI).

10.4.3.1 **Damage Rating Index (DRI)**

A semi-quantitative petrographic analysis, using the DRI, was performed on one specimen from each concrete mixture at determined periods of evaluation, according to the method described by Sanchez [53,56]. First, the samples were cut in half axially, polished by a hand polishing device, which uses diamond-impregnated rubber disks (nº. 50-coarse, 100, 400, 800, 1500 to 3000-very fine) and 1 cm^2 grids were drawn on the surface of the polished sections. Then a stereomicroscope (16× magnification) was used to perform the test. The DRI final number presented hereafter is the normalized 100 cm^2 value.

10.4.3.2 **Compressive Strength**

Compressive strength was measured through two different approaches with different and specific goals. First, to characterize all mixtures at 28 days compressive strength, samples were wrapped and placed at 12 °C, since some of the specimens contained highly reactive aggregates and ASTM C39 method could not be followed as they could develop some AAR. The cylinders were maintained at 12 °C for 47 days, according to the maturity concept as by ASTM C 1074. Moreover, considering the use of SCMs and the later strength gain, two additional measurements were taken after 93, 150 and 300 days (maturity equivalent to 56, 90 and 180 days, respectively). Second, the compressive strength measurements were carried out on three specimens from each concrete mixture after being subjected to SDT to verify the compressive strength loss of the material as ASR develops. This procedure was adopted and considered valid after Sanchez et al. [53,56] confirmed the largely non-destructive character of the SDT.

10.4.3.3 **Stiffness Damage Test (SDT)**

The SDT procedure was performed following Sanchez et al. publications [53,55,63], i.e. using five loading/unloading cycles at a controlled loading rate of 0.10MPa/s with a maximum load corresponding to 40% of the concrete strength. To characterize the compressive strength of all mixtures, the specimens were wrapped and placed at 12 °C, since some of the specimens contained highly reactive aggregates and CSA23.2-9C [64] method could not be followed as they could develop

some AAR. Therefore, for the test procedure, the samples were re-conditioned/prepared under 100% RH for 48 hours [65], and the test was conducted. The results obtained hereafter is an average value from three different specimens tested at each expansion level.

10.5 **Results**

10.5.1 **ASR Kinetics**

This section presents ASR expansion kinetics and amplitude results for all mixtures developed in the laboratory. Figure 7.2 displays the expansion results obtained through the accelerated mortar bar test (AMBT). A wide range of expansion kinetics was obtained as a function of the reactive aggregate and different binder compositions tested. In general, TX mixtures developed a faster expansion rate and amplitudes (Figure 7.2b) than mixtures made of crushed SPH aggregate (Figure 7.2a). However, the control mixtures of both aggregates yielded extremely high expansion levels at 14 days of exposure (i.e., 0.30% for SPH and 0.86% for TX). Moreover, the results demonstrate that all "chemically controlled" mortar mixtures (from #1 to #9) slowed ASR-kinetics for both crushed SPH and natural TX; yet the efficiency of the mortar mixtures to lessen the expansion development were more expressive for samples made of TX. Overall, the mixtures named #1, #2, #5, and #8 were the only mixtures able to mitigate ASR to levels below the limits proposed by ASTM C1567 and CSA A23.2-28A (i.e., 0.10% at 14 days) for both reactive aggregates, while #6 and #7 mixtures lowered the expansion to below 0.10% only for mortar bars made of SPH.

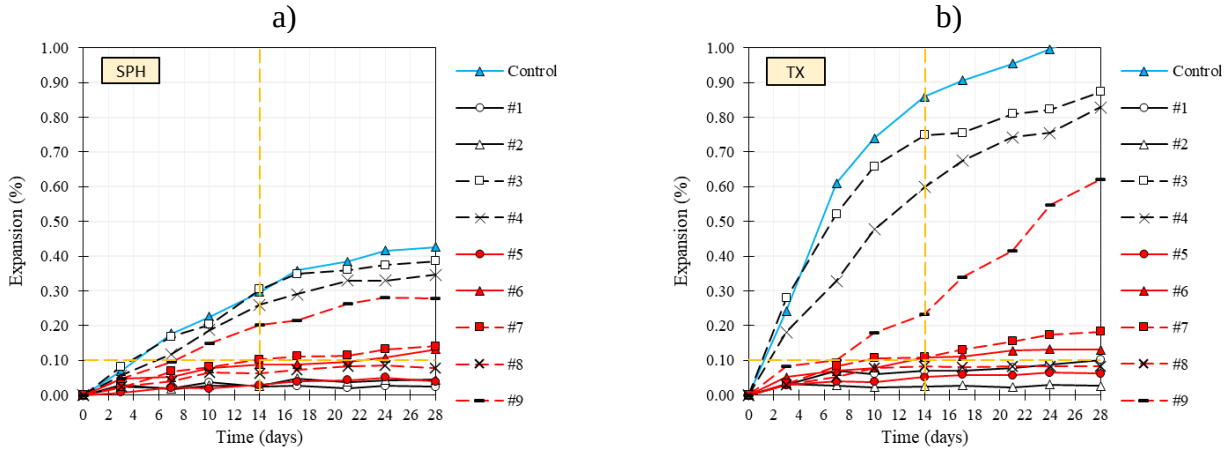

Figure 10.3: Accelerated mortar bar test (AMBT) expansion of mortar bars made of a) SPH crushed coarse and b) TX fine aggregates.

The expansion obtained for concrete specimens' are displayed in Figure 10.4 (through the ACPT) and Figure 10.5 (through CPT) as a function of time, over 180 days for ACPT, as per CSA A23.1-14 (Annex B) [41], and over one year of exposure (up to date results) for CPT. Correspondingly to ABMT results, rather for ACPT and CPT, mixtures made of TX fine aggregate showed faster kinetics and higher expansion amplitudes. Likewise, all mixtures (i.e., #1 to #4 for ACPT and from #1 to #9 for CPT) displayed lessen or at least exhibited lower but relatively close values (e.g., #3 mixture) than SPH and TX control specimens. The ACPT evaluation (i.e., 180 days) verifies that the vertical dashed line at 90 and 180 days indicates comparable results with CPT at 360 and 720 days [60,61]. After 180 days of curing at 60 ^{o}C, the only concrete mixture which displayed expansion amplitudes bellows 0.04% for both aggregates was #2 (i.e., 0.01% for SPH and 0.02% for TX). Curiously, #1 mixtures exhibited slightly higher expansion for concrete made of SPH than for TX, 0.05% and 0.04%; all others demonstrated opposite behaviour, #4 mixtures yielded 0.27% and 0.32% of expansion for SPH and TX, respectively, while #3 values were 0.41% for SPH and 0.57% for TX, the closest values with control specimens. Similar trends were also seen for the CPT method; #3 displayed the highest expansion values after 360 days of curing among the blended binder mixtures from #1 to #9 (i.e., 0.43% for SPH and 0.75% for TX-made concrete). Likewise, #4 achieved 0.34% and 0.62% of expansion for SPH and TX and followed by #9 (0.30% for SPH and 0.51% for TX), #7 (0.22% for SPH and 0.43% for TX), and #6 (0.12% for SPH and 0.33% for TX). The remaining mixtures (i.e., #1, #2, #5, and #8) gathered expansion values bellows 0.04% at 360 days of curing at 38 ^{o}C.

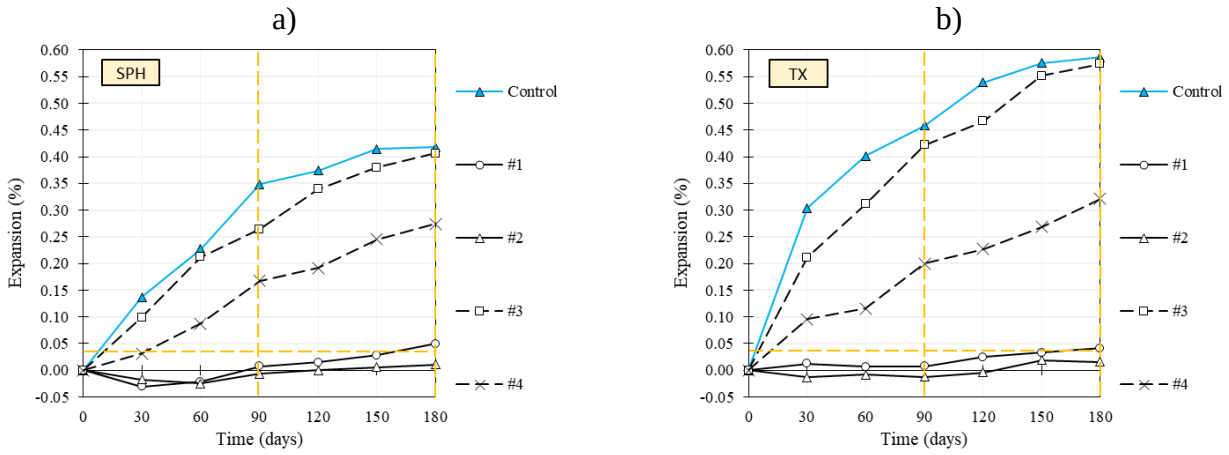

Figure 10.4: Accelerated concrete prism test (ACPT) expansion of concrete mixtures of a) SPH crushed coarse and b) TX fine aggregates.

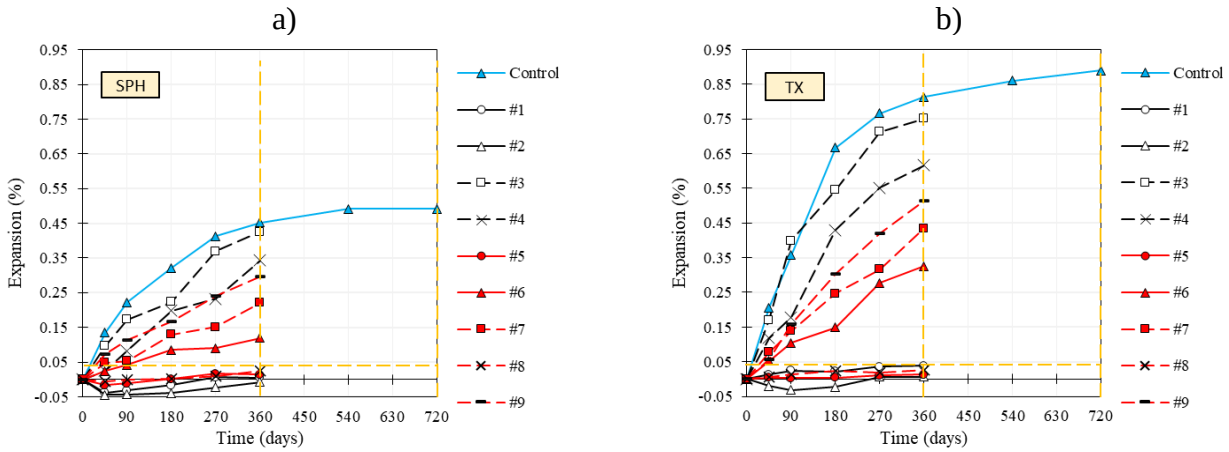

Figure 10.5: Concrete prism test (CPT) expansion of concrete mixtures made of a) SPH crushed coarse and b) TX fine aggregates.

10.5.2 Damage rating index (DRI)

Figure 7.3 presents the total DRI numbers obtained from the ASR-affected concrete specimens for ACPT (Figure 7.3a and b) and CPT (Figure 7.3c and d) methods. A complete description of the microscopic features over the ASR development of the SCMs-made concrete and the different types of reactive aggregates is given in the discussion section. Globally, the results suggest that all DRI numbers increase as a function of the specimens' expansions (i.e., the higher the expansion of the concrete mixtures, the higher the total DRI number) for both exposure conditions. Moreover, the ASR-reactive aggregates displayed somewhat similar values of DRI and almost with a linear behaviour with the expansion degrees (Figure 7.3). However, it verifies that #3 showed a higher DRI number (i.e., 977) than the control mixture (i.e., 925) made of SPH reactive coarse aggregate; whereas #4, #1, and #2 exhibit DRI numbers of 784, 345, and 206, respectively. Likewise, the DRI number of TX-made concrete specimens exposed to ACPT was equal to 1047, 1014, 890, 219, and 208 at 180 days of curing, respectively. The DRI number of the concrete mixtures evaluated through the CPT followed similar trends to ACPT after 360 days of curing. Overall, control mixtures reached the higher values (i.e., 1091 and 1117 for SPH and TX), and followed by #3 (i.e., 895 for SPH and 1052 for TX), #4 (i.e., 856 for SPH and 994 for TX), #9 (i.e., 794 for SPH and 914 for TX), #7 (i.e., 657 for SPH and 880 for TX), and #6 (i.e., 452 for SPH and 747 for TX), while mixtures #1, #2, #5 and #8 have all displayed DRI number lower than 200. The only exception was the #1 mixture made of TX, which achieved a DRI number of 280.

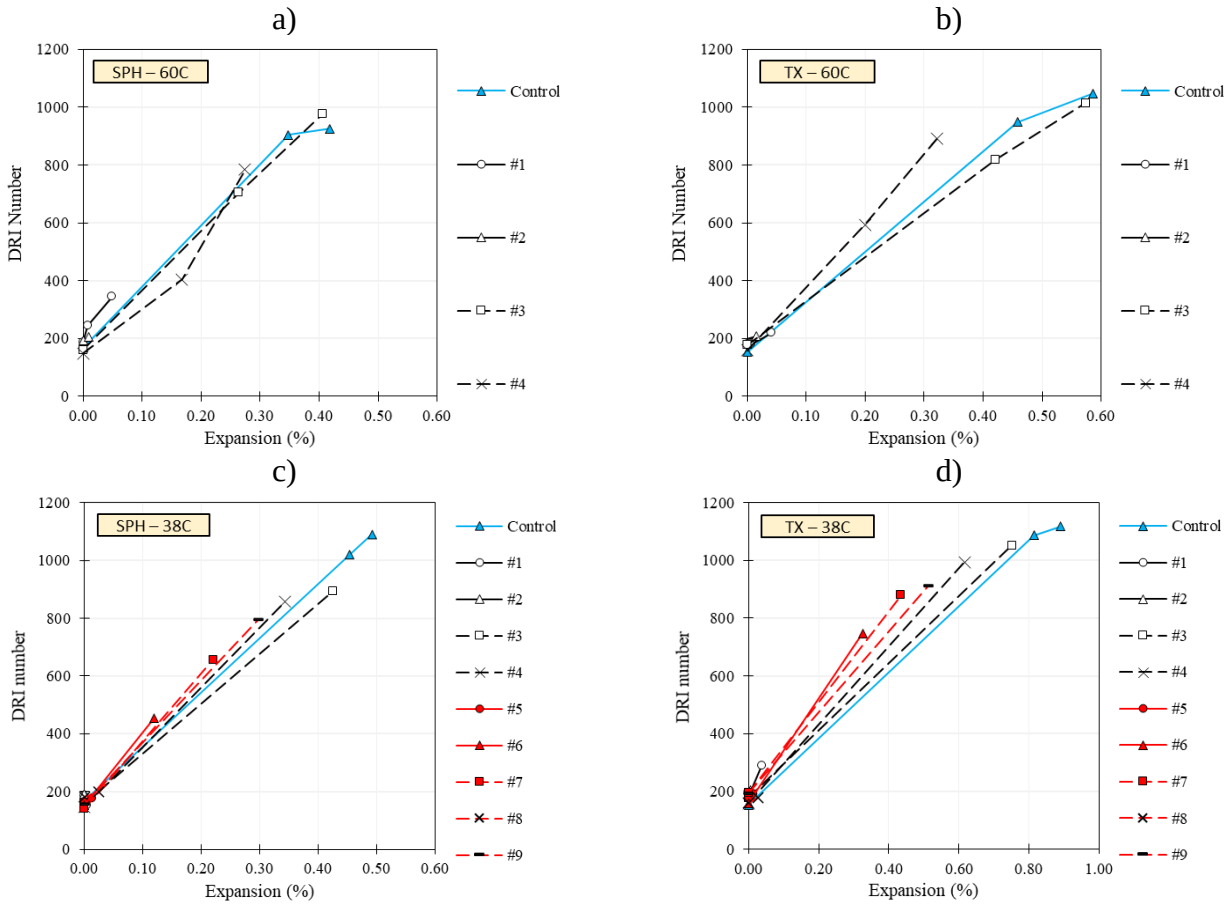

Figure 10.6: Damage Rating Index vs. expansion levels: ACPT of mixtures made a) SPH crushed coarse and b) TX fine aggregates; and CPT of mixtures made c) SPH crushed coarse and d) TX fine aggregates.

10.5.3 **Mechanical properties assessment**

In this section, the stiffness damage index (SDI) and the losses in modulus of elasticity (ME) and compressive strength (CS) of the various concrete mixtures are investigated. The mechanical data presented hereafter for ACPT and CPT methods displays the ratio of values obtained from an ASR-induced expansion over the values gathered on sound concrete specimens presenting “equivalent maturity” than the damaged samples as previously discussed in 10.4.3. Moreover, one may notice that the mentioned mechanical ratios are displayed in the function of their respective expansion amplitudes to better visualize the mitigative behaviour of the binder compositions after ASR has already started.

10.5.3.1 **Compressive strength (CS)**

Figure 7.4 illustrates the compressive strength reductions for the different concrete mixtures investigated and obtained at each selected "free" expansion level, for ACPT made of a) SPH reactive coarse and b) TX reactive fine aggregates; likewise, for CPT made of c) SPH reactive coarse and d) TX reactive fine aggregates. In general, the CS was found to decrease in a somewhat modest way in comparison with ME. Moreover, the control, #3, and #4 specimens yielded the highest CS losses (i.e.., 0.28, 0.22, and 0.19) for SPH coarse mixtures, while #1, and #2 presented gain of CS (i.e., -0.02 and -0.04). Similar trends can also be seen for TX-made concrete mixtures, control, #4, #3, #1, and #2 achieving CS losses of 0.26, 0.20, 0.17, 0.07, and -0.02 after 180 days of curing, respectively. Furthermore, for CPT, the overall behaviour of the concrete mixtures followed a somewhat similar trend. Yet, concrete mixtures #7 (i.e., 0.21 and 0.22 for SPH and TX) and #9 (i.e., 0.16 and 0.21 for SPH and TX) yielded higher losses than #4 mixture (i.e., 0.15 for both SPH and TX aggregates), even for lower expansion amplitudes than #4. The mixtures incorporating SCMs that reached the higher losses of CS was #3 (0.28 for both aggregates), while #6, #8, #1, #5, and #2 displayed values of about 0.16 and 0.11 (SPH and TX), 0.04 (both aggregates), -0.01 and 0.01 (SPH and TX), and -0.01 and -0.02 (SPH and TX), respectively.

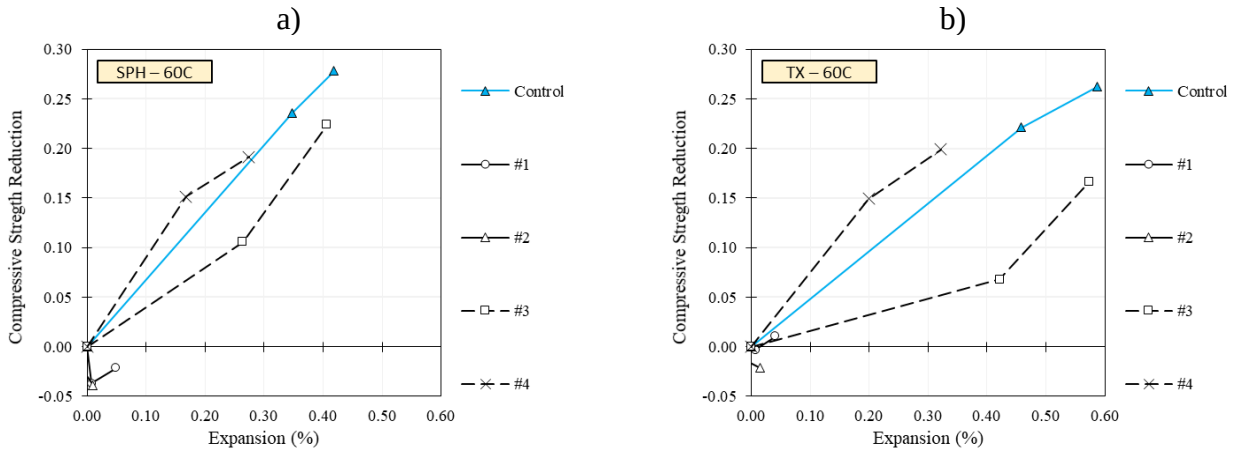

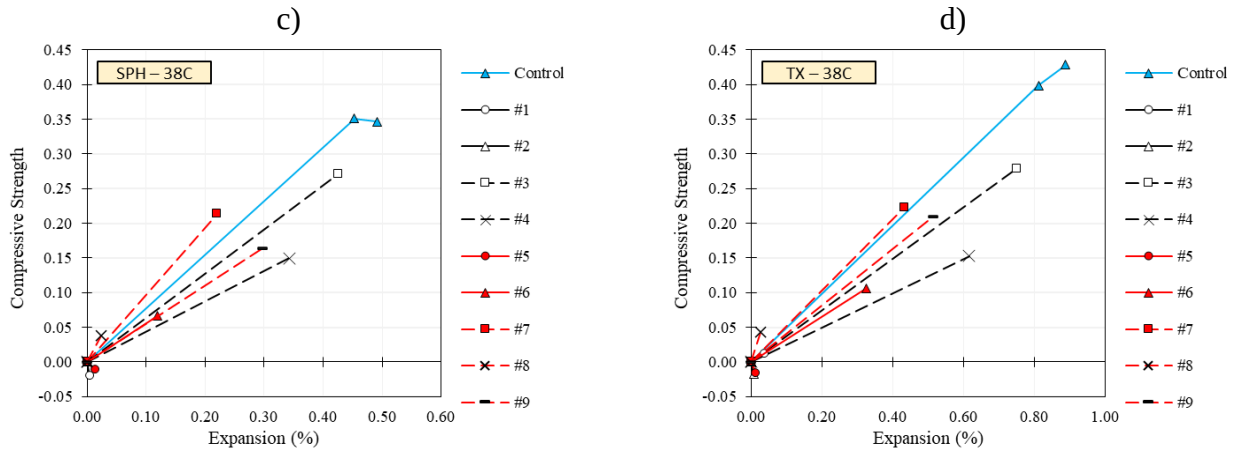

Figure 10.7: Compressive strength reduction vs. expansion levels: ACPT of mixtures made a) SPH crushed coarse and b) TX fine aggregates; and CPT of mixtures made c) SPH crushed coarse and d) TX fine aggregates.

10.5.3.2 **Stiffness damage index (SDI)**

Figure 7.5 illustrates the SDI obtained in this work through the *stiffness damage test* (SDT) method as per Sanchez et al. [53,55,63] of the different concrete mixtures investigated. Generally, SDI values increased towards ASR development for all mixtures; moreover, the higher the expansion amplitudes, the higher the SDI. By incorporating different reactive aggregates and supplementary cementing materials, SDI of ACPT were found to range from about 0.09 (#2 mixture) at 0.00% of expansion to 0.32 (Control) at 0.49% for SP-made concrete, and from about 0.08 (#2 mixture) at 0.00% to 0.38 (#3 mixture) at 0.57% for TX after 180 days of curing at 60 ^{o}C. For the CPT method, the control specimens displayed more distinguished values than the mixtures containing SCMs, achieving SDI values of 0.40 for SPH and 0.47 for TX at 360 days of exposure. The mixtures named as #3, #4, #6, #7, and #9 ranged from 0.17 (#6) at 0.12% of expansion to 0.35 (#3) at 0.43% of expansion for SPH-made concrete, whereas ranged from 0.26 (#6) at 0.33% to 0.39 (#4) at 0.62% of expansion for TX-made concrete. The remaining mixtures (i.e., #1, #2, #5, and #8) slightly change from their initial SDI values, averagely about 0.12.

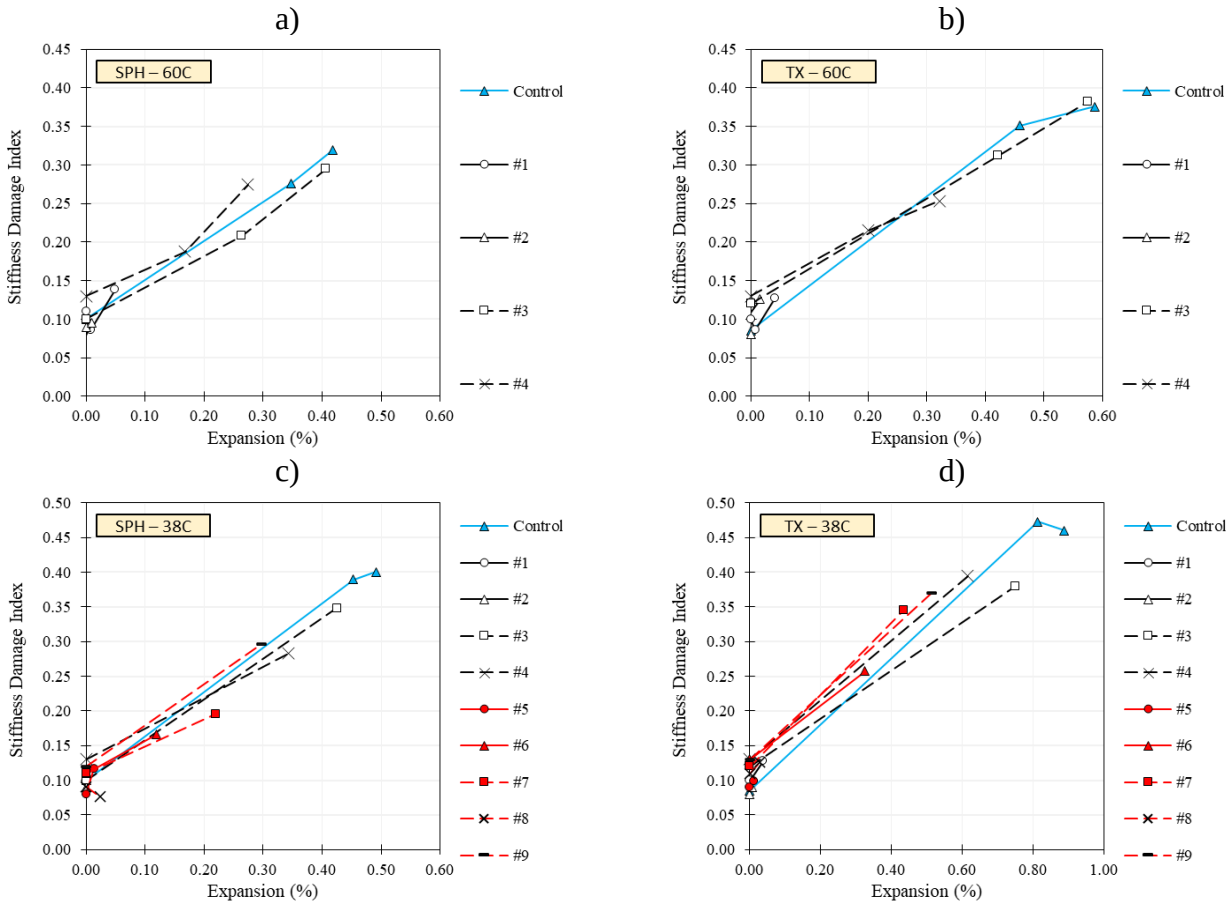

Figure 10.8: Stiffness Damage Index vs. expansion levels: ACPT of mixtures made a) SPH crushed coarse and b) TX fine aggregates; and CPT of mixtures made c) SPH crushed coarse and d) TX fine aggregates.

10.5.3.3 **Modulus of Elasticity (ME)**

The ME reductions (Figure 7.6a and b for ACPT and Figure 7.6c and d for CPT) presented an increase as a function of the expansion (i.e., the higher the expansion level, the higher the decrease in ME) for almost all mixtures. For the specimens exposed to ACPT, the control mixtures displayed the highest ME losses (i.e., 0.50 and 0.58 for SPH and TX) and, besides not exhibiting the greater expansion between SCMs-made concrete mixtures (i.e., from #1 to #4), #4 mixtures yielded the higher losses in ME disregarding control specimens. In general, the values obtained were about 0.45 for SPH-concrete at 0.27% of expansion and 0.52 for TX at 0.32% of expansion, whereas #3 concrete mixtures achieved 0.43 at 0.41% of expansion and 0.52 at 0.57% of expansion for SPH and TX-concrete, respectively. It is worth highlighting that the #1 mixture made of SPH demonstrated ME reduction of 0.13 at 0.05% of expansion; however, for concrete made incorporating TX, the value was around 0. Likewise, #2

mixtures for both SPH and TX aggregates did not develop ME losses for ACPT and CPT. However, the global results of specimens exposed to 38 ºC (i.e., CPT) demonstrated slightly higher results than ACPT. In which, the control specimens reached the higher losses (0.64 and 0.67 for SPH and TX at 360 days of exposure) and were followed by #3, #4, #6, #7, and #9 mixtures, i.e., values ranging from 0.33 to 0.59 for SPH-concrete and from 0.52 and 0.63 for TX-concrete. The concrete mixtures named #1, #2, #5, and #8 yielded ME losses values ranging from -0.01 (gain of ME) to 0.05.

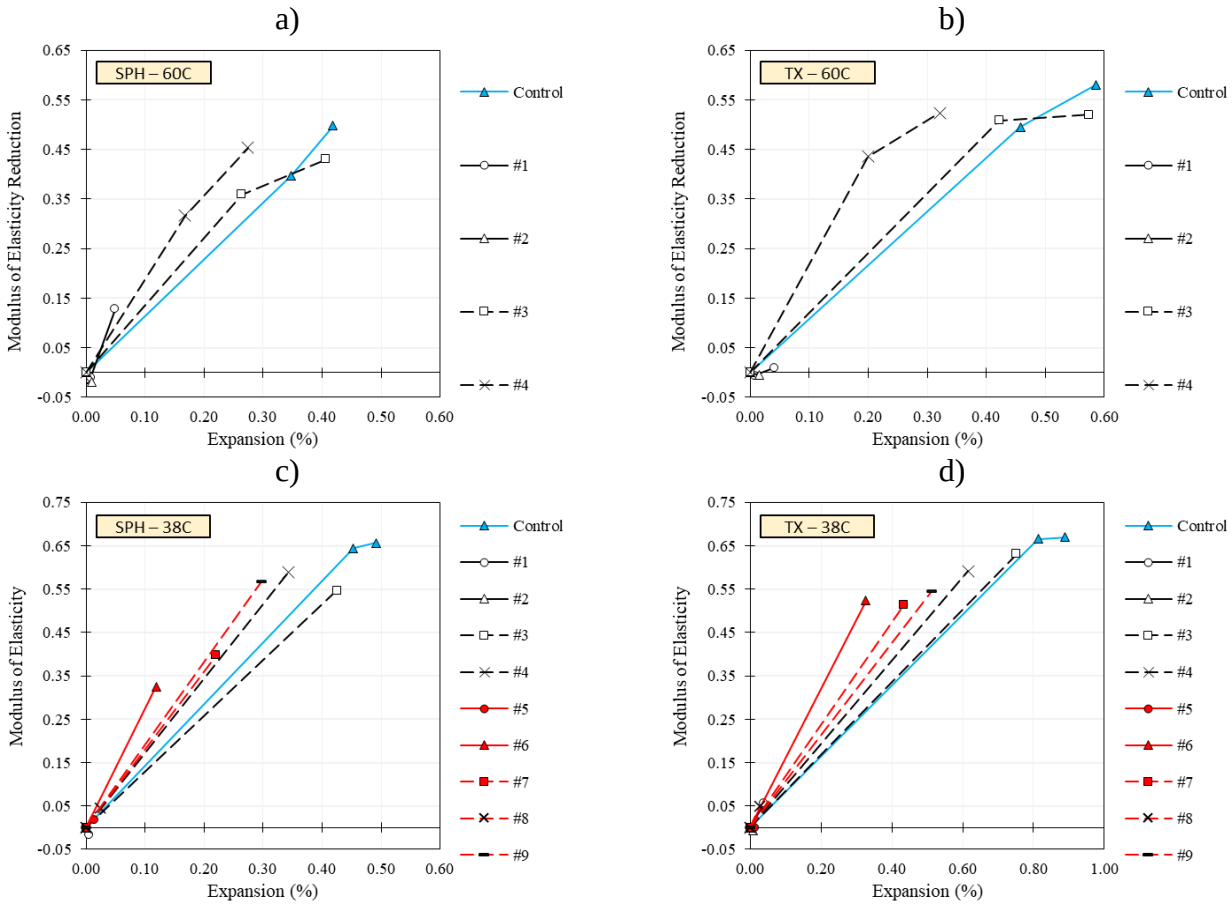

Figure 10.9: Modulus of Elasticity reduction vs. expansion levels: ACPT of mixtures made a) SPH crushed coarse and b) TX fine aggregates; and CPT of mixtures made c) SPH crushed coarse and d) TX fine aggregates.

10.6 **Discussions**

10.6.1 **ASR kinetics and induced development**

In this section, ASR-kinetics and expansion amplitudes of the various concrete mixtures are investigated and divided into three main topics. First of all, a discussion on the influence of the testing

method (i.e., accelerated mortar bar test – AMBT, accelerated concrete prism test – CPT, and concrete prism test – CPT) is presented. Second, the coupling is made between the "chemical composition" of the binder mixtures and ASR-induced expansion amplitudes; finally, a validation (statistical significance) of the expansion values is obtained through the different testing methods in this work.

10.6.1.1 Assessment of ASR-induced expansion through accelerated methods (AMBT, ACPT, and CPT)

Regardless of the testing procedure adopted in this research (i.e., AMBT, ACPT, and CPT), it is clear that concrete mixtures made of TX fine aggregate had faster ASR kinetics than SPH. This is likely explained by the general lower particle size of the TX that increases the surface contact area between the reactive particles and the alkali solution, thus accelerating the kinetics. Yet, it is quite curious that differently from CPT results, where TX-control displayed expansion amplitude was 0.86%, for ACPT, the maximum expansion yielded was 0.57%. Moreover, SPH-concrete specimens also displayed a similar trend; however, in a relatively smaller magnitude. Although not evaluated in the present study, this behaviour is likely explained by the fact that higher temperatures (i.e., 60 ^{o}C) potentially increase the alkali leaching from concrete specimens [61]. On the other hand, the expansion of SPH-made mortar bars soaked in 1M NaOH solution at 80 ^{o}C showed smaller results than both ACPT and CPT over 28 days of evaluation. Thus, one verifies that while the crushing process, some reactive mineral phases may be lost, which could significantly impact the reactivity of the assessed material.

Globally, the assessment of the effectiveness of distinct binder mixtures (i.e., from #1 to #9) to prevent alkali-silica reaction, the exposure conditions (i.e., AMBT, ACPT, and CPT) displayed a somewhat comparable trend; yet a few observations can be addressed. For instance, three out of nine binder mixtures (i.e., #1, #6, and #7) exhibits conflicting results among the accelerated testing methods regarding the limits to classify the reactivity of the mixtures. While in AMBT procedure, the samples named #1, #6, and #7 mitigated down SPH-made mortars to a non-reactive behaviour, for ACPT SPH-#1 yielded 0.05% after 180 days of exposure, whereas SPH-#6 and SPH-#7 tested through CPT method achieved 0.12% and 0.22% of expansion after "only" one year of exposure. Up to date, CPT SPH-#1 specimens have shown marginal expansion levels, yet the measurements until two years may confirm the behaviour of ACPT. Nevertheless, the results obtained in this work indicate the incompatibility between the mortar and concrete tests for assessing the efficiency of preventive measures. In this case,

a false-negative result has been gathered with AMBT, very likely due to either the crushing process of SPH or the extremely aggressive exposure condition.

10.6.1.2 **Influence of the distinct binder mixtures on ASR kinetics and expansion.**

The results demonstrate that all "chemically controlled" mixtures (from #1 to #9) displayed lessened or at least exhibited lower but close expansion values (e.g., #3 mixture) than SPH and TX control specimens. Moreover, considering the "position" of the points displayed in Figure 10.10a, the results showed a quite clear trend in which the farther the points are from the control mixture, the lower the expansion amplitudes at the end of the periods of analysis. In general, one of the reasons for this behaviour lies in the level of PC replacement by the distinct combinations of SCMs. However, peculiar trends pop out if the expansion amplitudes are analyzed closely with the ternary plot mixture points. In this regard, Figure 10.10a and b were developed to highlight the expansion behaviour of mixtures in which the Al_2O_3 content was fixed at three different portions (i.e., 5%, 10%, and 15%). In contrast, the amount of CaO was gradually replaced by SiO_2 (i.e., following the orientation of the blue dashed arrows). Overall, the increase in SiO_2 contribute to bound alkalis, form more C-S-H, and decrease portlandite in the concrete pore solution [19,20]. Furthermore, the amount of calcium either free in solution or combined as $Ca(OH)_2$ plays a central role in the degree of dissolution of reactive silica from the aggregates [33]; the higher the Ca^{2+} content, the higher the dissolution of silica. Therefore, the analysis displayed in Figure 10.10b indicates that the higher the replacement of CaO by SiO_2, the lower the expansion amplitudes of CPT mixtures. Moreover, it verifies that the difference between points #3, #6, and #1 (orientation 1) is resumed to "silica fume line", once from #3 to #1, only silica fume was used as SCM, and its dosages varied from 4.5% (#3) to 8% (#6), and 15% (#1). Thus, the results agreed with the data found in the literature.

a) b)

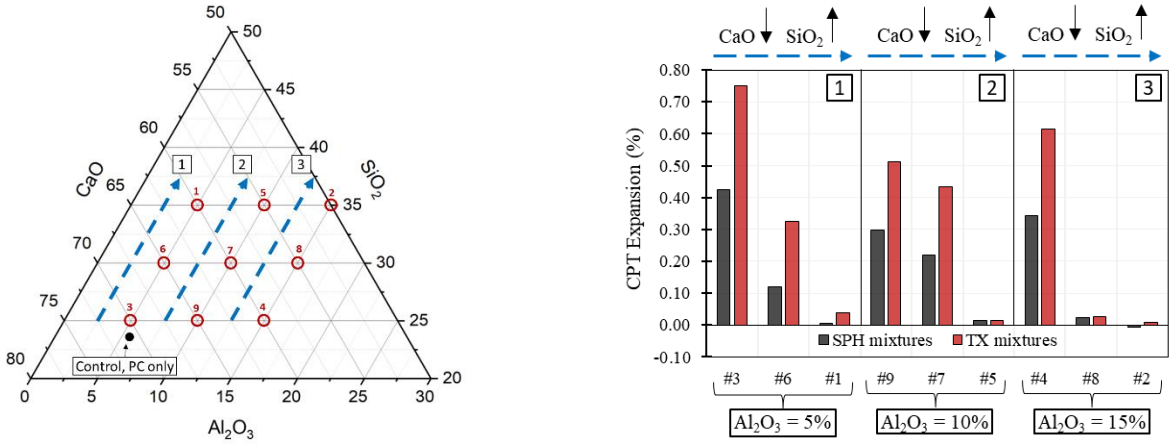

Figure 10.10: Comparative analysis between ternary plot mixtures and CPT expansion: a) ternary plot point and orientation path of the analysis displayed in b) fixed Al_2O_3 on mixtures vs. expansion behaviour.

Following the analysis on the influence of the three main oxides found in cementing materials, Figure 10.11 displays the same approach as previously discussed for Figure 10.10. Yet, setting three different portions of SiO_2 (i.e., 25%, 30%, and 35%) and lessening the amount of CaO and rising Al_2O_3 trends to decrease the final expansion of the concrete mixtures, although not as straightforward as replacing calcium with silicon ions. Nevertheless, the presence of aluminum in the pore solution, either from SCMs or cement, is absorbed on the surface of reactive SiO_2 from aggregates, slowing both the dissolution of SiO_2 and the formation of reaction products [8]. Analyzing Figure 10.10b, the orientation path 1 (i.e., SiO_2 fixed as 25%) reveals that from point #3 to point #9 the there is a decrease in the final expansion for both reactive aggregates, while from #9 to #4, the expansion increases. Likewise, for constant SiO_2 at 30%, higher expansions are also observed from points #6 to #7. This behaviour may be explained by two main factors: first, and unfortunately, to reach the chemical composition of #4 (i.e., 15% of Al_2O_3, 25% of SiO_2, and 60% of CaO), an expressive amount of calcium hydroxide was added in the mixture, enabling a faster release of Ca^{2+} ions in the concrete mixture. Second, mixture #7 was easily obtained by combining 82.5% of PC with 14.5% of FA and 3% of MK. However, the slower pozzolanic reactivity of FA may have consumed less portlandite from pore solution, enabling worsened ASR development. At SiO_2 fixed as 35%, changing Al_2O_3 content did not significantly modify the final expansion of the mixtures; all #1, #5, and #2 yielded expansion lower than 0.04%, up to date.

a) b)

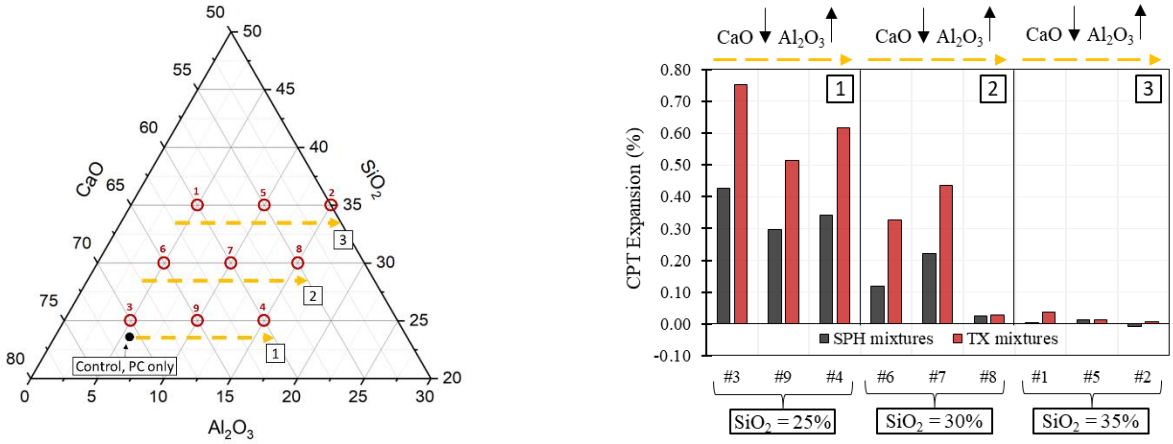

Figure 10.11: Comparative analysis between ternary plot mixtures and CPT expansion: a) ternary plot point and orientation path of the analysis displayed in b) fixed SiO_2 on mixtures vs. expansion behaviour.

As previously discussed, the amount of portlandite plays a central role in the dissolution of reactive silica from the aggregates. Moreover, SCMs consume a significant amount of $Ca(OH)_2$ during their pozzolanic reactivity; this consumption changes the viscosity and swelling properties of the ASR-gel and reduces the pH of the material. Thus, either replacing CaO with SiO_2 or Al_2O_3 slower ASR kinetics and decreases the final expansion amplitudes. However, another interesting analysis that can be done over the obtained results is the setting different portions of CaO (i.e., 65%, 60%, and 55%) and understand the influence on changing the contents of SiO_2 and Al_2O_3 (Figure 10.12a and b). The analysis indicates that for a fixed amount of CaO, the higher the amount of SiO_2, the lower the expansion of the CPT mixtures. However, this trend does not mean that silica fume is a "better" solution to mitigate ASR than metakaolin, for instance. In this case, the reason for this observed behaviour may lie in the portlandite consumption after the hydration of the concrete. For instance, the results obtained by De Souza and Sanchez [66] revealed that replacing 15% of PC's mass by MK mitigated down ASR expansion for both SPH and TX aggregates. This binder mixture used by the authors would results in a point (coordinates of 12%, 28%, and 60% for Al_2O_3, SiO_2, and CaO) almost halfway between points #4 and #7. Therefore, it emphasizes the importance of portlandite consumption from the pozzolanic reactivity of the SCMs. Moreover, the differences in the expansion results from points #5 and #8 are negligible, while both are composed of a high volume of SF and MK.

a) b)

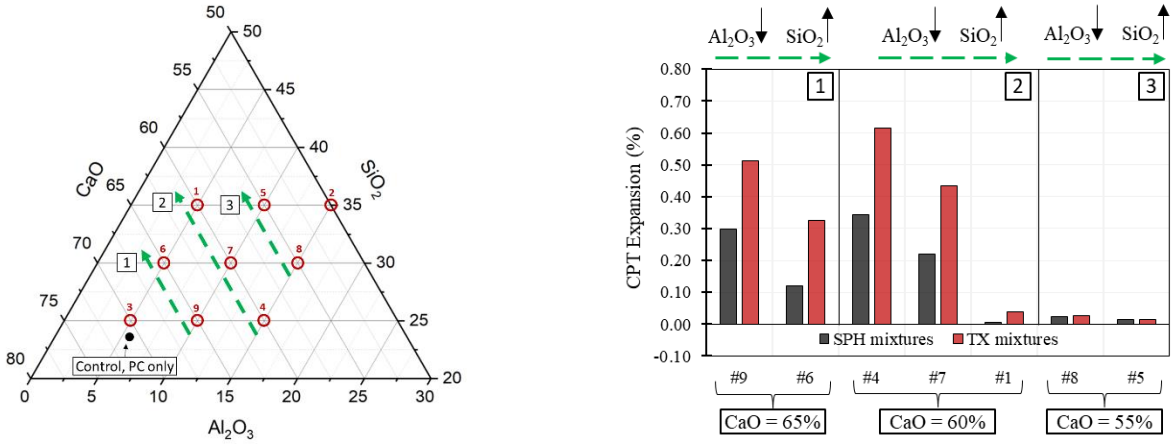

Figure 10.12: Comparative analysis between ternary plot mixtures and CPT expansion: a) ternary plot point and orientation path of the analysis displayed in b) fixed CaO on mixtures vs. expansion behaviour.

Finally, in the fourth analysis, all main oxides of the blended binder mixtures change over the orientation indicated by the red arrows illustrated in Figure 10.13a. For each step from one point to another (i.e., from #3 to #7), the percentage of CaO decreases in 10 units while SiO_2 and Al_2O_3 increase in 5 units each. Thus, expressive reductions in the final expansion values of the mixtures are observed by following orientations 1, 2, and 3 (Figure 10.13b). This was, in general, quite expected once the previous analysis suggested that individually replacing CaO either SiO_2 or Al_2O_3 could significantly slow ASR kinetics and mitigate the expansion development.

a) b)

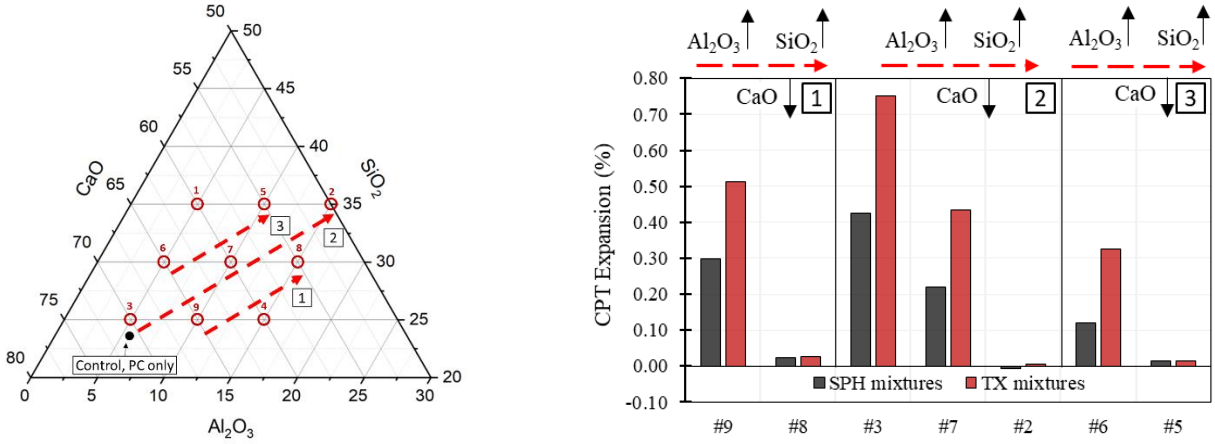

Figure 10.13: Comparative analysis between ternary plot mixtures and CPT expansion: a) ternary plot point and orientation path of the analysis displayed in b) varying all main oxides in mixtures vs. expansion behaviour.

10.6.1.3 **Data analysis and statistical significance.**

To assess the statistical validity and significance of the database generated as part of this study, analysis of variance (two-variable ANOVA), considering both the individual specimens and the various mortar/concrete mixtures for each exposure condition, were carried out. The results displayed in Table 10.6 show that the binder mixtures (i.e., control and mixtures from #1 to #9) significantly affect ASR development regardless of the type/nature of aggregates (i.e., SPH and TX) and the exposure condition (i.e., AMBT, ACPT, and CPT). Furthermore, all F_{values} were greater than F_{critic}; likewise, all P_{values} were smaller than 0.05. However, although ANOVA analysis can bring important validation of the data obtained in this research, a second statistical analysis (Tukey test) was performed to evaluate the significance of the individual results directly compared to each other. A summary of results is illustrated in Figure 10.14 (AMBT), Figure 10.15 (ACPT), and Figure 10.16 (CPT).

Table 10.6: Two-variable ANOVA analysis on the expansion amplitudes results for the mortar and concrete mixtures incorporating a wide range of binder combinations and different aggregate types/natures.

Method	Exposure Period	Aggregate	F_{value}	F_{critic}	$F_{value} > F_{critic}$	P_{value}	α	P < α
AMBT	14 days	SPH	145.95	2.39	Y	3.0E-16	0.05	Y
		TX	182.19	2.39	Y	3.4E-17	0.05	Y
	28 days	SPH	331.30	2.39	Y	9.2E-20	0.05	Y
		TX	374.18	2.39	Y	2.8E-20	0.05	Y
ACPT	90 days	SPH	621.22	2.64	Y	5.7E-32	0.05	Y
		TX	1196.33	2.64	Y	6.8E-37	0.05	Y
	180 days	SPH	457.77	3.06	Y	1.8E-15	0.05	Y
		TX	391.34	3.06	Y	5.7E-15	0.05	Y
CPT	360 days	SPH	234.87	2.02	Y	1.2E-48	0.05	Y
		TX	3102.75	2.02	Y	2.3E-87	0.05	Y

The comparative analysis between the average expansion values of the distinct mortar and concrete mixtures revealed that, due to the somewhat similar behaviour of mixture #3 with the control samples, both mixtures are statistically equivalent, which is quite reasonable once #3 has the closest “chemical composition” to control. Moreover, the mixtures named #1, #2, #5, and #8 displayed a general

statistical equivalency regarding their behaviour over ASR expansion development. Interestingly, mixtures #1, #2, and #5 have all the same amount of SiO_2 (i.e., 35%). Thus, the calcium oxide and aluminum oxide content variation did not imply any significant alteration in expansion development. Likewise, the difference between #5 and #8 mixtures sets on the variation of SiO_2 and Al_2O_3; while CaO is constant, their response on ASR development is also considered statistically equivalent. Finally, the comparative analysis reinforces the results found in this research, helping to better understand the behaviour of the distinct binder mixtures based on their chemical composition.

a)

	Control	#1	#2	#3	#4	#5	#6	#7	#8	#9
Control	x	2	2	1	1	2	2	2	2	2
#1		x	1	2	2	1	2	2	1	2
#2			x	2	2	1	2	2	1	2
#3				x	1	2	2	2	2	2
#4					x	2	2	2	2	2
#5						x	2	2	1	2
#6	SPH mixtures						x	1	1	2
#7								x	1	2
#8	1	Statistically similar							x	2
#9	2	Statistically significant difference								x

b)

	Control	#1	#2	#3	#4	#5	#6	#7	#8	#9
Control	x	2	2	1	2	2	2	2	2	2
#1		x	1	2	2	1	1	1	1	2
#2			x	2	2	1	1	1	1	2
#3				x	2	2	2	2	2	2
#4					x	2	2	2	2	2
#5						x	1	1	1	2
#6	TX mixtures						x	1	1	2
#7								x	1	2
#8	1	Statistically similar							x	2
#9	2	Statistically significant difference								x

Figure 10.14: Comparative analysis (Tukey Test for a significance level of 5%) between the average expansion of the distinct mortar mixture made of a) SPH and b) TX reactive aggregates and obtained through ABMT.

a)

	Control	#1	#2	#3	#4
Control	x	2	2	1	2
#1		x	1	2	2
#2			x	2	2
#3				x	2
#4	SPH mixtures				x
1	Statistically similar				
2	Statistically significant difference				

b)

	Control	#1	#2	#3	#4
Control	x	2	2	2	2
#1		x	2	2	2
#2			x	2	2
#3				x	2
#4	TX mixtures				x
1	Statistically similar				
2	Statistically significant difference				

Figure 10.15: Comparative analysis (Tukey Test for a significance level of 5%) between the average expansion of the distinct concrete mixture made of a) SPH and b) TX reactive aggregates and obtained through ACPT.

a)

	Control	#1	#2	#3	#4	#5	#6	#7	#8	#9
Control	x	2	2	1	2	2	2	2	2	2
#1		x	1	2	2	1	2	2	1	2
#2			x	2	2	1	2	2	1	2
#3				x	2	2	2	2	2	2
#4					x	2	2	2	2	2
#5						x	2	2	1	2
#6	SPH mixtures						x	2	2	2
#7								x	2	2
#8	1	Statistically similar							x	2
#9	2	Statistically significant difference								x

b)

	Control	#1	#2	#3	#4	#5	#6	#7	#8	#9
Control	x	2	2	2	2	2	2	2	2	2
#1		x	2	2	2	1	2	2	1	2
#2			x	2	2	1	2	2	1	2
#3				x	2	2	2	2	2	2
#4					x	2	2	2	2	2
#5						x	2	2	1	2
#6	TX mixtures						x	2	2	2
#7								x	2	2
#8	1	Statistically similar							x	2
#9	2	Statistically significant difference								x

Figure 10.16: Comparative analysis (Tukey Test for a significance level of 5%) between the average expansion of the distinct concrete mixture made of a) SPH and b) TX reactive aggregates obtained through CPT.

10.6.2 Microscopical and mechanical evaluation of ASR affected concrete mixtures

The extensive testing performed allowed some characteristics of the influence of distinct binder in the overall behaviour of ASR-affected concrete. In general, ASR damage development of the SCMs-made concrete mixtures (i.e., from #1 to #9) follows somewhat close distress characteristics than concrete made only with Portland cement as binder material. However, before exploring and discussing the influence of the different mixtures, a brief analysis of the impact of two concrete tests methods on the data gathered will be addressed as follows.

ASR distress development is often correlated to the level of expansion triggered by the concrete under ASR development. As widely studied by Sanchez et al. [56,58], the distress development due to ASR in concrete begins while cracks are formed within the aggregate particles (i.e., expansion level of about 0.05%). As the ASR-induced damage raises, new cracks are still developed within the aggregate particles; yet the pre-existing cracks keep increasing in length and width, reaching the cement paste. At higher levels of expansion (i.e., expansion of 0.30%), the cracks keep propagating through the aggregate particles and cement paste and due to the "minimum energy law", they start connecting, forming a high crack networking and compromising the mechanical properties of the affected concrete [56,58]. The exposure conditions of the concrete specimens (i.e., ACPT and CPT) implemented in this research proportioned different expansion kinetics, which was somewhat expected since there is an expressive variation in the exposure temperature (i.e., 38 ^{o}C and 60 ^{o}C). Yet, literature data indicates that the results obtained over 90 and 180 days of exposure to ACPT, although slightly lower, are quite comparable to CPT at 360 and 720 days. Globally, the data gathered in this study follows the findings from the literature. Moreover, the concrete mixtures' overall mechanical and microscopical results

follow similar trends and are well connected to the expansion development, yet a few observations can be addressed.

The DRI analysis revealed that the total DRI numbers obtained through either ACPT or CPT were, in general, quite comparable. However, the petrographic analysis of ACPT specimens (Figure 10.17) already verified the presence of an important and greater amount of cracks in the cement paste (CCP and CCPG) when compared to CPT samples (Figure 10.18). Furthermore, the specimens evaluated over ACPT also displayed fewer cracks in the aggregates (CCA, OCA, and OCAG). The higher temperature and further faster ASR kinetics proportioned by the ACPT seems to slightly modify the distress mechanism of ASR, although comparable total DRI numbers were found. Yet, it is necessary to highlight that besides a few exceptions, the expansion levels of ACPT specimens are not the same as CPT. Therefore, further analysis (e.g., at pre-determined expansion levels) must be performed to confirm these findings. Finally, the above information and the results displayed in Figure 10.17 and Figure 10.18 likely explain the differences observed in the mechanical analysis. Globally, ACPT specimens yielded lower SDI values (Figure 7.5) and modulus of elasticity losses (Figure 7.6), while higher but more variable compressive strength losses.

a) b)

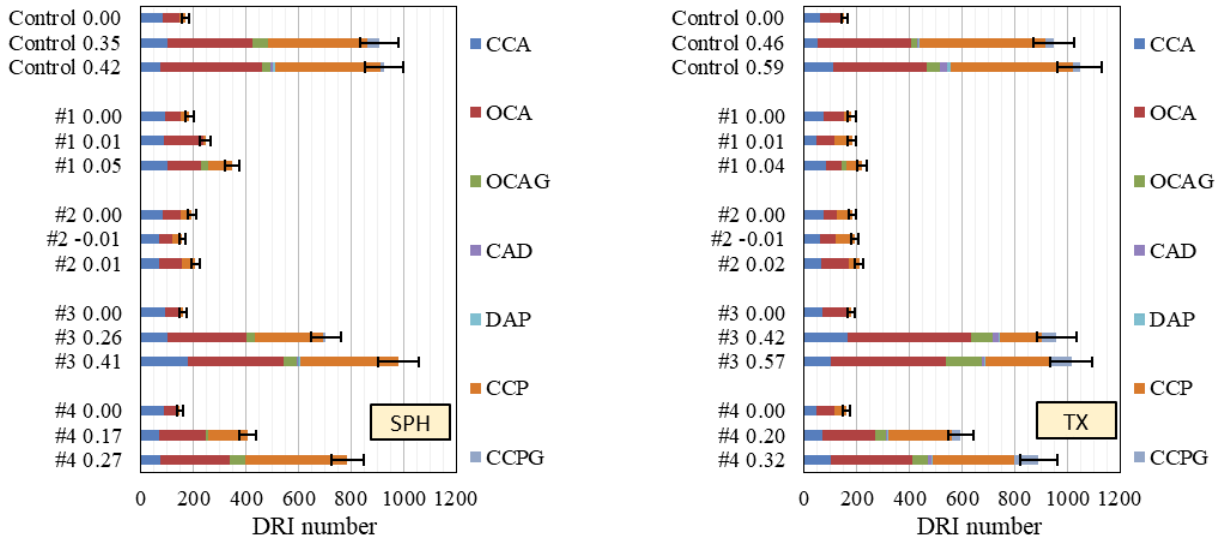

Figure 10.17: Petrographic features of the distinct concrete mixtures incorporating a) SPH coarse and b) TX fine aggregates and exposed to ACPT method.

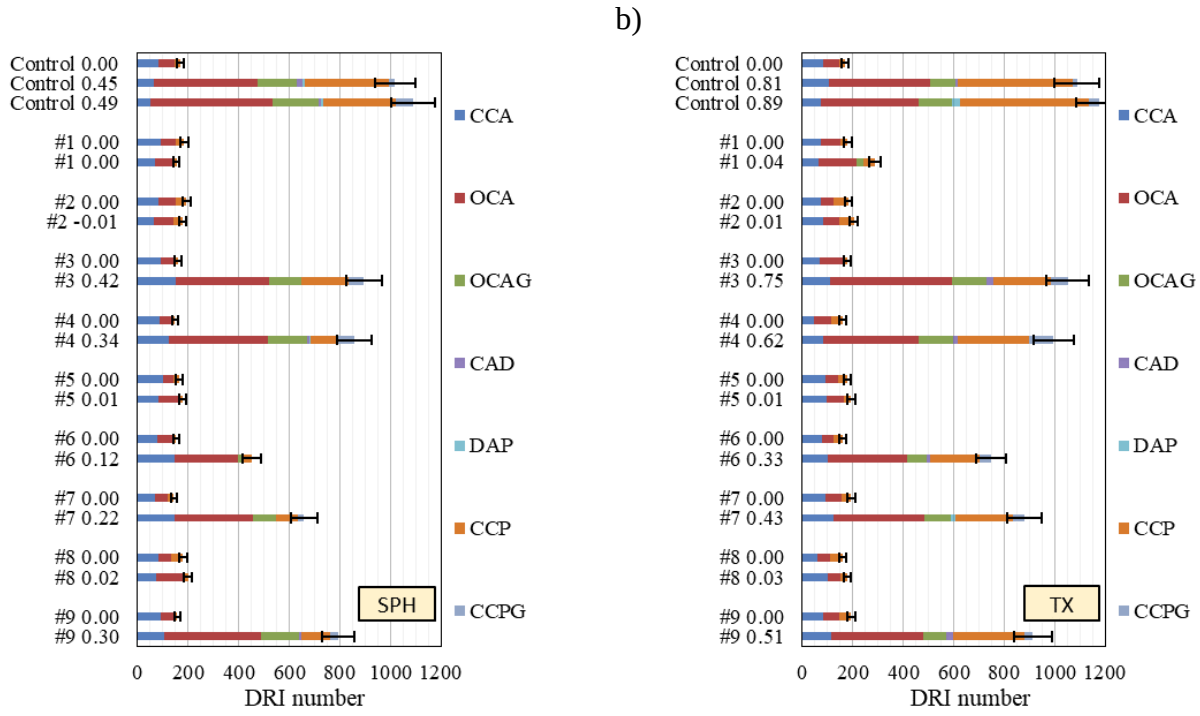

Figure 10.18: Petrographic features of the distinct concrete mixtures incorporating a) SPH coarse and b) TX fine aggregates and exposed to CPT method.

The mechanical properties of the ASR-affected concrete specimens are directly related to the quality of their microstructure (i.e., DRI). Overall, the mechanical behaviour and microscopical features of the concrete mixtures under ASR development correlated well with the expansion levels yielded over time. Moreover, the values likely followed the finding of De Souza and Sanchez [67] and ranges of properties loss proposed by Sanchez et al. [5]. In general, the higher the expansion level, the higher the DRI number and further losses in mechanical properties of the concrete mixtures. However, the different kinetics of the aggregates displayed an important role in the distress development. Concrete specimens made of TX fine aggregate developed significantly higher expansion amplitudes than SPH mixtures. Yet, at similar expansion levels, the global mechanical property losses, particularly the modulus of elasticity, were higher for concrete mixtures made of SPH coarse aggregate. This behaviour was quite expected, though, since coarse aggregates influence the concrete mechanical properties, particularly the stiffness or modulus of elasticity. Moreover, the DRI results displayed in Figure 10.17 and Figure 10.18 showed evidence of cracks in the aggregates for SPH coarse aggregate specimens compared to TX-concrete samples. This distinction in the cracking pattern explains the higher loss of modulus of elasticity obtained for SPH mixtures and confirms the mechanical results obtained. On the

other hand, the higher amount of cracks in the cement paste exhibited by the TX-concrete specimens likely explains the higher losses of compressive strength than concrete made of SPH coarse aggregate.

10.6.3 Proposal of a framework for the optimization of binder materials to avoid or mitigate ASR-induced expansion and deterioration

The extensive experimental program performed in this study on concrete mixtures designed with a new approach, based on pre-determined chemical compositions, and incorporating various aggregate types contributed to understanding the influence of the three main oxides found in binder materials on ASR development. Moreover, combining the data gathered with the data reported in the literature [12,20,35–37] became even more evident in the trends described and discussed in this work. For instance, Figure 10.19 was developed to illustrate and highlight the importance of the variation in the chemical composition of the concrete to mitigate the harmful development of ASR. Moreover, the main ternary oxides vs. the average ASR expansion development of concrete mixtures (Figure 10.19) take into account the incorporation of aggregates with marginal (Figure 10.19a), moderate (Figure 10.19b), high (Figure 10.19c); and extremely high reactivity (Figure 10.19d). The latter also considers the data from this study. Therefore, increasing the reactivity of the aggregate particles farther from the control mixtures area (black points in the plots), the binder composition needs to be set to suppress ASR development, likely following the trends displayed in section 10.6.1.2 (Figure 10.11, Figure 10.12, and Figure 10.13).

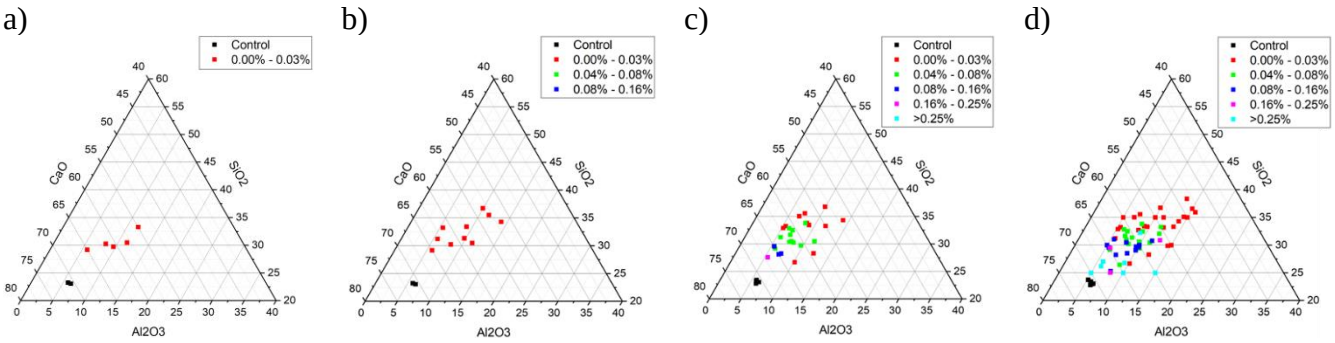

Figure 10.19: Main ternary oxides vs average ASR expansion development of concrete mixtures incorporating a) marginal reactive; b) moderate reactive; a) highly reactive; a) extremely high reactive aggregates.

In order to present a novel framework for the optimization of binder materials to avoid or mitigate ASR-induced expansion and deterioration in concrete, Figure 10.20 was elaborated and illustrated six

different regions, which indicates possible measures to suppress potential alkali-reactivity of aggregates according to each preventive measures, as per CSA A23.2-27A, allowing the selection of distinct binder combinations. It is worth mentioning that each coloured area represents the "minimum requirement" on the combination of the three main oxides of binder materials to mitigate ASR accordingly to the risk of ASR development, as indicated. However, further research is still required to better understand the potential of designing concrete mixtures based on the ternary plot approach. Second, to determine with higher precision the different proposed areas; particularly, for a wide range of reactive aggregates and different exposure conditions, such as field exposure. Nevertheless, this novel approach enables the optimization of the binder materials and provides support in the "decision making" to select optimized and efficient concrete mixtures against ASR-induced development.

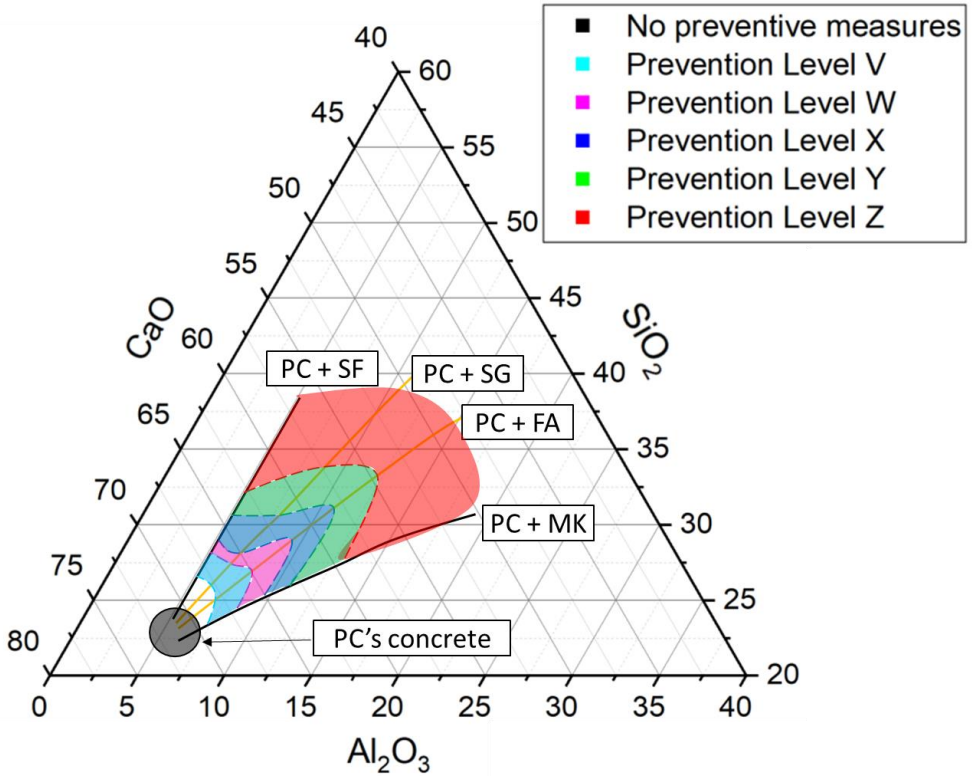

Figure 10.20: Global analysis charts for different combinations of supplementary cementing materials to counteract alkali-silica reaction (prevention levels from V to Z as per CSA A23.2-27A).

10.7 **Conclusions**

The main objective of this research was to evaluate a different mix-design approach to support concrete mix-designers to determine the appropriate preventive measures to fabricate supplementary cementing

materials-based concrete with minimum risk of ASR development. From the results obtained in this study, the following conclusions may be drawn:

- ASR kinetics, mechanical properties and microscopic changes are dependent on the aggregate's type (i.e., fine vs coarse aggregate). Samples incorporating the highly reactive Tx sand developed higher expansion levels and damage than SPH samples. Moreover, samples containing Tx have developed more cracks in shorter periods due to their faster ASR-induced kinetics.
- Three different accelerated methods were performed to assess ASR kinetics and expansion development of the distinct mixtures. Namely, accelerated mortar bar test (AMBT), accelerated concrete prism test (ACPT), and concrete prism test (CPT). Although the overall expansion behaviour of the mixtures agreed from one accelerated method to another, two out of nine binder mixtures (e.g., #1, #6, and #7) exhibits conflicting results among the accelerated testing methods. Furthermore, while in AMBT procedure, the samples mitigated down SPH-made mortars to a non-reactive behaviour (i.e., values below 0.10% of expansion at 14 days of exposure), for ACPT and CPT methods, they worsen behaviour, yielding values higher than 0.04% after 180 days and 360 days of exposure, respectively.
- The microscopic (i.e., DRI) and mechanical properties (i.e., SDI, modulus of elasticity, and compressive strength losses) agree with the expansion levels obtained for both ACPT and CPT: i.e., the higher the expansion amplitudes, the higher the DRI and SDI values, along with ME and CS losses. However, minor differences were observed between ACPT and CPT specimens. In general, ACPT provided samples with a slightly higher amount of cracks in the cement paste, thus increasing the losses in compressive strength.
- The results demonstrate that all "chemically controlled" mixtures (from #1 to #9) displayed a lower expansion value than SPH and TX control specimens. The statistical analysis performed

(i.e., ANOVA and Tukey Test) confirmed this behaviour, yet mixture #3 (the closest to control) was proven to have similar behaviour than control mixtures. Moreover, considering the "position" of the mixes points displayed in the ternary main oxides plot, the results showed a clear trend in which the farther the points are from the control mixture, the lower the expansion amplitudes at the end of the periods of analysis.

- Further analysis made by comparing the influence of the different portions of Al_2O_3, SiO_2, and CaO demonstrated that the higher the content of either Al_2O_3, SiO_2, or both, the lower ASR-induced expansion development. Yet, keeping constant the amount of CaO, the results suggest that mixtures with a higher amount of SiO_2 trends to be more efficient to mitigate ASR.
- Finally, a novel framework for the optimization of binder materials to avoid or mitigate ASR-induced expansion and deterioration in concrete was proposed. The qualitative chart provides interesting data to help in the "decision making" to select the best options (i.e., the combination of different SCMs and quantities) to apply in the concrete exposed to ASR development. Yet, further research is still required to first better understand the potential of designing concrete mixtures based on the ternary plot approach and, second, to determine the different proposed areas of composition with higher precision. Particularly for a wide range of reactive aggregates and different exposure conditions, such as field exposure.

10.8 Acknowledgment

The authors would like to thank Dr. Gamal Elnabelsya and Dr. Muslim Majeed, technical officers of Materials and Structures Laboratory in the Department of Civil Engineering at the University of Ottawa. As well as De Souza benefits from the University of Ottawa Excellence Scholarship, Collaborative Research & Development by NSERC (Natural Science and Engineering Research Council of Canada), and the prestigious Vanier CGS scholarship, also financed by the NSERC.

10.9 References

[1] B. Fournier, M.-A. Bérubé, Alkali-aggregate reaction in concrete: a review of basic concepts and engineering implications, Can. J. Civ. Eng. 27 (2000) 167–191. doi:10.1139/cjce-27-2-167.

[2] J. Lindgård, Ö. Andiç-Çakir, I. Fernandes, T.F. Rønning, M.D.A. Thomas, Alkali-silica reactions (ASR): Literature review on parameters influencing laboratory performance testing, Cem. Concr. Res. 42 (2012) 223–243. doi:10.1016/j.cemconres.2011.10.004.

[3] M. Rashidi, M.C.L. Knapp, A. Hashemi, J.Y. Kim, K.M. Donnell, R. Zoughi, L.J. Jacobs, K.E. Kurtis, Detecting alkali-silica reaction: A multi-physics approach, Cem. Concr. Compos. 73 (2016) 123–135. doi:10.1016/j.cemconcomp.2016.07.001.

[4] L.F.M. Sanchez, Contribution to the assessment of damage in aging concrete infrastructures affected by alkali-aggregate reaction, 2014.

[5] L.F.M. Sanchez, B. Fournier, M. Jolin, D. Mitchell, J. Bastien, Overall assessment of Alkali-Aggregate Reaction (AAR) in concretes presenting different strengths and incorporating a wide range of reactive aggregate types and natures, Cem. Concr. Res. 93 (2017) 17–31. doi:10.1016/j.cemconres.2016.12.001.

[6] M. Thomas, The effect of supplementary cementing materials on alkali-silica reaction: A review, Cem. Concr. Res. 41 (2011) 1224–1231. doi:10.1016/j.cemconres.2010.11.003.

[7] Z. Shi, C. Shi, J. Zhang, S. Wan, Z. Zhang, Z. Ou, Alkali-silica reaction in waterglass-activated slag mortars incorporating fly ash and metakaolin, Cem. Concr. Res. 108 (2018) 10–19. doi:10.1016/j.cemconres.2018.03.002.

[8] A. Leemann, L. Bernard, S. Alahrache, F. Winnefeld, ASR prevention - Effect of aluminum and lithium ions on the reaction products, Cem. Concr. Res. 76 (2015) 192–201. doi:10.1016/j.cemconres.2015.06.002.

[9] B. Fournier, M.A. Bérubé, Alkali-aggregate reaction in concrete: A review of basic concepts and engineering implications, Can. J. Civ. Eng. 27 (2000) 167–191. doi:10.1139/l99-072.

[10] CSA A23.2-27A, Standard practice to identify degree of alkali-reactivity of aggregates and to identify measures to avoid deleterious expansion in concrete, Can. Stand. Assoc. (2019) 439–451. doi:10.1520/C0618-15.2.

[11] CSA A23.2-28A, Standard Practice for Laboratory Testing to Demonstrate the Effectiveness of Supplementary Cementing Materials and Chemical Admixtures to Prevent ASR in Concrete, Can. Stand. Assoc. (2009).

[12] B. Fournier, R. Chevrier, A. Bilodeau, P.P.C. Nkinamubanzi, N. Bouzoubaa, R. Chevrier, Comparative field and laboratory investigations on the use of supplementary cementing materials (SCMs) to control alkali-silica reaction (ASR) in concrete, in: 15th Int. Conf. Alkali-Aggregate React., Bernardes, H.M & Hasparyk, N.P., São Paulo, 2016.

[13] P.J. Nixon, RILEM Recommendations for the Prevention of Damage by Alkali- Aggregate Reactions in New Concrete Structures, 2016.

[14] Folliard et. al, Selecting Appropriate Measures for Preventing Deleterious, (2008).

[15] ASTM C 1778-16, Standard Guide for Reducing the Risk of Deleterious Alkali-Aggregate Reaction, Annu. B. ASTM Stand. (2014) 1–11. doi:10.1520/C1778-20.2.

[16] Y. Kawabata, K. Yamada, The mechanism of limited inhibition by fly ash on expansion due to alkali–silica reaction at the pessimum proportion, Cem. Concr. Res. 92 (2017) 1–15. doi:10.1016/j.cemconres.2016.11.002.

[17] A.K. Saha, M.N.N. Khan, P.K. Sarker, F.A. Shaikh, A. Pramanik, The ASR mechanism of reactive aggregates in concrete and its mitigation by fly ash: A critical review, Constr. Build. Mater. 171 (2018) 743–758. doi:10.1016/j.conbuildmat.2018.03.183.

[18] D. Hester, C. McNally, M. Richardson, A study of the influence of slag alkali level on the alkali-silica reactivity of slag concrete, Constr. Build. Mater. 19 (2005) 661–665. doi:10.1016/j.conbuildmat.2005.02.016.

[19] M.C.G. Juenger, R. Siddique, Recent advances in understanding the role of supplementary cementitious materials in concrete, Cem. Concr. Res. (2015). doi:10.1016/j.cemconres.2015.03.018.

[20] M.H. Shehata, M.D.A. Thomas, Use of ternary blends containing silica fume and fly ash to suppress expansion due to alkali-silica reaction in concrete, Cem. Concr. Res. 32 (2002) 341–349. doi:10.1016/S0008-8846(01)00680-9.

[21] T. Nochaiya, W. Wongkeo, A. Chaipanich, Utilization of fly ash with silica fume and properties of Portland cement-fly ash-silica fume concrete, Fuel. 89 (2010) 768–774. doi:10.1016/j.fuel.2009.10.003.

[22] P. Lawrence, M. Cyr, E. Ringot, Mineral admixtures in mortars, Cem. Concr. Res. 33 (2003) 1939–1947. doi:10.1016/S0008-8846(03)00183-2.

[23] B. Lothenbach, K. Scrivener, R.D. Hooton, Supplementary cementitious materials, Cem. Concr. Res. 41 (2011) 1244–1256. doi:10.1016/j.cemconres.2010.12.001.

[24] R.B. Figueira, R. Sousa, L. Coelho, M. Azenha, J.M. de Almeida, P.A.S. Jorge, C.J.R. Silva,

Alkali-silica reaction in concrete: Mechanisms, mitigation and test methods, Constr. Build. Mater. 222 (2019) 903–931. doi:10.1016/j.conbuildmat.2019.07.230.

[25] M. Cyr, R. Pouhet, Resistance to alkali-aggregate reaction (AAR) of alkali-activated cement-based binders, Woodhead Publishing Limited, 2015. doi:10.1533/9781782422884.3.397.

[26] F. Rajabipour, E. Giannini, C. Dunant, J.H. Ideker, M.D.A. Thomas, Alkali-silica reaction: Current understanding of the reaction mechanisms and the knowledge gaps, Cem. Concr. Res. 76 (2015) 130–146. doi:10.1016/j.cemconres.2015.05.024.

[27] E.R. Latifee, State-of-the-Art Report on Alkali Silica Reactivity Mitigation Effectiveness Using Different Types of Fly Ashes, J. Mater. 2016 (2016) 1–7. doi:10.1155/2016/7871206.

[28] A. Gholizadeh-Vayghan, F. Rajabipour, The influence of alkali–silica reaction (ASR) gel composition on its hydrophilic properties and free swelling in contact with water vapor, Cem. Concr. Res. 94 (2017) 49–58. doi:10.1016/j.cemconres.2017.01.006.

[29] S. Diamond, Alkali silica reactions - Some paradoxes, Cem. Concr. Compos. 19 (1997) 391–401. doi:10.1016/s0958-9465(97)00004-8.

[30] S. Diamond, A review of alkali-silica reaction and expansion mechanisms 1. Alkalies in cements and in concrete pore solutions, Cem. Concr. Res. 5 (1975) 329–345. doi:10.1016/0008-8846(75)90089-7.

[31] D.W. Hobbs, W.H. Gutteridge, A. Samarin, Particle size of aggregate and its influence upon the expansion caused by the alkali-silica reaction, Mag. Concr. Res. 32 (1980) 251–252. doi:10.1680/macr.1980.32.113.251.

[32] H. Wang, J.E. Gillott, Mechanism of alkali-silica reaction and the significance of calcium hydroxide, Cem. Concr. Res. 21 (1991) 647–654. doi:10.1016/0008-8846(91)90115-X.

[33] A. Leemann, G. Le Saout, F. Winnefeld, D. Rentsch, B. Lothenbach, Alkali-Silica reaction: The Influence of calcium on silica dissolution and the formation of reaction products, J. Am. Ceram. Soc. 94 (2011) 1243–1249. doi:10.1111/j.1551-2916.2010.04202.x.

[34] A. Leemann, P. Lura, E-modulus of the alkali-silica-reaction product determined by micro-indentation, Constr. Build. Mater. 44 (2013) 221–227. doi:10.1016/j.conbuildmat.2013.03.018.

[35] J. Duchesne, M.A. Bérubé, Long-term effectiveness of supplementary cementing materials against alkali-silica reaction, Cem. Concr. Res. 31 (2001) 1057–1063. doi:10.1016/S0008-8846(01)00538-5.

[36] R.F. Bleszynski, The performance and durability of concrete with ternary blends of silica fume and blast-furnace slag, 2002.

[37] T. Ramlochan, M. Thomas, K.A. Gruber, Effect of metakaolin on alkali-silica reaction in concrete, Cem. Concr. Res. 30 (2000) 339–344. doi:10.1016/S0008-8846(99)00261-6.

[38] C. Yuksel, R.S. Ahari, B.A. Ahari, K. Ramyar, Evaluation of three test methods for determining the alkali-silica reactivity of glass aggregate, Cem. Concr. Compos. (2013). doi:10.1016/j.cemconcomp.2013.03.002.

[39] R.D. Hooton, F. Golmakani, Improving the reliability of the ASTM C1260 accelerated mortar bar test, in: Proc. 15th Int. Conf. Alkali-Aggregate React. Concr., 2016.

[40] ASTM C1293, Standard test method for determination of length change of concrete due to alkali-silica reaction, Annu. B. ASTM Stand. (2015) 1–7. doi:10.1520/C1293-08BR15.2.

[41] CSA A23.1-14, Concrete materials and methods of concrete construction, Can. Stand. Assoc. (2019).

[42] C.S. Shon, S.L. Sarkar, Evaluation of modified ASTM C 1260 accelerated mortar bar test for alkali-silica reactivity, Cem. Concr. Res. 32 (2002) 1981–1987. doi:10.1016/S0008-8846(02)00903-1.

[43] H. Yazıcı, A. Beglarigale, K. Tosun Felekoğlu, S. Türkel, Comparing the alkali-silica reaction mitigation potential of admixtures by using different accelerated test methods, Constr. Build. Mater. 197 (2019) 597–614. doi:10.1016/j.conbuildmat.2018.11.227.

[44] NP. Hasparyk, G. Gallo, T. Andrade, T.O. Santos, Potential of Metakaolin in Mitigating Expansions of Asr in Accelerated Tests, in: NP. Bernardes, H.M. & Hasparyk (Ed.), 15th Int. Conf. Alkali-Aggregate React., São Paulo, 2016.

[45] R. Deschenes, M. Waidner, W.H. Hale, Mitigation of Alkali-Silica Reaction in Concrete Pavements By Silane Treatment, in: NP. Bernardes, H.M. & Hasparyk (Ed.), 15th Int. Conf. Alkali-Aggregate React., São Paulo, 2016.

[46] G. Gudmundsson, H. Olafsson, Alkali-silica reactions and silica fume: 20 years of experience in Iceland, Cem. Concr. Res. 29 (1999) 1289–1297. doi:10.1016/S0008-8846(98)00239-7.

[47] BM. Pedersen, B.J. Wigum, J. Lindgård, Influence of Aggregate Particle Size on the Alkali-Silica Reaction – a Literature Review, in: 15th Int. Conf. Alkali-Aggregate React., 2016: pp. 1–11.

[48] R. Ranc, L. Debray, Reference test methods and a performance criterion for concrete structures, in: 9th Int. Conf. Alkali-Aggregate React. Concr., London, 1992.

[49] J. Lindgård, RILEM TC 219-ACS-P: Literature survey on performance testing, 2011.

[50] P.H. Kermit, Determining alkali content in ASR performance-tested concrete, (2017).

[51] J.B. Walsh, The effect of cracks on the uniaxial elastic compression of rocks, J. Geophys. Res. 70 (1965) 399–411. doi:10.1029/JZ070i002p00399.

[52] R.S. Crouch, Specification for the determination of stiffness damage parameters from the low cyclic uniaxial compression of plain concrete cores, 1987.

[53] L.F.M. Sanchez, Contribution to the assessment of damage in aging concrete infrastructures affected by alkali-aggregate reaction, (2014) 341.

[54] L.F.M. Sanchez, B. Fournier, M. Jolin, J. Bastien, Evaluation of the stiffness damage test (SDT) as a tool for assessing damage in concrete due to ASR: Test loading and output responses for concretes incorporating fine or coarse reactive aggregates, Cem. Concr. Res. 56 (2014) 213–229. doi:10.1016/j.cemconres.2013.11.003.

[55] L.F.M. Sanchez, B. Fournier, M. Jolin, J. Bastien, Evaluation of the Stiffness Damage Test (SDT) as a tool for assessing damage in concrete due to alkali-silica reaction (ASR): Input parameters and variability of the test responses, Constr. Build. Mater. 77 (2015) 20–32. doi:10.1016/j.conbuildmat.2014.11.071.

[56] L.F.M. Sanchez, B. Fournier, M. Jolin, M.A.B. Bedoya, J. Bastien, J. Duchesne, Use of Damage Rating Index to quantify alkali-silica reaction damage in concrete: Fine versus coarse aggregate, ACI Mater. J. 113 (2016) 395–407. doi:10.14359/51688983.

[57] V. Villeneuve, B. Fournier, Determination of the damage in concrete affected by ASR–the damage rating index (DRI), in: 14th Int. Conf. Alkali-Aggregate React. Concr., Austin (Texas), 2012: p. electronic.

[58] L.F.M. Sanchez, B. Fournier, M. Jolin, J. Duchesne, Reliable quantification of AAR damage through assessment of the Damage Rating Index (DRI), Cem. Concr. Res. 67 (2015) 74–92. doi:10.1016/j.cemconres.2014.08.002.

[59] ASTM International, WITHDRAWN- Standard Test Method for Determining the Potential Alkali-Silica Reactivity of Combinations of Cementitious Materials and Aggregate (Accelerated Mortar-Bar Method), Annu. B. ASTM Stand. (2008) 1–6. doi:10.1520/C1567-13.2.

[60] C. Tremblay, M.-A. Bérubé, B. Fournier, M.D.A. Thomas, K.J. Folliard, Effectiveness of Lithium-Based Products in Concrete Made with Canadian Natural Aggregates Susceptible to Alkali-Silica Reactivity, ACI Mater. J. 104 (2007). doi:10.14359/18583.

[61] J.H. Ideker, B.L. East, K.J. Folliard, M.D.A. Thomas, B. Fournier, The current state of the accelerated concrete prism test, Cem. Concr. Res. 40 (2010) 550–555. doi:10.1016/j.cemconres.2009.08.030.

[62] ASTM C1293, Standard test method for determination of length change of concrete due to alkali-silica reaction, Annu. B. ASTM Stand. (2015) 1–7. doi:10.1520/C1293-08B.2.

[63] L.F.M. Sanchez, T. Drimalas, B. Fournier, D. Mitchell, J. Bastien, Comprehensive damage assessment in concrete affected by different internal swelling reaction (ISR) mechanisms, Cem. Concr. Res. 107 (2018) 284–303. doi:10.1016/j.cemconres.2018.02.017.

[64] CSA23.2-9C, Compressive strength of cylindrical concrete specimens, in: CSA A23.119/CSA A23.219 Natl. Stand. Canada, 2019: pp. 733–748.

[65] L.F.M. Sanchez, B. Fournier, M. Jolin, J. Bastien, Evaluation of the Stiffness Damage Test (SDT) as a tool for assessing damage in concrete due to alkali-silica reaction (ASR): Input parameters and variability of the test responses, Constr. Build. Mater. 77 (2015) 20–32. doi:10.1016/j.conbuildmat.2014.11.071.

[66] DJ De Souza, L.F.M. Sanchez, The use of self-healing technology combined with supplementary cementing materials to mitigate the Alkali-Silica Reaction distress, Under Publ. (n.d.).

[67] DJ De Souza, L.F.M. Sanchez, Multi-level assessment of the AAR-affected concrete including Vickers' hardness in concrete., Under Publ. (2021).

Chapter Eleven: Conclusion and Future Recommendations

Alkali-aggregate reaction (AAR) is one of the main processes affecting the durability of concrete infrastructure in Canada and worldwide. Over the years, several approaches and recommendations, including a comprehensive variety of laboratory test procedures, have been developed around the world to assess the potential alkali-reactivity of concrete aggregates and the effectiveness of preventive measures (i.e., control of the cement & concrete alkali content, use of supplementary cementing materials, etc.) before their use in the field.

Various types of treatments, especially aiming to "physically" stop/reduce the ingress of moisture and/or to provide confinement of the affected members (i.e., silane/siloxane water repellents, coatings, prestress confinement, etc.) have been tested and have shown quite promising results. However, a number of contradictory data were also obtained, which reflects the current lack of consensus in the area. Furthermore, it has been verified that some products (i.e., crystalline admixtures, bacteria-based products, etc.), either applied in the bulk paste or externally, can provide concrete with self-healing properties, which may present an interesting "physical" solution for durability-related distress in concrete, especially AAR. Yet, very few data are available considering the competence of such products for mitigating/rehabilitating AAR-affected concrete, and some doubts remain regarding their ability to recover concrete integrity

In this context, this study focused on detailed laboratory investigations aiming first to understand the self-healing of the concrete (i.e., by the natural or engineered processes). Then, its further influence on ASR-induced expansion and deterioration, either applied internally or externally to the concrete. The main findings of this experimental program are presented hereafter:

11.1 Understanding the efficiency of autogenous and autonomous self-healing of conventional concrete mixtures through mechanical and microscopical analysis

The higher the pre-loading (PL) level in the concrete specimens, the higher the damage. However, PL of 40% of the ultimate compressive strength did not change the concrete samples' physical or mechanical properties. Yet, higher PL levels (70% and 90%) were able to generate internal

cracking measured by microscopic analysis and increased the total porosity of the specimens; thus, a decrease in compressive strength, modulus of elasticity, bulk electrical resistivity, ultrasonic pulse velocity and an increase in the stiffness damage index were noticed.

Both autonomous or autogenous healing processes partially recovered the physical and mechanical properties of the concrete specimens after 90 days of curing. Moreover, both approaches could self-heal only cracks formed in the cement paste; pre-existent and PL generated cracks within the aggregates were not even partially healed.

The autonomous healing property was significantly improved by replacing 30% of Portland cement (PC) with fly ash class F (FA); however, this property was negatively affected by the replacement of 10% of PC by silica fume (SF). Generally, control specimens could recover 32% of their physical and mechanical properties (on average) when damaged at 28 days and 19% at 180 days. On the other hand, FA concrete specimens achieved 46% and 26% at 28 and 180 days, while SF samples values were 21% and 18% at the same ages, respectively. Moreover, the control, FA, and SF mixtures could self-heal about 38%, 52% and 23% of their cracks in the cement paste for PL applied at 28 days, whereas they reached 17%, 26% and 25% of cracks healed at 180 days.

Concrete specimens treated with the commercially available crystalline admixture (CA), CA, CA-FA, CA-SF mixtures were able to achieve an average recovery of 67%, 66% and 61% of their physical and mechanical properties, respectively. Moreover, early age damage CA, CA-FA, and CA-SF samples self-healed 82%, 77% and 58% of cracks formed in the paste matrix. For specimens damaged at 180 days, the recovery ratio obtained was 61%, 55% and 48%, whereas the number of self-healed cracks was 61%, 58% and 50% for CA, CA-FA and CA-SF, respectively.

The chemically modified version of the CA (CA2 and CA3) reached even higher average values: the specimens of both mixtures were able to recover 73% of their physical and mechanical properties and self-seal 84% (CA2) and 93% (CA3) of the cracks in the paste matrix when damaged at 28 days. For specimens damaged at 180 days, the results showed that 51% and 69% of mechanical properties recovery and 67% and 74% of the cracks were self-healed for CA2 and CA3, respectively.

Finally, the chemo-mechanical evaluation of the products formed within the cracks showed a higher C-S-H formation was found in healed cracks of SCMs-made concrete specimens. On the other hand, in concrete mixtures without SCMs, the main products found filling the cracks were calcium

carbonate first, followed by portlandite, C-S-H, and ettringite. Moreover, the Vickers' Hardness (HV) analysis suggests that the HV of autonomous healed samples was higher, while the specimens made of CA and CA3 displayed the lowest HV values. This behaviour suggests that the "volume" of cracks healed plays a major role in the final physical and mechanical properties recovery of the concrete. At the same time, the inner "quality" of the healing products seems to be less important.

11.2 **Evaluating the efficiency of SCMs to avoid or mitigate AAR-induced expansion and deterioration through the use of the multi-level assessment**

Overall, the higher the Portland cement replacement level by the different types of SCMs, the slower the ASR-induced development (i.e., kinetics). However, once the specimens reach similar (and pre-determined) expansion levels, the mechanical outcomes of affected concrete (i.e., stiffness damage index, losses in modulus of elasticity and shear strength) are quite similar to conventional concrete, regardless of the binder composition of the mixture.

The microscopic investigations showed that the development of ASR-induced deterioration results in the formation of cracks within the reactive aggregate particles that propagate to the cement paste at advanced expansion levels. Yet, the results indicate that higher levels of PC replacement induced to fewer cracks' number and density in the cement paste at moderate and higher levels of expansion. Nonetheless, the number of cracks observed within the aggregate particles slightly increased in comparison to the control specimens. The above description and result agrees with the rate of mechanical properties loss (i.e., stiffness and shear strength losses) gathered. On the other hand, the lower formation of cracks in the cement paste of SCMs-made concrete lessened the compressive strength losses. In general, the higher the replacement level, the slower the rate of CS loss.

The evaluation of ASR-gel through micro-indentation indicates that whenever within the aggregates, ASR-gel presents lower Vickers hardness values, lower than the values found when the gel is in contact with the cement paste. However, at the interface aggregate/ITZ, the highest HV values were found. Moreover, the calcium content obtained through EDS analysis seems to be the main reason for this variation in the surface hardness. This behaviour highlights the importance of understanding ASR-gel features for assessing damage and developing models to predict ASR-induced distress development. Nevertheless, PC replacement impacts the micro indentation results;

in general, the higher the replacement level, the lower the Vickers hardness of the ASR-gel towards the paste matrix.

Finally, the evaluation of the AAR reaction products (ASR vs. ACR) through micro-indentation revealed that, in general, the properties (i.e., mechanical and chemical) of the gel found within the ASR reactive particles are somewhat similar between the different types/natures of the aggregates. However, HV values and the Ca/Si ratios of the ACR reaction products were 123% and 77% higher than the ASR-aggregates, respectively; this could explain the fasted reaction kinetics and distinct distress development displayed by KING mixtures. Yet, further research needs to be developed to better understand the mechanical and physical properties of the ACR reaction products.

11.3 **The use of self-healing technology combined with supplementary cementing materials to mitigate the Alkali-Silica Reaction distress**

ASR kinetics, mechanical properties and microscopic changes are dependent on the aggregate's type (i.e., fine vs coarse aggregate). Samples incorporating the highly reactive Tx sand were more damaged than SPH samples. Moreover, samples containing Tx have developed more cracks in shorter periods due to their faster ASR-induced kinetics.

The use of crystalline admixtures (CA), either commercially available or modified versions, could change ASR kinetics and distress for both reactive aggregates used. It is believed that the CAs can start healing cracks and modify ASR kinetics and further deterioration only when the cracks reach the cement paste.

The most effective crystalline admixtures in decrease the number of cracks in the cement paste of the affected concrete specimens was CA1MK2, CA1WRP and CA1. The latter is the commercially available formula of CA, and the first two are the modified versions incorporation coarse metakaolin particles (CA1MK2) and water repellent in powder (CA1WRP).

The combined use of different SCMs and crystalline admixtures was highly effective in mitigating ASR, either changing ASR-kinetics or damage development. Although the chemical composition of the SCMs plays a major role in the development of ASR, the use of CA enhanced the healing properties of the SCMs-made concrete favouring the slower damage development.

The use of metakaolin in combination with crystalline admixtures, nano-silica and silica fume (i.e., CA1-MK, CA1-NS-MK, and CA1-NS-SF-MK mixtures) yielded the best results, even better than the samples containing Lithium Nitrate in the proportion of 0.74 Li/Na. However, it is unlike that the crystalline admixture has a significant influence in these mixtures, yet CA can enhance the microstructure helping to prevent ASR development. Moreover, this material can be an important tool to modify ASR-kinetics once the reaction starts to damage the paste matrix, delaying the deterioration and giving extra time to intervene and reinforce affected structures.

11.4 Evaluation of the efficiency of distinct surface treatments to mitigate alkali-silica reaction induced expansion and deterioration

ASR kinetics, mechanical properties and microscopic changes are dependent on the aggregate's type (i.e., fine vs coarse aggregate). Concrete mixtures containing Tx developed faster ASR kinetics and higher ultimate expansion amplitudes (e.g., 0.85% for TX-Control against 0.52% for SPH-Control). Moreover, the residual expansion (i.e., the difference between ultimate expansion and the initial expansion before the surface treatment) plays an important role in the efficiency of the coating and sealers to mitigate further ASR development. Globally, the higher the residual expansion, the lower the treatment efficiency.

The application of coating and sealers on the surface of the concrete specimens showed promising evidence that, besides the different materials displayed high expansion values after 720 days of exposure, they significantly modify ASR-kinetics. Furthermore, the statistical analysis (Tukey's test) confirmed the significance of the surface treatments. The only exception was spraying lithium on the surface, which displays similar results to control samples. On the other hand, the coating containing crystalline waterproofing and water repellent (i.e., CAWRP) demonstrated the higher efficiency to mitigate ASR, followed by CA+Sil (i.e., crystalline waterproofing plus silane treatment), and CA-Fib (i.e., crystalline waterproofing mixed with acrylic fibres).

The microscopic observations revealed that the total DRI numbers were quite well linked to the expansion level of each different surface treatment. The sealers and coating materials could not modify the ASR distress development mechanism; yet they altered ASR-kinetics slowing and delaying the overall progress of the damage. The only exception was the coating CA-Fib, which slowed the expansion development, yet the inner damage and crack development found in CA-Fib

specimens were significantly higher, comparable to specimens that achieved expansions 1.5 to 3 times higher. Moreover, the three-dimensional confinement effect proportioned by the CA-Fib coating modified the distribution of cracks and the proportions of the microscopic features.

The use of crystalline waterproofing coatings, which contain artificial triggering healing agents, did not modify the distress mechanism of ASR or recovered mechanical properties of the affected concrete specimens. Although a few cracks were found to be self-healed close to the external layer of the specimens.

Finally, four qualitative charts (Figure 9.23) were developed to provide interesting data to help in the "decision making" of engineers to better select different types of coating and sealers and the most appropriate "timing" to apply them. Globally, the coating and sealers demonstrated higher efficiency as higher the initial damage degree due to ASR. However, the performance loss plots indicate that as earlier the surface treatment is applied, the lower the performance loss of the concrete cylinders. Moreover, the analysis indicates that at higher initial damage degree (i.e., 0.20% and 0.30%), the performance losses of the treated concrete were somewhat similar among each surface treatment and control group.

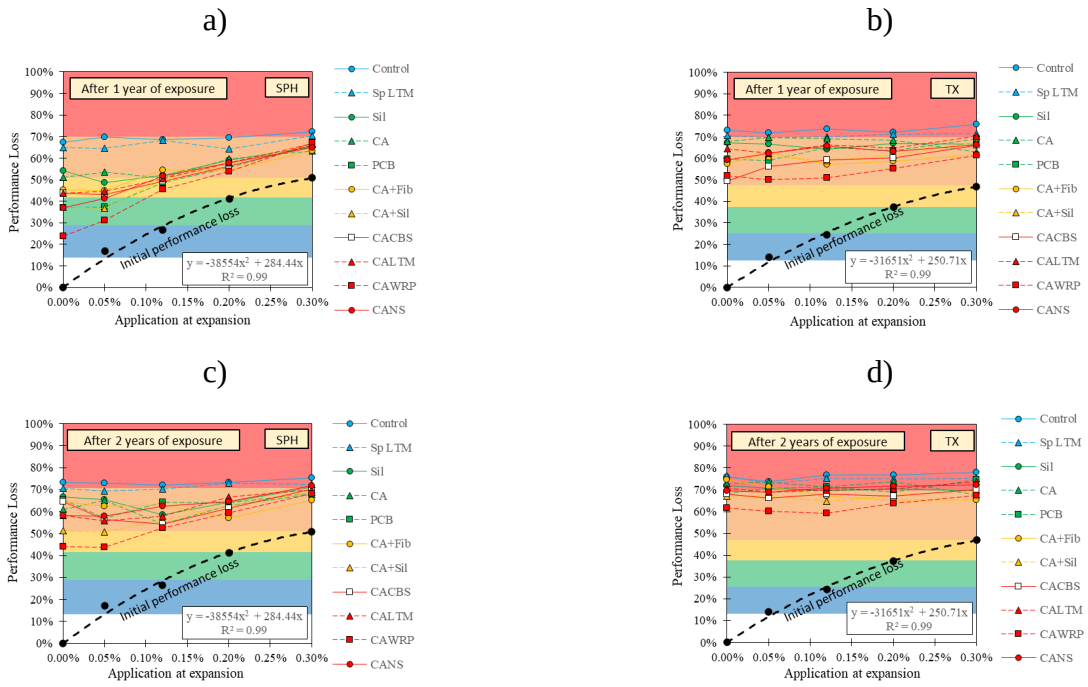

Figure 11.1: Performance losses of the surface-treated specimens after one year of exposure for a) SPH-concrete and b) TX-concrete, and after two years of exposure for c) SPH-concrete and d) TX-concrete.

11.5 **A proposed framework for an optimized selection of raw materials to avoid or mitigate ASR in concrete.**

ASR kinetics, mechanical properties and microscopic changes are dependent on the aggregate's type (i.e., fine vs coarse aggregate). Samples incorporating the highly reactive Tx sand developed higher expansion levels and damage than SPH samples. Moreover, samples containing Tx have developed more cracks in shorter periods due to their faster ASR-induced kinetics.

Three different accelerated methods were performed to assess ASR kinetics and expansion development of the distinct mixtures. Namely, accelerated mortar bar test (AMBT), accelerated concrete prism test (ACPT), and concrete prism test (CPT). Although the overall expansion behaviour of the mixtures agreed from one accelerated method to another, two out of nine binder mixtures (e.g., #1, #6, and #7) exhibits conflicting results among the accelerated testing methods. Furthermore, while in AMBT procedure, the samples mitigated down SPH-made mortars to a non-reactive behaviour (i.e., values below 0.10% of expansion at 14 days of exposure), for ACPT and CPT methods, they worsen behaviour, yielding values higher than 0.04% after 180 days and 360 days of exposure, respectively.

The microscopic (i.e., DRI) and mechanical properties (i.e., SDI, modulus of elasticity, and compressive strength losses) agree with the expansion levels obtained for both ACPT and CPT: i.e., the higher the expansion amplitudes, the higher the DRI and SDI values, along with ME and CS losses. However, minor differences were observed between ACPT and CPT specimens. In general, ACPT provided samples with a slightly higher amount of cracks in the cement paste, thus increasing the losses in compressive strength.

The results demonstrate that all "chemically controlled" mixtures (from #1 to #9) displayed a lower expansion value than SPH and TX control specimens. The statistical analysis performed (i.e., ANOVA and Tukey Test) confirmed this behaviour, yet mixture #3 (the closest to control) was proven to have similar behaviour than control mixtures. Moreover, considering the "position" of the mixes points displayed in the ternary main oxides plot, the results showed a clear trend in which the farther the points are from the control mixture, the lower the expansion amplitudes at the end of the periods of analysis.

Further analysis made by comparing the influence of the different portions of Al_2O_3, SiO_2, and CaO demonstrated that the higher the content of either Al_2O_3, SiO_2, or both, the lower ASR-induced expansion development. Yet, keeping constant the amount of CaO, the results suggest that mixtures with a higher amount of SiO_2 trends to be more efficient to mitigate ASR.

Finally, a novel framework (Figure 10.20) for the optimization of binder materials to avoid or mitigate ASR-induced expansion and deterioration in concrete was proposed. The qualitative chart provides interesting data to help in the "decision making" to select the best options (i.e., the combination of different SCMs and quantities) to apply in the concrete incorporating reactive aggregates. Yet, further research is still required to first better understand the potential of designing concrete mixtures based on the ternary plot approach and, second, to determine the different proposed areas of composition with higher precision. Particularly for a wide range of reactive aggregates and different exposure conditions, such as field exposure.

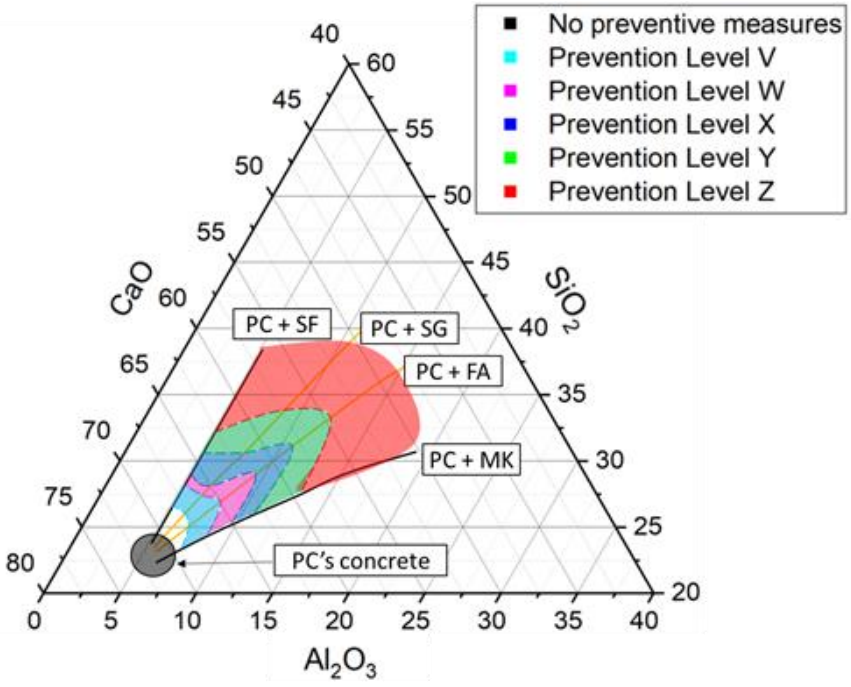

Figure 11.2: Global analysis charts for different combinations of supplementary cementing materials to counteract alkali-silica reaction.

11.6 **Recommendations for future work**

After conducting a very comprehensive experimental campaign (with over 4000 samples) and evaluating the main research outcomes, further investigations can be drafted as future research recommendations, as presented hereafter:

- A quite comprehensive experimental campaign was performed to better understand the influence of autogenous and autonomous healing to recover the physical and mechanical properties of damaged concrete specimens (laboratory-made concrete). Therefore, further research and investigations should be performed in concrete specimens exposed to field conditions and accounting for environmental influence in the self-healing ability of the concrete. This might give us some key information to understand the potential of self-healing in real concrete structures.
- Through a multi-level assessment of ASR-induced damage development, it became clear that SCMs can slightly modify ASR distress mechanisms in “unrestrained or free" expansion levels of concrete specimens. Further analysis needs to be performed to better understand the influence of SCMs on the rheological, swelling properties, alkalinity, and osmotic pressure of the ASR-gel. Since these parameters likely govern the overall expansive behaviour and damage of ASR-affected concrete.
- Likewise, investigations on mechanical, chemical, and rheological properties of the alkali-carbonate reaction products still need to be performed to understand the differences between ASR and ACR reaction products.
- The combination of engineered triggering self-healing agents and different types of supplementary cementing materials provided promising results regarding the prevention and mitigation of ASR. Yet, there are a few gaps to fully understand this technique of ASR mitigation, such as 1) the behaviour of these mixtures vs. a wide range of reactive aggregate,

including aggregates with different reactivity, ACR reactive aggregates, etc.; and 2) concrete specimens exposed to field conditions.

- It is necessary to further test the influence of autogenous and autonomous healing on other durability mechanisms (e.g., sulphate attack, corrosion, freezing and thawing, etc.) in order to gather a more holistic understanding of the impact of this engineering triggering self-healing agents on the durability-related properties of concrete.
- The qualitative chats proposed to help selecting different types of coating and sealers still require more data to improve its potential for further application. Likewise, the evaluation of the different coating and sealers is deemed crucial in field exposed specimens (i.e., cubes, blocks, etc.). Hence, to consider a critical aspect for waterproofing and repellent materials, the wet and drying cycles can significantly enhance their efficiency to maintain the relative humidity of the concrete at lower levels, thus increasing their performance against ASR development.
- Finally, a novel framework for optimizing binder materials to avoid or mitigate ASR-induced expansion and deterioration in concrete was proposed. Yet, further research is still required to first better understand the potential of designing concrete mixtures based on the ternary plot approach and, second, to determine the different proposed areas of composition with higher precision, particularly for a wide range of reactive aggregates and different exposure conditions, such as field exposure.